



DEVELOPMENT OF FLAT-PLATE SOLAR COLLECTORS
FOR THE HEATING AND COOLING OF BUILDINGS

By J. W. Ramsey, J. T. Borzoni, and T. H. Holland

(NASA-CR-134804) DEVELOPMENT OF FLAT-PLATE
SOLAR COLLECTORS FOR THE HEATING AND COOLING
OF BUILDINGS Final Report (Honeywell, Inc.)

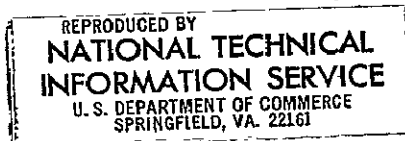
N75-26495

CSCL 10A

Unclassified

G3/44 26444

Distribution of this report is provided in the interest of
information exchange. Responsibility for the contents
resides in the author or organization that prepared it.



Prepared under Contract No. NAS3-17862 by
HONEYWELL INC.
Systems and Research Center
Minneapolis, Minnesota

for

NATIONAL AERONAUTICS AND SPACE ADMINISTRATION

1 Report No NASA CR-134804	2 Government Accession No	3 Recipient's Catalog No <i>N75-26495</i>
4. Title and Subtitle DEVELOPMENT OF FLAT-PLATE SOLAR COLLECTORS FOR THE HEATING AND COOLING OF BUILDINGS		5. Report Date June 1975
7 Author(s) J. W. Ramsey, J. T. Borzoni, and T. H. Holland		6. Performing Organization Code .
9. Performing Organization Name and Address Honeywell Inc. Systems and Research Center 2600 Ridgway Parkway N. E. Minneapolis, Minnesota 55413		8. Performing Organization Report No. 2852-40057
12 Sponsoring Agency Name and Address National Aeronautics and Space Administration Washington, D.C. 20546		10. Work Unit No.
		11 Contract or Grant No NAS3-17862
		13. Type of Report and Period Covered Contractor Report
		14 Sponsoring Agency Code
15 Supplementary Notes Project Manager, Frederick F. Simon, NASA Lewis Research Center, Cleveland, Ohio		
16 Abstract <p>The development of an efficient, low-cost flat-plate solar collector is the essential first step toward the effective utilization of solar energy for heating and cooling of buildings. This report describes a research and development program directed at examining the relevant design parameters in the fabrication of such a solar collector for heating liquids. The program objective was to design, fabricate, and test a flat-plate solar collector capable of a collection efficiency in excess of 50 percent at an inlet fluid temperature 93°C (200°F). Furthermore, the collector was to be of low cost, have high durability, and require little maintenance. To accomplish these objectives, the design task was approached with the use of computer-aided math models of the heat transfer processes in the collector. The analysis was used to determine the preferred physical design parameters from a heat transfer standpoint. This design process aided in defining the absorber panel configuration, the surface treatment of the absorber panel, the type and thickness of insulation, and the number, spacing and material of the covers. The outcome of this design task was a collector design (henceforth referred to as the baseline collector) which met the performance goals and which was producible using existing technology. In addition to the baseline collector, variations of this configuration were also identified for further study. These were of interest for a number of reasons. For example, some were predicted to have higher collector efficiency, others would be less expensive to build, while still others might have a longer life expectancy. Prototypes of each of the collector configurations were built and performance tested. All the collector configurations were tested using a solar simulator. The baseline collector and one additional configuration were also tested outside under natural sunlight. Each of the configurations was analyzed to determine the cost differential between designs. This was done both for the fabrication of a limited number of units and also for a limited mass-production level. Finally, based on the experimentally determined collector performance, simulated operation of the baseline collector configuration was combined with insolation data for a number of locations and compared with a predicted load to determine the degree of solar utilization.</p>		
17 Key Words (Suggested by Author(s)) Flat-plate solar collector Effective utilization of solar energy Heating and cooling of buildings Aluminum absorber panels Optically selective Black Nickel coating		18 Distribution Statement Unclassified - unlimited
19 Security Classif (of this report) Unclassified	20 Security Classif (of this page) Unclassified	21

FOREWORD

This is the final report describing the work performed by Honeywell Inc. for the NASA/Lewis Research Center, Cleveland, Ohio, under Contract Number NAS3-17862, "Development of Flat-Plate Solar Collectors for the Heating and Cooling of Buildings."

The authors acknowledge the guidance provided by Mr. F. F. Simon, NASA Project Manager, and Mr. R. N. Schmidt, Honeywell Urban and Environmental Systems. Ms. L. C. Cyrus and Ms. J. L. Byrne have the authors' sincere gratitude for their patience and cooperation.

The following personnel participated in the program:

J. W. Ramsey, Program Manager	P. R. Meyers
J. T. Borzoni	J. D. Moon
I. M. Bursch	R. E. Peterson
B. P. Gupta	R. L. Sampson
T. H. Holland	A. M. Severson
R. W. Kemna	

Preceding page blank

TABLE OF CONTENTS

	Page
SUMMARY	1
INTRODUCTION	2
Statement of the Problem	2
Review of Requirements	3
Synopsis of Program Results	4
COLLECTOR ANALYSIS	8
Thermal Performance Analysis Discussion	9
Analysis of the Flow Distribution in Solar Collector Arrays	13
Other Considerations for Sizing the Flow Tubes	17
Baseline Tube Size and Spacing	20
BASELINE COLLECTOR DESIGN	20
The Absorber Panel	21
The Solar Absorber Coating	23
Heat Transfer Fluid	26
Insulation	26
Collector Cover System	34
Collector Housing	39
COLLECTOR PERFORMANCE PREDICTIONS	43
BASELINE TESTING	52
Baseline Test Objectives	52
Indoor Test Facility	52
Baseline Test Matrix	54
Test Results	57
ALTERNATE COLLECTOR CONFIGURATION TESTING	63
COMPARISON OF TEST RESULTS TO PREDICTED PERFORMANCE	76
OUTDOOR TESTING	82
COST ANALYSIS	89

PREVIOUS PAGE BLANK FOR INFORMATION

Preceding page blank

TABLE OF CONTENTS (CONTINUED)

	Page
UTILIZATION STUDY	99
Study Approach	99
Energy Collection Calculations	102
Load Calculations	106
Typical Solar Utilization System	110
CONCLUSIONS AND RECOMMENDATIONS	114
Conclusions	114
Recommendations	118
APPENDIX A - FLAT-PLATE COLLECTOR PROGRAM	123
Introduction	123
Flat-Plate Collector Program	123
Solar Energy Absorption	125
Single Layer	126
Multiple Layers	128
Multiple Layers Plus Absorber	130
Heat Losses	142
Heat Absorbed by Collector Fluid	144
Solution Stability	145
APPENDIX B - FLOW DISTRIBUTIONS IN SOLAR COLLECTOR ARRAYS	147
Introduction	147
Flow Analysis	148
Header Pressure Drop Due to Wall Shear	148
Cross-Tube Pressure Drop	149
Pressure Changes Due to Removal or Addition of Flow at Branches	149
Cross-Tube Flow Distribution	151
APPENDIX C - SOLAR SIMULATOR AND OUTDOOR TEST DATA	157
Solar Simulator Test Data	157
Outdoor Test Data	157
APPENDIX D - HEATING AND COOLING LOAD AND SOLAR-LEVEL COLLECTION DATA	189
Heating and Cooling Load	189
Solar-Level Collection Data	189

TABLE OF CONTENTS (CONCLUDED)

	Page
APPENDIX E - BLACK NICKEL SELECTIVE COATING AND ANTIREFLECTIVE GLASS-ETCH PROCESS DESCRIPTIONS	207
Black Nickel Coating Process Description	207
Antireflective Glass-Etch Process Description	208
REFERENCES	209

LIST OF ILLUSTRATIONS

Figure		Page
1	Photograph of Baseline Collector	5
2	Baseline Collector Assembly	5
3	Nodal Subdivision of Flat-Plate Solar Collector	10
4	Schematic of Individual Collector and Potential Collector Array Configuration	13
5	Flow Distribution for 0.13 cm x 1.3 cm (0.05 in. x 0.50 in.) Cross Tube	15
6	Flow Distribution for 0.25 cm x 1.3 cm (0.10 in. x 0.50 in.) Cross Tube	15
7	Flow Distribution for 0.5 cm x 1.3 cm (0.20 in. x 0.50 in.) Cross Tube	16
8	ΔT from Absorber Tube to Fluid	19
9	Solar Collector Assembly	20
10	Solar Absorber Panel	23
11	Performance Curve for Selective Black Nickel Coating from Baseline Collector	24
12	Humidity Degradation of Black Nickel, Bright Nickel Coatings on Aluminum	25
13	Standoff Support	27
14	Heat Loss Test Arrangement	30
15	Initial Collector Configuration for Heat Loss Test	32
16	Mod. 1. Improved Edge Insulation	32
17	Mod. 2. Removal of Cross Braces and Variation of Insulation	33
18	Mod. 3. Revised Mechanical Supports	33
19	Baseline Configuration Resulting from Heat Loss Experiment	34
20	Spectral Transmission of Common and Low-Iron Glass	36

LIST OF ILLUSTRATIONS (CONTINUED)

Figure		Page
21	Solar Transmission Spectra of Two Plexiglass Products	36
22	Plexiglass Infrared Transmission	37
23	Transmission Spectra of Tedlar	38
24	Transmission Spectra of Polyethylene	38
25	Base-Solar Collector Box.	40
26	End-Solar Collector Box	40
27	Solar Collector Box	41
28	Glass Frame - Bottom Layer	41
29	Cover Spacer	42
30	Top Cover Bracket	42
31	Predicted Performance of the Baseline Collector (Selective Coated Absorber/Two Glass Covers).	44
32	Predicted Performance for a Collector with a Nonselective Absorber and Two Glass Covers	45
33	Predicted Performance for a Collector with a Selective Absorber and One Glass Cover.	46
34	Predicted Performance for a Collector with a Nonselective Absorber and One Glass Cover.	47
35	Predicted Effect on Wind on Performance of a Collector with Selective Absorber.	48
36	Predicted Effect of Wind on Performance of a Collector with Nonselective Absorber.	48
37	Predicted Effect of Changing Diffuse to Direct Ratio for a Collector with Selective Absorber	49
38	Predicted Effect of Changing Diffuse to Direct Ratio for a Collector with a Nonselective Absorber	50
39	Predicted Effect of Varying Incident Angle on Collector Performance	51

LIST OF ILLUSTRATIONS (CONTINUED)

Figure		Page
40	Spectral Total Reflectance for Several Angles of Incidence on a Black Nickel Coating Sample	51
41	Solar Simulator in Operation	53
42	Diagram of Indoor Collector Test Loop	55
43	Baseline Collector Performance with 0° Incident Flux Angle .	58
44	Baseline Collector Performance with 40° Incident Flux Angle	60
45	Baseline Collector Performance with 60° Incident Flux Angle	60
46	Effect of Incident Flux Angle on Performance	61
47	Performance of Baseline Collector under Changing Diffuse to Direct Ratio for Incident Flux	62
48	Startup Test Results for Baseline Collector	62
49	Radiation Properties of Black Chrome on Steel	63
50	Absorber Plate Comparisons for Collectors with Two Glass Covers - Low Temperature Operation	66
51	Absorber Plate Comparisons for Collectors with Two Glass Covers - High Temperature Operation	66
52	Cover Comparison for Collectors with Black Nickel Aluminum Absorbers - Low-Temperature Operation	67
53	Cover Comparison for Collectors with Black Nickel Aluminum Absorbers - High-Temperature Operation	67
54	Cover Comparison for Collectors with Black Painted Aluminum Absorbers - Low-Temperature Operation	69
55	Cover Comparison for Collectors with Black Painted Aluminum Absorbers - High-Temperature Operation	69
56	Comparison of Reflectance of Plain Glass and AR Etched Glass	70

LIST OF ILLUSTRATIONS (CONTINUED)

Figure		Page
57	Performance Curve for Black Nickel/Aluminum/2 Plain Glass Covers	70
58	Performance Curve for Black Nickel/Aluminum/1 Plain Glass Cover	71
59	Performance Curve for Black Nickel/Aluminum/1 Lexan Cover	71
60	Performance Curve for Black Nickel/Aluminum/Glass-Tedlar Cover	72
61	Performance Curve for Black Nickel/Aluminum/2 AR Glass Cover	72
62	Performance Curve for Black Paint/Aluminum/2 Plain Glass Covers	73
63	Performance Curve for Black Paint/Aluminum/1 Plain Glass Cover	73
64	Performance Curve for Black Paint/Aluminum/1 Lexan Cover	74
65	Performance Curve for Black Paint/Aluminum/Glass-Tedlar Cover	74
66	Performance Curve for Black Paint/Aluminum/2 AR Glass Covers	75
67	Performance Curve for Black Nickel/Steel/2 Plain Glass Covers	75
68	Performance Curve for Commercial Black Chrome/Steel/2 Plain Glass Covers	76
69	Comparison of Predicted and Test Results - Baseline Collector	78
70	Comparison of Predicted and Test Results - Nonselective - 2 Plain Collector Glass	78
71	Comparison of Predicted and Test Results - Selective - 1 Plain Collector Glass	79

LIST OF ILLUSTRATIONS (CONTINUED)

Figure		Page
72	Comparison of Predicted and Test Results - Nonselective - 1 Plain Collector Glass	79
73	Schematic of Outdoor Test Setup	83
74	Outdoor Test Setup	83
75	Outdoor Test Results--9/26/74	85
76	Outdoor Test Results--10/2/74	85
77	Outdoor Test Results--10/18/74	86
78	Outdoor Test Results--10/20/74	86
79	Outdoor Test Results--10/24/74	87
80	Outdoor Test Results--10/26/74	87
81	Outdoor Test Results--10/25/74	88
82	Outdoor Test Results--10/8/74	88
83	Outdoor Test Results--10/15/74	89
84	Collector Assembly (Prior to the Start of Assembly)	91
85	Collector Assembly (Adding the Insulation)	91
86	Collector Assembly (Installing the Absorber Panel)	92
87	Collector Assembly (Assembling the Cover System)	92
88	Collection Curves for a Clear Winter Day Insolation	98
89	Collection Curves for a Clear Summer Day Insolation	98
90	Geographic Comparison of Solar Heating	101
91	Geographic Comparison of Solar Cooling	101
92	Total Yearly Heating and Cooling Loads	102

LIST OF ILLUSTRATIONS (CONTINUED)

Figure		Page
93	Energy Delivered to a Load by 69.7 m^2 (750 ft^2) of Baseline Collector in Minneapolis	106
94	Heating and Cooling Load for a 139 m^2 (1500 ft^2) Minneapolis House	109
95	Heating and Cooling Load and Solar-Supplied Portion of a Load for a Minneapolis House	109
96	Heating and Cooling Load and Solar-Supplied Portion of a Load for an Atlanta House	111
97	Cooling Load and Solar-Supplied Portion of a Load for a Miami House	111
98	Heating and Cooling Load and Solar-Supplied Portion of a Load for an Industrial Building in Philadelphia	113
99	Typical Solar-Assisted-HVAC System	113
100	Nodal Subdivision of Flat-Plate Solar Collector	124
101	One Layer	131
102	Two Layers	132
103	Three Layers	133
104	Four Layers	135
105	N Layers, Diffuse Incident Flux	137
106	N Layers + Absorber: Direct Incident, Specular Absorber	138
107	N Layers + Absorber: Diffuse Incident, Specular Absorber	139
108	N Layers + Absorber: Direct Incident, Diffuse Absorber	140
109	N Layers + Absorber: Diffuse Incident, Diffuse Absorber	141
110	Flat-Plate Solar Collector	147
111	Control Volume Computation	150

LIST OF ILLUSTRATIONS (CONCLUDED)

Figure		Page
i12	Flow Distribution for 0.13 cm x 1.3 cm (0.05 in. x 0.50 in.) Cross Tube	154
i13	Flow Distribution for 0.25 cm x 1.3 cm (0.10 in. x 0.50 in.) Cross Tube	155
i14	Flow Distribution for 0.5 cm x 1.3 cm (0.20 in. x 0.50 in.) Cross Tube	156

LIST OF TABLES (CONTINUED):

Table		Page
19	Solar Simulator Test Data for Black Nickel on Aluminum	158
20	Solar Simulator Test Data for Black Paint on Aluminum	166
21	Solar Simulator Test Data for Black Nickel on Steel	171
22	Solar Simulator Test Data for Black Chrome on Steel	172
23	Outdoor Test Data for 9/26/74 , ;	173
24	Outdoor Test Data for 10/2/74 ;	175
25	Outdoor Test Data for 10/8/74 , ,	177
26	Outdoor Test Data for 10/15/74 ;	179
27	Outdoor Test Data for 10/18/74 . . , ,	180
28	Outdoor Test Data for 10/20/74 ;	182
29	Outdoor Test Data for 10/24/74 ;	184
30	Outdoor Test Data for 10/25/74 , ;	185
31	Outdoor Test Data for 10/26/74 ;	187
32	Heating and Cooling Load for Atlanta ;	190
33	Heating and Cooling Load for Chicago ;	191
34	Heating and Cooling Load for Dallas ;	192
35	Heating and Cooling Load for Los Angeles ;	193
36	Heating and Cooling Load for Miami ;	194
37	Heating and Cooling Load for Pittsburg ;	195
38	Heating and Cooling Load for Philadelphia ;	196
39	Heating and Cooling Load for Seattle ;	197
40	Incident and Collected Solar Energy Including Cloud Cover for Atlanta ;	198

LIST OF TABLES

Table	Page
1 Fiberglass Insulation	28
2 Nonfiberglass Insulation	28
3 Summary of Heat Loss Results	31
4 Baseline Collector Test Matrix (Test Date)	56
5 Alternate Configuration Test Matrix (Test Date)	65
6 Comparison of Performance Coefficients Derived from Testing and Analysis	81
7 Baseline Collector Design Present Fabrication Cost	94
8 Baseline Collector Design Fabrication Costs with Limited Mass Production	94
9 Estimated Component Cost with Limited Mass Production	95
10 Comparative Cost of Various Collector Design Iterations	95
11 Cost Effectiveness for Various Collector Designs	97
12 Cost Effectiveness for Various Collector Designs	97
13 Locations and Conditions Used for the Utilization Analysis	99
14 Percent of Load Supplied by 69.7 M ² (750 ft ²) of Baseline Solar Collectors for a 139.4 M ² (1500 ft ²) House	100
15 Incident and Collected Solar Energy without Cloud Cover for Minneapolis	104
16 Incident and Collected Solar Energy Including Cloud Cover (Based on 1956 Weather Data) for Minneapolis	105
17 Heating and Cooling Load for Minneapolis	108
18 Heating and Cooling Load for Philadelphia Industrial Building	112

LIST OF TABLES (CONCLUDED)

Table		Page
41	Incident and Collected Solar Energy Including Cloud Cover for Chicago	199
42	Incident and Collected Solar Energy Including Cloud Cover for Dallas	200
43	Incident and Collected Solar Energy Including Cloud Cover for Los Angeles	201
44	Incident and Collected Solar Energy Including Cloud Cover for Miami	202
45	Incident and Collected Solar Energy Including Cloud Cover for Pittsburgh	203
46	Incident and Collected Solar Energy Including Cloud Cover for Philadelphia	204
47	Incident and Collected Solar Energy Including Cloud Cover for Seattle	205

DEVELOPMENT OF FLAT-PLATE SOLAR COLLECTORS
FOR THE HEATING AND COOLING OF BUILDINGS

By J. W. Ramsey, J. T. Borzoni, and T. H. Holland
Honeywell Inc.

SUMMARY

This is the final report describing the work performed by Honeywell Inc. for the NASA Lewis Research Center, Cleveland, Ohio, under Contract Number NAS3-17862 on "Development of Flat-Plate Solar Collectors for the Heating and Cooling of Buildings."

The development of an efficient, low-cost flat-plate solar collector is the essential first step toward the effective utilization of solar energy for heating and cooling of buildings. This report describes a research and development program directed at examining the relevant design parameters in the fabrication of such a solar collector for heating liquids.

The program objective was to design, fabricate, and test a flat-plate solar collector capable of a collection efficiency in excess of 50 percent at an inlet fluid temperature 93°C (200°F). Furthermore, the collector was to be of low cost, have high durability, and require little maintenance.

To accomplish these objectives, the design task was approached with the use of computer-aided math models of the heat transfer processes in the collector. The analysis was used to determine the preferred physical design parameters from a heat transfer standpoint. This design process aided in defining the absorber panel configuration, the surface treatment of the absorber panel, the type and thickness of insulation, and the number, spacing and material of the covers.

The outcome of this design task was a collector design (henceforth referred to as the baseline collector) which met the performance goals and which was producible using existing technology. In addition to the baseline collector, variations of this configuration were also identified for further study. These were of interest for a number of reasons. For example, some were predicted to have higher collector efficiency, others would be less expensive to build, while still others might have a longer life expectancy.

Prototypes of each of the collector configurations were built and performance tested. All the collector configurations were tested using a solar simulator. The baseline collector and one additional configuration were also tested outside under natural sunlight. Each of the configurations was analyzed

to determine the cost differential between designs. This was done both for the fabrication of a limited number of units and also for a limited mass-production level.

Finally, based on the experimentally determined collector performance, simulated operation of the baseline collector configuration was combined with insulation data for a number of locations and compared with a predicted load to determine the degree of solar utilization.

INTRODUCTION

Statement of the Problem

Interest in solar energy as a potential contributor to the U.S. energy economy has risen again primarily on the basis of impending reductions in the supplies of economically recoverable conventional fuels (particularly those having low sulfur content and other desirable properties) and on the idea that the utilization of solar energy leads to a minimum of environmental impact.

An examination of the potential applications of solar energy in the United States indicates that the most likely significant early contribution to energy economy is in the area of heating and air conditioning. In particular, summer air conditioning results in heavy peak loads on many public utilities. Residential energy uses represent approximately one-fifth of the total U.S. energy consumption. While some of this energy is used in metropolitan areas where solar heating and cooling would be difficult to apply, approximately 75 percent of the U.S. families live in single-family dwellings and are potential users of solar heating-cooling systems. Population trends and housing needs in the next two decades indicate that some millions of new dwellings will be constructed in this country which may be conditioned by solar processes. Solar heating-cooling systems can also have, as an integral feature, water heating capability to provide domestic hot water. Domestic solar water heating is already widely practiced in other countries such as Australia, where the economic benefits are more favorable than in the United States.

Higher temperature performance is more desirable for collectors used for building climate control than for those used for domestic water heating. In both cases, however, economics governs the design. The task becomes one of developing a collector which can operate at the higher temperatures with reasonably high efficiency without increasing the costs significantly. The primary measure will be cost per unit energy delivered at the required temperature. Long life, low maintenance, and architectural aesthetics must also be considered in the design, evaluation and selection.

Review of Requirements

The flat-plate solar collector is the basic element of a solar heating and cooling system and can represent 50 percent or more of the total system cost. Collector development is directed toward three objectives: increase of the temperature at which collectors operate, improvement in performance, and reduction in cost. To achieve these objectives, a set of requirements must be met.

1) High thermal performance. - The thermal performance of the collector can be measured by the temperature at which the collected thermal energy can be delivered and the collection efficiency (useful energy/incident energy) of the collector system at that delivery temperature. To effectively use the collected heat, the energy must be delivered to the heating-cooling system (or leave the collector) at a temperature of approximately 50-90°C (120-200°F), or higher. In the described program, the emphasis was on the higher temperature performance, as required for air conditioning. The required outlet temperature must be attainable for typical environmental conditions such as those specified in the contract: -23 to 38°C (-10°F to 100°F) ambient temperature, 0 to 32 kph (0 to 20 mph) wind speed. The collector must be designed for high efficiency at the required collector fluid outlet temperature; however, it is essential that the effect of the performance improvements on the cost of the collector be considered.

The specific performance goal for the collector in this contract was a collection efficiency in excess of 50 percent at an inlet fluid temperature of 93°C (200°F).

2) Low cost. - The acceptable cost for a flat-plate collector can be determined by comparing the cost of the heat delivered from a collector ("solar fuel") with the cost of the fuel replaced. The cost of the "solar fuel" is proportional to the ratio of the collector cost (\$/area) to the heat delivered by the collector. The ability of a collector to deliver heat is indicated by its efficiency. Therefore, there is a one-to-one correlation in the cost and efficiency which must be considered in evaluating collector designs.

3) Low maintenance/high durability. - It is necessary that the solar collector require low maintenance. One method of establishing the cost for owning and operating a solar collector is to assume a standard 15-percent annual discount rate (or operating expense). This value of 15 percent includes only a minimum amount of maintenance, nominally less than 1 percent per year of the capital cost. Even if the maintenance cost could be allowed to become as large as 3 percent, however, it still precludes the replacement of any major component or the renewal of the absorber surface. Any acceptable collector design will require high durability for the design goal of 15-year life. The collector must be resistant to degradation due to environmental conditions such as wind, rain, hail, temperature extremes, UV radiation, and possibly snow.

Allowance for thermal expansion must also be made and, to maximize durability, the collector must be made of materials compatible with each other and with the heat transport fluid.

4) Design for condition of no heat removal. - The collector must be designed to withstand the high temperature which will occur under conditions of no heat removal (e.g., no flow of the heat transfer fluid). The absorber plates of well-designed collectors can reach temperatures as high as 260°C (500°F) for a condition of no heat removal. This high temperature imposes severe restrictions on the use of plastics and foam insulations.

5) Fast startup. - The thermal capacity of the collector must be low to allow rapid startup of the system. The contract goal for the startup time was from 10 to 30 minutes.

6) Suitable collector fluid. - A collector fluid compatible with the absorber plate and other plumbing must be selected so that any corrosion which takes place does not limit the durability of the system. Contact of other parts of the system with the fluid, due to leakage, should not result in permanent degradation. As large amounts of fluid will be needed for a complete heating and cooling system, a low-cost fluid is required. Other requirements such as a very low freezing point, safety, health and inflammability are also factors in the fluid selection.

7) Low weight. - It is preferable that the collector be lightweight. Such a collector will simplify installation and eliminate the need for the use of costly erection equipment. Also, it is anticipated that it may be desirable to retrofit existing buildings with roof construction that may not have been designed for heavy loads.

Synopsis of Program Results

A baseline collector was designed based on the above-listed requirements. This collector, plus a number of variations of the basic configuration, was built, tested and priced. The baseline collector design determined for this program has an aluminum absorber plate with an optically selective Black Nickel coating. The absorber plate is backed with 7.6 cm (3 in.) of rigid fiberglass insulation and surrounded with 5 cm (2 in.) of rigid fiberglass insulation on its four edges. This absorber/insulation sandwich is encased in a sheet metal box and covered with two layers of glass with a 3-cm (1.25-in.) air gap between sheets and a 3-cm (1.25-in.) air gap between the absorber and the lower layer of glass. The outside dimensions of the collector are 122 x 122 x 15.2 cm (48 x 48 x 6 in.). The baseline collector thus described is pictured in Figure 1 and displayed in an exploded view in Figure 2.

Variations of the baseline collector design were also examined to evaluate the effect on cost and performance for various collector materials. The variations were concentrated in two major design areas: the absorber and the cover

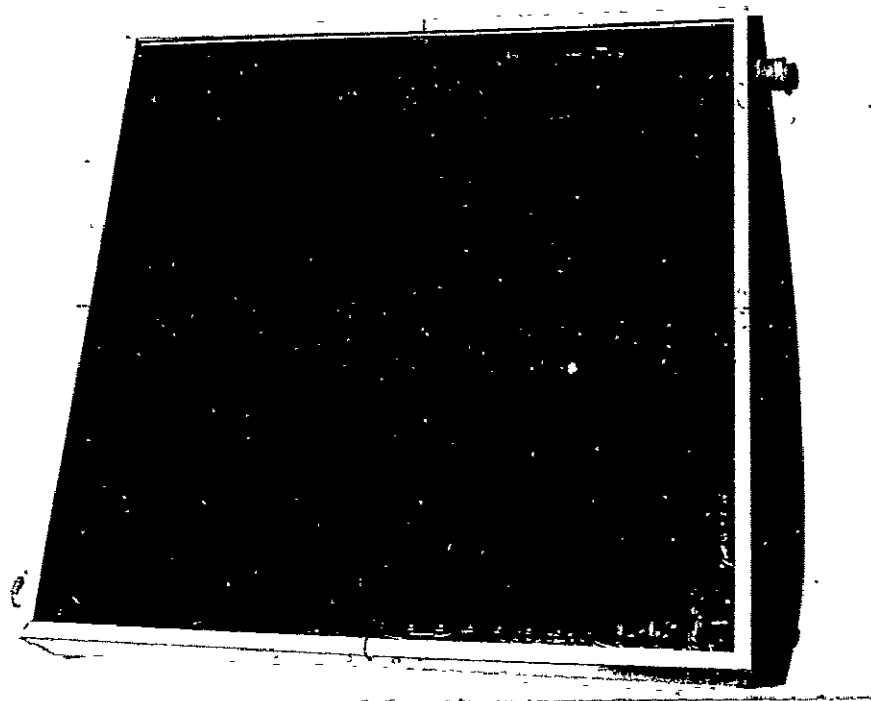


Figure 1. Photograph of Baseline Collector

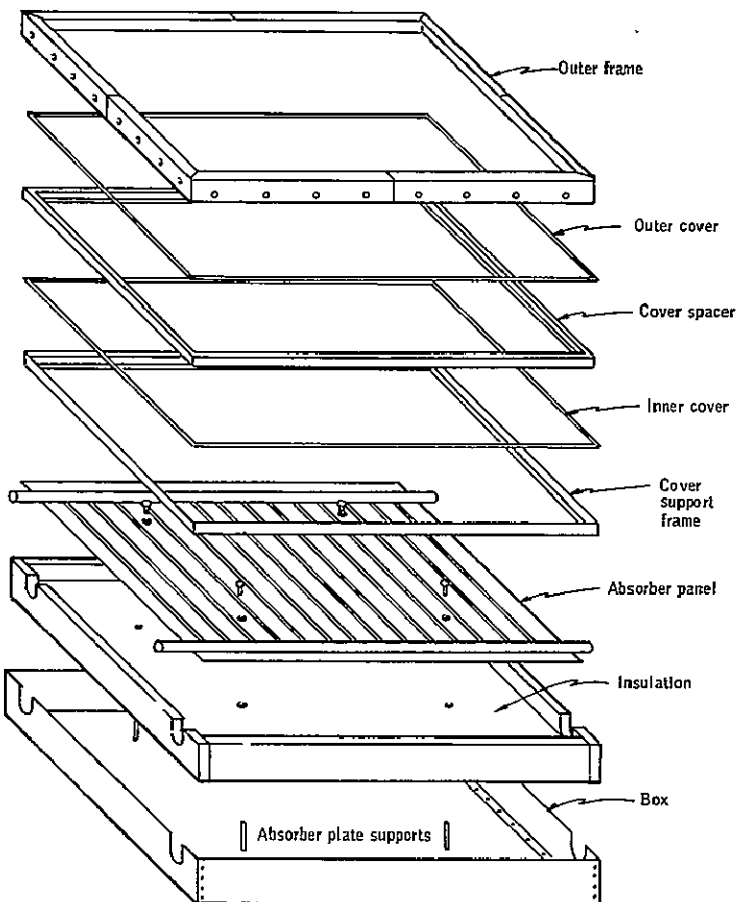


Figure 2. Baseline Collector Assembly

system. Absorber plates were made of both steel and aluminum and coated with selective Black Nickel (steel and aluminum), nonselective black paint (aluminum only) and selective Black Chrome (steel only). The cover systems examined consisted of one glass cover, two glass covers, one outer glass - one inner Tedlar cover, one Lexan cover, and two antireflection (AR) etched glass covers. The box design and insulation type and thickness were held constant, as was the cover spacing.

The performance results determined from the solar simulator testing indicated that the selective Black Nickel absorber, on either steel or aluminum panel, covered with two sheets of antireflection etched glass provides the greatest collector efficiency; 61.5 percent* at 93°C (200°F) inlet temperature, 27°C (80°F) ambient temperature, and 1009 w/m² (320 Btu/hr-ft²) incident flux.

Within the bounds of experimental accuracy, the following collector configurations are considered to have met or exceeded the performance goal of 50-percent collection efficiency with a 93°C (200°F) inlet temperature, 27°C (80°F) ambient temperature, and 1009 w/m² (320 Btu/hr-ft²) incident flux:

- Black Nickel-coated aluminum absorber panel and two glass covers -- 50.5 percent collection efficiency.
- Black Nickel-coated steel absorber panel and two glass covers -- 51.5 percent collection efficiency.
- Black Nickel-coated aluminum absorber panel and two AR etched glass covers -- 61.5 percent collector efficiency.
- Black Nickel-coated aluminum absorber panel and a glass outer cover and Tedlar inner cover -- 52.5 percent collection efficiency.
- Black-painted aluminum absorber panel and two AR etched glass covers -- 51.5 percent collection efficiency.
- Black Nickel-coated aluminum absorber panel and a single glass cover -- 49.5 percent collection efficiency.
- Black Nickel-coated aluminum absorber panel and a single Lexan cover -- 49 percent collector efficiency.
- Black Chrome-coated steel absorber panel and two glass covers -- 49 percent collection efficiency.

*The efficiency is defined as the heat delivered to the collector fluid per unit area of absorber divided by the incident solar flux based on the absorber area.

The following collectors did not meet the design goal:

- Black-painted aluminum absorber panel and two glass covers -- 42.5 percent collection efficiency.
- Black-painted aluminum absorber panel and an outer glass cover and an inner Tedlar cover -- 40.5 percent collection efficiency.
- Black-painted aluminum absorber panel and a single glass cover -- 39 percent collection efficiency.
- Black-painted aluminum absorber panel and a single Lexan cover -- 34.5 percent collection efficiency.

The companion objective to performance was cost. As might be expected, the best performing collector design was also the most costly. A cost analysis performed on each of the collector configurations revealed that the greatest cost effectiveness, measured in dollars per unit heat delivered to the working medium, was available from a collector with a Black Nickel-coated steel absorber panel with one glass outer cover and one Tedlar inner cover. However, only small differences were found in the cost effectiveness of a number of the best units. The top four units had a total cost-effectiveness spread of only 13 percent. All of these have selectively coated absorbers. The cost analysis also revealed, as expected, considerable disparity between present costs of fabricating small quantities of collectors, such as 93 m^2 (1000 ft^2) and moderate limited production quantities of 9300 m^2 ($100,000 \text{ ft}^2$).

Estimates of thermal heating and cooling loads for both a house and small industrial building were made and compared with estimates of the amount of solar energy which would be collected by a flat-plate array with an area equal to approximately one-half the floor area of the house or building. The calculations for the house were made for nine geographical locations utilizing actual weather data and insulation from a typical year. The industrial building was analyzed for a single location. Sufficient daytime storage was assumed to supplement nighttime heating and cooling, but heat collected in excess of monthly demand was assumed to be dumped, instead of accrued from month to month. Under these storage assumptions, 49 percent or more of the estimated energy required for cooling the house was delivered by the baseline collector array for all nine geographic locations. With the exception of Minneapolis and Seattle, 50 percent or more of the heating load was also satisfied by the same baseline collector array.

COLLECTOR ANALYSIS

The design of the baseline collector was guided by the results of a computer-generated flat-plate performance analysis. In addition to performing a thorough thermal analysis, including consideration of the transient response, detailed calculations were made to analyze the flow distribution, both within a single collector and throughout a multicollector array. The flow analysis was considered particularly relevant because most applications of the baseline collector would in fact use an array rather than a single collector.

The thermal analysis performed two primary functions: The initial effort of setting up the various heat transfer equations forced an early examination of the physical and mechanical characteristics of the components of a flat-plate collector. From this examination, such parameters as thickness of insulation and spacing between flow tubes were derived. The second, and perhaps more significant result of the thermal analysis, was the generation of a computer code that enabled an analytic prediction of flat-plate collector performance, given a set of design conditions and a set of input parameters. The computer code was to predict the comparative performance of one cover versus two covers; the effect of a selective absorber coating as compared with a nonselective black; the effect of wind; the effect of variable diffuse to direct ratio; the effect of the incident angle of the flux on flat-plate performance; and finally, the substantiation of the validity of using the following linear equation to describe flat-plate collector performance over a wide range of conditions:

$$\eta = k_1 \alpha_{\text{absorber}} \tau_{\text{cover}} - k_2 \frac{\Delta T_{\text{collector to ambient}}}{Q_{\text{incident}}} \quad (1)$$

where

- α = absorptance
- k_1, k_2 = thermal efficiency factors dependent of definition of ΔT
- η = collection efficiency
- Q_{incident} = incident solar flux
- τ = transmittance
- ΔT = temperature difference between collector and ambient

This equation is of particular interest, since it has been previously used by Hottel and Woertz, (1) Hottel and Whillier, (2) and Bliss (3) for predicting flat-plate performance, and also by Hottel and Whillier (5) and Simon and Harlamert (6) for presenting performance results.

The following collectors did not meet the design goal:

- Black-painted aluminum absorber panel and two glass covers -- 42.5 percent collection efficiency.
- Black-painted aluminum absorber panel and an outer glass cover and an inner Tedlar cover -- 40.5 percent collection efficiency.
- Black-painted aluminum absorber panel and a single glass cover -- 39 percent collection efficiency.
- Black-painted aluminum absorber panel and a single Lexan cover -- 34.5 percent collection efficiency.

The companion objective to performance was cost. As might be expected, the best performing collector design was also the most costly. A cost analysis performed on each of the collector configurations revealed that the greatest cost effectiveness, measured in dollars per unit heat delivered to the working medium, was available from a collector with a Black Nickel-coated steel absorber panel with one glass outer cover and one Tedlar inner cover. However, only small differences were found in the cost effectiveness of a number of the best units. The top four units had a total cost-effectiveness spread of only 13 percent. All of these have selectively coated absorbers. The cost analysis also revealed, as expected, considerable disparity between present costs of fabricating small quantities of collectors, such as 93 m^2 (1000 ft^2) and moderate limited production quantities of 9300 m^2 ($100,000 \text{ ft}^2$).

Estimates of thermal heating and cooling loads for both a house and small industrial building were made and compared with estimates of the amount of solar energy which would be collected by a flat-plate array with an area equal to approximately one-half the floor area of the house or building. The calculations for the house were made for nine geographical locations utilizing actual weather data and insulation from a typical year. The industrial building was analyzed for a single location. Sufficient daytime storage was assumed to supplement nighttime heating and cooling, but heat collected in excess of monthly demand was assumed to be dumped, instead of accrued from month to month. Under these storage assumptions, 49 percent or more of the estimated energy required for cooling the house was delivered by the baseline collector array for all nine geographic locations. With the exception of Minneapolis and Seattle, 50 percent or more of the heating load was also satisfied by the same baseline collector array.

COLLECTOR ANALYSIS

The design of the baseline collector was guided by the results of a computer-generated flat-plate performance analysis. In addition to performing a thorough thermal analysis, including consideration of the transient response, detailed calculations were made to analyze the flow distribution, both within a single collector and throughout a multicollector array. The flow analysis was considered particularly relevant because most applications of the baseline collector would in fact use an array rather than a single collector.

The thermal analysis performed two primary functions: The initial effort of setting up the various heat transfer equations forced an early examination of the physical and mechanical characteristics of the components of a flat-plate collector. From this examination, such parameters as thickness of insulation and spacing between flow tubes were derived. The second, and perhaps more significant result of the thermal analysis, was the generation of a computer code that enabled an analytic prediction of flat-plate collector performance, given a set of design conditions and a set of input parameters. The computer code was to predict the comparative performance of one cover versus two covers; the effect of a selective absorber coating as compared with a nonselective black; the effect of wind; the effect of variable diffuse to direct ratio; the effect of the incident angle of the flux on flat-plate performance; and finally, the substantiation of the validity of using the following linear equation to describe flat-plate collector performance over a wide range of conditions:

$$\eta = k_1 \alpha_{\text{absorber}} \tau_{\text{cover}} - k_2 \frac{\Delta T_{\text{collector to ambient}}}{Q_{\text{incident}}} \quad (1)$$

where

- α = absorptance
- k_1, k_2 = thermal efficiency factors dependent of definition of ΔT
- η = collection efficiency
- Q_{incident} = incident solar flux
- τ = transmittance
- ΔT = temperature difference between collector and ambient

This equation is of particular interest, since it has been previously used by Hottel and Woertz, (1) Hottel and Whillier, (2) and Bliss (3) for predicting flat-plate performance, and also by Hottel and Whillier (5) and Simon and Harlamert(6) for presenting performance results.

Thermal Performance Analysis Discussion

The flat-plate collector, a relatively simple device, operates on equally simple thermal principles. Nevertheless, the prediction of its thermal efficiency necessitates a detailed and fairly complex analytical approach. An accounting must be made of all the heat flow paths by which energy may enter and/or leave the collector.

This accounting requires the calculation of the radiation absorption in the solar spectrum; the radiation losses in the infrared; the natural convection between inclined parallel plates; external natural or forced convection from inclined plates; the heat conduction; and the heat transfer by forced or free convection to the collector fluid. Analytical correlations are available in the heat transfer literature which apply to the processes in varying degrees.

The published literature on the analysis of solar energy collection dates back to the 1880s, one of the well-known treatments being the work of Hottel and Woertz⁽¹⁾ in 1942. Hottel and Whillier⁽²⁾ in 1958 and Bliss in 1959⁽³⁾ presented certain plate efficiency factors, the use of which simplifies the calculation of the collector performance. Although these procedures reduce labor involved, they have some shortcomings. Their principal shortcoming is their inability to treat adequately the transient condition. A second drawback also lies in the method of handling the effects of a nonuniform temperature distribution (in the flow direction) in the absorber and other components. Although the derived efficiency factors do partially account for this effect, the variation of the radiation and convection heat transfer coefficient along the surfaces is not included in the analysis.

The computer program developed for this analysis of flat-plate collector performance does consider the transient conditions and the nonuniform temperature distribution. One of the inputs to the program is the incident solar flux. This flux may be a constant or a function of time, depending upon the response desired. The instantaneous and average performance may be calculated by inputting a daily record of solar flux. The time constant and, consequently, the system warmup time, may be obtained from an analysis of the response to a sudden inception of solar flux.

The flat-plate transient analysis program was developed with the following goals:

- The transient nature of the problem must be adequately treated.
- Effects of nonuniform temperature distributions must be considered.
- System energy balance and efficiency must be calculated on both an instantaneous and a daily basis.

- The program input routine must be able to handle conveniently a wide variety of geometrical and environmental parameters.
- The output routine must provide temperatures, temperature rates, heat flows, heat transfer coefficients, etc., to furnish good physical insight into the thermal performance.
- The output routine must summarize collector performance in the form of a system energy balance.

The program, as developed, uses all the pertinent geometrical, environmental and operational parameters of a particular collector design configuration and computes the desired thermal performance parameters. This computer program was utilized to obtain the predicted performance for collectors using both selective and nonselective absorber surfaces and also to predict the effect on performance of using one or more transparent covers. Wind effects, as related to collector performance, and the effect of varying solar incidence angle, were also analyzed and predicted.

A summary of the analytical procedures and the main features of the program is presented here. For greater analytical detail, refer to Appendix A.

To treat the transient condition and the nonuniform temperature distribution, the collector is subdivided into a number of physical elements or nodes (see Figure 3).

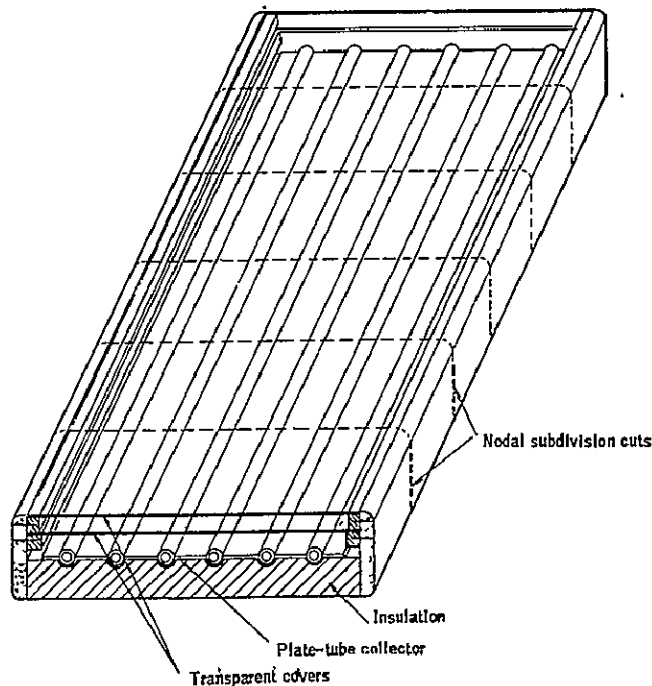


Figure 3. Nodal Subdivision of Flat-Plate Solar Collector

The effect of the fluid temperature from inlet to outlet is best examined by the indicated subdivision. The temperature of each node is computed as a function of time using the straightforward explicit method in which the rate change of the temperature of node i is related to its present temperature and the temperatures of the neighboring nodes j by:

$$C_i \frac{dT_i}{dt} = \sum_j K_{ij} (T_j - T_i) + S_i \quad (2)$$

C_i is the heat capacity of node i , T_i its temperature, dT_i/dt its rate of change of temperature, T_j is the temperature of node j , and S_i is the solar heat absorption. The coupling coefficients, K_{ij} , called conductance, depend on the heat transfer mode and, in general, on the temperature.

There are M such equations, one for each mass element, and the solution of these simultaneous, nonlinear, first-order, ordinary differential equations yields the temperature history at M discrete points throughout the collector. Since the temperature of each node is assumed to be given at some initial time, t_0 , the rates $(dT_i/dt)_{t=t_0}$ are given and the temperatures at $t_0 + \Delta t$ are obtained by:

$$T_i(t_0 + \Delta t) = T_i(t_0) + \left(\frac{dT_i}{dt} \right)_{t_0} \Delta t \quad (3)$$

Then the rates at $t_0 + \Delta t$ can be calculated and the procedure is repeated until the desired time range is covered.

The solar input, S_i , to each element is obtained by an analysis of the reflection, transmission, and absorption of incoming energy in the solar spectrum by a system of covers over an absorbing surface. This analysis has been carried out taking into consideration the two components of polarization, the reflection of each cover-air interface, the absorption of each cover and the absorption and reflection of the absorber plate. The program is then able to treat the four important combinations of specular and/or diffuse conditions:

- 1) Direct solar flux with specular reflecting absorber
- 2) Direct solar flux with diffuse reflecting absorber
- 3) Diffuse solar flux with specular reflecting absorber
- 4) Diffuse solar flux with diffuse reflecting absorber

The program analyzes the reflection, absorption, and transmission of the direct and diffuse components of the incident solar flux separately and then combines the results to obtain the total heat absorption.

The absorber loses heat to the environment by:

- 1) Emission of energy in the infrared spectrum and subsequent absorption, transmission, and re-emission of this energy by the cover system
- 2) Convection of energy to the adjacent cover and subsequent radiation and convection of the energy by the cover system
- 3) Conduction through the layer of insulation on the rear surface of the absorber
- 4) Conduction, convection, and radiation from the absorber to the side walls of the collector.

The final heat rejection to the environment is by convection and radiation from the external surfaces of the collector. The effective sky temperature is assumed equal to the ambient temperature.

Details on the pertinent heat transfer equations and their application in the heat losses are given in Appendix A.

The assumption is made that the absorber plate has parallel flow tubes. The fluid is assumed to enter the flow tubes from a common supply header and empty into a common collection header.

Intimately connected with the absorber-fluid heat transfer is the question of the temperature drop in the absorber plate because the heat must flow laterally in the absorber to the flow tubes. This temperature drop results in a higher absorber temperature than would occur if the absorber were a perfect conductor, or were very thick. Since the collector cost depends upon the type and amount of material used in the absorber, there exists an optimization problem.

Investigators have treated the absorber-to-fluid tube conduction problem as that of a fin exchanging heat with its surroundings through a heat transfer coefficient constant over the fin surface. But since the largest heat flow quantity is the solar flux and since this flux is uniform over the fin surface, it appears that it is appropriate to treat the fin surface heat flow as uniform. This is the approach used in the present analysis. The actual condition lies between these two approaches, considering the conduction, radiation and natural convection loss terms to be proportional to the temperature difference between the absorber and its surroundings.

Analysis of the Flow Distribution in Solar Collector Arrays

A typical solar collector installation consists of many flat-plate collector modules assembled as an array. Collection fluid is supplied to the modules in some form of series-parallel network. The piping network must be designed to provide the proper flow to each module. Also, within a module, the goal is to provide uniform flow per unit area of the collector. In the usual case of uniformly spaced tubes running from a supply header to a collection header, it is desirable to provide, as nearly as possible, equal flow to each tube. Figure 4 illustrates the flow configuration described above. The problem of uniform flow within a module is addressed in the following paragraphs. Appendix B provides a more detailed description of the procedure used for the flow analysis.

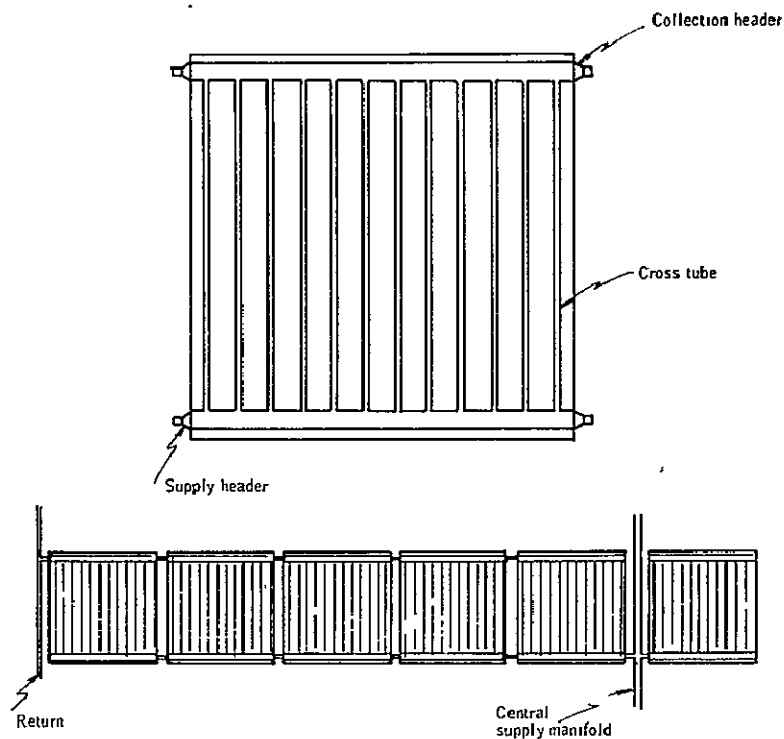


Figure 4. Schematic of Individual Collector and Potential Collector Array Configuration

The flow in a tube is determined by the difference in pressure between the supply header and the collection header at the tube ends. Header pressures will vary along their length from wall friction losses and momentum flux changes in the headers as fluid is withdrawn or added. The pressure in the supply manifold will fall in the flow direction owing to wall shear stress, but the drop will be reduced by pressure recovery at each cross tube because of extraction of fluid and subsequent loss of momentum in the supply header flow.

In the collection header the frictional drop is reinforced by the acceleration drop due to the increased momentum. The resulting pressure difference at the ends of a tube will therefore vary from one tube to the next and the flow rate will vary from tube to tube.

Pressure drop in the flow in a header between adjacent tubes depends upon the flow rate and the flow condition; e.g., laminar or turbulent, developing or fully developed. Because only a little of the header flow is extracted or added at each cross tube, the header flow is assumed to be fully developed at all locations. The flow is assumed to be laminar for Reynolds numbers below 2000 and turbulent above 2000. The above discussion applies equally well to the cross-tube pressure drop. However, the flow in a cross tube will almost always be laminar.

Based on the foregoing discussion, the flow distribution in the tubes was calculated. The analysis was programmed for solution on a digital computer (see Appendix B). Results were obtained for a row of 10 collectors as indicated in Figure 4. This number of collectors was chosen as typical; however, a complete array would consist of several rows. The analysis was concerned primarily with the distribution of flow in one row. The pressure drop in the supply and collection headers in the collectors can be reduced by a central supply manifold as indicated in Figure 4, with the flow passing both ways to the outer edge of the array.

The analysis thus may be carried out for a row of five collectors, each having 12 cross tubes, for a total of 60 tubes as shown in Figure 4. The supply and collection headers are on 107-cm (42-in.) centers and the cross tubes are 102 cm (40 in.) long on 9-cm (3.552-in.) centers. The headers are rectangular ducts, with 1.3-cm by 5-cm (0.5-in. by 2-in.) inside dimensions. The cross tubes are also rectangular in section. Their dimensions were varied and the flow distributions for the various sizes were analytically determined.

Figures 5 through 7 present the results of the flow distribution calculations for three possible cross-tube dimensions: 0.13-cm by 1.3-cm (0.050-in. by 0.50-in.), 0.25-cm by 1.3-cm (0.10-in. by 0.500-in.) and 0.5-cm by 1.3-cm (0.20-in. by 0.50-in.). The sensitivity of the flow distribution to the cross-tube dimensions is immediately evident. Referring to Figure 5 for the 0.13-cm by 1.3-cm (0.050-in. by 0.50-in.) tube, it is seen that the cross-tube pressure drop at a nominal flow of 49 kg/hr-m^2 (10 lbm/hr-ft^2) is about 6.4 cm (2.5 in.) of water. This is a relatively large pressure difference compared with the header pressure variation and, consequently, the cross-tube flow distribution is quite uniform.

As the cross-tube inner height is increased, the associated pressure drop falls rapidly and, as shown in Figure 6 for the 0.25-cm by 1.3-cm (0.10-in. by 0.50-in.) tubes, the header pressure variation causes a significant nonuniformity in the flow distribution. The distribution for the 0.5-cm by 1.3-cm (0.200-in. by 0.500-in.) tubes, Figure 7, is badly out of balance.

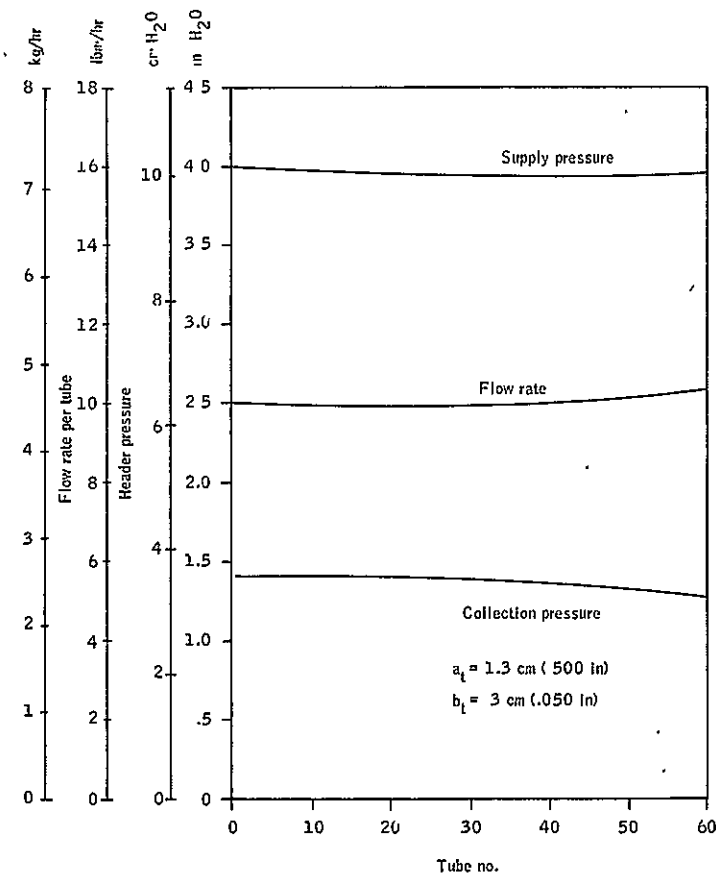


Figure 5. Flow Distribution for 0.13 cm x 1.3 cm (0.05 in. x 0.50 in.) Cross Tube

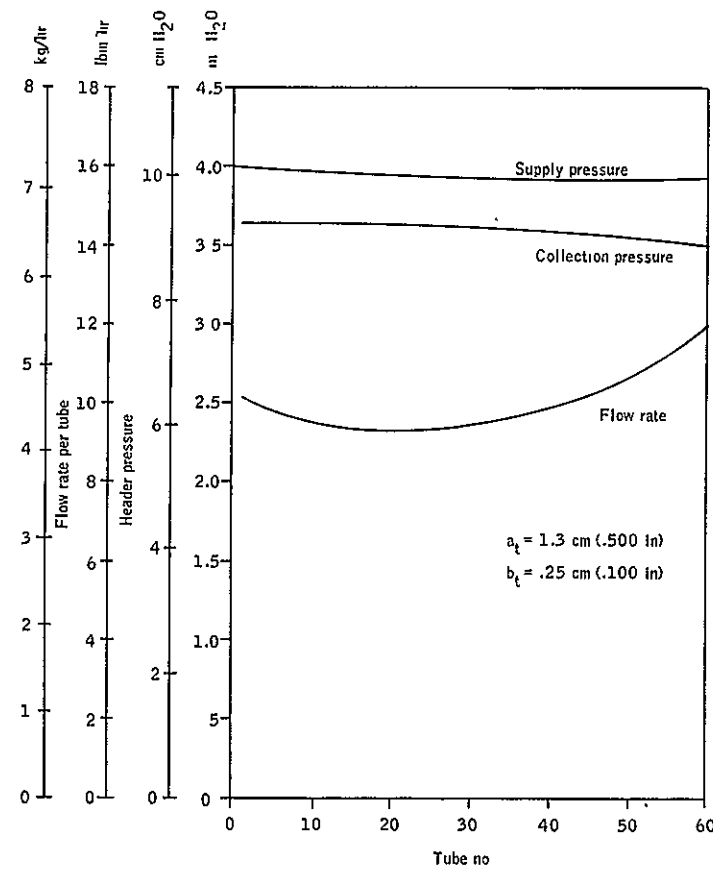


Figure 6. Flow Distribution for 0.25 cm x 1.3 cm (0.10 in. x 0.50 in.) Cross Tube

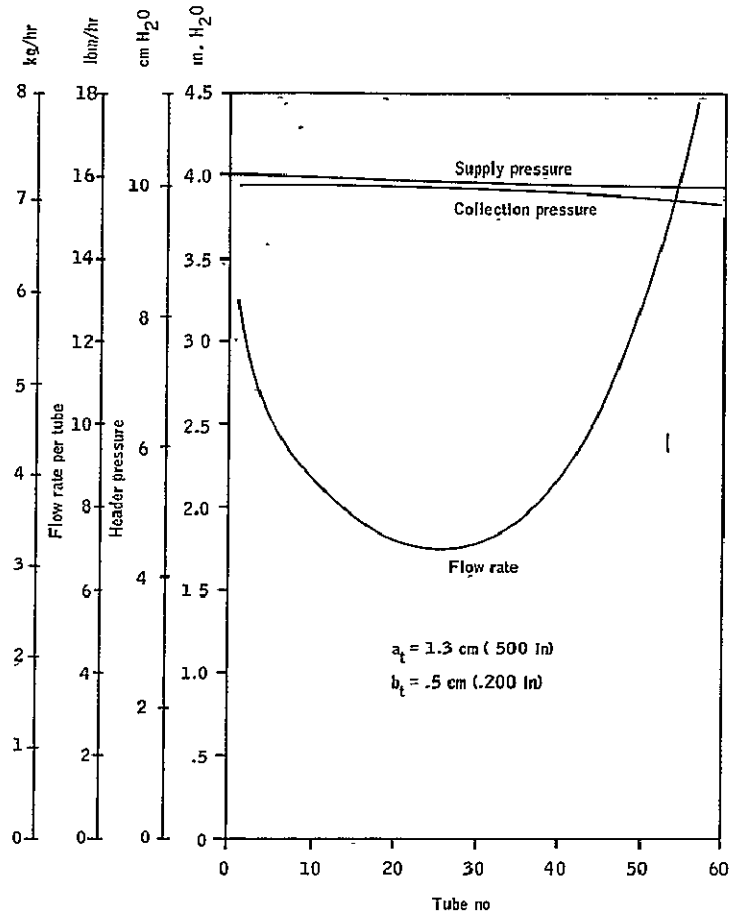


Figure 7. Flow Distribution for $0.5 \text{ cm} \times 1.3 \text{ cm}$ ($0.20 \text{ in.} \times 0.50 \text{ in.}$) Cross Tube

Increasing the cross-sectional dimensions of the headers results in less header pressure variation and more uniform flow. However, the mass of fluid and collector heat capacity increase as the header dimensions are increased. For 1.3-cm by 5-cm (0.5-in. by 2.0-in.) headers and 0.13-cm by 1.3-cm (0.050-in. by 0.50-in.) cross tubes, the fluid heat capacity is about 25 percent of the total collector heat capacity (assuming an aluminum panel), and 90 percent of the fluid is in the two headers.

It should be noted that if a nonuniform flow is present, the resulting variation in the fluid temperature (i.e., higher temperatures for tubes with less flow) will produce a variation in the hydrostatic pressure distribution which acts in a direction to reduce the nonuniformity. Since the hydrostatic pressure of a 102-cm (40-in.) column of a 50-percent mixture of ethylene glycol and water decreases 0.073 cm of water per °C (0.016 in. of water per °F), the temperature variation will significantly improve the flow distribution for the 0.5-cm by 1.3-cm (0.20-in. by 0.50-in.) tubes, but will give little improvement for the thinner tubes.

Other Considerations for Sizing the Flow Tubes

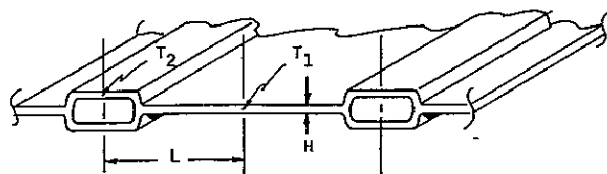
The choice of cross-tube dimensions and spacings cannot be made solely on the basis of flow uniformity. Two thermal considerations enter into the problem: One is the desirability of minimizing the lateral temperature gradient in the collector plate which is necessary to carry the absorbed heat to the cross tubes. The other consideration is to minimize the temperature difference between the surface of the cross tube and the collection fluid.

The collection and flow of heat laterally in the collector can be treated by one-dimensional heat conduction methods because the collector plate thickness is much less than the tube spacing. One approach to analyzing this part of the collector thermal design is to employ the well-known formulae for a fin exchanging heat via a uniform loss coefficient and to use the usual hyperbolic relations. However, the largest term in the energy collection and loss process is the solar input, which represents a uniform heat flux boundary condition. Furthermore, part of the heat loss is by radiation, a fourth-power term. It therefore appears that neither the uniform heat transfer coefficient condition, nor the uniform heat flux condition, is totally correct. However, since the solar input is the largest term, the uniform flux condition approximates most closely the existing condition and was therefore used.

Under this assumption, it can be demonstrated that the temperature difference ($T_1 - T_2$) between a location midway between two tubes and the tube centerline is given by:

$$T_1 - T_2 = \frac{qL^2}{2kH} \quad (4)$$

where



k = thermal conductivity of the plate

q = net heat flux into the plate per unit area

The baseline collector design used a Roll-Bond aluminum panel with 12 cross tubes. This configuration had the following parameters:

- $L = 4.5 \text{ cm (1.78 in.)}$
- $H = 0.15 \text{ cm (0.060 in.)}$
- $k = 173 \text{ w/m} \cdot ^\circ\text{C (100 Btu/hr-ft-}^\circ\text{F)}$

Assuming a 50-percent efficient collector and a maximum solar flux of 1100 w/m^2 (350 Btu/hr-ft^2), from the equation above, $q \leq 550 \text{ w/m}^2$ (175 Btu/hr-ft^2) and $T_1 - T_2 \leq 2.1^\circ\text{C (3.8}^\circ\text{F)}$. This temperature differential is considered to be acceptable.

The temperature difference between a cross tube and the collection fluid was calculated from established relations for laminar flow in rectangular ducts. The flow will be laminar since the Reynolds number is 170 for typical flow of 49 kg/hr-m^2 (10 lbm/hr-ft^2) of 50 percent ethylene glycol-water solution in $0.13 \text{ cm by } 1.3 \text{ cm (0.050 in.} \times 0.500 \text{ in.)}$ tubes spaced 9 cm (3.5 in.) apart.

Most of the tube length was assumed to be in the fully developed flow and temperature regime. This occurs for:

$$\frac{x}{D_t} \frac{1}{Re Pr} > 10^{-2} \quad (5)$$

where

D_t = hydraulic diameter of the tube

Pr = Prandtl number

Re = Reynolds number

x = entrance length

For the conditions listed above, the entrance length is approximately 3.6 cm (1.4 in.). This is less than 5 percent of the total cross-tube length. Hence, it may be assumed that the fully developed relations can be used over the entire tube length.

The heat transfer coefficient for fully developed flow and temperature fields in rectangular ducts is presented in Ref. (4) as a function of the duct aspect ratio (ratio of side dimensions). From this information the curves on Figure 8 were computed for water and a 50 percent ethylene-glycol-water mixture. The tube-to-fluid temperature difference for the 0.13 cm by 1.3 cm (0.050 in. by 0.500 in.) duct is about 1.9°C (3.5°F) for the ethylene-glycol-water mixture. It can be seen that this value rises sharply as the duct thickness is increased, reaching a value of 7.2°C (13°F) for the 0.51 cm by 1.3 cm (0.200 in. by 0.500 in.) duct.

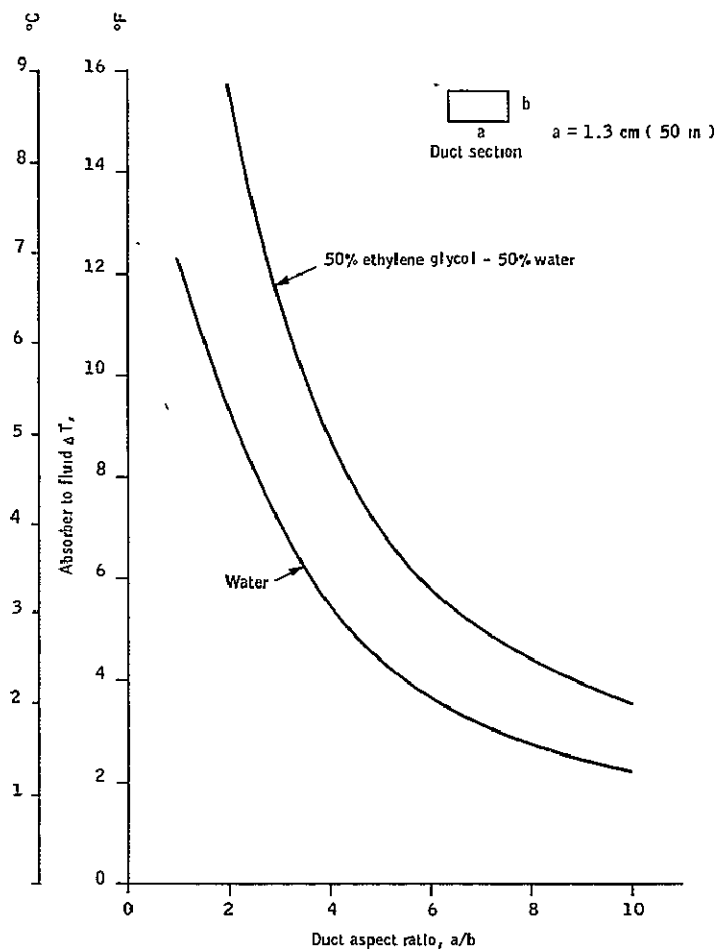


Figure 8. ΔT from Absorber Tube to Fluid

Baseline Tube Size and Spacing

Based on the results of the flow distribution analysis and the thermal consideration described above, it was decided to design the baseline collector with 1.3 cm by 5 cm (0.5 in. by 2 in.) headers and 0.13 by 1.3 cm (0.05 in. by 0.50 in.) cross tubes.

BASELINE COLLECTOR DESIGN

The design selected for the baseline collector is shown in Figure 9. It contains an aluminum absorber panel coated with an optically selective Black Nickel coating. The heat transfer fluid is a 50 percent (by volume) mixture of ethylene-glycol and water. The absorber panel has 5 cm (2 in.) of foil-coated, semi-rigid fiberglass insulation around its edges and 7.6 cm (3 in.) of the same insulation on the bottom side of the absorber. A sheet steel housing surrounds the absorber panel and its insulation. The absorber panel is supported and located by use of four, linen-filled bakelite standoffs that fasten to the housing on one end, pass through the bottom side insulation and fasten to the absorber panel on the other end.

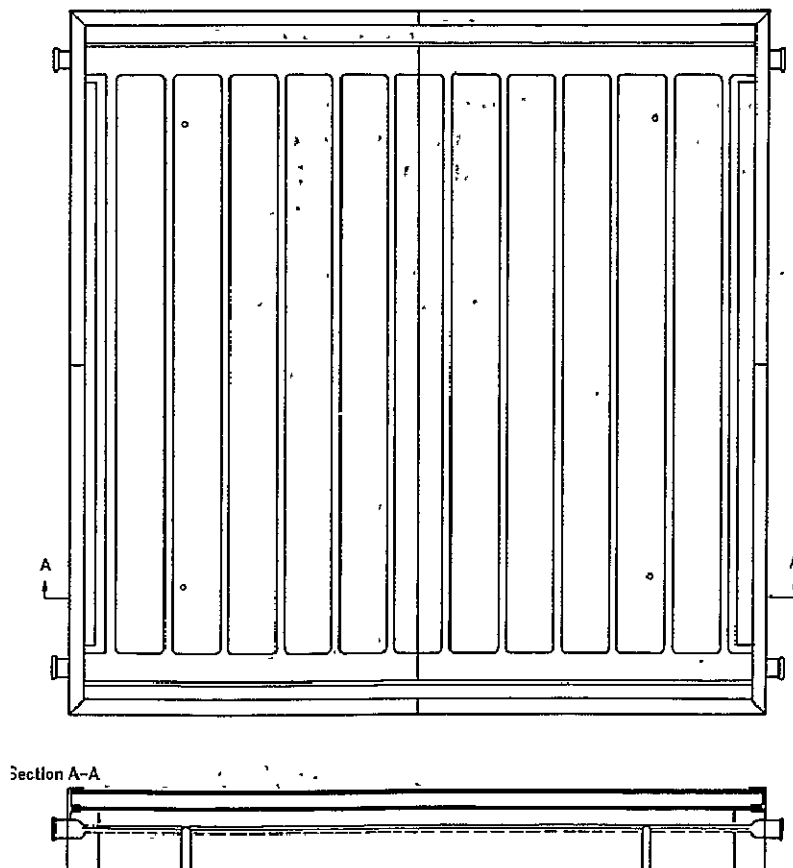


Figure 9. Solar Collector Assembly

The sheet steel housing also supports the collector cover system. The cover system itself is composed of two sheets of low-iron glass on either side of a "u" shaped 2.5 cm (1 in.) steel spacer. The lower sheet of glass is supported by a lip around the edge of the sheet steel housing that suspends the glass approximately 3.2 cm (1.25 in.) above the installed absorber panel. All surfaces that would have glass-metal contact are protected by 0.3-cm. (0.125 in.) thick Butyl rubber weatherstripping. An aluminum cap strip is fastened over the installed cover system and then fastened to the sheet steel housing. Finally, heavy rubber gaskets are bolted around the absorber panel outlet tubes so that there is not a thermal short where the absorber outlet tubes pass through the sheet steel housing.

Details of the component design and specific considerations made in the material choices are presented in the following subsections.

The Absorber Panel

The basic requirement for an absorber panel design is that it consists of a plate which absorbs incident solar energy and that it contains flow passages through which the absorbed heat flux may be transferred to the collector working fluid. There are two basic configurations which meet this requirement: a plate with attached flow tubes, or a multilayer panel with internal flow passages.

The plate with attached tube design provides good mechanical integrity, has little chance of fluid leakage, and can withstand high fluid pressure. However, this type of construction is typically costly. Even the relatively simple flow pattern of a common header with parallel flow tubes is expensive in that it requires many connections, both between header and flow tube and also between plate and tubing. Furthermore, it is difficult to make a good thermal connection between tubing and plate.

The integral flow passage design has been successfully commercialized by Olin Brass as their Roll-Bond aluminum panel. This panel is formed by hot rolling two thin sheets of aluminum. The combination of heat and pressure diffusion bonds the sheets everywhere except for the predetermined flow passages. In these areas, bonding is prevented by printing or silk screening the flow passage pattern on one aluminum sheet with an inhibiting paint. The final step in the process is to hydraulically expand the unbonded flow passage pattern. The advantages of this product are twofold: it provides good thermal joints, and even complex flow passage configurations can be provided without significantly increasing fabrication cost.

The aluminum roll-bond panel was selected as the baseline absorber panel because of its manufacturing potential, high thermal conductivity, and light weight; however, there were reservations regarding aluminum's corrosion resistance. To reduce potential corrosion problems, Olin Brass

recommended that the panels be manufactured from either standard aluminum (1100) or from an aluminum-manganese alloy (3003). The 3003 was preferred because it is easier to weld and has superior mechanical strength; however, the 1100 alloy was used because of better availability. An inquiry was made regarding the use of a clad aluminum (7072 over 1100), which is generally regarded as being more corrosion resistant. However, it appears that when used with high-temperature water ($\sim 100^{\circ}\text{C}$), there is a strong possibility that the 7072 cladding on either 1100 or 3003 will reverse its polarity with reference to the base aluminum. Consequently, instead of inhibiting pitting, the cladding would then tend to promote corrosion.

To reduce internal corrosion, it is necessary to use deionized water mixed with ethylene-glycol and also to add 500 ppm of sodium chromate as a corrosion inhibitor. As a further precaution, it is recommended that a combination filter/getter column be installed at the collector array inlet. This component consists of a plastic or glass tube filled with aluminum turnings and screen. Particles in the collector working fluid are thus filtered, and heavy metal ions are sacrificially consumed in a getter column before they reach the absorber panels. To minimize the contamination of the collector system by heavy metals, special care must be taken in selecting materials for the other system components, such as pumps, storage tank, plumbing, etc.

In general, we have serious reservations about the long-term durability of the aluminum absorber panels when considered for the desired 20-year operating life of a solar collection system. One of the design modifications performed as part of this program was to design and manufacture a mild steel absorber panel of similar configuration to the baseline aluminum roll-bond panel. This design consists of two steel sheets spot and seam welded together.

The mechanical configuration of the roll-bonded aluminum absorber panel used in the baseline design is shown in Figure 10. The nominal material thickness is 0.15 cm (0.060 in.). Supply and collection headers are roughly rectangular and of dimensions 5.08 x 1.27 x 111.76 cm (2.00 x 0.500 x 44 in.). The supply and collection headers are joined by an array of rectangular cross tubes 1.27 x 0.127 cm (0.500 x 0.050 in.). The cross tubes are approximately 96.5 cm (38 in.) long and are spaced on 9.78 cm (3.85 in.) centers. The supply and collection headers have 3.175 cm (1.25 in.) diameter aluminum outlet connections heli-arc welded on each end. The connectors are approximately 7.62 cm (3 in.) long.

Each 112 x 112 cm (44 x 44 in.) absorber panel is made by shearing two standard 61 x 122 cm (24 x 48 in.) roll-bond panels down to 46 x 112 cm (22 x 44 in.) each. The two sheared panels are connected by heli-arc welding the sheared header edges together.

The sheet steel housing also supports the collector cover system. The cover system itself is composed of two sheets of low-iron glass on either side of a "u" shaped 2.5 cm (1 in.) steel spacer. The lower sheet of glass is supported by a lip around the edge of the sheet steel housing that suspends the glass approximately 3.2 cm (1.25 in.) above the installed absorber panel. All surfaces that would have glass-metal contact are protected by 0.3-cm (0.125 in.) thick Butyl rubber weatherstripping. An aluminum cap strip is fastened over the installed cover system and then fastened to the sheet steel housing. Finally, heavy rubber gaskets are bolted around the absorber panel outlet tubes so that there is not a thermal short where the absorber outlet tubes pass through the sheet steel housing.

Details of the component design and specific considerations made in the material choices are presented in the following subsections.

The Absorber Panel

The basic requirement for an absorber panel design is that it consists of a plate which absorbs incident solar energy and that it contains flow passages through which the absorbed heat flux may be transferred to the collector working fluid. There are two basic configurations which meet this requirement: a plate with attached flow tubes, or a multilayer panel with internal flow passages.

The plate with attached tube design provides good mechanical integrity, has little chance of fluid leakage, and can withstand high fluid pressure. However, this type of construction is typically costly. Even the relatively simple flow pattern of a common header with parallel flow tubes is expensive in that it requires many connections, both between header and flow tube and also between plate and tubing. Furthermore, it is difficult to make a good thermal connection between tubing and plate.

The integral flow passage design has been successfully commercialized by Olin Brass as their Roll-Bond aluminum panel. This panel is formed by hot rolling two thin sheets of aluminum. The combination of heat and pressure diffusion bonds the sheets everywhere, except for the predetermined flow passages. In these areas, bonding is prevented by printing or silk screening the flow passage pattern on one aluminum sheet with an inhibiting paint. The final step in the process is to hydraulically expand the unbonded flow passage pattern. The advantages of this product are twofold: it provides good thermal joints, and even complex flow passage configurations can be provided without significantly increasing fabrication cost.

The aluminum roll-bond panel was selected as the baseline absorber panel because of its manufacturing potential, high thermal conductivity, and light weight; however, there were reservations regarding aluminum's corrosion resistance. To reduce potential corrosion problems, Olin Brass

recommended that the panels be manufactured from either standard aluminum (1100) or from an aluminum-manganese alloy (3003). The 3003 was preferred because it is easier to weld and has superior mechanical strength; however, the 1100 alloy was used because of better availability. An inquiry was made regarding the use of a clad aluminum (7072 over 1100), which is generally regarded as being more corrosion resistant. However, it appears that when used with high-temperature water ($\sim 100^{\circ}\text{C}$), there is a strong possibility that the 7072 cladding on either 1100 or 3003 will reverse its polarity with reference to the base aluminum. Consequently, instead of inhibiting pitting, the cladding would then tend to promote corrosion.

To reduce internal corrosion, it is necessary to use deionized water mixed with ethylene-glycol and also to add 500 ppm of sodium chromate as a corrosion inhibitor. As a further precaution, it is recommended that a combination filter/getter column be installed at the collector array inlet. This component consists of a plastic or glass tube filled with aluminum turnings and screen. Particles in the collector working fluid are thus filtered, and heavy metal ions are sacrificially consumed in a getter column before they reach the absorber panels. To minimize the contamination of the collector system by heavy metals, special care must be taken in selecting materials for the other system components, such as pumps, storage tank, plumbing, etc.

In general, we have serious reservations about the long-term durability of the aluminum absorber panels when considered for the desired 20-year operating life of a solar collection system. One of the design modifications performed as part of this program was to design and manufacture a mild steel absorber panel of similar configuration to the baseline aluminum roll-bond panel. This design consists of two steel sheets spot and seam welded together.

The mechanical configuration of the roll-bonded aluminum absorber panel used in the baseline design is shown in Figure 10. The nominal material thickness is 0.15 cm (0.060 in.). Supply and collection headers are roughly rectangular and of dimensions 5.08 x 1.27 x 111.76 cm (2.00 x 0.500 x 44 in.). The supply and collection headers are joined by an array of rectangular cross tubes 1.27 x 0.127 cm (0.500 x 0.050 in.). The cross tubes are approximately 96.5 cm (38 in.) long and are spaced on 9.78 cm (3.85 in.) centers. The supply and collection headers have 3.175 cm (1.25 in.) diameter aluminum outlet connections heli-arc welded on each end. The connectors are approximately 7.62 cm (3 in.) long.

Each 112 x 112 cm (44 x 44 in.) absorber panel is made by shearing two standard 61 x 122 cm (24 x 48 in.) roll-bond panels down to 46 x 112 cm (22 x 44 in.) each. The two sheared panels are connected by heli-arc welding the sheared header edges together.

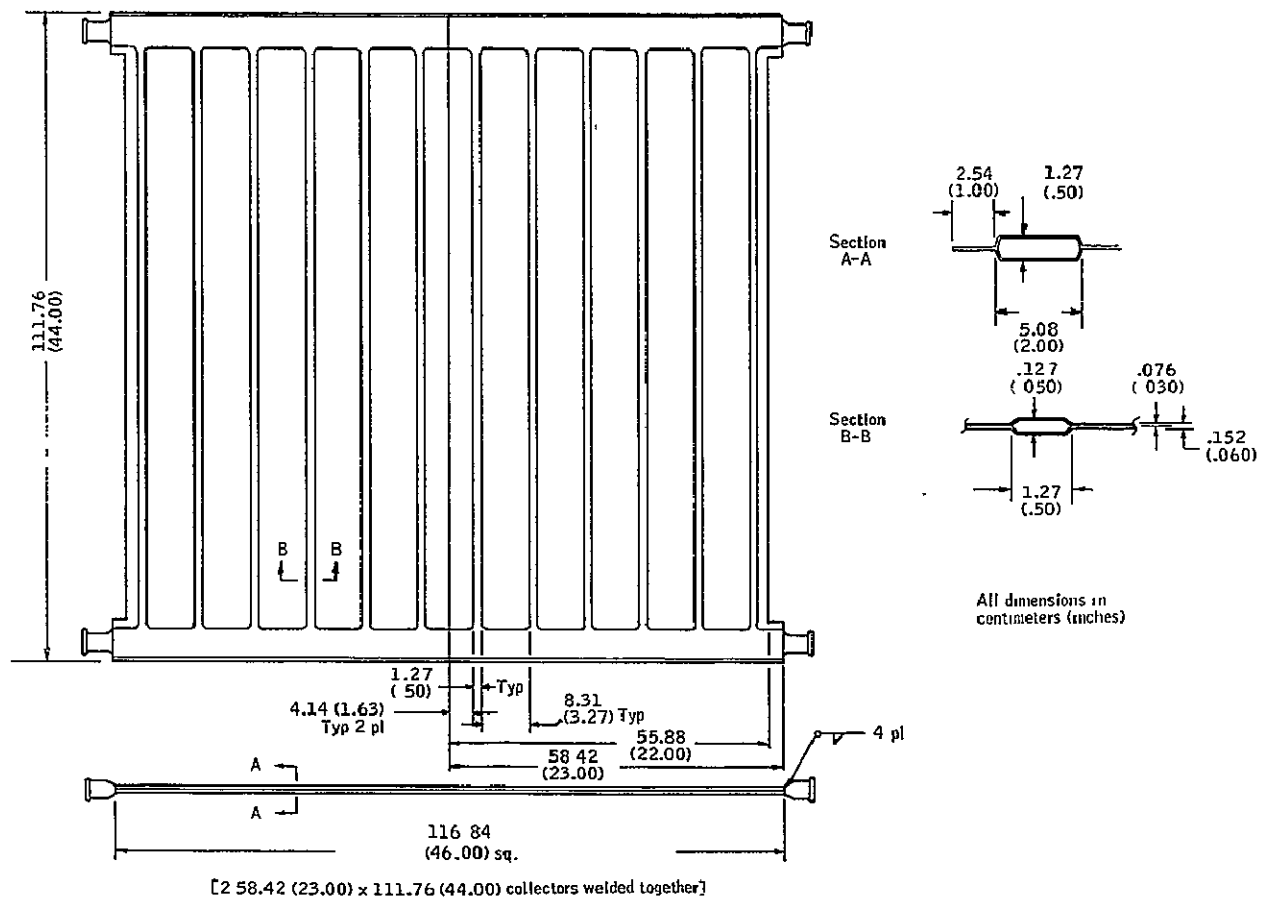


Figure 10. Solar Absorber Panel

The Solar Absorber Coating

The net amount of solar energy absorption depends on the optical surface properties of the absorber panel. Solar absorptance values up to 95 percent can be achieved by simply blackening the absorber panel by painting, oxidizing, or anodizing; however, these surfaces also tend to have equally high emittance levels in the infrared, the wavelength region where energy is emitted from the plate.

An improved type of surface preparation is the selective black solar absorber coating. This surface has a relatively high solar absorptance and a low infrared emittance. Most of the practical selective black surfaces are produced by taking a polished metal base with its intrinsic low emittance, and coating it with a very thin surface layer which is optically dark in the short wavelengths in which most of the incident solar energy is contained. By making the layer quite thin it is essentially transparent for wavelengths

longer than 2-3 microns and the low natural emittance of the base metal is essentially undisturbed by the superimposed layer. Some typical selective coatings include: dielectric interference layers on aluminum; iron oxide on steel; copper oxide on aluminum; copper oxide on copper; and a nickel-zinc-sulfide complex, known as Black Nickel, on nickel.

Black Nickel was selected as the absorber coating for the baseline collector configuration because of its high performance and projected low cost. During the course of this program, the Black Nickel electroplating process was sufficiently refined to repetitively produce absorber panels with a solar absorptance, α , of 0.94 and an emissivity, ϵ , of 0.06. The coating on the absorber panel used for the baseline collector test program had an α of 0.955 and an ϵ of 0.07. Its performance curve, reflectance as a function of incident flux wavelength, is presented as Figure 11. This significant improvement in performance was achieved by exploiting a unique property of the Black Nickel complex. If the current density is changed during the Black Nickel deposition, the composition and refractive index of the deposited nickel-zinc-sulfide complex can be changed. This makes two layer coatings possible, thereby increasing optical flexibility. A selective Black Nickel coating developed by NASA Marshall Space Flight Center, Huntsville, Alabama, routinely produces an α of 0.90 and an ϵ of 0.06. The NASA-MSFC process does not use the two-layer coating.

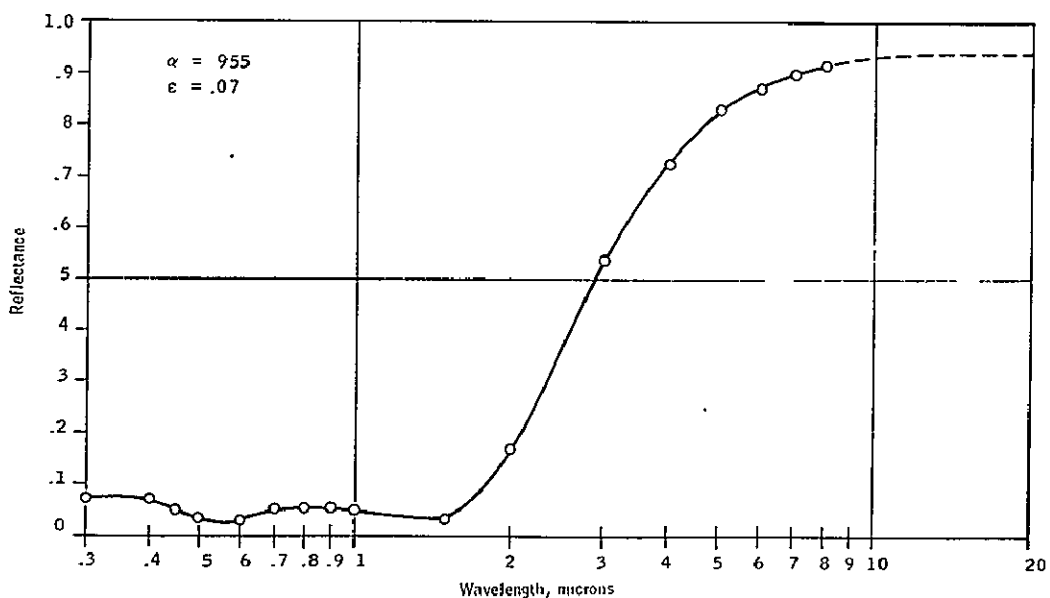


Figure 11. Performance Curve for Selective Black Nickel Coating from Baseline Collector

The process used for electroplating the Black Nickel coating is discussed in Appendix E.

Coating lifetime and durability are still areas of concern and have not yet been well evaluated. The coating has been found to degrade on exposure to 274°C (525°F); however, exposure at 204°C (400°F) does not cause degradation. Humidity degradation has also been examined. Figure 12 shows three samples coated with Black Nickel. The sample on the left is as deposited. The center sample was soaked in distilled water for 10 days. Except for a residue that could be wiped off, the coating was unaffected. The sample on the right was subjected to MIL-STD-810B, Procedure I humidity testing; 10 days of 24-hour cycles from 28°C (82°F) to 71°C (160°F) with 85 to 95 percent relative humidity. The combination of heat and humidity completely degraded the coating. Although this test is more severe than might be expected in normal collector operation, coating durability is still considered an area requiring further investigation. One of the design modifications examined as part of this program was the performance of a different selective absorber coating known as Black Chrome. This is a commercially available electroplating process presently used for decorative applications; however, when applied properly and in thin enough depositions, it becomes selective. Black Chrome may be more durable than an equivalent Black Nickel coating.



Figure 12. Humidity Degradation of Black Nickel,
Bright Nickel Coatings on Aluminum

ORIGINAL PAGE IS
OF POOR QUALITY

Heat Transfer Fluid

The heat transfer fluid required for use in a solar collector can range from water to various oils; however, to be suitable for general purpose use, the fluid should exhibit the following properties:

- 1) Low viscosity over the range of ambient temperatures encountered
- 2) Noncorrosive (with inhibitors, if necessary)
- 3) Chemically stable over 15-20 year life
- 4) Good heat transfer properties
- 5) High heat capacity
- 6) Low freezing point if low ambient temperatures are anticipated

It should also be readily available at a reasonable price.

There are several fluids that can meet most or all of these requirements, but an ethylene-glycol-based "antifreeze" appears to be best suited for the application. The heat transfer fluid selected for use in the baseline collector testing and also in the test program for the alternate design configurations was Dowtherm SR-1, produced by the Dow Chemical Company. Mixed with water in a 50-50 ratio by volume, SR-1 yields a fluid capable of providing efficient heat transfer over a temperature range of -40°C (-40°F) to 149°C (300°F).

Insulation

The thermal analysis revealed that conduction losses from the absorber panel to the collection housing would be a significant constraint on collector efficiency if not adequately controlled. To reduce these conduction losses, the baseline design incorporates 7.5 cm (3 in.) of insulation on the underside of the absorber panel, and 5 cm (2 in.) of insulation between the edges of the absorber panel and the walls of the collector housing. Furthermore, the mechanical connection between the absorber panel and the collector housing is accomplished via four bakelite standoffs 7.5 cm (3 in.) in length and 1.9 cm (0.75 in.) in diameter. Machine screws fasten the respective ends to the standoff to the collector housing and to the absorber panel, leaving 5 cm (2 in.) of solid bakelite for the heat flow path. Figure 13 shows the standoff in detail.

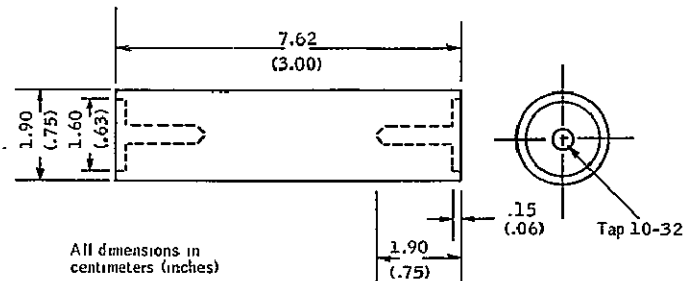


Figure 13. Standoff Support

The most cost-effective insulation available today is fiberglass, which is produced in a variety of densities and corresponding thermal conductance values, and a variety of binder conditions. Table 1 lists three fiberglass product types which vary in binder content. Regular building fiberglass insulation, such as Owens-Corning PF-3340, has a bakelite binder which limits its upper use temperature to 121°C (250°F). When heated above 121°C (250°F) the binder burns, giving off both odor and fumes. If the fumes are not objectionable and do not fog the cover, the material can be used to 371°C (700°F). The insulating value is not degraded at these higher temperatures, provided the material is not compressed. Vibration or mechanical compression will tend to compress the glass fibers, thereby reducing insulating value. Fiberglass insulation with little or no binders is made specifically for higher temperature applications. One such product is Certainteed Products No. 850 fiberglass board, which is semi-rigid and can be used to temperatures of 454°C (850°F). This figure is well above the predicted maximum collector temperature of 232°C (450°F), which could occur with no heat removal (i.e., no fluid flow through the collector).

Loose fill, such as Conwed Mineral Wool, is inexpensive and is capable of withstanding temperatures up to 649°C (1200°F); however, loose fill insulation tends to settle, particularly in the presence of moisture, and therefore loses its insulating qualities.

The common plastic foams, styrofoam and urethanes, are good insulators but cannot withstand the collector zero-flow temperatures. High temperature foam insulation, such as Pittsburg Corning Foamglas, is available but is quite costly. Table 2 presents data for some nonfiberglass insulations.

TABLE 1. - FIBERGLASS INSULATION

Insulation type	Upper use temperature, °C (°F)	K at 93°C (200°F), W/m-°C (Btu/ft²-°F-hr/in.)	\$/m²** at 2.5 cm thick (\$/ft² at 1 in. thick)
Regular building insulation (e.g., Owens-Corning PF-3340)	121 (250)	.0414 (.287)	.462 (.043)
Industrial fiberglass board (e.g., CertainTeed Products No. 850)	454 (850)	.0432 (.28)	.926 (.086)
Loose fill (e.g., Conwed Mineral Wool)	649 (1200)	.0461 (.32)	.161 (.015)

TABLE 2. - NONFIBERGLASS INSULATION

Insulation type	Upper use temperature, °C (°F)	K at 24°C (75°F), W/m-°C (Btu/ft²-°F-hr/in.)	\$/m²** at 2.5 cm thick (\$/ft² at 1 in. thick)
Closed cell urethane (e.g., Owens-Corning)	107 (225)	.0216 (.15)*	2.42 (.225)
Foam glass (e.g., Pittsburgh-Corning)	493 (919)	.0548 (.38)	2.37 (.22)

*Freon diffuses out and air diffuses in, causing increase in conductivity within 1 year.

**Cost figures are for 9290 m² (100,000 ft²) or carload quantities and are March 1975 prices.

The insulation selected for the baseline collector was Johns-Manville 814. It is a semi-rigid fiberglass board capable of continuous operation at 177°C (350°F) and brief exposures to 232°C (450°F). Its thermal conductivity is 0.042 w/m·°C, (0.29 Btu/ft²·hr·°F/in.), and it costs \$1.21/m² (\$0.112/ft²) for 2.5 cm (1 in.) thickness. This insulation represented a reasonable compromise between cost, performance, and physical properties.

To substantiate the importance of good insulation between the absorber panel and the collector housing, an experiment was performed to examine and evaluate the heat losses due to mechanical support of the absorber panel and to edge conduction losses from the absorber panel to the collector housing. The heat loss experiment consisted of operating a collector with no incident flux and measuring the temperature drop of the heat transfer fluid as it passed through the collector. This test was iterated several times with modifications to the collector design which provided greater insulation between the absorber panel and the collector housing.

A detailed description of the heat loss experiment and its results is presented in the following paragraphs.

Isolation and measurement of the heat loss components was accomplished by a series of indoor test runs utilizing the test arrangement shown in Figure 14. Ambient temperature was held at approximately 19°C (66°F) and there was zero wind velocity. Fluid inlet temperature was maintained at approximately 93°C (200°F) by the series connection of a 189.25 L (50-gallon) commercial hot water heater and an Isotemp constant temperature bath. A uniform mass flow rate was achieved by pumping from the fluid reservoir to an overhead secondary reservoir, utilized as a gravity feed head tank of adjustable height. All test configurations of the collector used a single glass cover, and the complete unit was inclined at 40° from horizontal. The inlet and outlet temperatures were measured with platinum resistance sensors. Flow rate was measured by both a flowmeter and by a stopwatch and graduated cylinder.

Heat loss was defined as:

$$q_{\text{loss}} = \dot{m} (h_{\text{in}} - h_{\text{out}}) \quad (6)$$

where

q_{loss} heat loss per unit absorber area per hour

\dot{m} = mass flow rate per unit absorber area

$h_{\text{in}} - h_{\text{out}}$ = enthalpy difference of the fluid (water) at the inlet and outlet temperatures

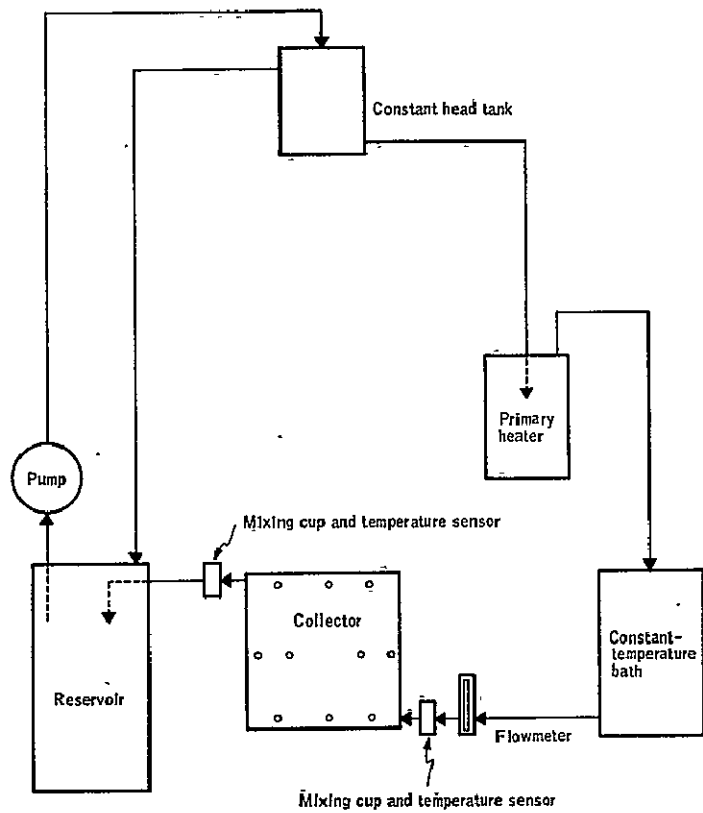


Figure 14. Heat Loss Test Arrangement

The mass flow rate was calculated at the average fluid temperature, and the enthalpy values were obtained from "Thermodynamic Properties of Steam" by Keenan and Keyes. (These tests were performed using water and not the ethylene-glycol-water mixture.)

The heat loss was measured first on an initial test design configuration and then on modified versions of that design. The initial design was defined as a sheet metal box 122 x 122 x 15 cm (48 x 48 x 6 in.) with cross braces six wall supports for a 117 x 117 cm (46 x 46 in.) absorber panel, and 7.5 cm (3 in.) of soft fiberglass insulation beneath the panel (refer to Figure 15).

The series of modifications was as follows:

- 1) The absorber panel was trimmed to 112 x 112 cm (44 x 44 in.) and 5 cm (2 in.) of semi-rigid fiberglass insulation were placed around the walls of the box (Figure 16).
- 2) The cross bracing from the bottom of the box was removed (Figure 17), and the type and thickness of insulation beneath the absorber panel was varied.
- 3) The six mechanical supports from the walls of the box were removed and replaced with bakelite standoffs to support the absorber panel. The insulation type and thickness were varied (Figure 18).

The results of the heat loss experiment are shown in Table 3. It is seen that in going from the initial design to the first modifications, i.e., making the absorber panel smaller and adding insulation to the edges, the heat loss per unit absorber area dropped by six percent.

TABLE 3. - SUMMARY OF HEAT LOSS RESULTS

Configuration	Heat loss/absorber area	
	W/m ²	(Btu/hr-ft ²)
Initial configuration	410.2	130
Modification 1	384.9	122
Modification 2		
With soft insulation	386.8	122.6
With semi-rigid insulation	379.5	120.3
Modification 3		
With soft insulation	367.9	116.6
With semi-rigid insulation	347.4	110.1

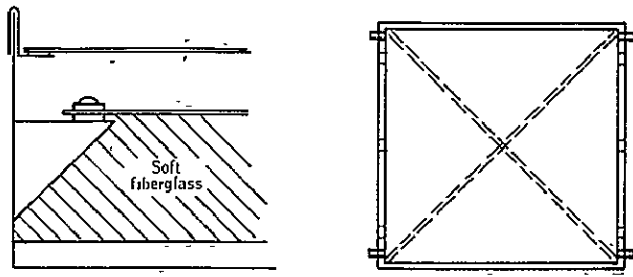


Figure 15. Initial Collector Configuration
for Heat Loss Test

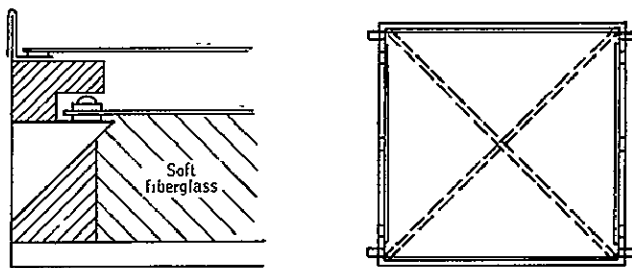


Figure 16. Mod. 1. Improved Edge
Insulation

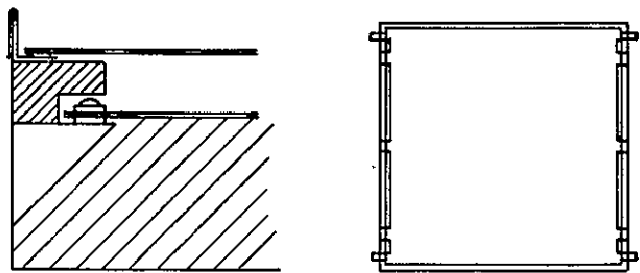


Figure 17. Mod. 2. Removal of Cross
Braces and Variation of
Insulation

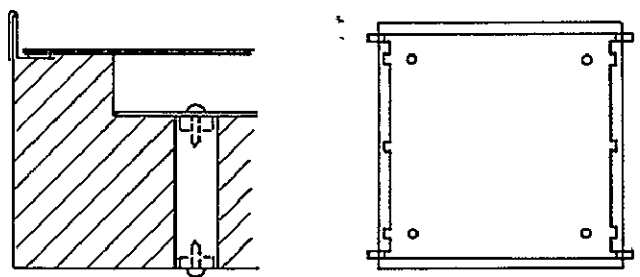


Figure 18. Mod. 3. Revised Mechanical
Supports

Removal of the cross bracing in the collector box produced a negligible change in performance, whereas changing the absorber plate support design significantly reduced the heat loss. A noticeable improvement was also achieved by using the semi-rigid type of fiberglass insulation. The overall improvement in heat loss going from the initial test design configuration to modification three with semi-rigid fiberglass insulation was 15.3 percent. All three modifications were therefore adopted for the program's baseline collector design configuration. A detailed section of this collector is presented as Figure 19.

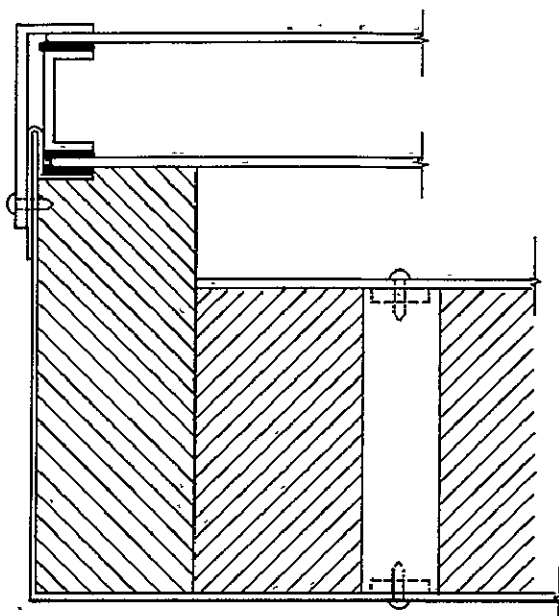


Figure 19. Baseline Configuration
Resulting from Heat
Loss Experiment

Collector Cover System

The thermal analysis program predicted that heat losses through the collector cover would be a significant constraint to achieving a high-efficiency collector design; however, two sets of design considerations could be employed to reduce the amount of reradiation losses through the cover.

The initial consideration was to utilize a selective absorber coating to reduce the amount of energy reradiated from the absorber panel. The baseline collector design includes a selective Black Nickel absorber panel coating. A detailed explanation of the coating and further rationale for its selection have already been discussed in the section entitled "Absorber Panel Coating."

The second set of design considerations was in the design of the cover system itself. The analysis program predicted that collector performance could be improved appreciably by adding a second cover to the collector. This performance increase resulted regardless of whether the absorber coating was selective or nonselective, although the impact of the second cover was greater when a nonselective absorber coating was specified. This improvement in collector performance could be negated, however, if the reduction in incident flux level due to the transmission loss through a second cover layer became significant when compared to the level of energy reradiated from the absorber panel. This condition will occur for a selectively coated absorber panel if the desired mode of collector operation is to run slightly above ambient; for example, providing solar-heated water at 38°C (100°F) with a 21°C (70°F) ambient and fairly high incident flux levels.

Recognizing that the more important applications of a solar collection system require operation well above ambient, e.g., 67°C (120°F), as would be necessary for air conditioning, the baseline collector design configuration was determined to include two covers.

The choice of materials used for the two covers may be varied for each cover. The outer cover must provide structural strength, transmit a maximum amount of the incident solar energy, and limit reradiation and convection losses. It should not be subject to degradation due to ultraviolet radiation; in fact, it is desirable that it be at least partially opaque to the ultraviolet component. The inner cover should also transmit as much of the incident radiation as possible while limiting convection and reradiation losses. However, it needs only enough structural strength to be self-supporting, and if the outer cover serves as an ultraviolet filter, the inner cover need not be highly resistant to ultraviolet degradation.

Candidate materials for the cover layers include various commercially available glasses; glass substitutes such as Lucite, Kel-F, and Lexan; and plastic films such as Tedlar, Mylar and polyethylene. Each of these materials is readily available and obtainable over a range of costs.

The spectral transmission characteristics of common glass are shown in Figure 20. Included in the same figure is the spectral transmission characteristics of less common low-iron glass. The low-iron glass has the more desirable higher solar transmission. Both common and low-iron glass are reasonably opaque to infrared, thereby absorbing the long wave reradiation emitted from the absorber panel. They are also resistant to ultraviolet radiation. In addition, both glasses are structurally strong; not only self-supporting, but able to carry wind, rain and snow loads. These glasses are also more abrasion resistant than plastics.

The spectral transmission characteristics of two plexiglass products, Lucite and Kel-F, are shown in Figure 21. The Lucite has a particularly high transmission in the solar wavelength region; however, plexiglass is not

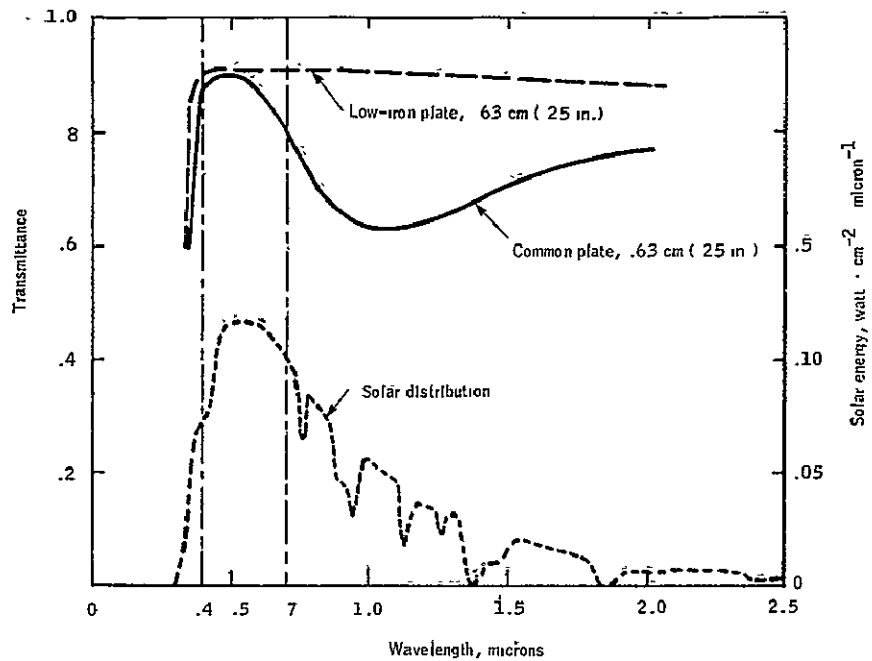


Figure 20. Spectral Transmission of Common and Low-Iron Glass

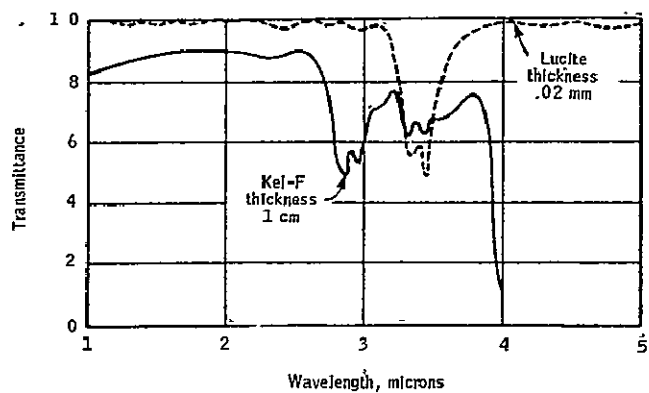


Figure 21. Solar Transmission Spectra of Two Plexiglass Products

very opaque in the infrared region, as is shown in Figure 22. This lack of infrared absorption effectively cancels the transmission advantage of plexiglass. Its physical softness reduces its desirability for use as an outer cover; however, it is self-supporting and may therefore serve as an inner cover. Care must still be used, even if it is selected as an inner cover, for when heated to 72°C (162°F) it may distort.

The plastic films are potentially attractive candidates because of their low cost. Dupont Tedlar is quite transmissive in the solar region; however, it is not particularly opaque in the infrared. The transmission spectra of Tedlar is given in Figure 23. The material is reasonably durable with regard to ultraviolet exposure; however, if it is used as an inner cover, ultraviolet durability may not be required. If Tedlar is used it must be mounted in a frame or other supportive device, thus reducing its cost effectiveness.

Other films such as polyethylene can be considered for the inner cover. The transmission of polyethylene is shown in Figure 24. Solar transmission is again good, but long wavelength opacity is poor. This film would also require a support device, such as a wire mesh or frame.

Despite the potential attractiveness of the plastic films as an inner cover, glass was selected for both the inner and outer cover of the baseline design configuration. This decision was influenced by the unknown cost factors of frame design and material life expectancy inherent to using the plastic films.

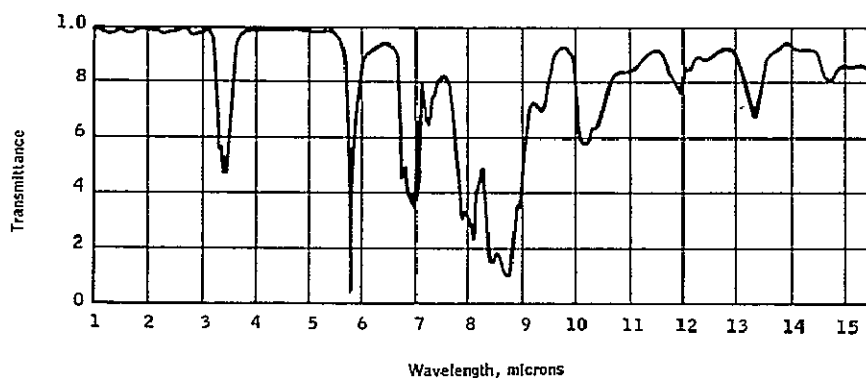


Figure 22. Plexiglass Infrared Transmission

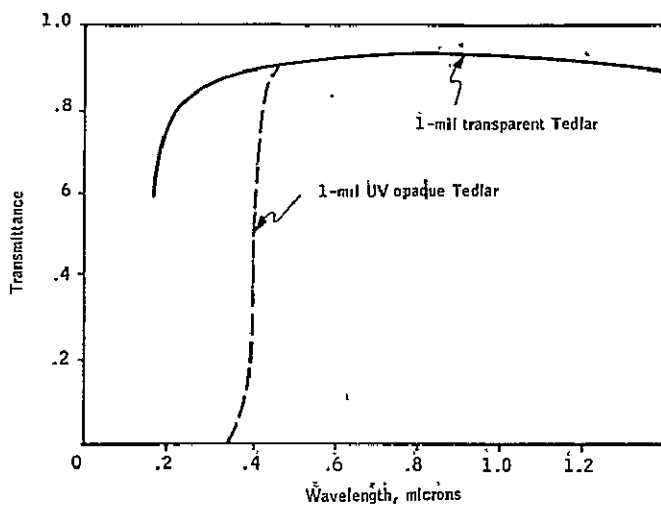


Figure 23. Transmission Spectra of Tedlar

ORIGINAL PAGE IS
OF POOR QUALITY.

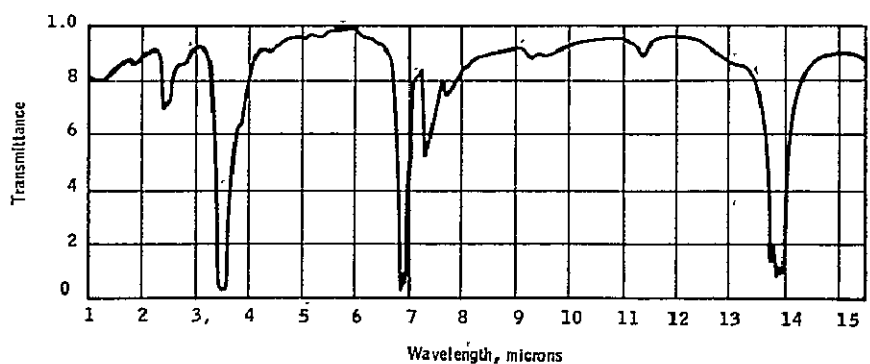


Figure 24. Transmission Spectra of Polyethylene

The glass used was Fourco Clearlite, a low-iron glass, untempered and in single strength, 0.23 cm (0.090 in.) thick. Based on the results of the thermal analysis, the two cover layers were spaced 3.0 cm (1.25 in.) apart, and the inner cover was placed 3.2 cm (1.25 in.) above the absorber panel. The space between the two covers was not hermetically sealed. An investigation of alternate cover materials was performed during the course of the program. The investigation included evaluation of a Tedlar inner cover, a Lexan outer cover, and antireflection-etched glass surface for both inner and outer covers.

Collector Housing

The collector housing serves three functions: it is a pan in which all the other collector components are nestled; it locates the absorber panel and fixes its relationship with the cover system; and finally it functions as a weather barrier.

The housing design selected for the baseline design configuration is composed of 15 piece parts, grouped into 4 different subassemblies: the pan or box, the cover support, the cover spacer, and the top cover bracket. All the piece parts are fabricated from sheet metal. The exterior sides of the assembled housing are coated with a chromide primer to prevent rusting and then painted with a decorative enamel.

The pan or box is assembled from three pieces of 24-gauge steel. The base is folded up to form two sides of the box. The other two sides are fabricated separately and spot-welded to the base to complete the box. Four U-shaped troughs are cut in opposing corners of the box to accommodate the absorber panel inlet and outlet tubes. Figures 25 and 26 show the piece parts, and Figure 27 shows the assembled box. Figure 27 also includes the next subassembly: the cover support. The cover support consists of four pieces of folded 24-gauge sheet steel which are gas welded together at the corners to form a frame. This frame slips over the top edge of the assembled box and forms an internal lip on which the inner cover glass sits. Figure 28 shows the cover support piece part. Locating the cover support on the top edge of the assembled box automatically fixes the 3.2 cm (1.25 in.) spacing between the inner cover and the absorber panel.

The cover spacer is formed by gas welding four sections of U-shaped 20-gauge steel together to form a frame. This welded frame rests on top of the inner cover and supports the outer cover. The cover spacer automatically establishes the 3 cm (1.25 in.) spacing between inner and outer covers. Figure 29 shows the cover spacer piece part.

The top cover bracket is formed by folding strips of 0.15 cm (0.060 in.) aluminum sheet stock. See Figure 30 for the shape. The choice of aluminum instead of steel was dictated by the desirability of having folded corners for the top cover bracket. As can be noted from Figure 30, the

All dimensions in
centimeters (inches)

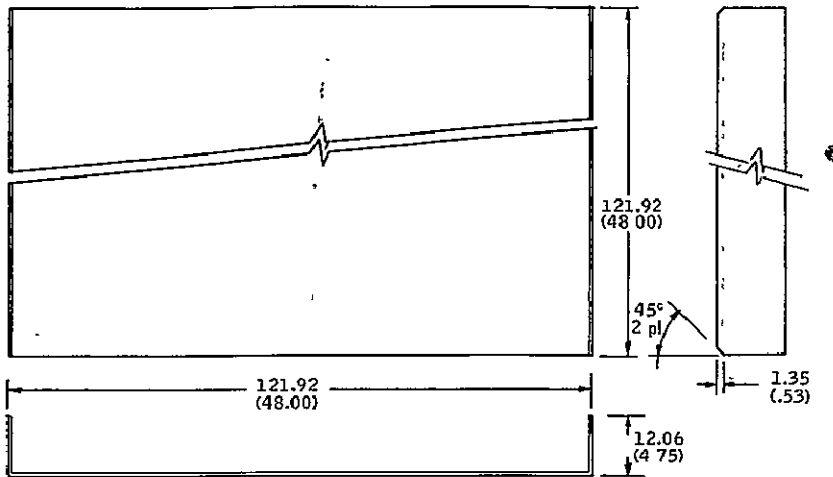


Figure 25. Base-Solar Collector Box

ORIGINAL PAGE IS
OF POOR QUALITY

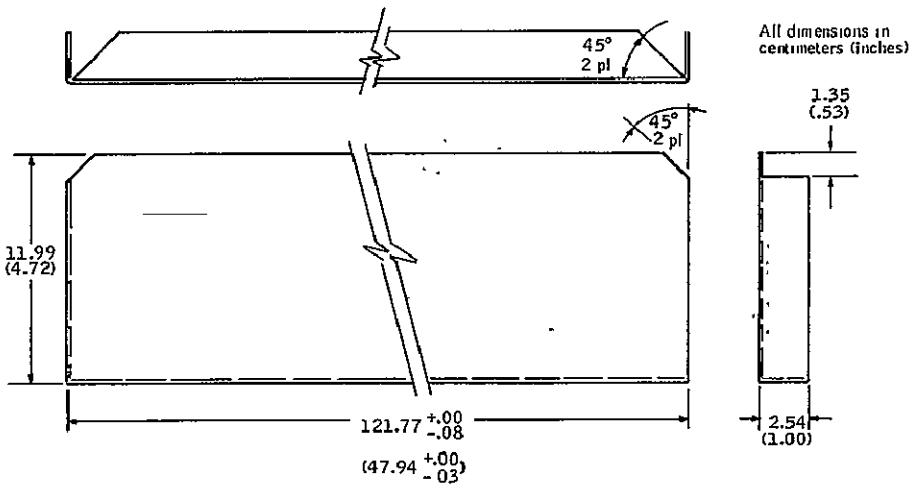


Figure 26. End-Solar Collector Box

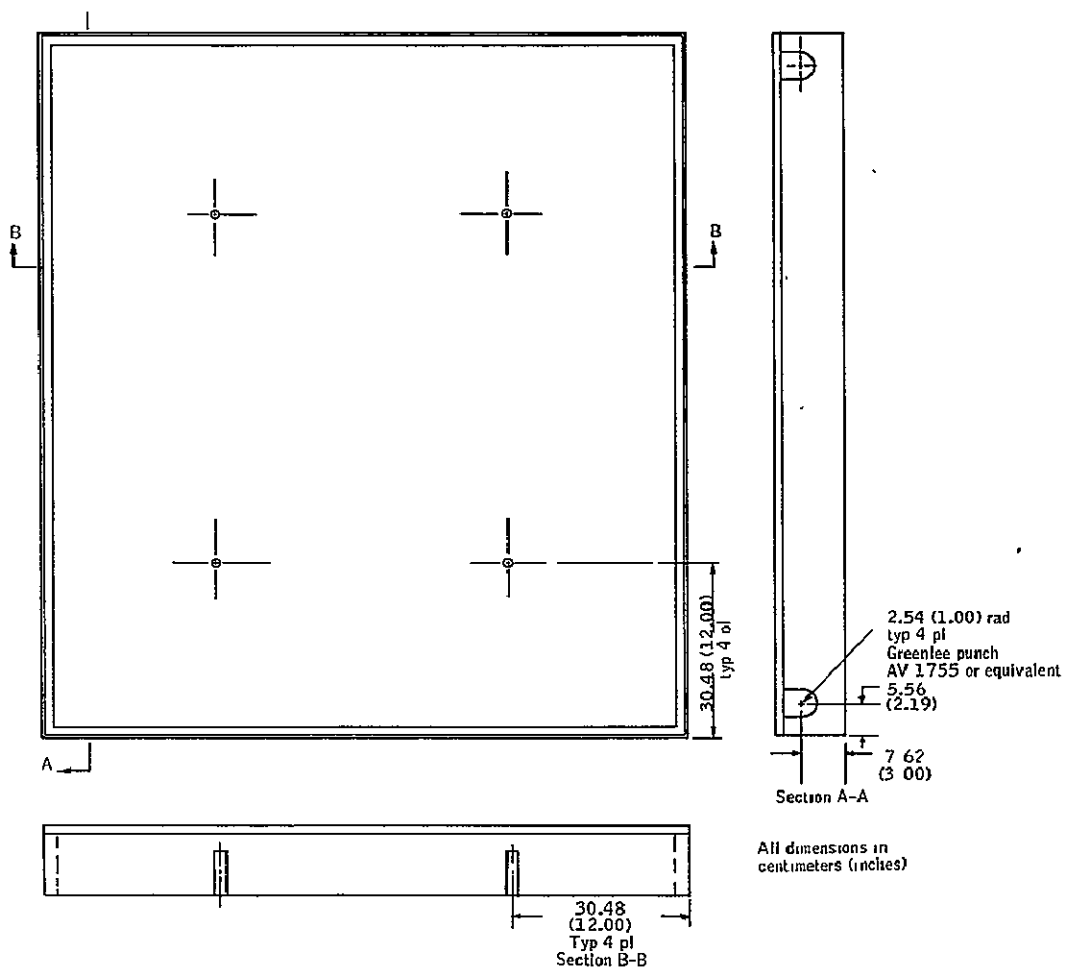


Figure 27. Solar Collector Box

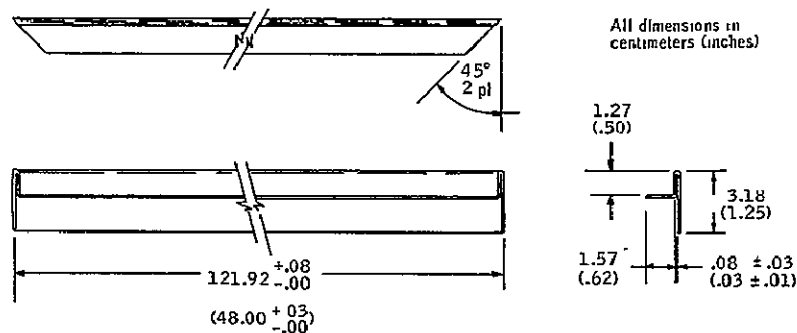


Figure 28. Glass Frame - Bottom Layer

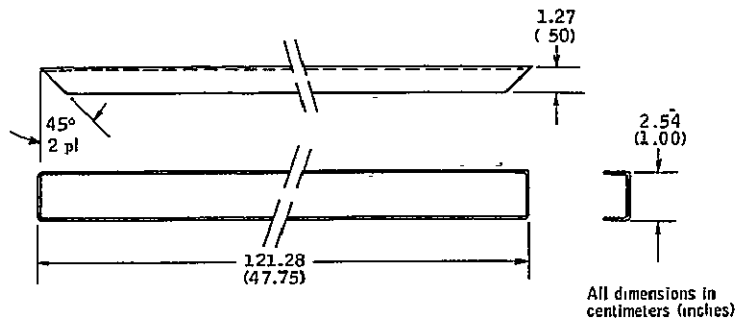


Figure 29. Cover Spacer

**ORIGINAL PAGE IS
OF POOR QUALITY**

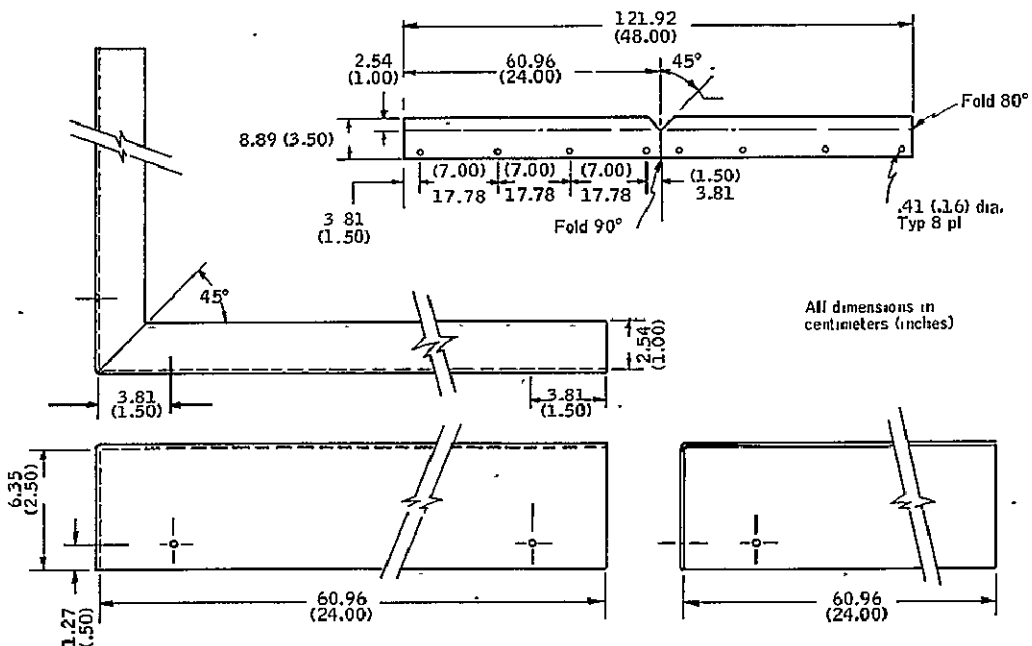


Figure 30. Top Cover Bracket

assembled top cover bracket has a joint in the middle of each side of the housing, instead of at the corners. This design makes the corners neater and safer. The top cover bracket is placed over the outer cover and fastened to the sides of the housing by sheet metal screws. Before placing the top cover bracket over the outer cover, a strip of butyl rubber weather stripping is attached to the inside top edge of each bracket section so that it will form a weather seal for the outer cover when the top cover bracket is fastened down.

Sheet metal was chosen for the housing piece parts primarily for expediency. Folded sheet metal parts are readily fabricated with a minimum of machines and tooling, yet they retain the potential for being adapted to automated fabrication techniques for production quantities. Other material candidates for the housing might be extruded or injection molded plastics, wood and wood composites, aluminum extrusions and sheets, or combinations of these materials.

Using materials other than metal presents certain problems: A plastic housing must include an ultraviolet inhibitor to reduce degradation and a fire retardant to reduce flammability. A wooden housing must be treated to reduce weathering and to make it fire resistant. Yet these problems are not insurmountable, and a careful study program might enable the design of a non-metallic collector housing that would certainly be lighter, and perhaps, cheaper.

COLLECTOR PERFORMANCE PREDICTIONS

Based on the thermal analysis it was possible to predict the performance of a fixed collector design given a set of input parameters. This process was programmed for operation on a CDC 6600 computer. The analytically predicted response to a given input could then be calculated for a number of input parameter sets to generate points to form a collector performance curve. This collector performance curve could then be characterized by the well-known form:

$$\eta = k_1 \alpha_{\text{absorber}} T_{\text{cover}} - k_2 \frac{\Delta T_{\text{collector to ambient}}}{Q_{\text{incident}}} \quad (7)$$

where

α = absorptance

k_1, k_2 = thermal efficiency factors dependent of definition of ΔT

η = collection efficiency

Q_{incident} = incident solar flux

τ = transmittance

ΔT = temperature difference between collector and ambient

Figure 31 presents the resulting predicted performance curve for the baseline collector design configuration. The performance prediction graph presents collection efficiency, η , as a function of the temperature differential between collector fluid inlet and ambient, divided by the incident flux level. The adequacy of representing this function by a linear equation can be gauged by examining the data points indicated in Figure 31. The single line drawn through the points is actually the graphical average of four distinct sets of points. The four sets were generated by fixing the ambient temperature and the fluid inlet temperature and modulating the incident flux level. Two fairly obvious conclusions may be drawn from these data: for a fixed temperature differential between ambient and fluid inlet, collection efficiency is directly proportional to the incident flux level; secondly, the rate of change of collection efficiency increases as the size of the temperature differential between ambient and fluid inlet increases. However, as may be seen from the total spread of the four sets of data points, a linear approximation of the performance curve presents a reasonably good fit to the actual predicted performance level, except perhaps at the intercepts.

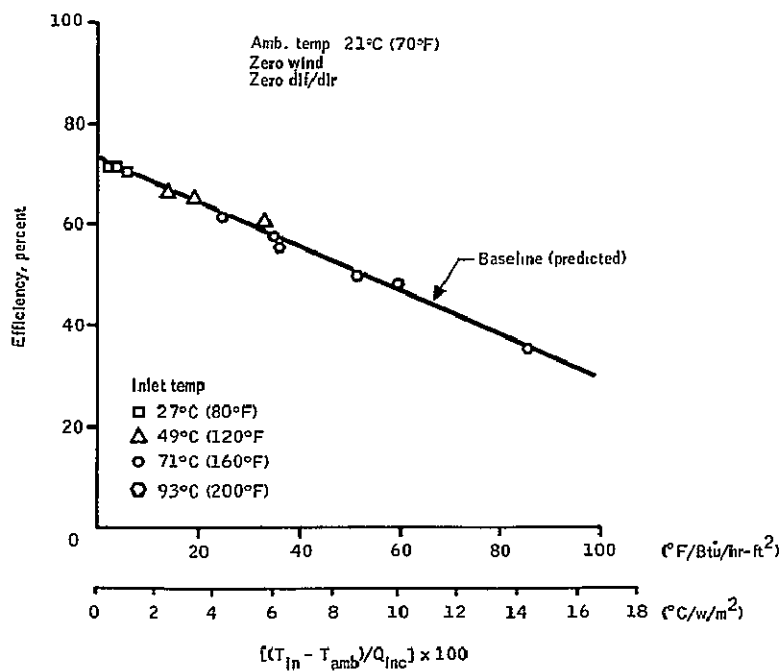


Figure 31. Predicted Performance of the Baseline Collector (Selective Coated Absorber/Two Glass Covers)

Once the predicted performance for the baseline collector design configuration was established, it became possible to evaluate the anticipated effects of design modifications. Two particular design modifications were of primary interest: the change in performance attributable to the use of a selective coating; and the change in performance attributable to the second cover layer.

The analytically predicted performance for a two-cover collector with a nonselective absorber coating is shown in Figure 32. The data are presented in the same format as that for the baseline collector design configuration in Figure 31. The predicted performance line for the baseline collector is added for purpose of reference. A comparison of the two predicted performance lines presented in Figure 32 indicates that a selective absorber coating provides significantly greater collection efficiency, except if the differential temperature between ambient and fluid inlet is small and the incident flux level is high. This statement may be generalized to say that the improvement in collection efficiency obtained by adding a selective coating to the absorber panel is directly proportional to the temperature differential, ΔT , and inversely proportional to the incident flux level, Q_{inc} .

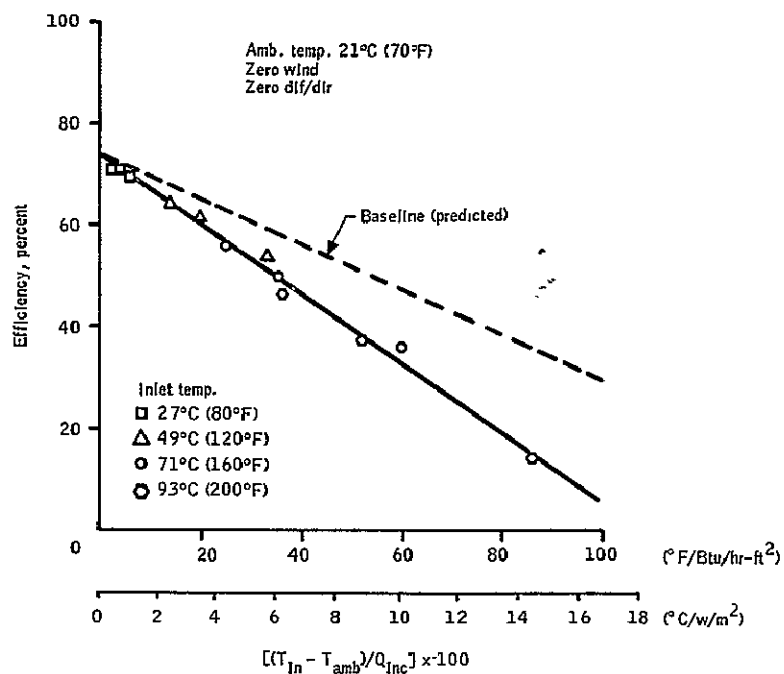


Figure 32. Predicted Performance for a Collector with a Nonselective Absorber and Two Glass Covers

The predicted effect of adding the second cover layer was examined for both the selective and nonselective absorber coating. Figure 33 shows the predicted performance for a collector with a selectively coated absorber panel and one cover layer. The baseline performance reference line is also included. Losses from a selectively coated collector are sufficiently low that the reduction in convection loss gained by adding a second cover is offset by the reduction in incident flux level caused by passing through that second cover; that is, until the combination of ΔT and Q_{inc} produces a sufficiently large ratio. In terms of the potential applications, it appears that air-conditioning would generally benefit from the second cover, as would heating in northern climates or low solar flux levels.

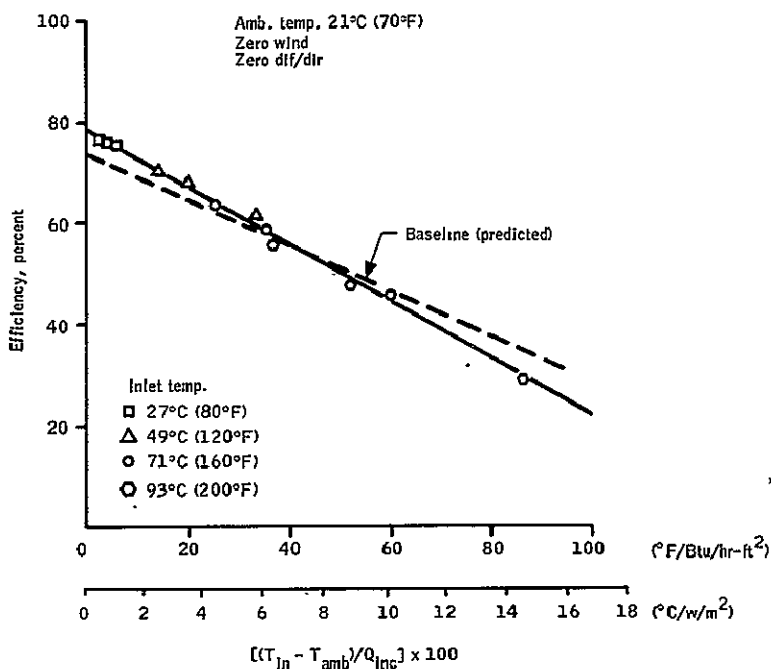


Figure 33. Predicted Performance for a Collector with a Selective Absorber and One Glass Cover

The question of whether or not to add a second cover appears more clear-cut for a nonselective absorber. Figure 34 presents the predicted performance for a collector with a nonselective absorber and one cover. Here, the second cover improves collector performance significantly for essentially all operating conditions (compare Figure 34 with Figure 32).

It may also be noted when comparing Figures 34 and 33 that a collector with a nonselective absorber coating, even with the benefit of a second cover layer, is not expected to perform as efficiently as a collector with a selective coating and only one cover.

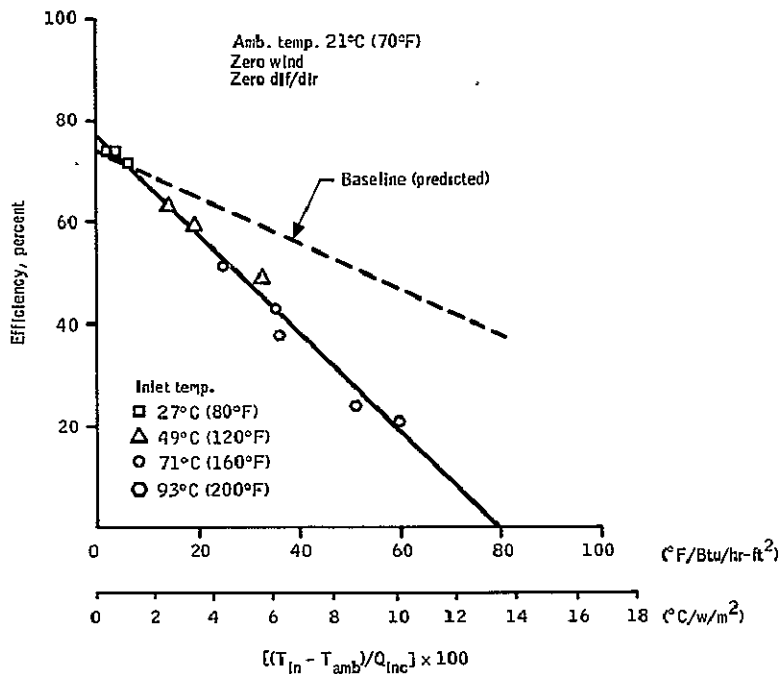


Figure 34. Predicted Performance for a Collector with a Nonselective Absorber and One Glass Cover

The performance predictions examined thus far contained some simplifying assumptions with regard to ambient conditions: that wind velocity was zero across the face of the collector, that the incident solar flux was entirely direct radiation, and that the incident solar flux was orthogonal to the front surface of the collector. The effect of these assumptions was also investigated.

The predicted effect of wind on collector performance is presented in Figures 35 and 36, for selective and nonselective absorber coatings, respectively. Figure 35 examines the effect of a 32-kph (20-mph) wind on a collector with a selective absorber and either one or two covers. A 32-kph (20-mph) wind reduces collector performance, regardless of whether there are one or two covers; but the impact is significantly greater with only one cover. Comparing this response to that for a collector with a nonselective absorber, as shown in Figure 36, it is obvious that the effect of wind is more pronounced with a nonselective absorber. Some interesting conclusions may be tentatively drawn from comparing Figures 35 and 36. The performance of a collector with a selective absorber and two covers under a 32-kph (30-mph) wind is essentially equal to that of a collector with a nonselective absorber, two covers and no wind. A second conclusion is that a collector with a selective absorber and one cover still performs better than a collector with a nonselective absorber and two covers, even with the added factor of a 32-kph (20-mph) wind.

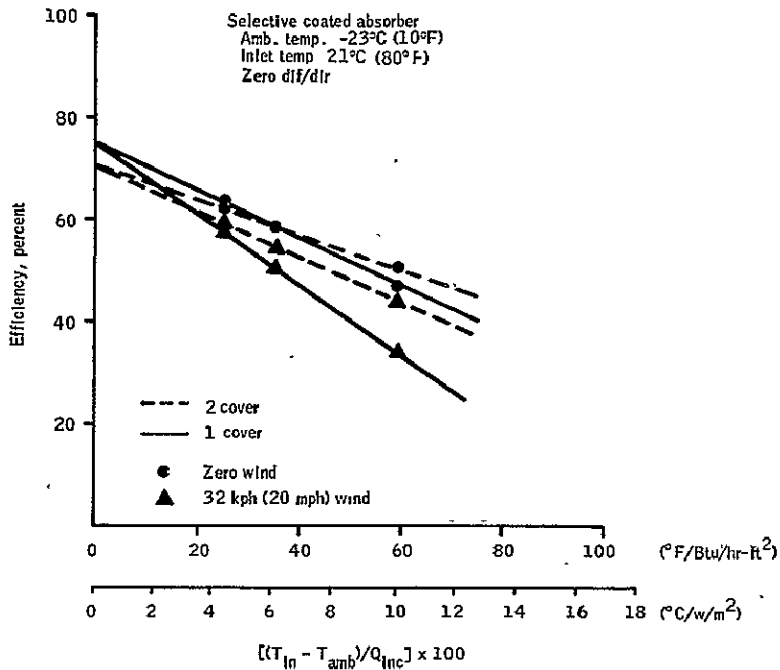


Figure 35. Predicted Effect on Wind on Performance of a Collector with Selective Absorber

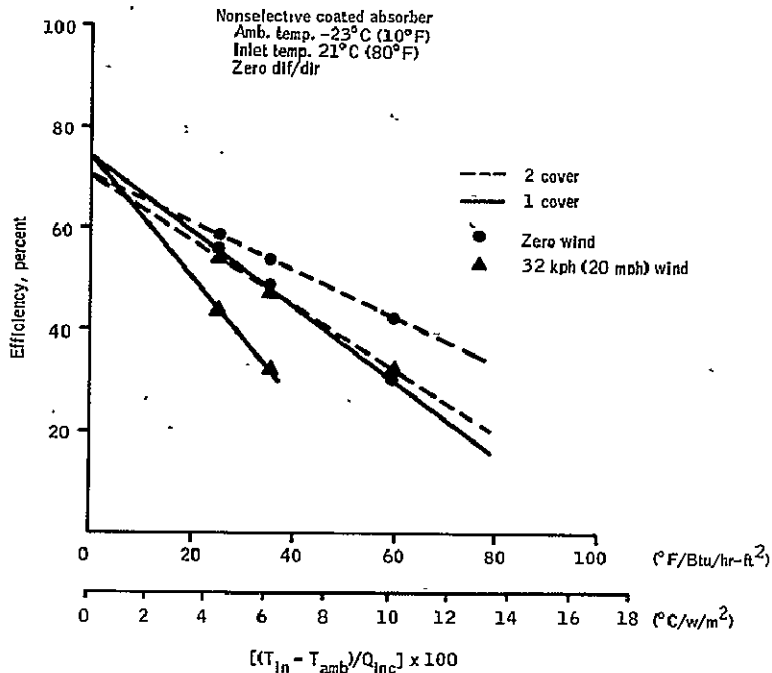


Figure 36. Predicted Effect of Wind on Performance of a Collector with Nonselective Absorber

Figure 37 shows predicted performance of a collector with a selective absorber when operating under the condition of a large diffuse component in the incident solar flux, such as would be expected on a cloudy day. Here the performance for the collector is compared between operation with an incident flux that is 100-percent direct radiation, and one that is 50-percent direct radiation and 50-percent diffuse radiation. This comparison is made for both one-cover and two-cover configurations. The net effect of a large diffuse solar flux component appears to be a uniform reduction in collection efficiency, amounting to a few percentage points all along the operating line. This small uniform loss in collection efficiency appears to be independent of the choice of one or two covers for the collector. Figure 38 presents the same analysis for a collector with a nonselective absorber. Here, too, there is a small uniform loss in efficiency for both one- and two-cover configurations. In addition, by comparing Figures 37 and 38, it appears that the presence of a large diffuse component causes about the same performance loss whether the collector has a selective or nonselective coating on the absorber panel.

The uniform change predicted for variations in the diffuse component is of particular interest in light of the test program, to be described in the next section of this report. The conclusions drawn from Figures 37 and 38 lend credibility to the use of a solar simulator for testing collector designs under controlled conditions. The incident flux output from the solar simulation is effectively 100-percent direct radiation, and yet, based on the results of the foregoing analysis, test results using a solar simulator should be applicable even for cloudy day collector operation.

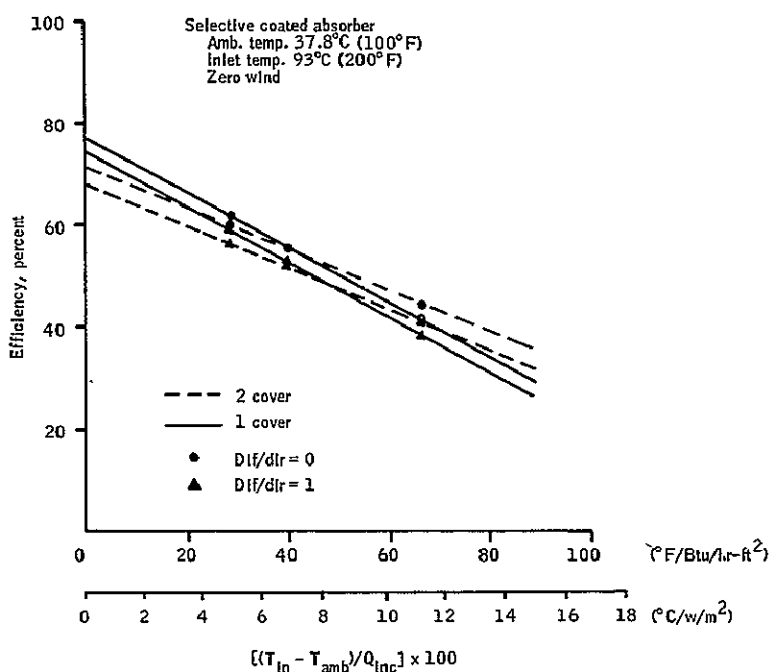


Figure 37. Predicted Effect of Changing Diffuse to Direct Ratio for a Collector with Selective Absorber

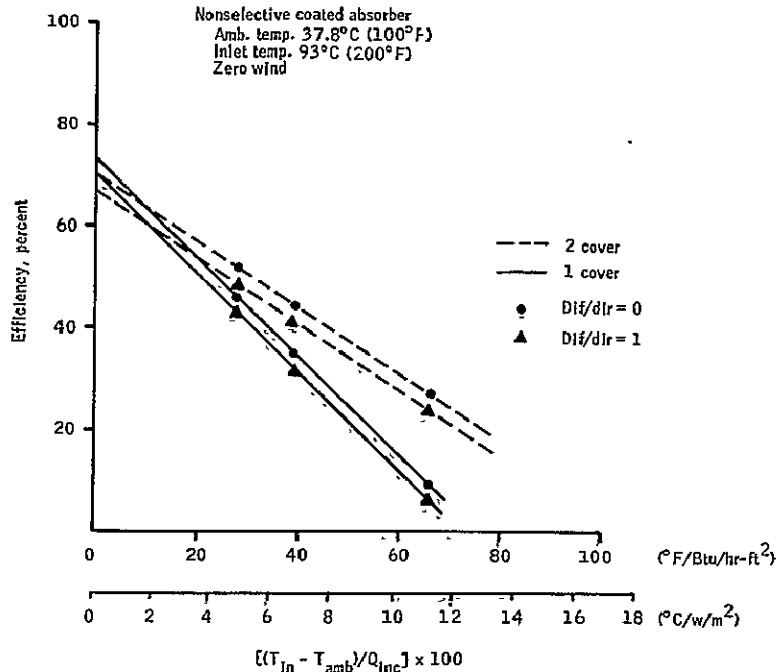


Figure 38. Predicted Effect of Changing Diffuse to Direct Ratio for a Collector with a Nonselective Absorber

The final variation considered in the analysis program was the effect on collector performance of changing the incident angle of the incoming solar flux. Figure 39 contains the expected performance of both a selective and a nonselective absorber, each with one cover or two covers, when subjected to a given solar flux applied at varying incident angles. As can be seen from the figure, collector performance varies only slightly until the flux incidence angle gets out to 45 degrees off-normal; from there it drops off more rapidly, approaching zero as the flux incidence angle passes 60 degrees from the normal. This result indicates that a fixed collector position would allow adequate response to the varying sun angle for most of the operating day.

To determine the effect of variable incident angle for a collector with a selectively coated absorber panel, it was necessary to understand the degree of angular dependence which a selective coating would be subject to. This relationship was established by performing a series of tests on a sample coated with Black Nickel, the baseline collector design configuration absorber coating. Figure 40 presents the family of reflectance spectra for off-angle testing of the Black Nickel sample. As can be seen from the figure, reflectance as a function of incident energy wavelength does not vary appreciably until the incident angle of the incoming flux reaches 60 degrees from the normal.

To establish the validity of the analysis and performance prediction code, a test program was devised to provide correlation. The details of the test program and its performance results are the subject of the next section of this report.

ORIGINAL PAGE IS
OF POOR QUALITY

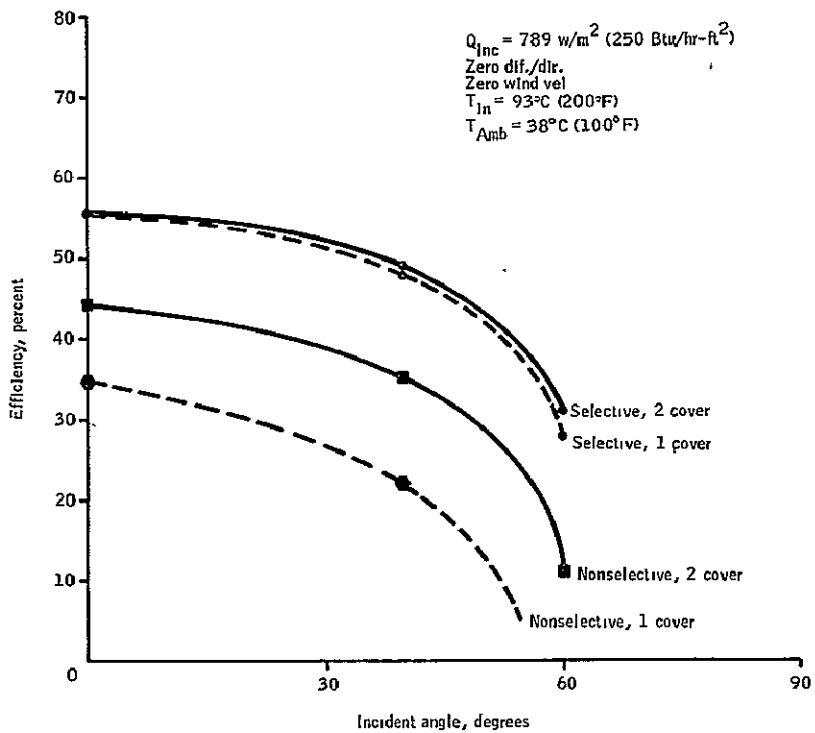


Figure 39. Predicted Effect of Varying Incident Angle on Collector Performance

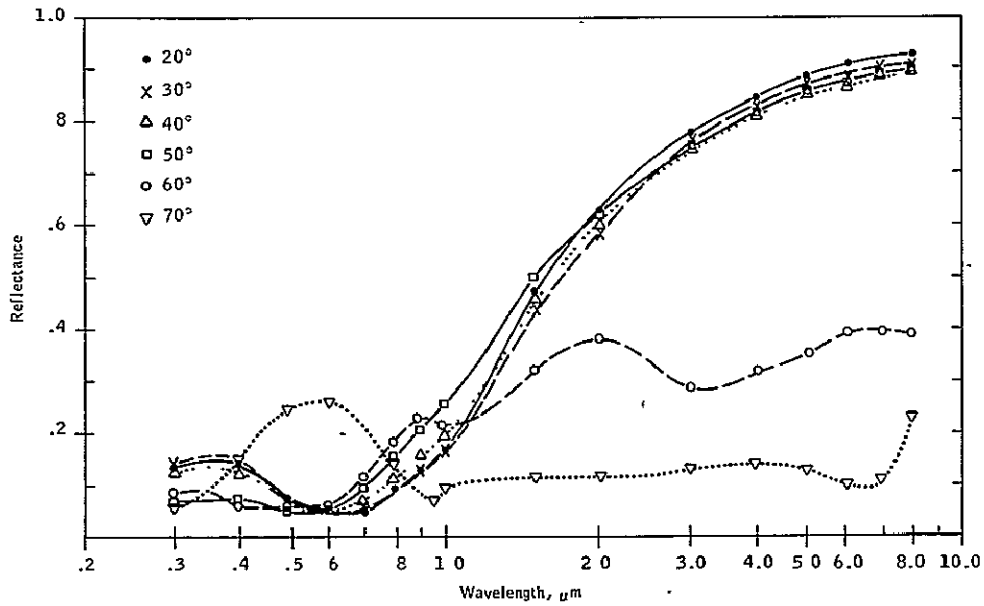


Figure 40. Spectral Total Reflectance for Several Angles of Incidence on a Black Nickel Coating Sample

BASELINE TESTING

The test and evaluation program had three primary objectives: to investigate the performance of the baseline collector design configuration when subjected to known input parameters, to examine alternate materials and their effect on performance, and to establish correlation between actual operation and the predicted performance. The last point applies to both the analytically predicted performance and also to the correlation between testing with the solar simulator and outdoor operation.

Baseline Test Objectives

The test matrix performed on the baseline collector design configuration investigated the effects of variations in four input parameters: fluid inlet temperature, incident flux level, flux angle of incidence, and diffuse/direct component ratio of the incident flux. In addition, tests were performed to determine collector startup time, startup time being defined as the time required for the average absorber panel temperature to reach 93°C (200°F), with a given incident flux level and a zero fluid inlet mass flow rate.

Indoor Test Facility

The baseline collector test matrix was performed in an indoor test facility that utilizes a solar simulator to provide the incident flux, as advocated by Simon and Harlamert. (6) The solar simulator generates a range of flux levels that closely approximate the distribution of the solar spectrum at air mass 2. The simulator consists of 143 projection lamps evenly spaced in a 1.83 m (6 ft) square array containing 13 rows and 11 columns. The output from each lamp is collimated by a 15-cm (6 in.) diameter plastic Fresnel lens set in an array 23 cm (9 in.) in front of the lamp array. Using the Fresnel lenses results in a flux output that is essentially 100 percent direct radiation.

The solar simulator is powered by a 3-phase, 208-volt wye configuration circuit capable of providing 43,000 volt-amperes of power. Each phase of the circuit is monitored by an SCR power controller which restricts the power output from zero to full scale, dependent on an operator-supplied control signal. The full scale output from the solar simulator is 1010 w/m² (320 Btu/hr-ft²) at a distance of 4.57 m (15 ft) from the lens array. This solar simulator is similar in design to that at the NASA-Lewis Research Center, Cleveland, Ohio. A detailed discussion of solar simulator design and operation may be found in NASA Technical Memorandum TMX-3059, "Low-Cost Air Mass 2 Solar Simulator."(11) The simulator in actual operation is illustrated in Figure 41.

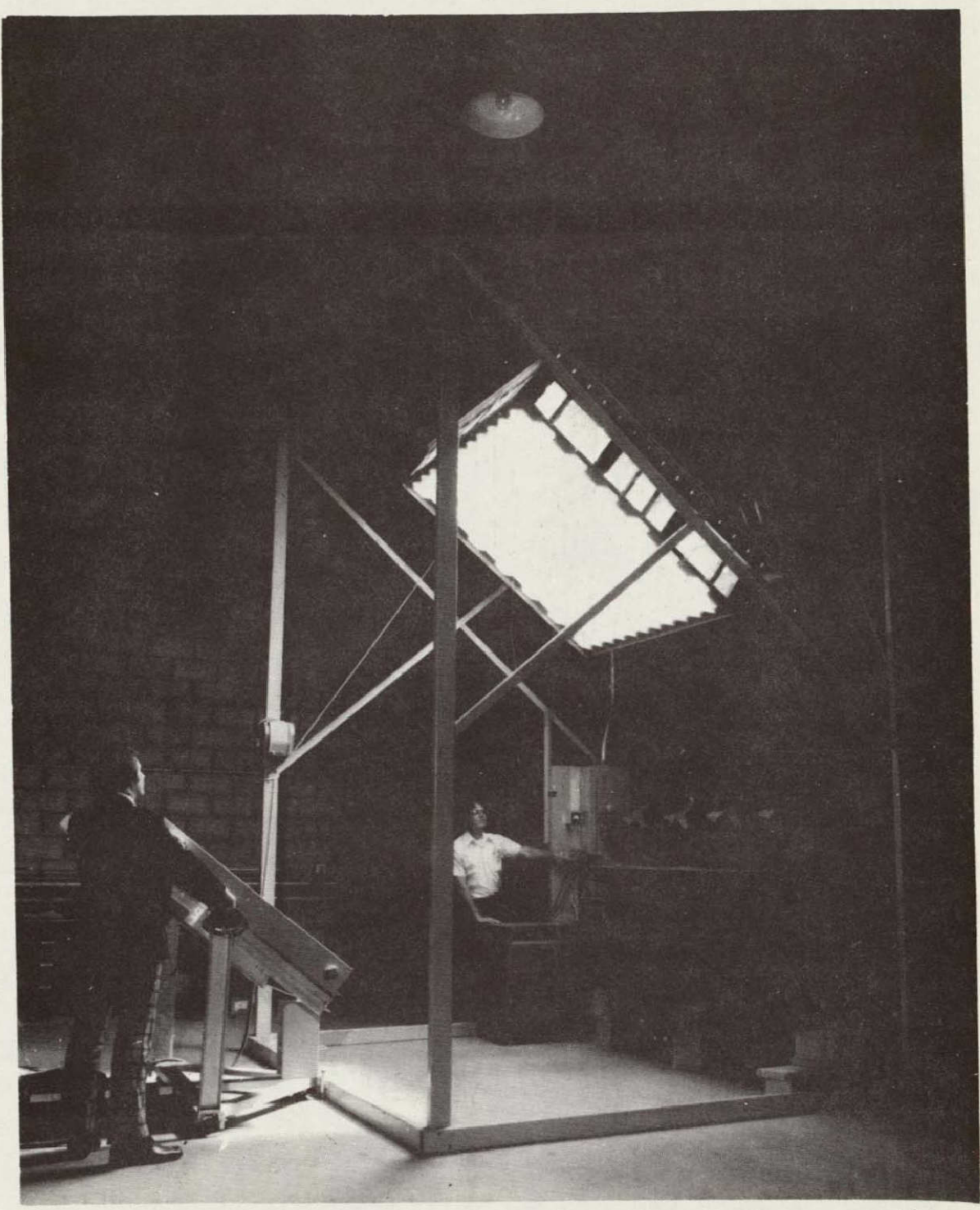


Figure 41. Solar Simulator in Operation

ORIGINAL PAGE IS
OF POOR QUALITY

The collector test loop is presented diagrammatically in Figure 42. System operation is as follows:

The glycol/water mixture was pumped from the reservoir to a 4.57 m (15 ft) constant head tank. An overflow line to return fluid to the reservoir maintained a constant pressure head. This pressure head drove fluid to a conventional hot water heater and then through a constant temperature bath. From there, the fluid went through the flowmeter and to the collector. The outlet from the collector returned fluid to the reservoir and completed the cycle. A valve placed between the constant temperature bath and the flowmeter regulated the flow.

Mixing cups were inserted at the inlet and outlet of the collector. A five-junction thermopile and a thermocouple were placed in each mixing cup. From these, the fluid temperature difference across the panel and fluid inlet and outlet temperatures was found. Another thermocouple placed behind the collector stand measured the ambient temperature. These temperatures were recorded on a digital recorder. Iron-constantan thermocouple wire was used.

The flow rate was determined using a calibrated flowmeter. As the system approached steady state, the flow rate was maintained at a constant value. This flow rate was also periodically checked by measuring the time for the return fluid to fill a 1000-ml graduated cylinder.

The flux from the simulator was determined using an Eppley pyranometer. A 16-point flux map at the collector surface was made and recorded for each experimental run. The average value was used as the effective incident radiation level.

Baseline Test Matrix

The tests performed on the baseline collector are listed in Table 4. As can be seen from this table, each performance test was run with a $48.9 \text{ kg}/\text{hr}\cdot\text{m}^2$ ($10 \text{ lbm}/\text{hr}\cdot\text{ft}^2$) flow rate of nominally 50-50 water-ethylene-glycol solution. The collector was tilted at an angle of 40 degrees with respect to horizontal and had a zero effective wind velocity across the face of the collector.

A test cycle consisted of preheating the fluid reservoir to the desired inlet temperature, 27°C (80°F), 49°C (120°F), 71°C (160°F) or 93°C (200°F), allowing flow through the collector to maintain inlet temperature equilibrium throughout the system. Once the desired inlet temperature was attained, the primary heater was shut off, the flow rate adjusted to $48.9 \text{ kg}/\text{hr}\cdot\text{m}^2$ ($10 \text{ lbm}/\text{hr}\cdot\text{ft}^2$), and the inlet temperature trimmed and maintained by the constant temperature bath.

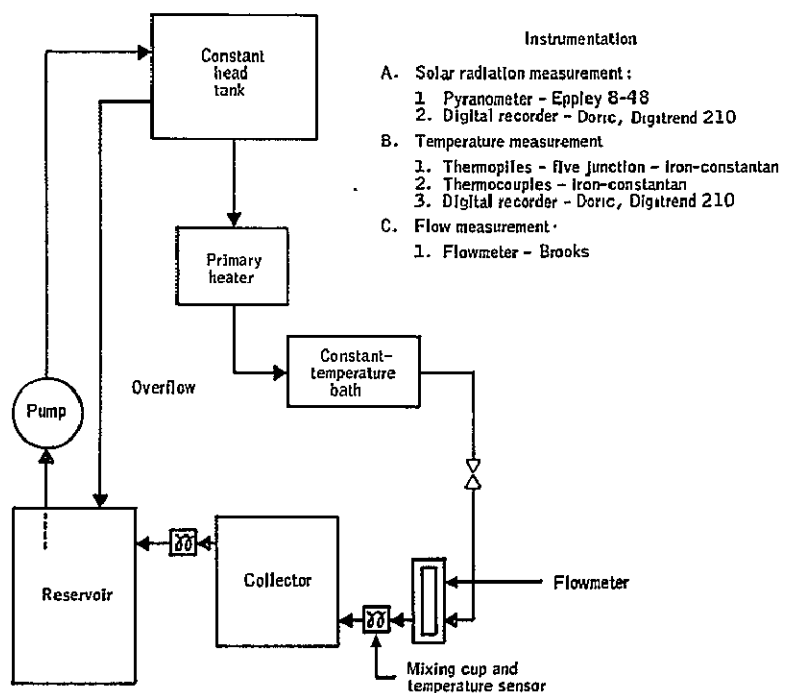


Figure 42. Diagram of Indoor Collector Test Loop

TABLE 4, - BASELINE COLLECTOR TEST MATRIX
(TEST DATE)

		Aluminum panel Selective Black Nickel coating, $\alpha = .955$ Ambient temperature = 21°C (70°F) Wind velocity = 0 kph (0 mph) Collector tilt angle = 40° Mass flow rate = 48.9 kg/hr-m ² (10 lbm/hr-ft ²)			
Angle of incidence, deg	Flux, W/m ² (Btu/hr-ft ²)	Inlet temperature			
		27°C (80°F)	49°C (120°F)	71°C (160°F)	93°C (200°F)
0 Diffuse/direct = 0	473 (150)	8/14	8/14	N/A	8/7
	789 (250)	8/14	8/14	8/14	8/7
	1010 (320)	8/14	8/14	N/A	8/7
40 Diffuse/direct = 0	473 (150)	8/30	9/9	N/A	9/13
	789 (250)	8/30	9/9	9/10	9/18
	1010 (320)	8/30	9/9	N/A	9/18
60 Diffuse/direct = 0	473 (150)	8/30	9/9	N/A	9/13
	789 (250)	8/30	9/9	9/10	9/18
	1010 (320)	8/30	9/9	N/A	9/18
0 Diffuse/direct = 1	789 (250)	10/10	11/14	11/16	11/19
	1010 (320)	10/10	11/14	N/A	11/19
Startup test:					
Plate temperature: 27°C to 93°C (80°F to 200°F)					
Mass flow rate: 0 kg/hr-m ² (0 lbm/hr-ft ²)					
Flux, W/m ² (Btu/hr-ft ²):		<u>Date</u>			
789 (250)		8/29			
1010 (320)		8/29			

After firing up the solar simulator, the flux map for the intended incident flux level was measured, and the illuminated collector was allowed to run until equilibrium was observed for the fluid temperature rise across the collector. Values for the inlet temperature, fluid temperature rise, fluid mass flow rate, and incident flux level were then recorded. The actual measurement process took approximately one half hour, once initial fluid inlet temperature equilibrium had been achieved.

The measurement process was then repeated for the next incident flux level, without altering the flow rate or fluid inlet temperature.

Test Results

The test data is presented and discussed in the following sections. The bulk of the data is presented by plotting the efficiency, η , as a function of $(T_{in} - T_{amb})/Q_{inc}$. The efficiency is defined as:

$$\eta = Q_{coll}/Q_{inc} \quad (8)$$

where

Q_{coll} = heat flux delivered to the collector fluid (per unit absorber area)

Q_{inc} = incident solar flux measured in the plane of the collector surface (per unit absorber area)

T_{amb} = ambient temperature

T_{in} = fluid inlet temperature

The heat flux collected is obtained from the test data by:

$$Q_{coll} = \dot{m} C_{p_{fluid}} (T_{out} - T_{in}) \quad (9)$$

where

$C_{p_{fluid}}$ = heat capacity of the collector fluid

\dot{m} = collector fluid mass flow rate (per unit absorber area)

$(T_{out} - T_{in})$ = collector fluid temperature difference between the outlet and inlet (as measured with the differential thermopile)

As will be seen from the test results, the parameters used do a good job of correlating the data. In addition, they allow direct comparison with one of the commonly used collector performance models:

$$\eta = F_r \left(\alpha \tau_e - U_L \frac{T_{in} - T_{amb}}{Q_{inc}} \right) \quad (10)$$

where

α = absorptance of the collector plate

F_r = heat removal efficiency factor

τ_e = transmittance of the covers

U_L = collector heat loss coefficient

Baseline performance results. - The performance of the baseline collector is shown in Figure 43. Note that this performance curve is only applicable for 100-percent direct radiation impinging on the collector with a 0-degree incident angle; however, it does demonstrate the effect of varying inlet temperature and incident flux level.

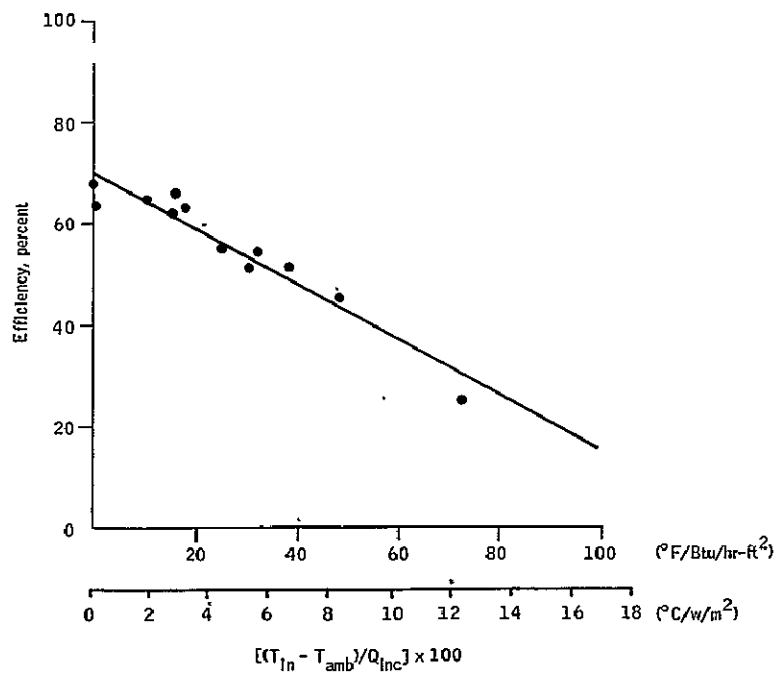


Figure 43. Baseline Collector Performance with 0° Incident Flux Angle

Efficiency varies inversely as the differential temperature from ambient to operating temperature. This, of course, is reasonable as heat losses from both convection and conduction will increase as the driving force of the temperature difference between collector and ambient increases.

A second interesting point relative to the effect of varying inlet temperature is the case when $T_{in} - T_{amb} = 0$. When the losses due to the external temperature differential are held to zero, approximately 30 percent of the incident radiation is still not utilized. This points out an area of collector design that requires considerable care. As evidenced in Equation (10), the intercept of the performance curve is a function of cover transmission and collector absorptance. Improving either of these two factors will tend to increase the intercept, assuming the heat loss factors are not impacted by the improvement in τ_e or α . This effect became evident later in the research program as varying absorber materials and cover materials were tested while retaining the same collector configuration. The results of these tests will be examined further.

The other factor exhibited by the graph of Figure 43 is the effect of varying incident flux level. Collection efficiency increases as incident flux level increases. This is the logical response in that heat losses through the collector are a function of $T_{in} - T_{amb}$ and not a function of Q_{inc} ; therefore, for a given operating temperature, losses will be fairly consistent, thereby reducing the effective heat available for transfer to the working medium. Incident flux levels exceeding that required for collector losses are then available for transfer.

As mentioned previously, Figure 43 does not represent collector performance as a function of flux incidence angle. Performance graphs that allow comparison of 0-, 40- and 60-degree flux incidence angles are presented as Figures 44 and 45. The reduced performance is primarily the result of decreased window transmittance as the angle increases. An experiment performed to determine the effect of flux incidence angle on collector cover transmission did indicate that glass transmission decreased as a function of increasing incident angle, dropping off quite sharply as the angle of incidence approached 60 degrees. This experimental result for the glass transmission correlated well with the published data from Hottel and Whillier's paper "Evaluation of Flat Plate Solar Collector Performance."⁽⁵⁾ It also provided good correlation with the predicted performance variation with incident angle (see Figure 46) at least for high inlet temperatures. As previously described, experiments performed on a Black Nickel-coated absorber sample indicated only a weak angular dependence for the absorptance over the range of angles considered. It should be noted however, that off-normal collector performance is still lower than predicted by glass transmission loss alone.

The final variable considered in the baseline test matrix was the effect of variation in the diffuse/direct component ratio of the incident flux. To evaluate this effect, the solar simulator was modified by placing a grid between the collector and the simulator. This grid was a checkerboard arrangement of 1.25 cm (0.5 in.) squares alternating between clear glass and

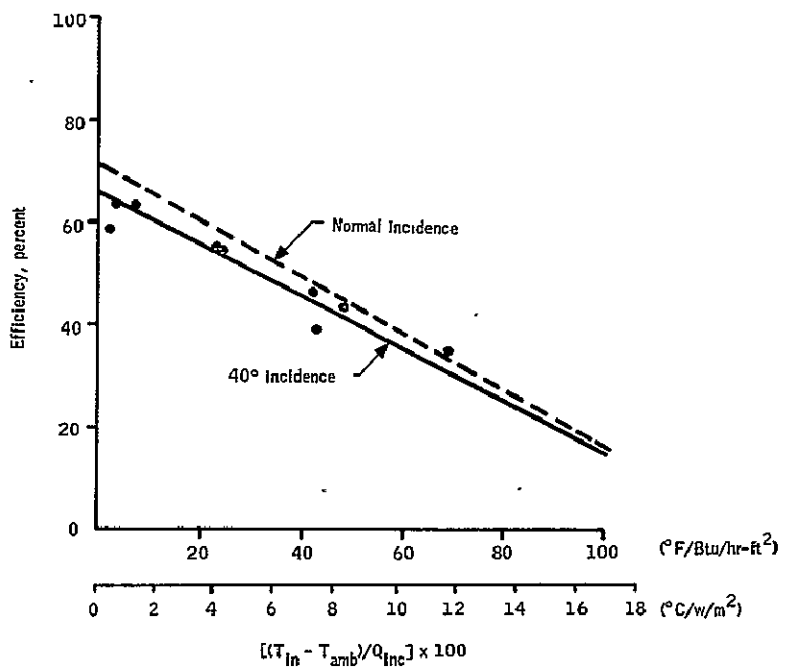


Figure 44. Baseline Collector Performance with 40° Incident Flux Angle

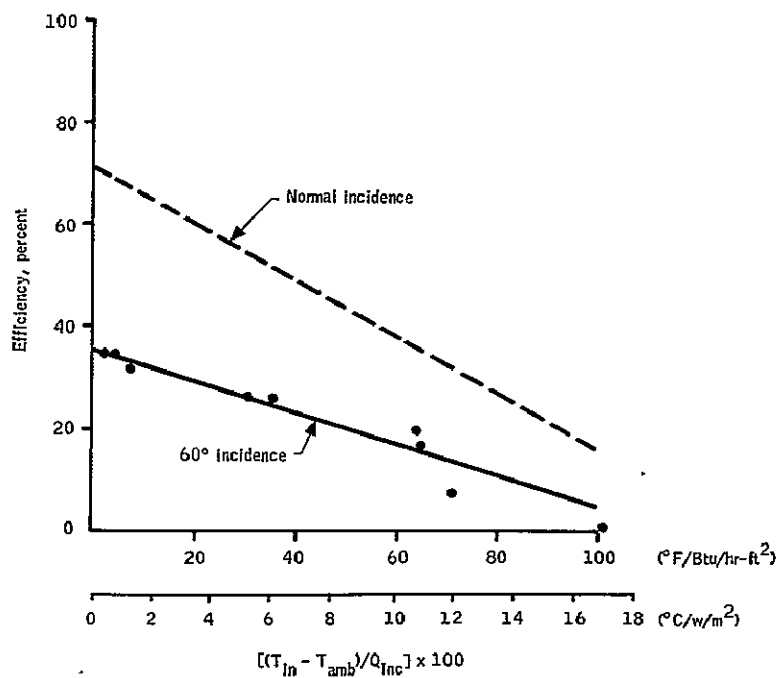


Figure 45. Baseline Collector Performance with 60° Incident Flux Angle

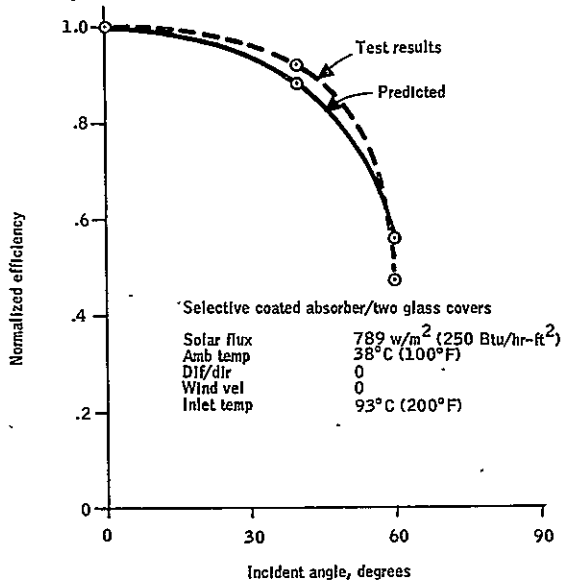


Figure 46. Effect of Incident Flux Angle on Performance

"frosted" or sand blasted glass. Measurements performed on a grid sample indicated the radiation from the solar simulator was modified from essentially 100 percent direct radiation to 46 percent diffuse and 54 percent direct radiation by passing through the grid prior to irradiating the collector. Collector performance under these modified radiation conditions is presented as Figure 47. By comparison to the results for all direct flux, it may be noted that the effect of increasing the diffuse component appears to be a slight overall reduction in effective transmission of the collector covers.

Figure 48 presents the test series performed on the baseline collector to determine startup time. As mentioned earlier, this test measured the time required for the absorber plate to reach a desired operating temperature; in these cases 93°C (200°F), given a sudden inception of incident radiation. The tests were performed with liquid in the collector, but with no flow. The figure shows that startup time for the baseline collector design configuration is significantly shorter than the design objective startup time of 30 minutes or less.

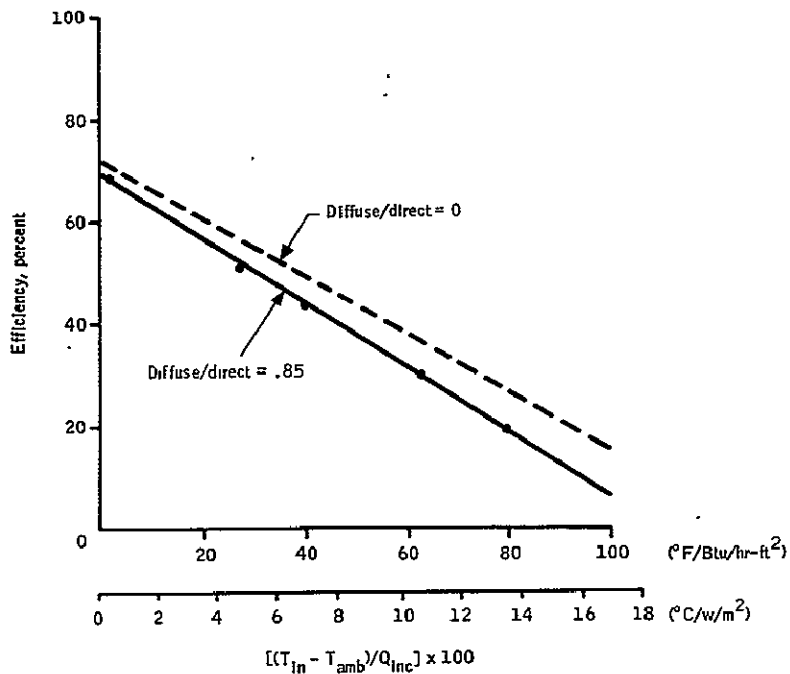


Figure 47. Performance of Baseline Collector under Changing Diffuse to Direct Ratio for Incident Flux

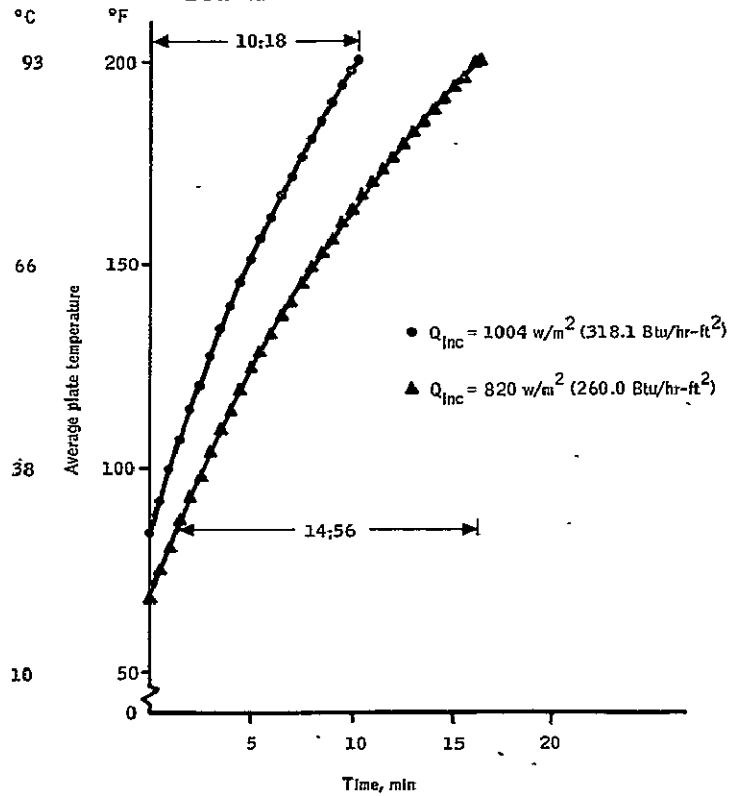


Figure 48. Startup Test Results for Baseline Collector

ALTERNATE COLLECTOR CONFIGURATION TESTING

Another objective of the test and evaluation program was to examine other materials as candidates for the collector absorber and the collector covers. Of particular interest was the comparative performance of a collector using a nonselective black paint as its absorber. Surveys of current literature reveal that black paint is probably the most commonly used absorber coating. The paint used was 3M Black Velvet which has a solar absorptance of approximately 0.95 and an infrared emittance of approximately 0.9. In addition to examining black paint on the aluminum absorber panel, selective Black Nickel on a steel absorber panel and selective Black Chrome(12) on a steel absorber panel were also evaluated. The radiation properties of a sample of Black Chrome on steel are shown in Figure 49.

It should be noted, however, that the commercial Black Chrome (Harshaw Process) left a black soot-like deposit on the absorber panels. Removal of this deposit reduced the coating's α to 0.80.

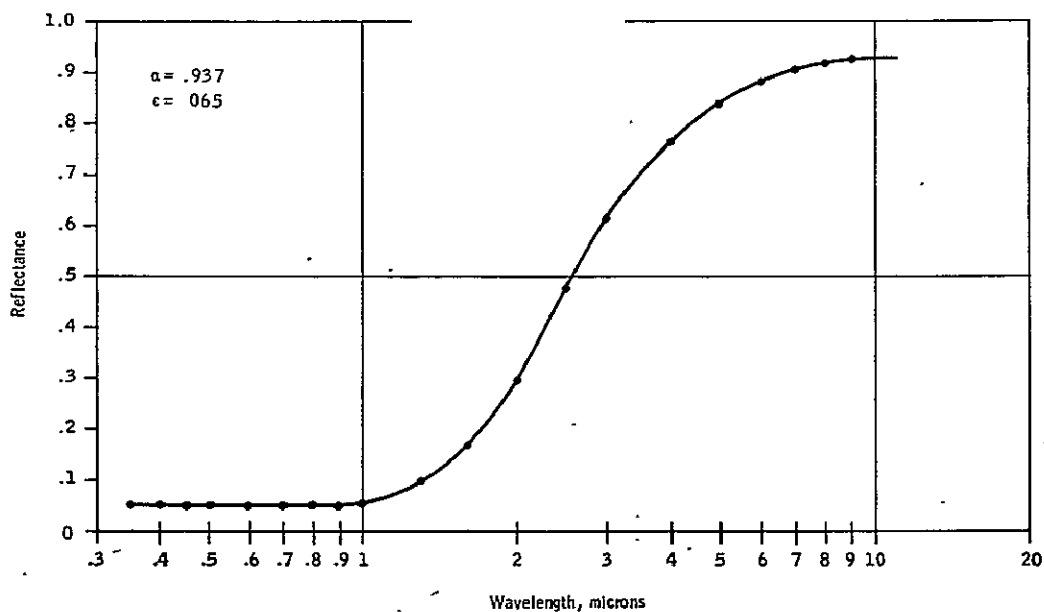


Figure 49. Radiation Properties of Black Chrome on Steel

The choice of cover materials was examined by performance testing five different cover types on the same baseline collector used for baseline testing, and also by testing the same five cover types on a collector with a nonselective black paint on aluminum absorber panel. The five cover

1000
100

types investigated and examined for comparative performance were: two sheets of glass; one sheet of glass; an outer sheet of glass and an inner sheet of Tedlar; one sheet of Lexan; and two sheets of surface etched antireflection glass.

Table 5 presents the test matrix performed to complete the evaluation of the various absorber and cover choices. It should be noted that here, unlike the baseline test matrix, only one incident flux level was used; i.e., 789 W/m^2 ($250 \text{ Btu/ft}^2\text{-hr}$). By testing at four different inlet fluid temperatures, it was possible to generate a performance curve, such as was done for the baseline collector. The tests listed on the matrix were performed on the same test arrangement used for the baseline testing, with the collector tilted at 40 degrees with respect to the horizontal and an inlet fluid mass flow rate of 48.9 kg/hr-m^2 (10 lbm/hr-ft^2).

Graphs comparing collector performance for the four absorber material combinations are presented in Figures 50 and 51. Figure 50 is for low-temperature operation. An inlet temperature of 49°C (120°F) compares performance under conditions of low collector heat losses. The data presented in this figure show that for high incident flux levels and low-to-moderate temperature differentials between ambient and the collectors, a nonselective absorber is adequate.

Figure 51 presents the same four absorbers at the other end of their operating spectrum: a fluid inlet temperature of 93°C (200°F) and a collector-ambient temperature differential of -72°C (130°F). Under this set of conditions, the reradiation losses of the nonselective absorber become much more dominant and performance of both the Black Nickel-aluminum and the Black Nickel-steel absorbers is significantly better than that of the nonselective black paint absorber.

A final point of interest is evident in both this figure and the previous figure. Both the Black Nickel-steel absorber and the Black Nickel-aluminum absorber have essentially the same performance levels. This is reasonable as samples of both coatings exhibited the same response; as a weighted average over the solar spectrum both Black Nickel samples had an absorptance (α) of 0.95 and an emissivity (ϵ) of 0.7. In addition, the spacing between flow tubes was adjusted for the steel absorber panel design to give it the same thermal resistance between tubes as the aluminum absorber panel.

The full range performance curves for the four absorber types are presented at the end of the next section with the performance curves of the cover choice investigation.

Figures 52 and 53 present the comparative performance of five various cover types when used in conjunction with a Black Nickel-aluminum absorber. As in the absorber material investigation, the graphs presented show comparative performance with a small 28°C (50°F) temperature differential

TABLE 5.- ALTERNATE CONFIGURATION TEST MATRIX
(TEST DATE)

		Inlet temperature			
Panel	Cover	27°C (80°F)	49°C (120°F)	81°C (160°F)	93°C (200°F)
Aluminum, selective Black Nickel coating, $\alpha = .95$	One glass, $\tau = .92$	8/22	8/19	8/22	8/23
	One Lexan, $\tau = .85$	9/3	9/9	9/10	9/12
	Two glass, $\tau = .85$	8/14	8/14	8/14	8/7
	Glass/Tedlar, $\tau = .86$	11/26	11/21	11/21	11/28
	Two AR glass, $\tau = .92$	11/26	11/26	11/28	11/28
Aluminum, black paint coating, $\alpha = .97$	One class, $\tau = .92$	11/22	11/14	11/19	11/28
	One Lexan, $\tau = .85$	9/4	9/6	9/10	9/12
	Two glass, $\tau = .85$	7/30	9/6	9/10	9/12
	Glass/Tedlar, $\tau = .86$	11/26	11/21	11/21	11/19
	Two AR glass, $\tau = .92$	11/26	11/26	11/27	11/28
Steel, selective Black Nickel coating, $\alpha = .94$	Two glass, $\tau = .85$	11/12	11/14	11/19	11/19
Steel, selective Black Chrome coating, $\alpha = .935$	Two glass, $\tau = .85$	2/2	2/2	2/2	2/2

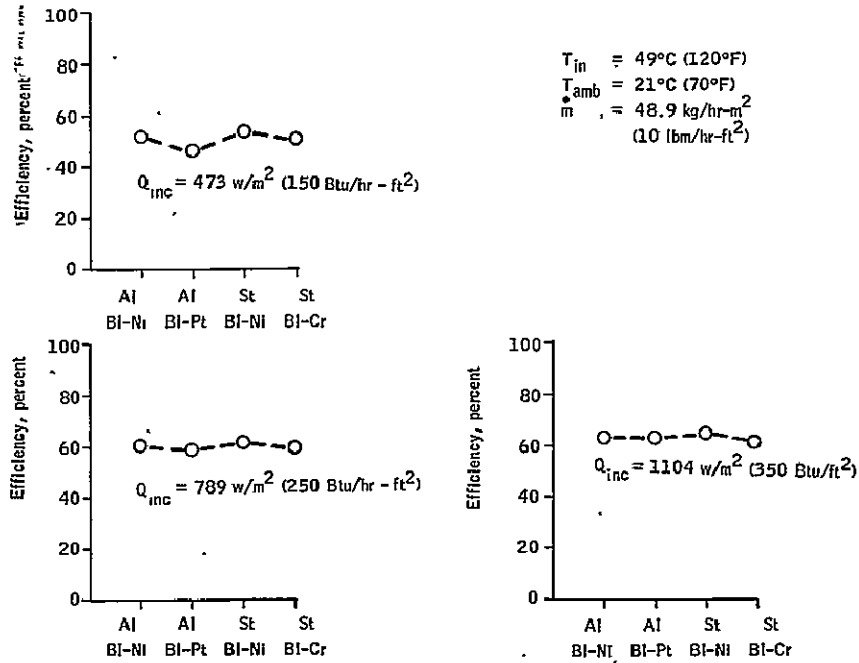
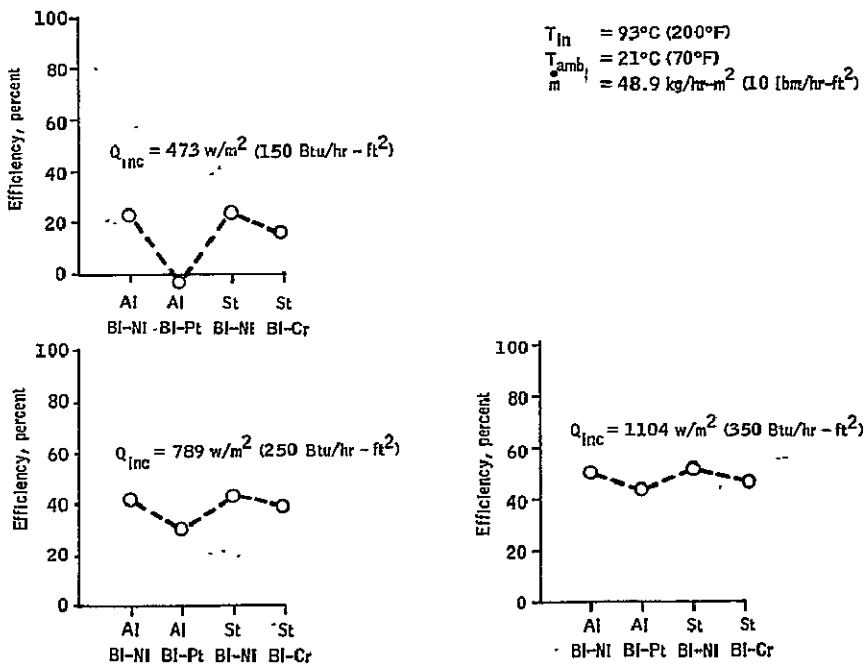


Figure 50. Absorber Plate Comparisons for Collectors with Two Glass Covers - Low-Temperature Operation



ORIGINAL PAGE IS
OF POOR QUALITY

Figure 51. Absorber Plate Comparisons for Collectors with Two Glass Covers - High-Temperature Operation

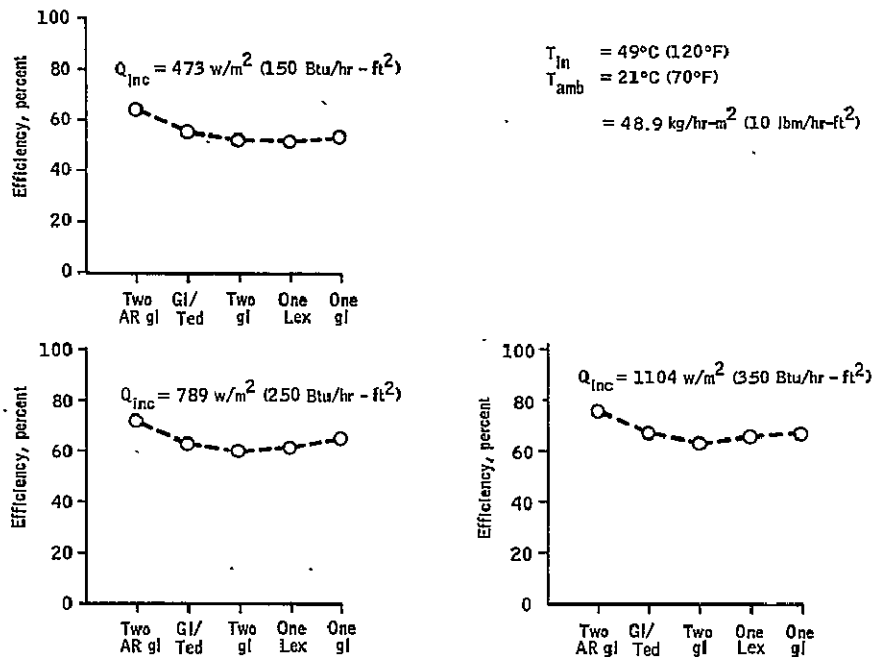


Figure 52. Cover Comparison for Collectors with Black Nickel Aluminum Absorbers - Low-Temperature Operation

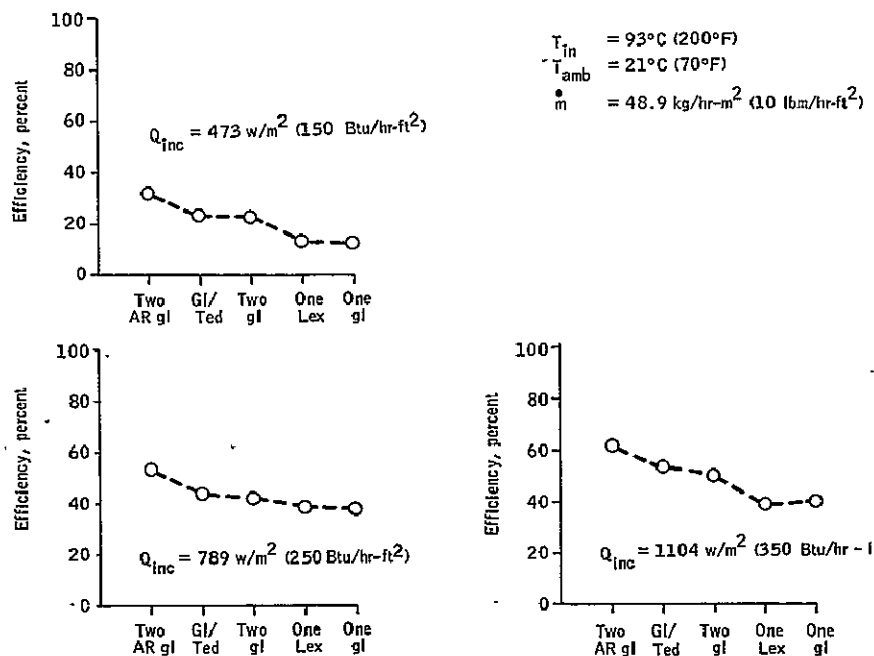


Figure 53. Cover Comparison for Collectors with Black Nickel Aluminum Absorbers - High-Temperature Operation

between ambient and fluid inlet temperature and again with a large temperature differential 72°C (130°F). This pair of comparisons is made for low, medium, and high incident flux levels.

Using the baseline collector (two glass covers) performance as a baseline, the following conclusions may be drawn from these two figures: at low fluid inlet temperature the transmission factor, T_e , determined by both the cover material and cover configuration (i. e., one or two covers), is the dominant factor in setting the comparative performance levels. At high inlet fluid temperature, the losses are a significant factor, and the additional reduction in losses created by adding a second cover outweighs the effect of differences in the effective transmission factor of the cover.

Figures 54 and 55 are the same performance comparison except that the collector tested had a nonselective black paint absorber. Similar conclusions may be drawn about the impact of the various covers with regard to collector performance. The major difference in the test results is that the greater amount of reradiation loss from a nonselective absorber causes losses in the collector to be a greater factor at much lower temperature differentials. As can be seen from Figure 54, unlike the case for the selective absorber, the performance of the glass/Tedlar cover and the single Lexan cover is not better than the two-glass cover, even at low fluid inlet temperatures, although they both have higher transmission factors. The one-glass cover, on the other hand, has better performance than the two-glass cover. The apparent explanation here is that the glass is opaque to infrared and therefore provides a greater greenhouse effect and reduces the losses. However, at low operating temperatures, one sheet of glass is about as effective as two sheets, and its transmission is significantly greater, giving better performance.

The higher operating temperature testing shows essentially the same phenomena, although here, the one cover-two cover difference in reducing losses is great enough to overcome the improved transmission of one cover versus two covers.

A final point in connection with these last four figures is the performance of the two AR (antireflection surface etched) glass cover. Figure 56 illustrates the impact of using AR glass for the collector cover. The transmission of the glass is improved to the extent that two sheets of AR glass still yields a higher effective transmission than one sheet of ordinary glass. Combining this high effective transmission with the reduction in convection losses available from using two sheets of glass results in the best performing cover configuration independent of absorber material or operating conditions. A description of the glass etching process is included in Appendix E.

The full performance curve generated for each combination of cover and absorber tested is included herein as Figures 57 through 68. They allow comparison of the various combinations of operating points other than those already presented. The actual test data taken to generate these performance curves, as well as the baseline testing, are presented in Appendix C.

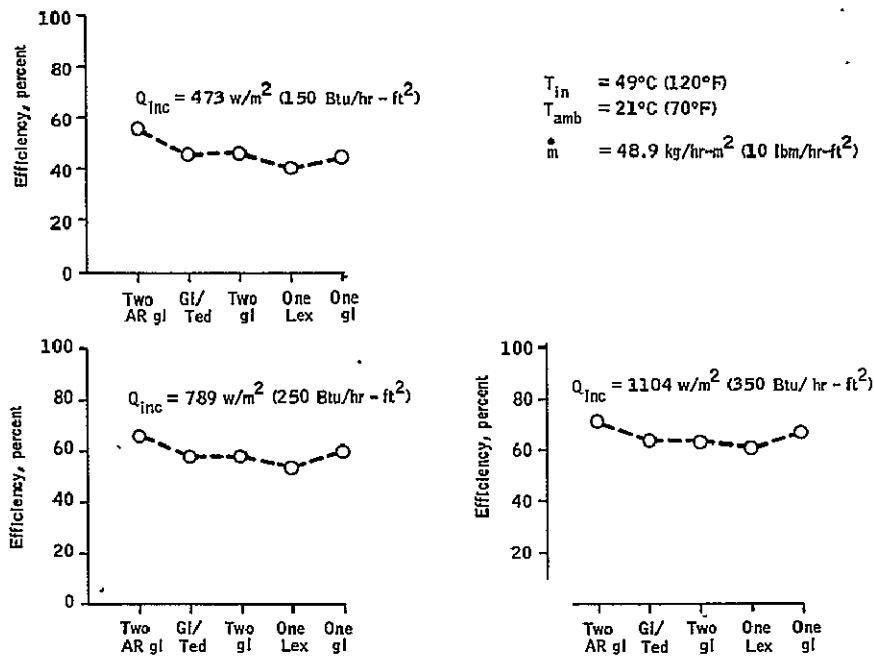


Figure 54. Cover Comparison for Collectors with Black Painted Aluminum Absorbers - Low-Temperature Operation

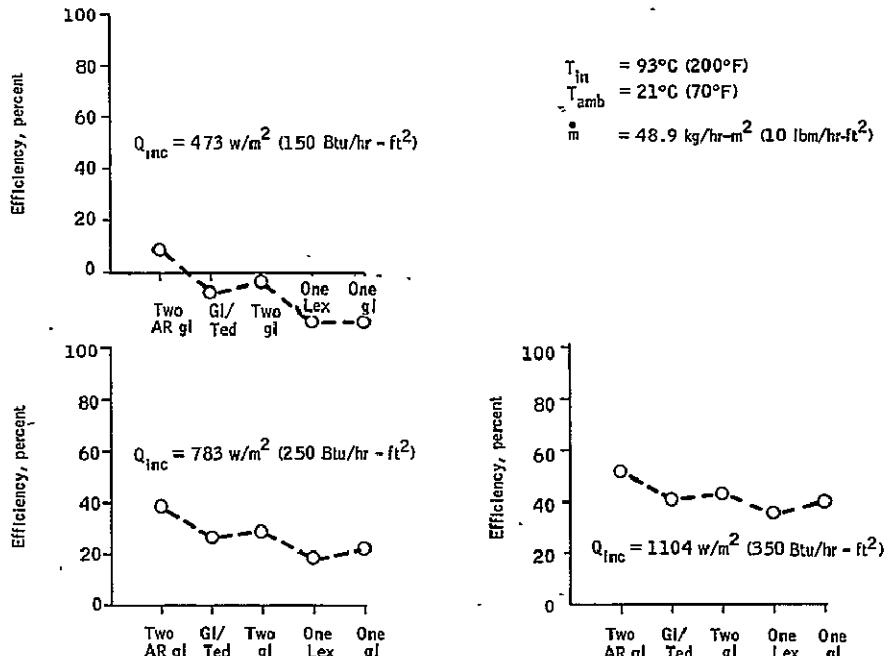


Figure 55. Cover Comparison for Collectors with Black Painted Aluminum Absorbers - High-Temperature Operation

ORIGINAL PAGE IS
OF POOR QUALITY

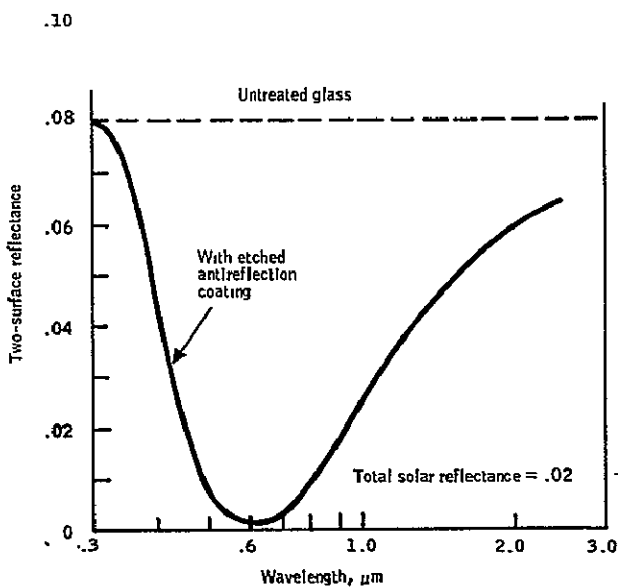


Figure 56. Comparison of Reflectance of Plain Glass and AR Etched Glass

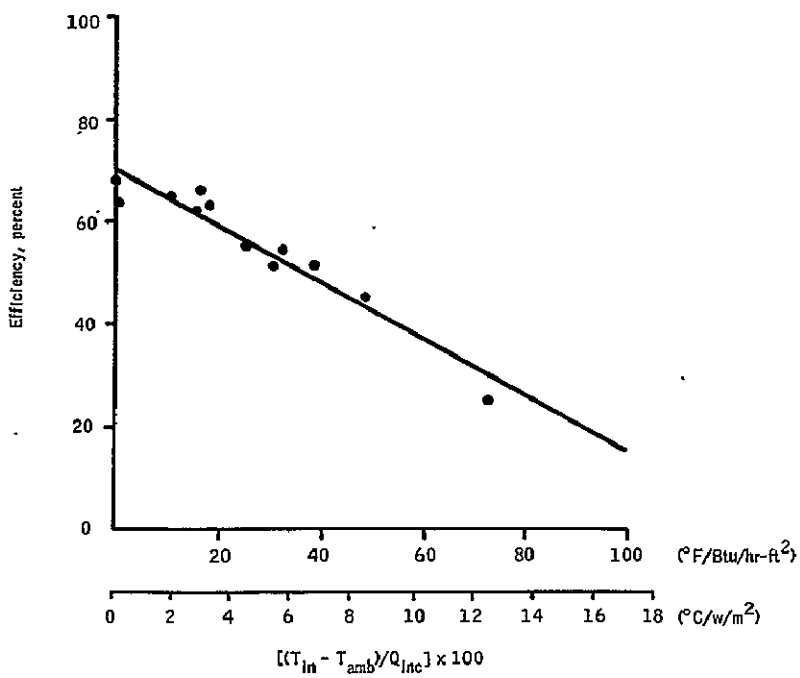


Figure 57. Performance Curve for Black Nickel/Aluminum/2 Plain Glass Covers

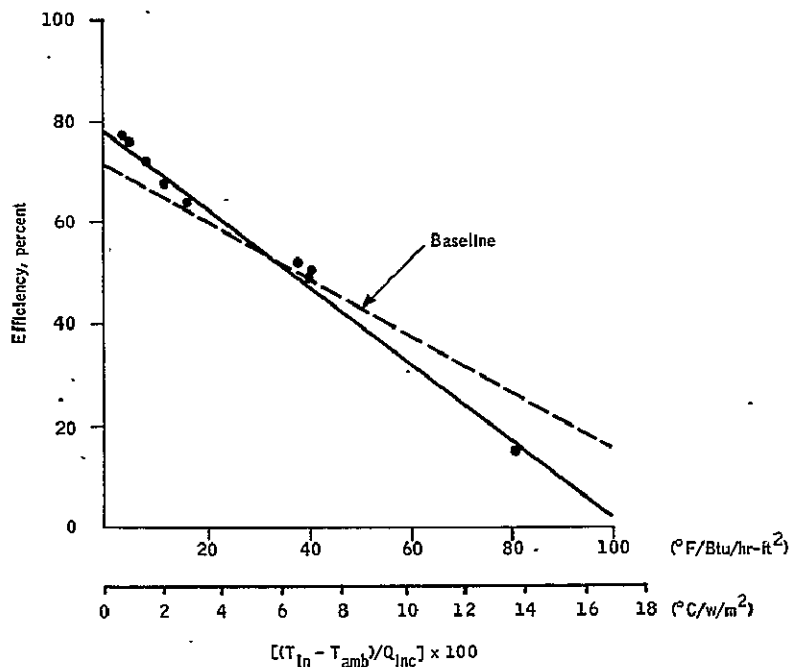


Figure 58. Performance Curve for Black Nickel/
Aluminum/1 Plain Glass Cover

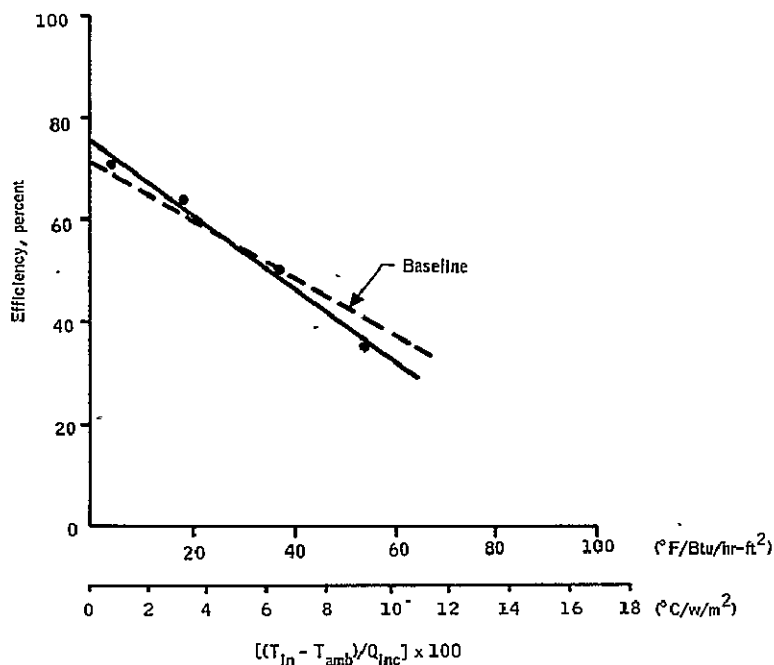


Figure 59. Performance Curve for Black Nickel/
Aluminum/1 Lexan Cover

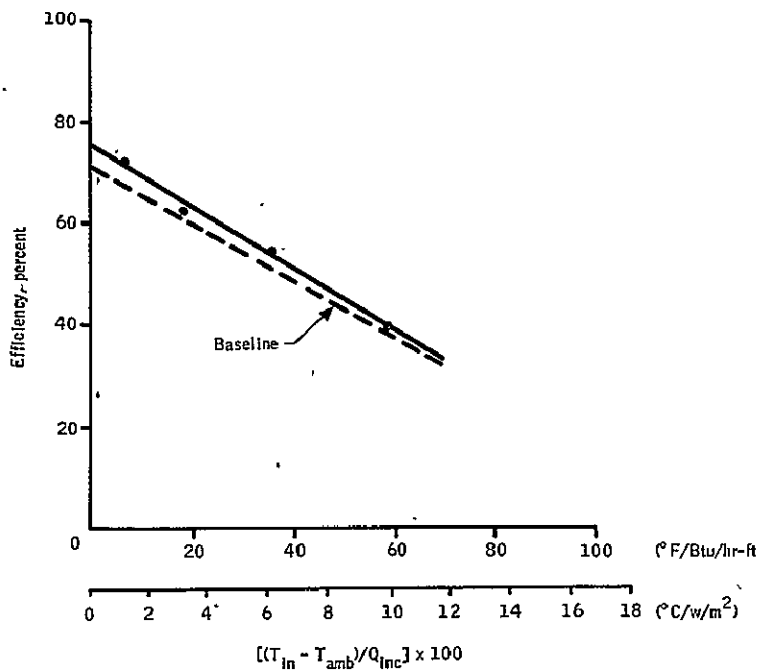


Figure 60. Performance Curve for Black Nickel/
Aluminum/Glass-Tedlar Cover

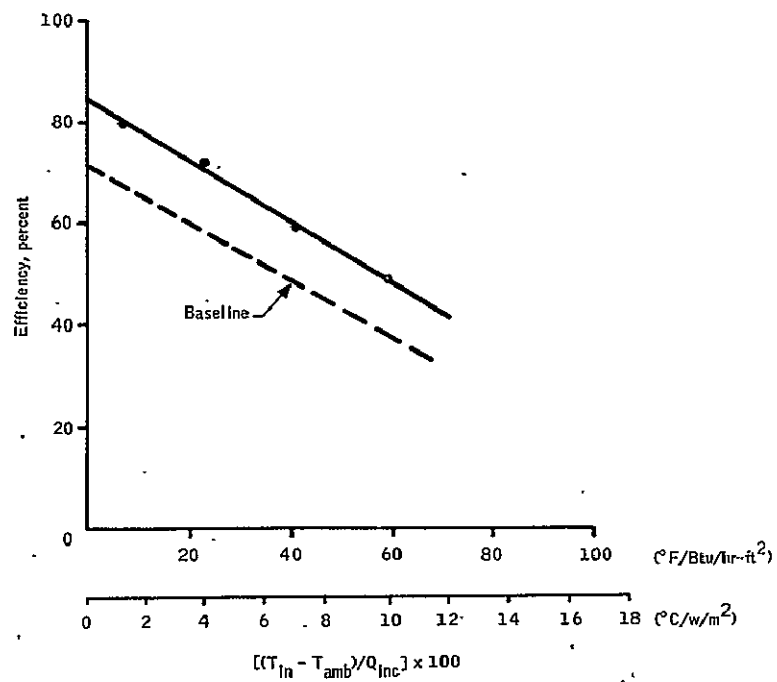


Figure 61. Performance Curve for Black Nickel/
Aluminum/2 AR Glass Cover

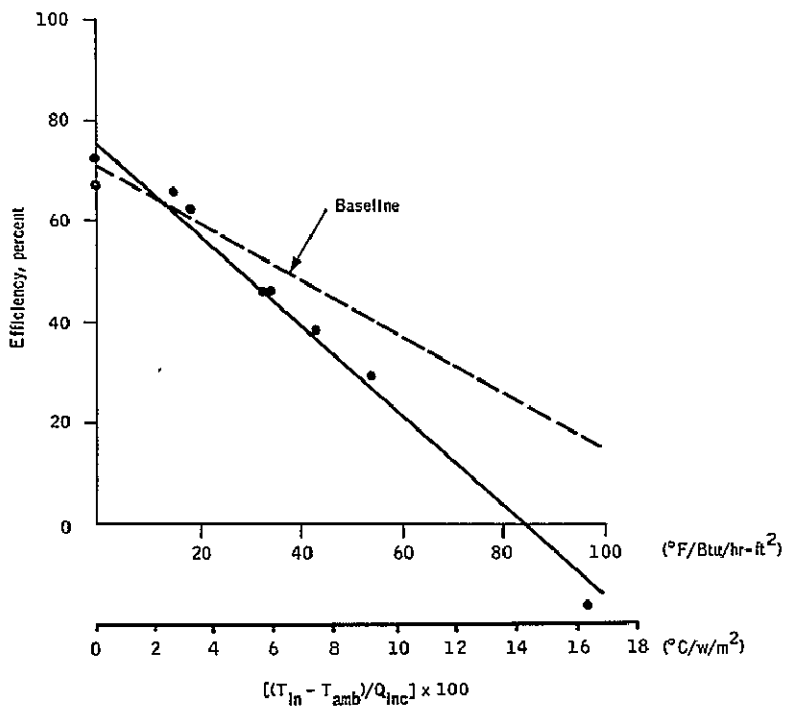


Figure 62. Performance Curve for Black Paint/
Aluminum/2 Plain Glass Covers

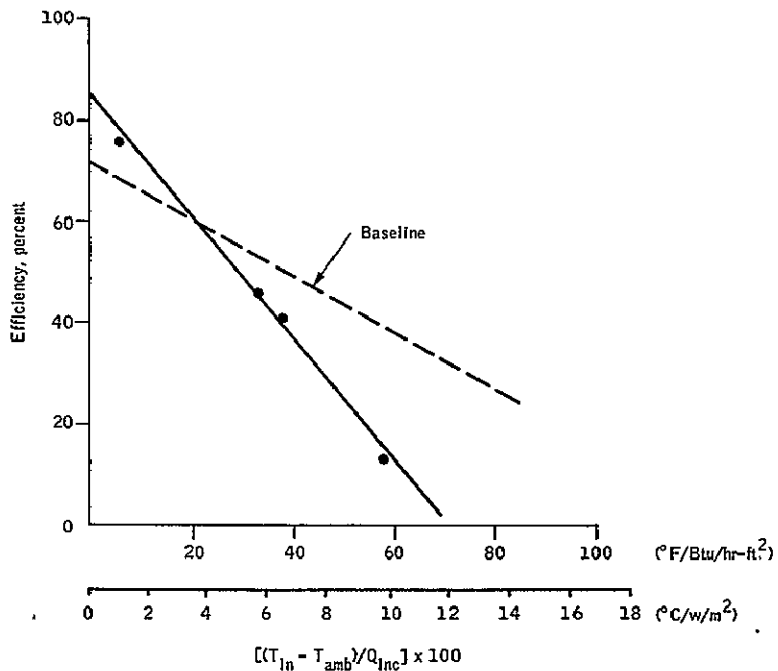


Figure 63. Performance Curve for Black Paint/
Aluminum/1 Plain Glass Cover

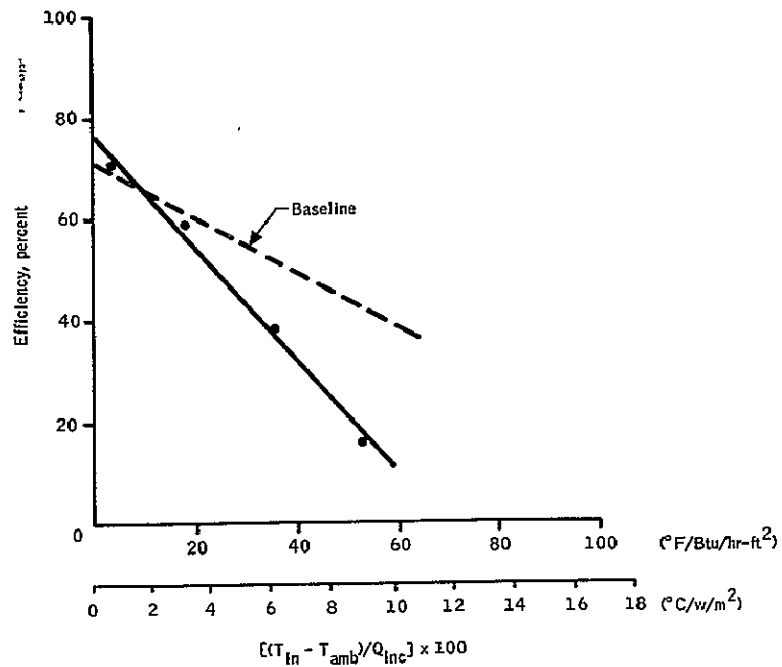


Figure 64. Performance Curve for Black Paint
Aluminum/1 Lexan Cover

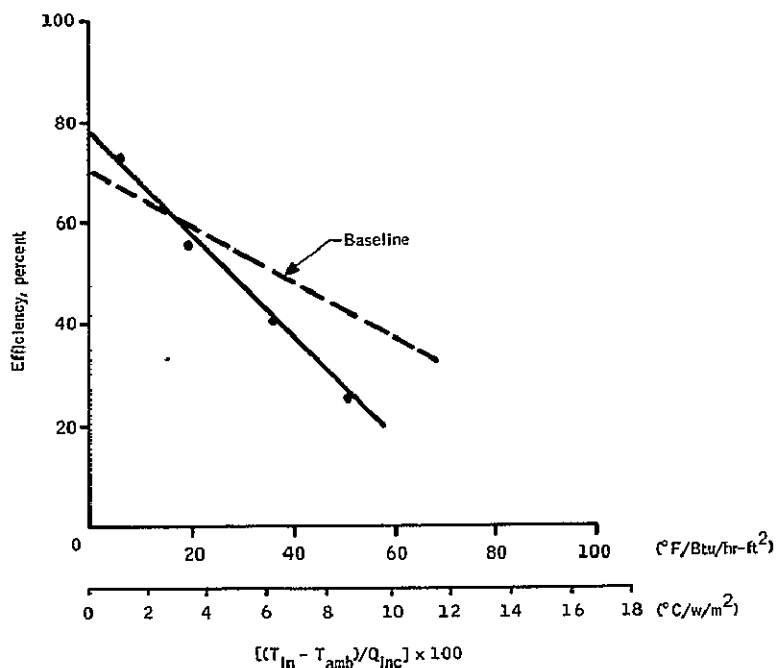


Figure 65. Performance Curve for Black Paint,
Aluminum/Glass-Tedlar Cover

ORIGINAL PAGE IS
OF POOR QUALITY

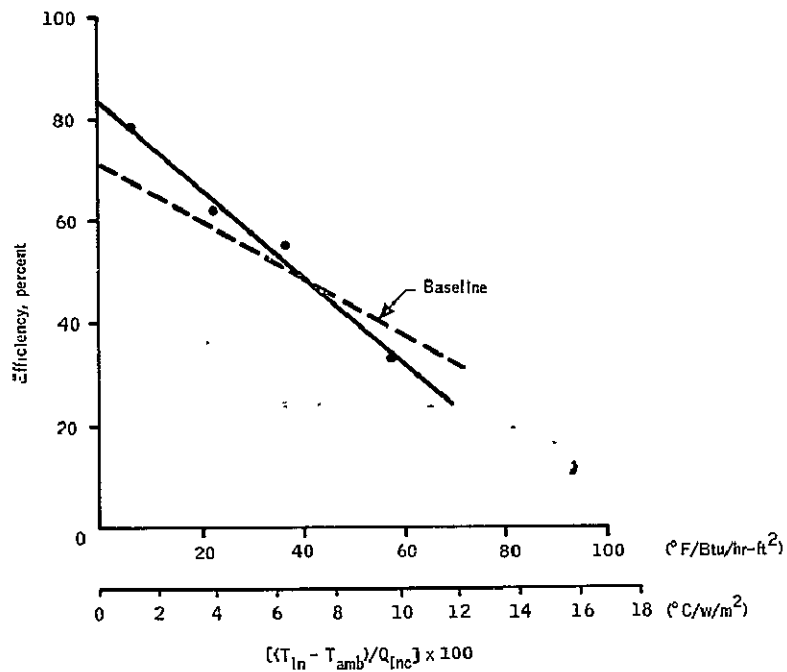


Figure 66. Performance Curve for Black Paint/
Aluminum/2 AR Glass Covers

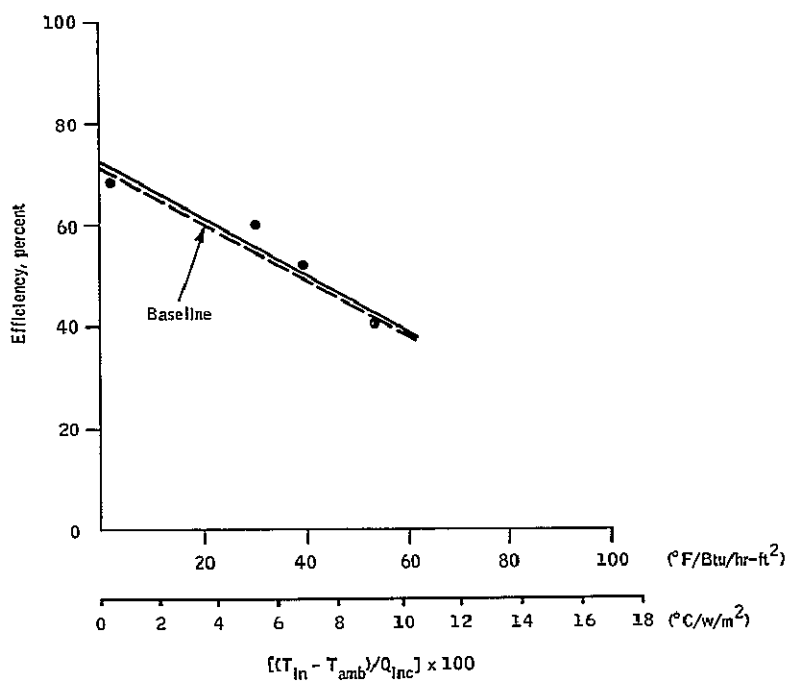


Figure 67. Performance Curve for Black Nickel/
Steel/2 Plain Glass Covers

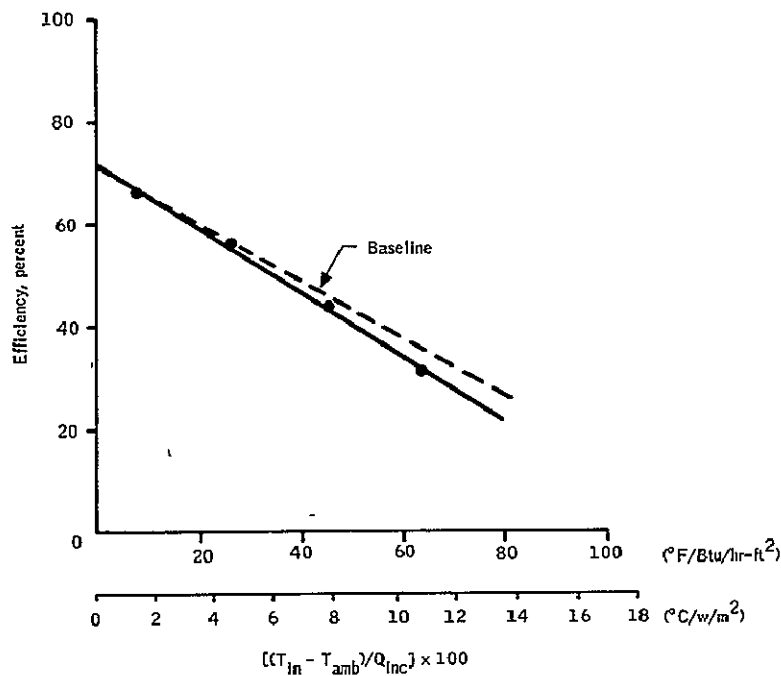


Figure 68. Performance Curve for Commercial Black Chrome/Steel/2 Plain Glass Covers

COMPARISON OF TEST RESULTS TO PREDICTED PERFORMANCE

The performance data obtained by testing with the solar simulator provides a means for establishing the degree of correlation between the analysis effort that guided the collector design and the actual performance of the resultant collector. The analytical predictions of performance can be compared with the empirical results for the baseline collector design, a collector with a nonselective absorber and two glass covers, a collector with a selective absorber and one glass cover, and a collector with a nonselective absorber and one cover.

The performance predictions generated during the analysis phase of the program utilized assumed values of component performance variables in determining the expected collector performance. Tests performed during the fabrication phase of the program indicated that some of these assumed values were not sufficiently accurate. The variation between assumed and actual values for the absorptance and emittance of the absorber coatings, both selective and nonselective, and the transmission factor of the glass used in the covers is tabulated below:

<u>Variable</u>	<u>Analytic assumption</u>	<u>Experimental value</u>
<u>Selective coating</u>		
α	0.90	0.94
ϵ	0.10	0.06
<u>Nonselective coating</u>		
α	0.90	0.97
ϵ	0.90	0.97
<u>Cover glass</u>		
τ	0.92	0.92

Attempts to correlate the performance predictions and actual test data must consider these variations in value.

The variation between experiment and analysis can best be seen by examining the graphs. Figures 69 through 72 present the comparison of the performance curves for the four collector designs considered in the analysis. Each performance curve is an equation of the form:

$$\eta = F_R \left[\alpha \tau_e - U_L \left(\frac{T_{in} - T_{amb}}{Q_{inc}} \right) \right]$$

where

- η = collection efficiency
- F_R = heat removal efficiency factor
- α = absorptance of absorber coating
- τ_e = transmission of cover system
- U_L = collector heat loss coefficient
- Q_{inc} = incident flux level
- T_{in} = fluid temperature at collector inlet
- T_{amb} = ambient temperature surrounding collector

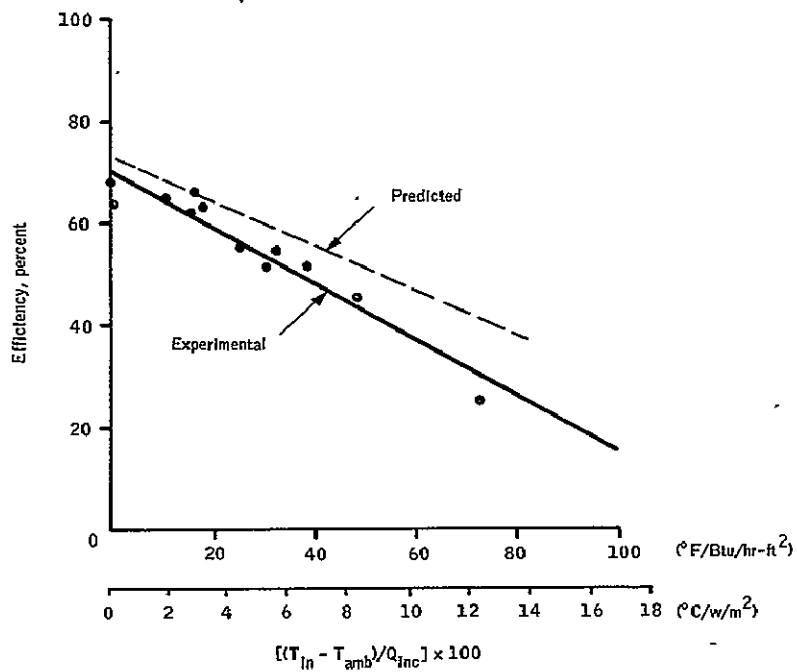


Figure 69. Comparison of Predicted and Test Results - Baseline Collector

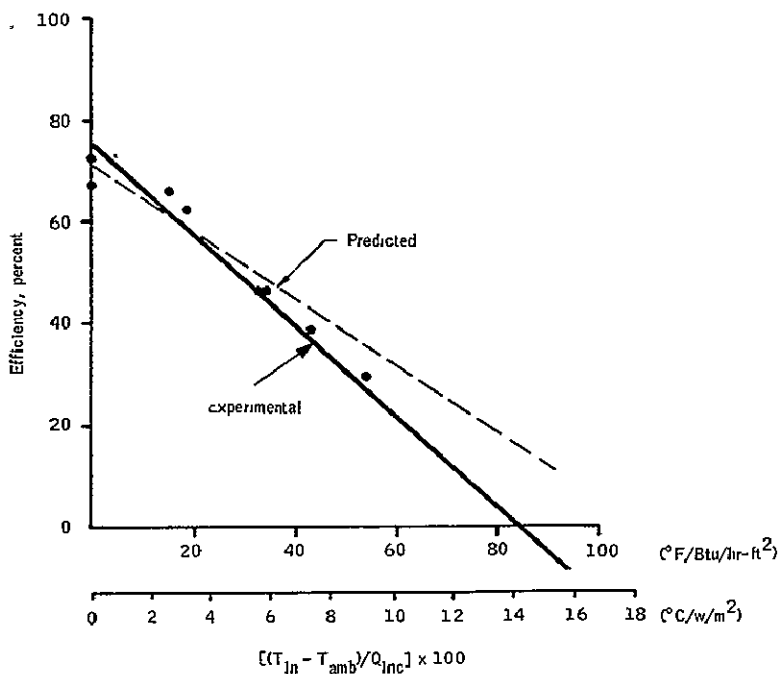


Figure 70. Comparison of Predicted and Test Results - Nonselective - 2 Plain Collector Glass

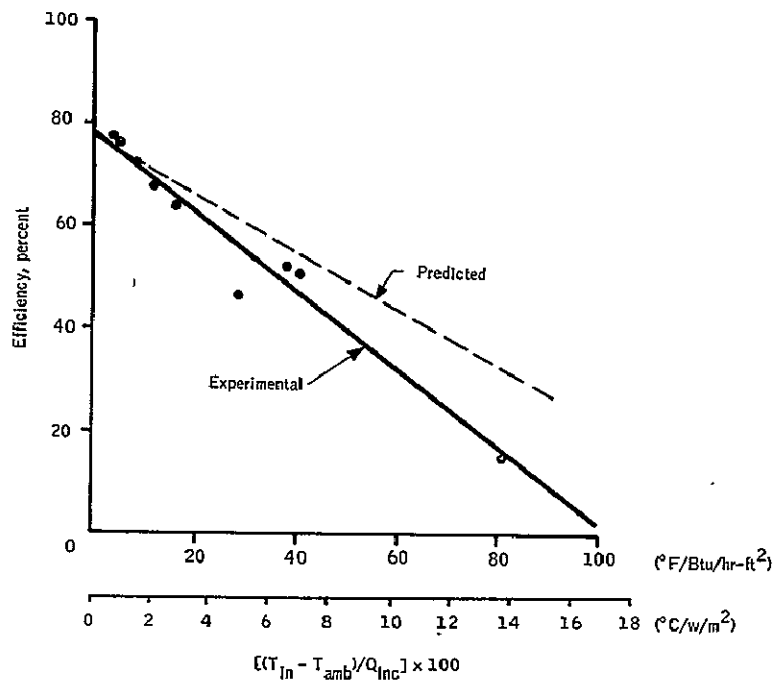


Figure 71. Comparison of Predicted and Test Results - Selective - 1 Plain Collector Glass

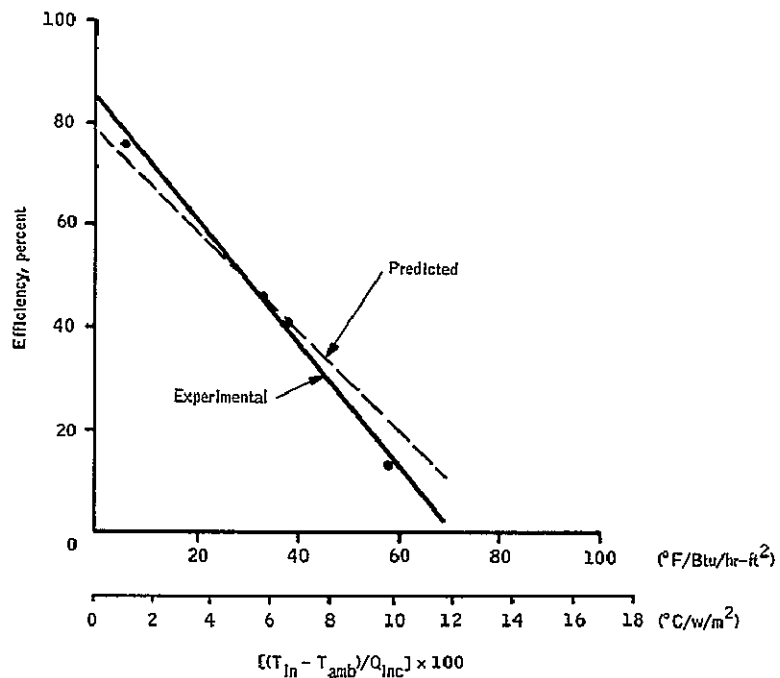


Figure 72. Comparison of Predicted and Test Results - Nonselective - 1 Plain Collector Glass

In graphical terms, $F_R\alpha\tau_e$ corresponds to the intercept on the ordinate and F_RU_L is the slope of the curve. Since the values of α and τ_e used in the analysis differ somewhat from the experimental, it is reasonable to expect imperfect correlation between the experimental and analytic values of $F_R\alpha\tau_e$; however, given the discrepancy in input values, the variation exhibited between experimental and analytic results probably provides a satisfactory degree of correlation. The values determined for F_RU_L , however, are consistently low in the analytic predictions.

To provide a more detailed examination of the differences between the analysis and the test results, Table 6 presents a comparison of the coefficients from the performance curves of the four collector configurations examined in the analysis section and their actual performance results from the testing done with the solar simulator.

The values are derived as follows:

$$F_R = \frac{\text{Intercept of performance curve}}{\alpha\tau_e}$$

$$U_L = \frac{\text{Slope of performance curve}}{F_R}$$

The transmittance, τ , of a single cover and the absorptivity, α , of the absorber panel are found experimentally. From these values, the product of $\alpha\tau_e$ can be found from the equation below⁽²⁾

$$\alpha\tau_e = \alpha \left[\tau^n + \left(\frac{1 - \tau_a}{C\alpha} \right) \right]$$

where

τ = single cover transmittance

n = number of covers

τ_a = transmittance of cover system, allowing for absorption losses only = $.99^n$, where n = number of covers

C = constant, a function of the number of covers*

By comparing the U_L values from the chart, it becomes obvious that the analysis has underestimated the heat losses from the collector.

*Number of covers	1	2	3	4
Value of C	4.6	3	2.7	2.6

TABLE 6.- COMPARISON OF PERFORMANCE COEFFICIENTS DERIVED FROM TESTING AND ANALYSIS

Collector configuration	Experimental result						Analytic prediction					
	Intercept	$\alpha\tau$	$\alpha\tau_e$	F_R	Exp. slope	U_L	Intercept	$\alpha\tau$	$\alpha\tau_e$	F_R	Anal. slope	U_L
Selective aluminum absorber with two glass covers (baseline collector)	0.74	0.80	0.80	0.93	0.57	0.63	0.74	0.73	0.77	0.96	0.44	0.46
Nonsselective aluminum absorber with two glass covers	0.80	0.82	0.83	0.96	0.94	0.98	0.74	0.73	0.77	0.96	0.68	0.71
Selective aluminum absorber with one glass cover	0.82	0.86	0.87	0.94	0.84	0.84	0.79	0.81	0.83	0.95	0.57	0.61
Nonsselective aluminum absorber with one glass cover	0.89	0.89	0.89	1.0	1.3	1.3	0.78	0.81	0.83	0.94	0.97	1.03

These results can be compared with typical values found in the literature. For a nonselective black panel with fluid bathing the entire black surface, Hottel and Whillier⁽²⁾ found $U_L = 1.2$ for a one-cover system and 0.7 for a two-cover system. Our analysis compares well for the two-cover system, but is quite low in comparison with their one-cover result.

OUTDOOR TESTING

Outdoor collector performance tests were conducted in Minneapolis. Two configurations, the baseline and the black-painted-aluminum absorber, two glass cover, were tested. The two collectors were operated simultaneously to allow direct performance comparisons to be made for the same conditions of solar flux, ambient environment, and inlet temperature. The outdoor tests also provided a means for correlating the solar simulator results with actual collector performance.

The outdoor test set-up is presented schematically in Figure 73 and photographically in Figure 74. As shown in Figure 73, fluid is supplied to the collectors using a constant head-tank type of flow loop similar to that used in the indoor tests. The ethylene-glycol/water mixture was pumped from the reservoir to the constant head tank. To help achieve the required inlet temperature, auxiliary heaters were placed in the flow line between the pump and the head tank. From the head tank, the fluid flowed through a conventional hot water heater and then through a constant temperature bath. A tee was used to direct the flow through each of the two collectors. Valves were placed downstream of the collector outlets to regulate the fluid flow. Return lines brought the fluid back to the reservoir to complete the cycle.

Mixing cups were placed at the inlet and outlet of each collector. These contained both thermocouples to measure inlet and outlet temperatures, and five junction thermopiles to give a more accurate measurement of the temperature difference across the collector. Another thermocouple with wind and radiation shield was used to measure the ambient temperature. Iron-Constantan thermocouple wire was used. These temperatures were recorded both continuously on a multipoint chart recorder and at 15-minute intervals using a digital multimeter.

The fluid in the return line could be directed into a beaker to determine the flow rate. Using a 1000-ml graduated cylinder and a stop watch, the time to fill the cylinder can be checked and thus determine the flow rate. The flow rate was recorded at 15-minute intervals. To measure the incident solar radiation, an Eppley pyranometer was mounted between, and in the plane of, the two collectors. The flux was recorded continuously on a chart recorder and at 15-minute intervals on the digital multimeter.

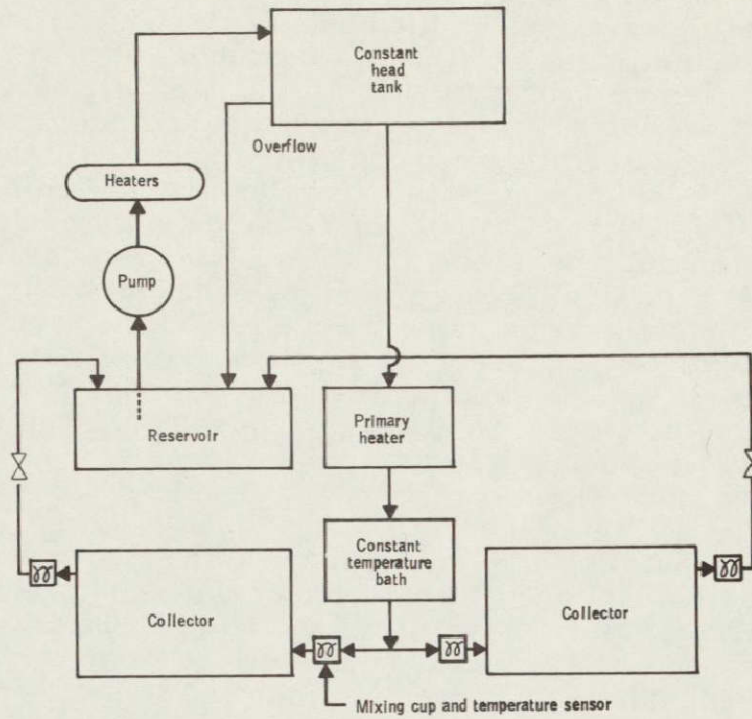


Figure 73. Schematic of Outdoor Test Setup

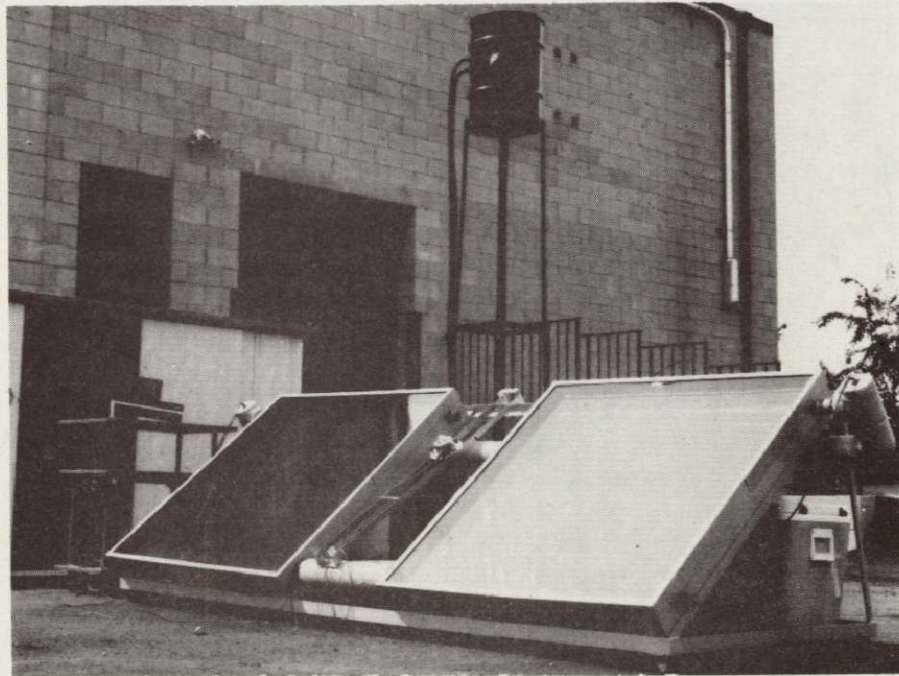


Figure 74. Outdoor Test Setup

The experiments were performed with the collectors facing south and with a tilt angle of 40 degrees from the horizontal. The collectors were operated with a constant mass flow rate of nominally 48.9 kg/hr-m^2 (10 lbm/hr-ft^2). The inlet fluid temperature was 82.2°C (180°F). Figures 75 through 83 present test results for typical days representing clear, partly cloudy, and cloudy conditions. Each figure includes five plots: (1) the instantaneous solar flux incident on the collector; the heat flux actually collected at each corresponding instant of time for both the (2) selectively coated (S), and (3) nonselectively coated collectors; and the simulator empirically predicted flux collected by the (4) selectively coated, and (5) nonselectively coated collectors. The predictions are made using the measured incident flux, inlet temperature and ambient temperature, and the linear correlations for the collector performance as measured using the solar simulator. All the data are plotted as a function of time of day (CDT). Typical wind velocity and the ambient temperature at noon are listed in the figures to give an indication of the environmental conditions.

It was common that the fluid temperature in the test system reservoir would drop during the night and an hour or more of startup time was required before the inlet fluid temperature reached the nominal 82°C condition. During the startup, the collectors were used to add energy to the system and their heat output recorded. These data are also included in Figures 75 through 83.

Test results obtained on six relatively clear days are shown in Figures 75 through 80. The results verify that there is a significant difference between the performance of the two collectors. The correlation between the empirical results, based on the simulator tests and the outdoor tests, is seen to be reasonably good. In most cases, the two agree to within less than 10 percent.

The effect of the morning startup is apparent in the data. During this period it is seen that less heat is going into the collector fluid than is predicted by the steady-state simulator empirical calculation. The difference, of course, is the heat required to raise the collector temperature.

The data in Figure 81 were obtained on a partially cloudy day. In this case, as before, the correlation between the indoor and outdoor results is seen to be good. The differences, neglecting the startup period, are less than 10 percent. It is also observed that the two collectors tested responded rapidly to the variations in flux conditions. The data taken on cloudier days, Figures 82 and 83, also show the rapid response to sudden flux change. This is particularly apparent in Figure 82 where between 1:00 and 1:45 p.m., a cloud passed over, and the flux dropped suddenly from 984 w/m^2 (312 Btu/hr-ft^2) and just as suddenly rose to 1072 w/m^2 (340 Btu/hr-ft^2). Both collectors are seen to have followed this change with a time lag of less than 10 minutes.

The actual test data for the outdoor testing are presented in Appendix C.

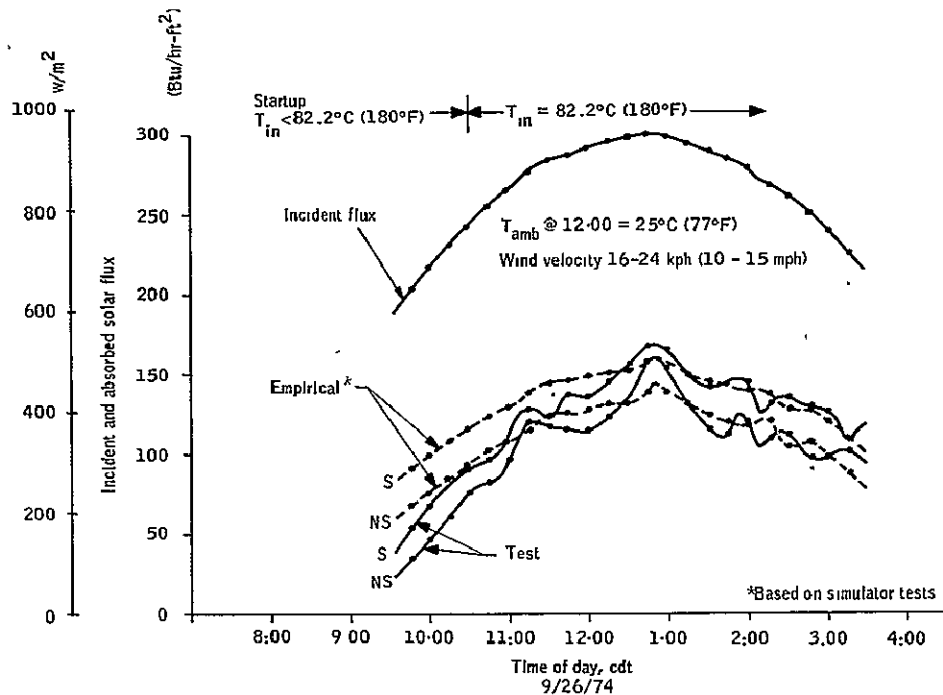


Figure 75. Outdoor Tests Results--9/26/74

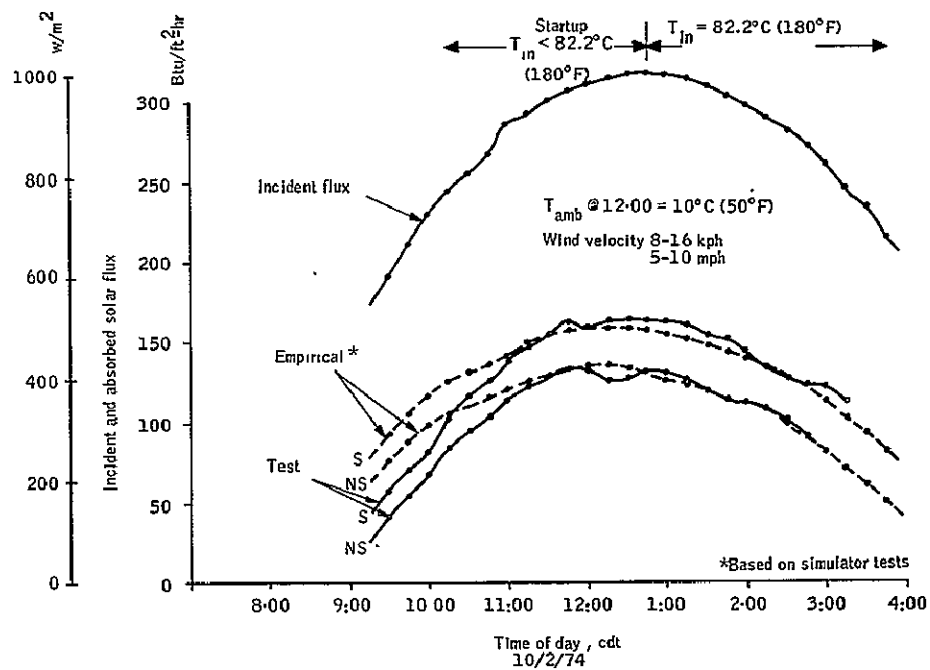


Figure 76. Outdoor Test Results--10/2/74

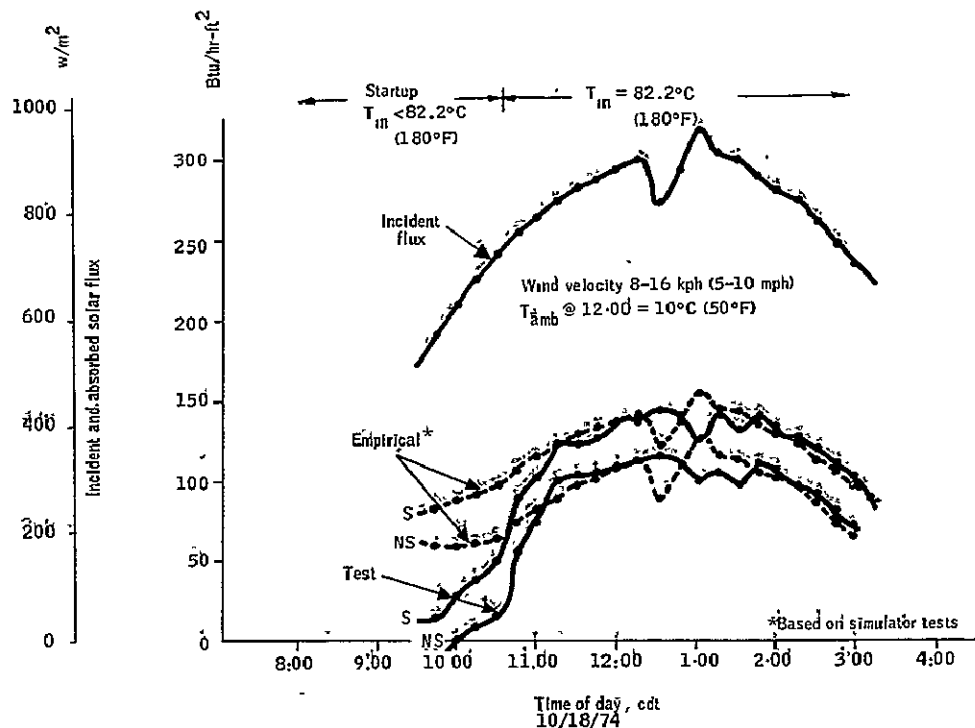


Figure 77. Outdoor Test Results--10/18/74

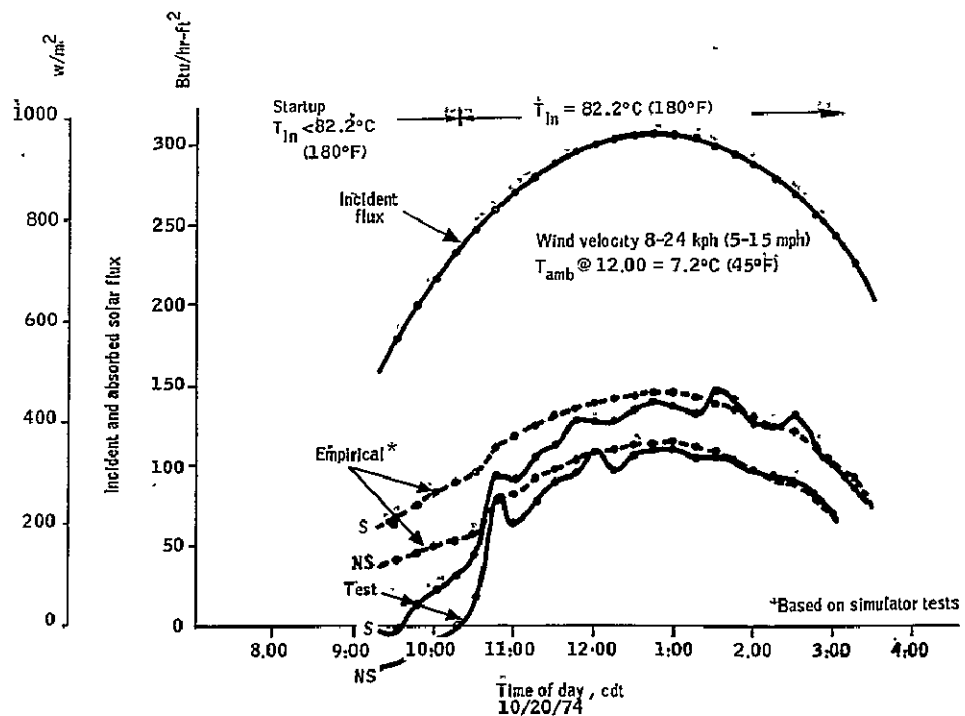


Figure 78. Outdoor Test Results--10/20/74

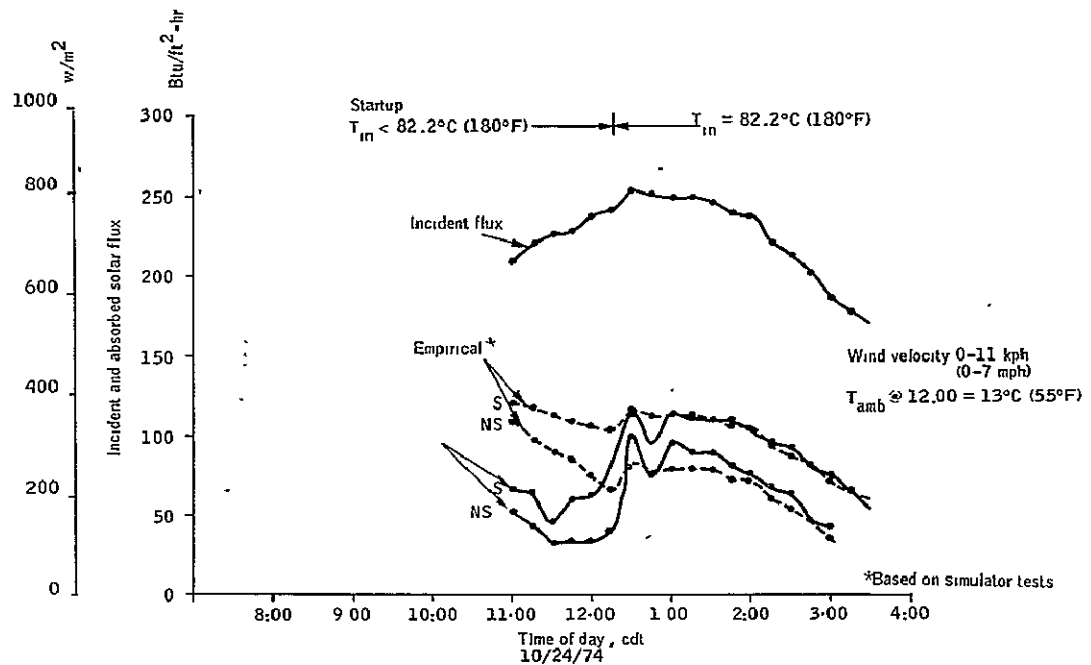


Figure 79. Outdoor Test Results--10/24/74

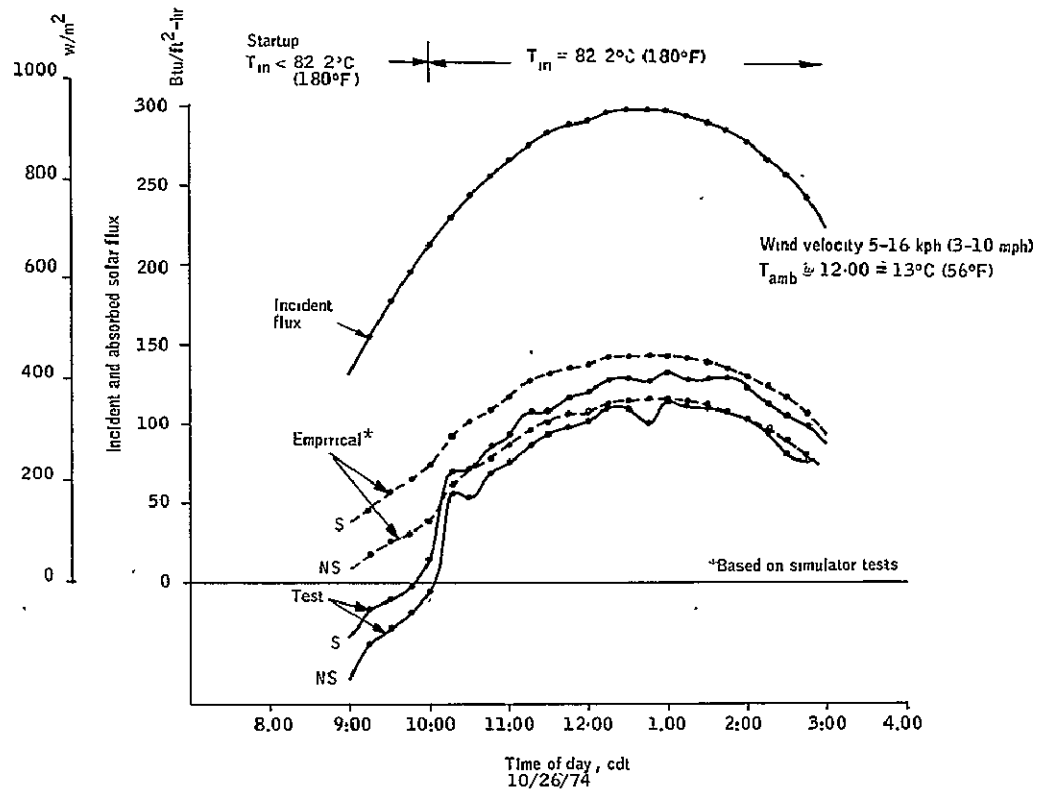


Figure 80. Outdoor Test Results--10/26/74

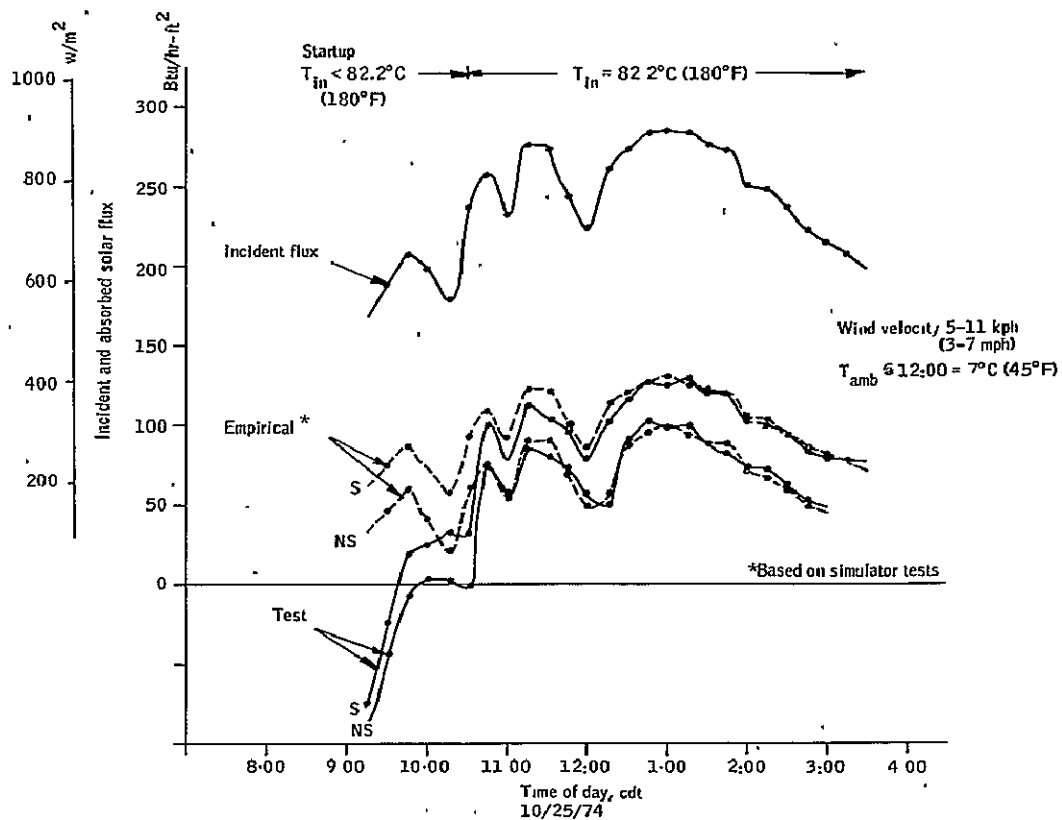


Figure 81. Outdoor Test Results--10/25/74

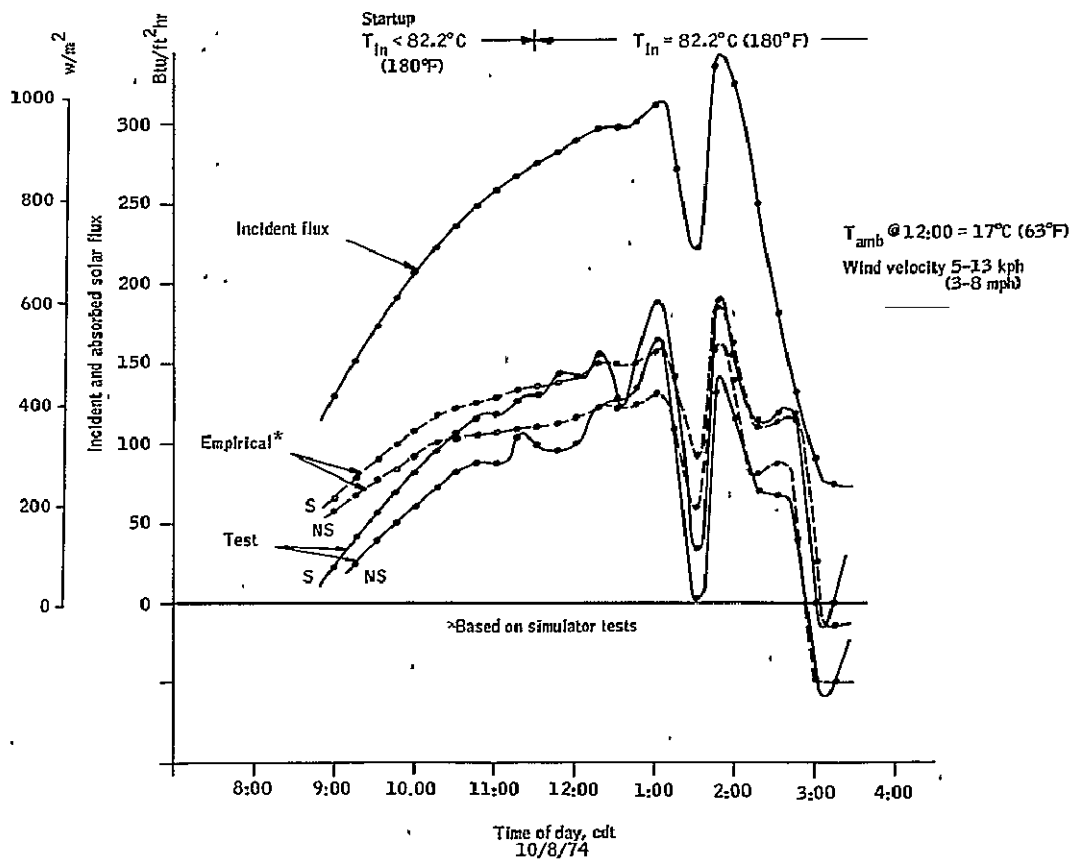


Figure 82. Outdoor Test Results--10/8/74

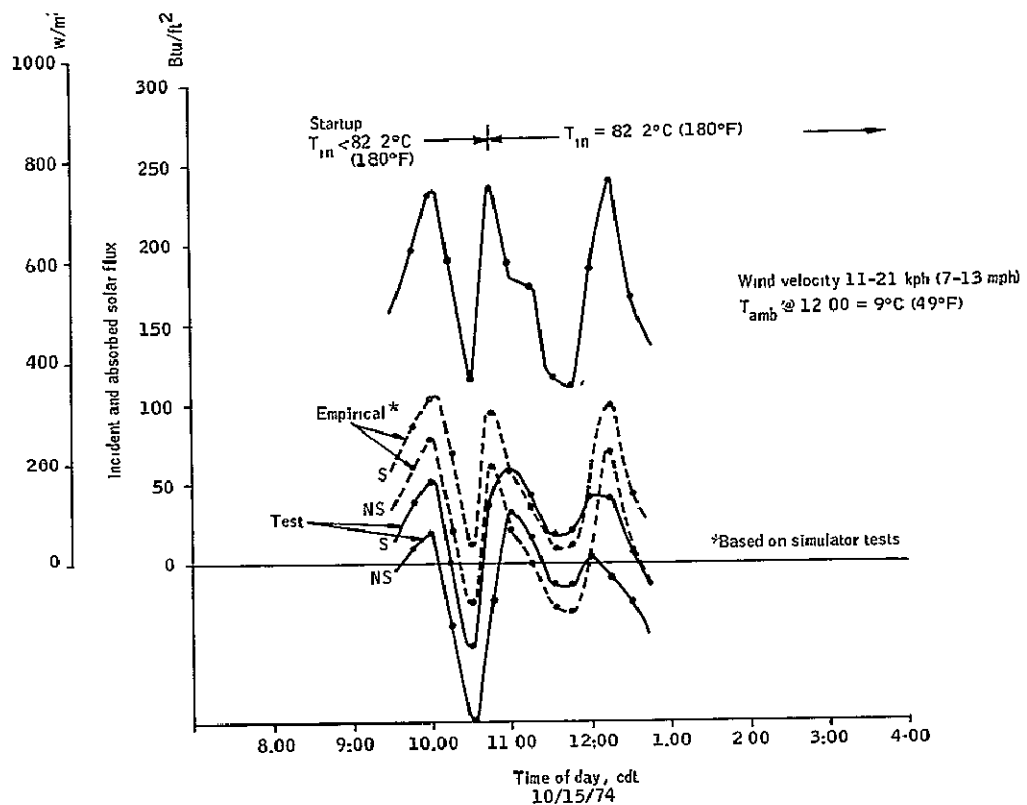


Figure 83. Outdoor Test Results--10/15/74

COST ANALYSIS

Costs associated with the fabrication of the baseline collector today are obviously not representative of what may be expected should the baseline design ever reach mass production. In fact, the baseline design itself may not be totally representative of the collectors that would be fabricated in a production mode.

During the program certain desirable design considerations became obvious and should be mentioned. The initial choice of collector envelope was a box 1.22 m x 1.22 m x 15 cm (4 ft x 4 ft x 6 in.). This choice gave rise to several fabrication difficulties. The maximum standard width for sheet steel presently available is 122 cm (48 in.); thus, we were unable to benefit from the cost advantages of a one-piece folded box and were forced to a three-piece box. [It is recognized that sheet steel is manufactured in widths up to 198 cm (78 in.) wide, but these widths are only available on special order, in large quantity and at a premium price.] Furthermore, the completed collector is too large for one man to carry comfortably, yet not heavy enough to require two men to lift it.

Physical size considerations also affected the absorber panel. The absorber panel selected for the baseline collector was an aluminum roll-bonded panel produced by Olin Brass. The maximum panel width presently

available is 91 cm (3 ft). To produce a 122-cm (4-ft) panel, we trim two panels down to 61 cm (22 in.) wide each, and then heliarc weld the two trimmed panels together. Obviously, this approach is not cost effective.

The choice of aluminum for the absorber panel also presented some definite drawbacks. In addition to the major question of corrosion, which has not yet satisfactorily been investigated, aluminum requires extensive surface preparation (Zincate and Copper processes) before applying the bright nickel-Black-Nickel selective coating. A steel absorber panel, on the other hand, requires only a mild surface cleaning before bright nickel-Black Nickel plating; and the steel absorber panel can be made in a four-foot width.

Because a production mode collector likely would adopt at least the size change recommendation, the cost analysis has been performed on a 91 cm x 122 cm (3 ft x 4 ft) collector of the baseline design configuration.

The fabrication of small quantities of collector, say 46.5 to 139.4 m² (500 to 1500 ft²), would remain much the same process as that for those built during the program: the sheet metal piece parts -- including the three-piece welded box, cover support frame, welded cover spacer frame, and collector top cover -- would be built or procured as a box subassembly. The box subassembly would be treated with a chromide rust inhibitor and then painted. Insulation would be cut to fit the bottom and sides of the box subassembly. Formed aluminum pipe would be welded to the aluminum absorber panel, and the completed absorber panel would then be zincate processed and Black Nickel coated. The coated absorber panel would be mounted on its standoffs in the box assembly, the cover support frame added to the top of the box, the glass-spacer-glass sandwich laid on the support frame, and the top covers fastened on.

Figures 84 through 87 illustrate steps in the assembly process.

Figure 84 shows the materials gathered before start of assembly. The coil of thermocouple wire is for instrumentation purposes only.

Figure 85 shows the insulation being added to the box. Note that the standoffs are installed at this time.

Figure 86 shows the installation of the absorber panel. The U-shaped channels for the absorber panel outlet tubes have been cut by this time. Collectors assembled later in the program had boxes with pre-cut outlet tube channels.

Figure 87 illustrates the assembly of the two-cover system. The cover support frame has already been installed on the top edge of the box, and the inner layer of glass has been laid in place. The assembler is now inserting the cover spacer frame and is about to apply the weather stripping before adding the second cover and top cover bracket. Note also that the heavy rubber gasket has been fitted around the outlet tube to prevent a thermal short to the box.



Figure 84. Collector Assembly (Prior to the Start of Assembly)



Figure 85. Collector Assembly (Adding the Insulation)

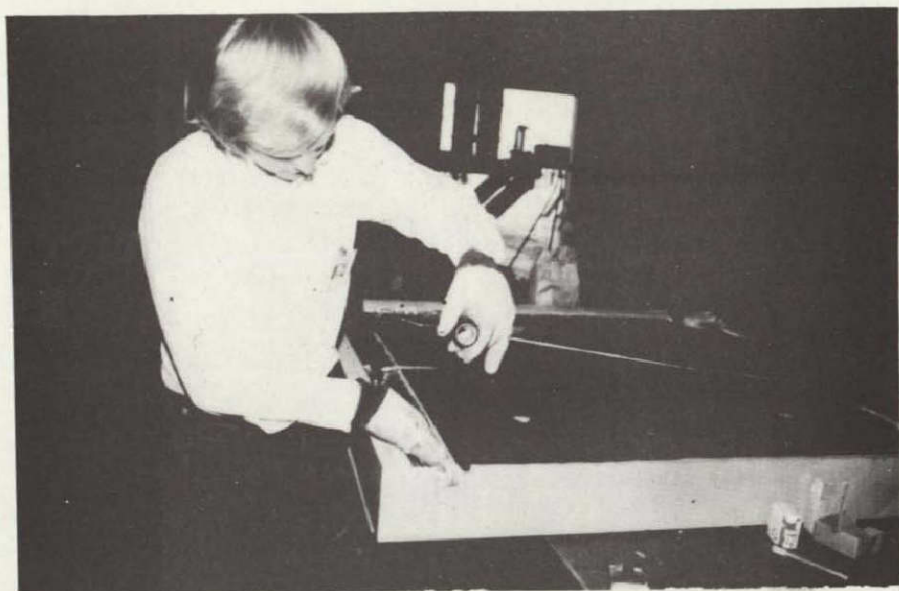


Figure 86. Collector Assembly (Installing the Absorber Panel)



Figure 87. Collector Assembly (Assembling the Cover System)

The costs associated with this present fabrication process for the base-line collector design configuration are presented as Table 7. The total presented in Table 7 includes material and direct labor costs but does not reflect the cost of assembly supervision, engineering support, material acquisition, or labor overhead. These additional costs would probably increase the manufacturer's cost to approximately \$323/m² (\$30/ft²).

In a limited mass production mode, i. e., production quantities of the order of 10,000 m²/yr (100,000 ft²/yr), costs may be reduced as shown in Table 8. These costs are total factory cost and do include factory overhead, but do not provide for engineering support.

This analysis includes another recommended design change: the substitution of a two-piece welded steel absorber. This change would enable the manufacturer to produce the absorber panels in-house and realize the attendant production economies, rather than procuring the absorber panels from an aluminum supplier. This change in design does not compromise collector performance in that the simulator testing has shown the steel absorber panel to be at least as efficient as the aluminum absorber panels, and perhaps somewhat better. The flow tube spacing, of course, must be modified to compensate for the change in material.

The estimated cost of the selective coating is also reduced by using a steel substrate. This approach enables the use of a bright nickel-Black Nickel coating. An aluminum absorber, however, requires a zincate-copper-bright nickel-Black Nickel process. These additional processing steps more than double the estimated cost. Table 8 presents the estimated limited mass production cost with both the aluminum absorber panel and the proposed steel absorber panel.

The estimated cost for limited mass production quantities of the alternate configurations evaluated during the test program can be determined by pricing out the component changes. Table 9 lists the estimated component costs for limited mass production quantities.

As an example of the use of this figure: To determine the cost of a collector with a nonselective steel absorber and two AR glass covers, take the \$50.70/m² (\$4.71/ft²) cost of the baseline steel collector; (1) subtract the 15 percent scrap and salvage, leaving \$44.24/m² (\$4.11/ft²), (2) subtract \$3.23/m² (\$0.30/ft²) for the difference between a selective and a nonselective absorber coating, leaving \$41.01/m² (\$3.81/ft²), (3) add on the \$8.61/m² (\$0.80/ft²) difference between two plain glass and two AR glass covers, leaving \$49.62/m² (\$4.61/ft²), and (4) add on 15 percent scrap and salvage, making a total of \$58.02/m² (\$5.39/ft²).

The other configurations considered during the course of the test program have been priced out by the technique of using the baseline collector design cost from Table 8 and adding in the component cost changes from Table 9. The results are shown in Table 10. This figure again presents comparative costs with both a steel and an aluminum absorber panel.

TABLE 7. - BASELINE COLLECTOR DESIGN
PRESENT FABRICATION COST

Component/process	Cost (dollars)
Box subassembly	31.00
Chromide treatment	3.00
Painting	5.00
2 glass layers	9.00
Insulation	7.00
Standoffs (4)	2.00
Aluminum absorber	25.00
Connectors (installed)	20.00
Zincate - Black Nickel coating	45.00
Assembly labor (4 hours)	30.00
Leak check	6.00
Packing	5.00
Total	188.00 per collector 168.68/m ² (15.67/ft ²)

TABLE 8. - BASELINE COLLECTOR DESIGN FABRICATION
COSTS WITH LIMITED MASS PRODUCTION

Component/process	Cost (dollars)	Cost (dollars)
Box	8.28	
Covers	12.12	
Insulation	3.72	
Standoffs	1.68	
Absorber	12.36 (steel)	14.04 (alum)
Selective coating (bright Ni/Black Ni)	4.80 (on steel)	12.96 (on alum) Zincate/Br Ni/Bl Ni
Assembly labor	6.36	
Scrap and salvage (15%)	7.20	8.87
Total	56.52 (4.71/ft ²) 50.70/m ²	68.03 (5.67/ft ²) 61.03/m ²

TABLE 9. - ESTIMATED COMPONENT COST WITH LIMITED MASS PRODUCTION

Component/process	Cost (dollars)	
	\$/m ²	\$/ft ²
Tempered glass cover	4.31	0.40
Tedlar cover	1.08	0.10
Lexan cover	9.15	0.85
AR glass cover	8.61	0.80
Cover frame (1 or 2 covers)	2.26	0.21
Black Nickel coating on steel	4.31	0.40
Black Nickel coating on aluminum	11.63	1.08
Nonselective (paint)	1.08	0.10
Black chrome coating on steel	4.84	0.45
Black chrome coating on aluminum	12.16	1.13
Absorber panel - steel	11.09	1.03
Absorber panel - aluminum	12.59	1.17

TABLE 10. - COMPARATIVE COST OF VARIOUS COLLECTOR DESIGN ITERATIONS

Configuration	Cost (dollars) with steel absorber			Cost (dollars) with aluminum absorber		
	\$/m ²	\$/ft ²	Δ Cost, percent	\$/m ²	\$/ft ²	Δ Cost, percent
Baseline (Black Ni - 2 glass)	50.70	4.71		61.03	5.67	
Black Nickel - 1 glass	45.96	4.27	- 9.3	56.08	5.21	- 8.1
- Glass/Tedlar	47.15	4.38	- 7.0	57.27	5.32	- 6.2
- 1 Lexan	51.45	4.78	+ 1.5	61.68	5.73	+ 1.1
- 2 AR glass	60.80	5.65	+19.9	70.94	6.59	+16.2
Nonselective - 2 glass	47.15	4.38	- 7.0	48.87	4.54	-10.9
- 1 glass	42.20	3.92	-16.8	43.42	4.08	-28.0
- Glass/Tedlar	43.49	4.04	-14.2	45.21	4.20	-25.9
- 1 Lexan	47.79	4.44	- 5.7	49.52	4.60	-18.9
- 2 AR glass	57.05	5.30	+12.5	58.77	5.46	- 3.7
Black Chrome - 2 glass	51.45	4.78	+ 1.5	61.68	5.73	+ 1.1

Based on the results from Table 10, the least costly collector design is a collector with a nonselective steel absorber and one plain glass cover; however, this conclusion is deceptive as it does not consider the improvement in collection performance obtaining by adding the various component changes. The additional factor of collector performance enables the computation of an effective cost for a flat plate collector. This means that the increased cost of each component change must produce at least an equivalent increase in collection efficiency, assuming that the objective of a particular component change is not the resolution of some particular constraint, such as limited space availability, or perhaps maximum acceptable cost per unit area.

Table 11 presents a comparison of the cost effectiveness of the collector design configurations evaluated during the course of the program. Cost effectiveness here is calculated by computing the ratio of cost per unit area and collection efficiency for each collector design configuration and then comparing it to the value determined for the baseline collector design configuration. The cost values used here are for the limited mass production quantity of 9300 m² (100,000 ft²). In keeping with the previous cost analysis figures, Table 11 presents collectors with both a steel and an aluminum absorber. Based on this figure, one may conclude that the most cost-effective collector design is actually a collector having a selectively coated steel absorber panel and a two-cover system consisting of a plain glass outer cover and a Tedlar inner cover.

It should be noted that the collection efficiency value, η , used in Table 11 was calculated for a specific set of input conditions; a temperature differential between the fluid inlet and ambient, ΔT , of 67°C (120°F), a tilt angle of 40° and an incident flux level of 789 w/m² (250 Btu/hr-ft²), normal to the collector surface. The actual value of η was determined from the performance lines established by testing with the solar simulator.

Use of a single-point collection efficiency may also be deceptive in calculating cost effectiveness. Instead of determining collection efficiency at a single design point, it may be more accurate to integrate the heat flux gathered over an operating day and compare it to the integrated insolation level for that day. Table 12 presents this type of cost-effectiveness analysis for two typical clear operating days. The insolation curves and the resultant collected flux levels for three collector design configurations are presented as Figures 88 and 89. Based on the analysis in Table 12, it again is obvious that the lowest cost collector is not necessarily the more cost effective. This analysis approach can be extended even further to bring in cloud cover, variable ambient temperature, and long-term collection intervals. Collection performance integrated over a calendar year is included as a subject of the utilization study in the next section of this report.

TABLE 11.- COST EFFECTIVENESS FOR VARIOUS COLLECTOR DESIGNS

Configuration	Cost effectiveness, dollars		η , percent (a)	$\Delta\eta$, percent
	steel	aluminum		
Baseline (Black Nickel - 2 glass)	1.00	1.00	44.5	
Black Nickel - 1 glass	1.03	1.01	41.5	- 6.7
- Glass/Tedlar	1.13	1.11	46.5	- 4.5
- 1 Lexan	0.92	0.92	41.5	- 6.7
- 2 AR glass	1.03	1.06	55.0	+23.6
Nonselective - 2 glass	0.80	0.93	33.0	-25.8
- 1 glass	0.72	0.83	26.5	-40.4
- Glass/Tedlar	0.79	0.91	30.0	-32.6
- 1 Lexan	0.55	0.64	23.0	-48.3
- 2 AR glass	0.85	0.99	42.5	- 4.5
Black Chrome - 2 glass	0.93	0.93	42.0	- 5.6

^a At 789 w/m^2 (250 Btu/hr-ft^2), $\Delta T = 49^\circ\text{C}$ (120°F), and tilt angle = 40° ,

$$\text{cost effectiveness} = \frac{\left(\frac{\text{Cost/area}}{\eta} \right)_{\text{Baseline}}}{\left(\frac{\text{Cost/area}}{\eta} \right)_{\text{Alternate configuration}}}$$

TABLE 12.- COST EFFECTIVENESS FOR VARIOUS COLLECTOR DESIGNS

Configuration/cost	η , percent (a)		Cost effectiveness, dollars	
	6/21	12/21	6/21	12/21
Black Nickel - 2 glass \$50.70/m ² (\$4.71/ft ²) steel \$61.03/m ² (\$5.67/ft ²) aluminum	39	29	1.00	1.00
Nonselective - 2 glass \$47.18/m ² (\$4.38/ft ²) steel \$48.87/m ² (\$4.54/ft ²) aluminum	27	15	0.74	0.56
Black Nickel - 2 AR glass \$60.82/m ² (\$5.65/ft ²) steel \$70.94/m ² (\$6.59/ft ²) aluminum	50	38	1.07	1.09
			1.10	1.13

^a Integrated over the solar day.

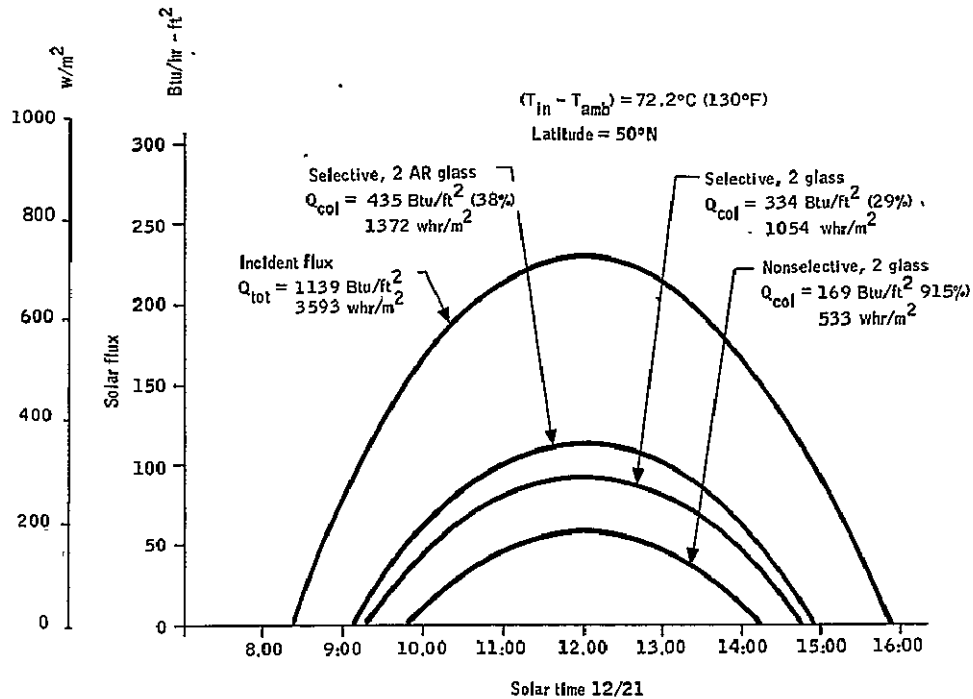


Figure 88. Collection Curves for a Clear Winter Day Insolation

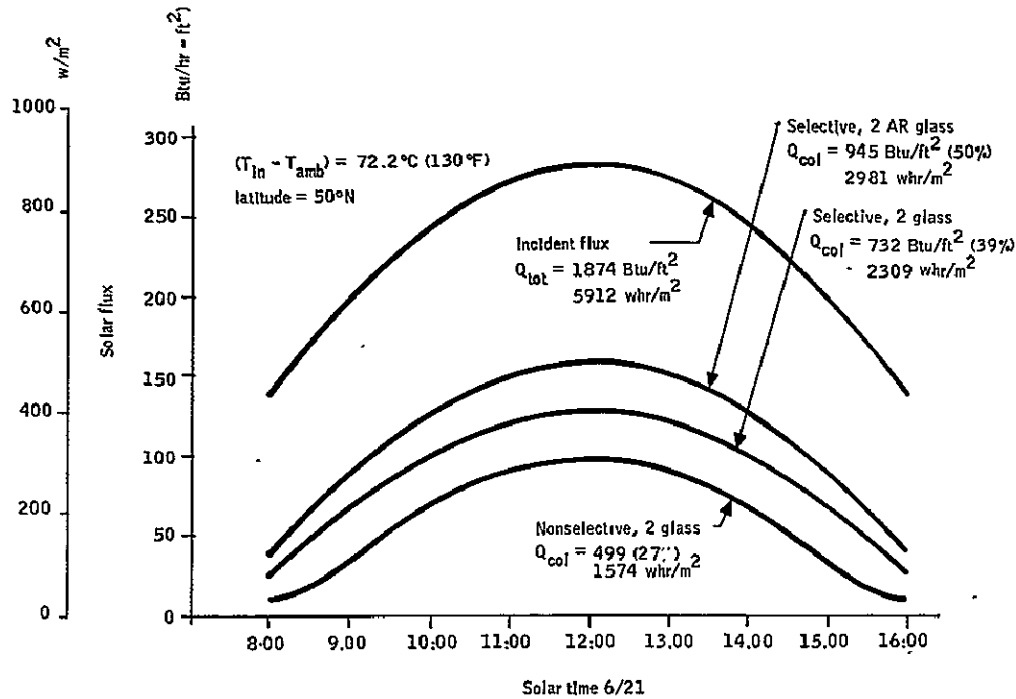


Figure 89. Collection Curves for a Clear Summer Day Insolation

UTILIZATION STUDY

Study Approach

Calculated collection efficiencies based on a given set of input parameters, or even integrated over a specified design day, may be misleading in terms of just how much a collector system will do to supply energy to a given load. Variations in the incident flux level due to clouds, haze, rain, etc., and the seasonal nature of the ambient temperature must be considered to produce a realistic picture of just how well a particular collector installation will perform. To interpret more accurately the effectiveness of the baseline collector design, the collected heat flux was calculated and totalled by month, over a full calendar year, for cities in nine geographic locations in the United States. The heating and cooling load for a typical residential installation was also calculated for the same locations throughout the year. The collected flux was then matched to the load to determine the degree to which a solar installation would satisfy the load. The ability to satisfy the load determines the degree of potential solar utilization.

Table 13 lists the nine selected cities, their latitude and collector tilt angle, and their typical heating and cooling seasons. Assuming that a tilt angle equal to the latitude of the city would provide equal solar utilization for heating and cooling all year long, the tilt angles used in this analysis were biased slightly to provide the greater amount of energy during the time of year it is needed most. Chicago, Minneapolis, and Seattle were biased towards heating, whereas Atlanta, Dallas, Los Angeles, Miami, and Philadelphia were biased towards cooling.

TABLE 13. - LOCATIONS AND CONDITIONS USED FOR THE UTILIZATION ANALYSIS

City	Latitude (degrees)	Collector tilt angle (degrees)	Typical heating months	Typical cooling months
Atlanta	33.6	25	Oct-Apr	May-Sep
Chicago	41.5	55	Sep-May	June-Aug
Dallas	32.1	25	Nov-Apr	May-Oct
Los Angeles	34.0	25	Nov-May	June-Oct
Miami	25.1	20	---	Jan-Dec
Minneapolis	44.5	55	Sep-May	June-Aug
Pittsburgh	40.1	40	Oct-May	June-Sep
Philadelphia	39.1	35	Oct-May	June-Sep
Seattle	47.5	55	Sep-June	July-Aug

Table 14 summarizes the percentages of heating and cooling loads that the solar energy collected from 69.7 m^2 (750 ft^2) of baseline collectors will provide to a typical 139.4 m^2 (1500 ft^2) house in the nine selected cities. Also tabulated is the ratio of the typical yearly flux level, which includes cloud cover, to the maximum possible flux level without clouds.

TABLE 14.- PERCENT OF LOAD SUPPLIED BY 69.7 M^2 (750 FT^2)
OF BASELINE SOLAR COLLECTORS FOR A 139.4 M^2
(1500 FT^2) HOUSE

Site	Typical flux/ maximum flux	Percent of load provided by solar collector	
		Percent of heating load	Percent of cooling load ¹
Atlanta	0.67	85	63
Chicago	0.60	50	67
Dallas	0.63	88	57
Los Angeles	0.71	99	98
Miami	0.66	99	49
Minneapolis	0.62	45	92
Pittsburgh	0.56	50	85
Philadelphia	0.58	57	77
Seattle	0.50	46	99
Philadelphia ²	0.58	40	41

¹ Assumes an air conditioner coefficient of performance of 0.6.

² A 464.5 m^2 (5000 ft^2) industrial building with 232.25 m^2 (2500 ft^2) collector area.

The utilization summaries of Table 14 may be separated into heating and cooling loads. These loads are graphed separately in Figures 90 and 91 and their sum is shown in Figure 92. The percentages of the load which can be supplied by solar energy from 69.7 m^2 (750 ft^2) of baseline collectors are visually presented on these graphs. Also included on the graph is the yearly total of the monthly load for each of the cities.

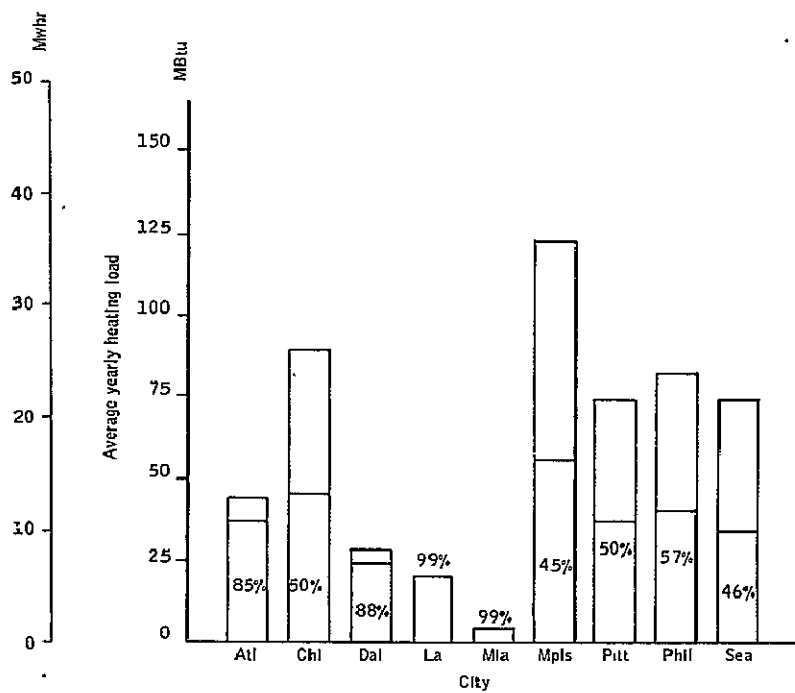


Figure 90. Geographic Comparison of Solar Heating

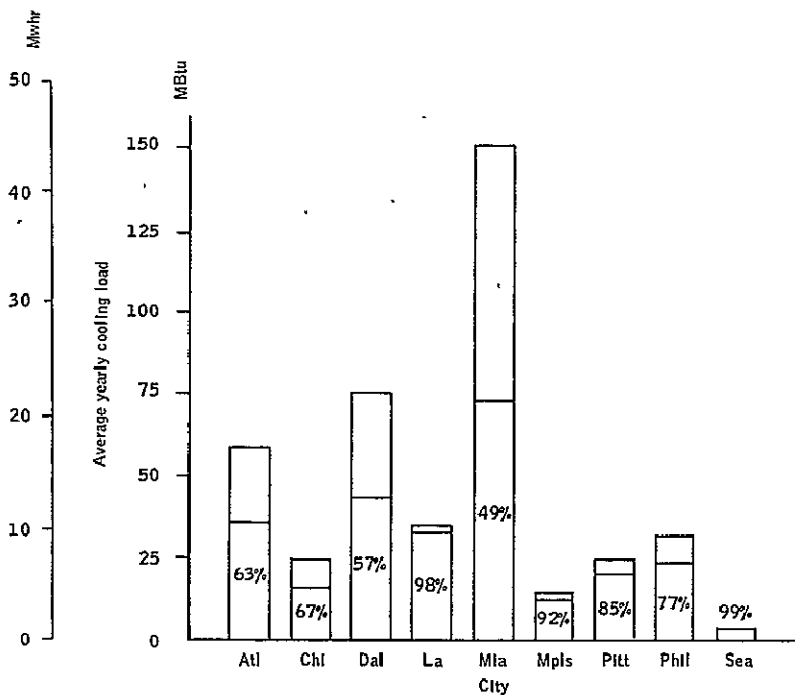


Figure 91. Geographic Comparison of Solar Cooling

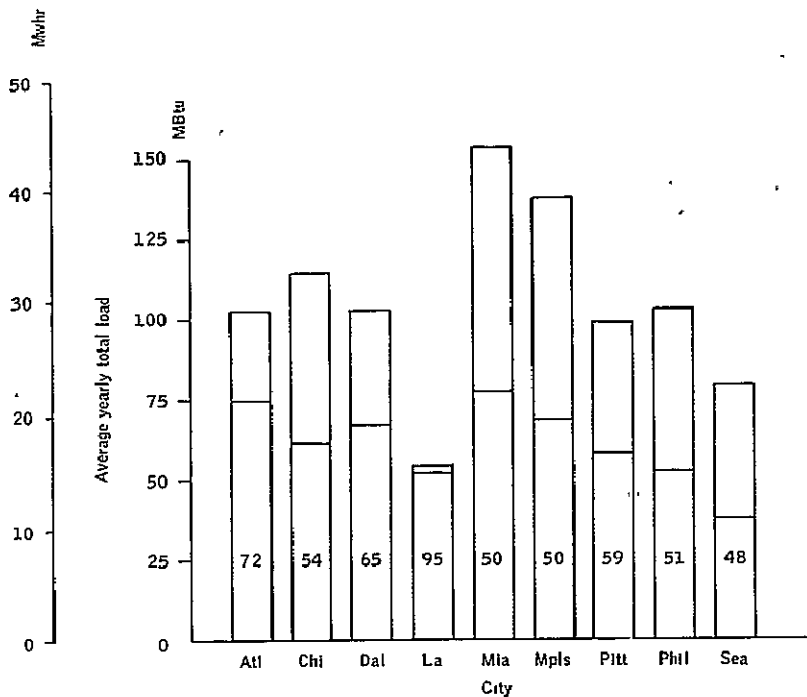


Figure 92. Total Yearly Heating and Cooling Loads

Energy Collection Calculations

The energy which can be collected in a particular geographic region with 69.7 m^2 (750 ft^2) of baseline collectors was calculated using two subroutines prepared for the ASHRAE task group on energy requirements, weather tapes for the city, and the semi-empirical expression for collector performance. The ASHRAE subroutines are called SUN and CCM (cloud cover modifier). The SUN subroutine is an algorithm to find solar position and intensity of direct normal and diffuse radiation without cloud cover. The CCM subroutine is an algorithm for modifying the solar radiation available in accordance with the cloud cover. Input for the CCM subroutine is provided from the weather tape. Incident radiation is also modified by a subroutine which modifies the energy transmitted through the glass cover sheets due to hourly changes in the incident angle.

The energy collected per unit area for the baseline collector design was calculated for each of the nine cities.

Based on the solar simulator tests on this collector, its performance can be expressed as:

Selective Black-Nickel Coated Collector

$$\frac{Q}{Q_{\text{inc}}} = 0.712 - 0.551 \left(\frac{T_{\text{in}} - T_{\text{amb}}}{Q_{\text{inc}}} \right) \quad (11)$$

where

Q = heat delivered (Btu per hour per square foot of absorber area)

Q_{inc} = incident solar flux (Btu per hour per square foot of absorber area)

T_{in} = fluid inlet temperature, °F

T_{amb} = ambient temperature, °F

Calculations were made for two inlet temperatures: 60°C (140°F), typical of a heating application, and 93°C (200°F), typical of an air conditioning application. Ambient temperature is input from the weather tapes. The mass flow rate is held constant at 48.9 kg/hr-m² (10 lbm/hr-ft²).

The monthly energy these collectors could deliver per unit area in Minneapolis, for example, is presented in Tables 15 and 16. The collectors are facing south and tipped 55 degrees from the horizontal.

Table 15 presents the data for clear sky conditions. This data gives an estimate of the maximum energy available and the maximum energy which could be collected with the baseline collectors. Table 16 presents the monthly energy totals when the incident flux is modified by the cloud cover. The particular year considered in Table 16 is 1956.

To utilize this collected energy for space heating or cooling, it is necessary to factor in a heating efficiency or air conditioning coefficient of performance (COP). For space heating, the efficiency may be considered to be 100 percent, but for cooling the typical COP is approximately 0.6. Applying the COP to the collected energy totals from Table 16, it is then possible to determine the amount of energy per unit area of baseline collector that can be actually delivered to satisfy a given load requirement. Figure 93 presents the amount of energy that can be delivered to a load by 69.7 m² (750 ft²) of baseline collector for the typical year in Minneapolis.

TABLE 15. - INCIDENT AND COLLECTED SOLAR ENERGY
WITHOUT CLOUD COVER FOR MINNEAPOLIS

Month	Incident flux, Whr/m ² - mo. (Btu/ft ² - mo.)	Collected energy from selective coated collector, Whr/m ² - mo. (Btu/ft ² - mo.)	
		T _{in} = 60°C (140°F)	T _{in} = 93°C (200°F)
1	167,691 (53,151)	66,182 (20,977)	44,826 (14,208)
2	188,823 (59,849)	79,534 (25,209)	55,543 (17,605)
3	220,383 (69,852)	96,394 (30,553)	69,684 (22,087)
4	208,895 (66,211)	96,123 (30,467)	68,346 (21,663)
5	202,528 (64,193)	97,732 (30,977)	68,176 (21,609)
6	188,044 (59,602)	97,139 (30,789)	67,529 (21,404)
7	196,493 (62,280)	99,855 (31,650)	69,302 (21,966)
8	206,542 (65,465)	108,519 (34,396)	77,685 (24,623)
9	206,141 (65,338)	139,258 (44,139)	76,126 (24,129)
10	202,592 (64,213)	103,777 (32,893)	75,436 (23,910)
11	170,723 (54,112)	75,704 (24,016)	53,376 (16,918)
12	154,418 (48,944)	64,090 (20,314)	42,321 (13,414)
Total	2,313,274 (733,209)	1,089,708 (345,391)	768,425 (243,558)

TABLE 16. - INCIDENT AND COLLECTED SOLAR ENERGY
INCLUDING CLOUD COVER (BASED ON 1956
WEATHER DATA) FOR MINNEAPOLIS

Month	Incident flux, Whr/m ² - mo. (Btu/ft ² - mo.)	Collected energy from selective coated collector, Whr/m ² - mo. (Btu/ft ² - mo.)	
		T _{in} = 60°C (140°F)	T _{in} = 93°C (200°F)
1	95,240 (30,187)	23,924 (7,583)	13,897 (4,405)
2	125,673 (39,883)	41,598 (13,185)	27,060 (8,577)
3	112,526 (35,666)	30,253 (9,589)	18,257 (5,787)
4	131,945 (41,821)	49,176 (15,587)	29,688 (9,410)
5	130,998 (41,521)	54,057 (17,134)	32,578 (10,326)
6	140,069 (44,396)	66,075 (20,943)	41,463 (13,142)
7	130,002 (41,205)	57,089 (18,095)	33,720 (10,668)
8	141,413 (44,822)	65,857 (20,874)	42,160 (13,363)
9	134,936 (42,769)	57,853 (18,337)	37,131 (11,769)
10	134,320 (42,574)	57,531 (18,235)	37,478 (11,879)
11	80,490 (25,512)	19,892 (6,305)	10,947 (3,470)
12	66,712 (21,145)	11,862 (3,760)	5,694 (1,805)
Total	1,424,485 (451,501)	535,176 (169,628)	330,016 (104,601)

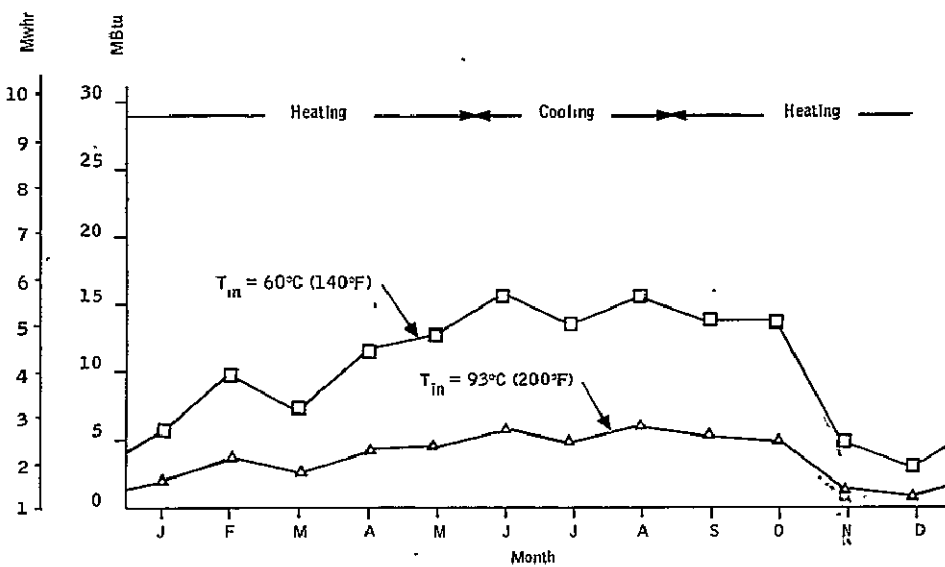


Figure 93. Energy Delivered to a Load by 69.7 m² (750 ft²) of Baseline Collector in Minneapolis

Load Calculations

To determine the percent utilization of the solar energy delivered to the load, it was necessary to establish the heating and cooling load levels for a typical residence in each of the nine selected cities for the typical year provided by the weather tapes.

The house load in this analysis is based on an area of 139.4 m² (1500 ft²) and a volume of 340 m³ (12,000 ft³). It is assumed that a typical house for all nine cities has a wall coefficient of transmission (U) of 0.942 (0.166) and a roof U of 0.233 (0.041), where U is measured in watt/m² °C (Btu/hr·ft² °F). The indoor design temperatures used were 21 °C (70 °F) in the winter and 24 °C (75 °F) in the summer, with a summer relative humidity comfort level of 40 percent. A volume exchange rate of 1.5 exchanges per hour was used as a typical infiltration value. The load was calculated directly from degree days by determining an average daily temperature difference and using the following equations:

$$\begin{aligned}
 H_{\text{heating}} &= H_{\text{infiltration}} + H_{\text{transmission}} \\
 &= C_p V N_p (t_i - t_o) + AU(t_i - t_o)
 \end{aligned}$$

$$\begin{aligned}
 H_{\text{cooling}} &= H_{\text{infiltration}} + H_{\text{transmission}} \\
 &= VN_p C_p (t_o - t_i) + (h_o - h_i) + AU(t_o - t_i)
 \end{aligned}$$

where

A = surface area of wall or roof

C_p = 0.278 watt/hr/kg- °C (0.240 Btu/lbm- °F)

h_o = outside enthalpy (Btu/lbm) of air determined from average monthly dry bulb temperature and relative humidity on psychrometric chart

H = load level

h_i = inside enthalpy of 24 °C (75 °F) dry bulb temperature and 40 percent relative humidity

N = number of volume exchanges per hour (1.5)

$(t_i - t_o)$ = inside-outside temperature difference

U = coefficient of transmission of wall or roof (Btu/ft²-hr- °F)

V = house volume

ρ = 1.2 kg/m³ (0.075 lbm/ft³)

These heating and cooling load levels, determined from the equations, are then multiplied by hours per month to get an average monthly load. The internal sensible heat associated with electricity use (light bulbs, appliances, etc.) is not included in this analysis. For geographical areas where heating and cooling load levels are similar, the total yearly effect of internal sensible heat may be negligible as it increases the load in the summer but decreases the load in the winter.

Table 17 tabulates the calculated heating and cooling load for the house in Minneapolis. These load levels are also presented graphically as Figure 94

By combining the graphs for energy delivered by 69.7 m² (750 ft²) of baseline collector with the load level graphs for the 139 m² (1500 ft²) house for each of the selected cities, it is possible to calculate the degree of utilization of the solar system. Figures 95 through 97 show the utilization for three of the cities. A COP of 0.6 is still assumed for cooling, and all of the heat collected is considered delivered for heating. The cross-hatched area in each figure indicates the portion of the load actually supplied by the solar system. System operation is assumed to switch from the heating to cooling mode and back again, as required by the load.

ORIGINAL PAGE IS
OF POOR QUALITY

TABLE 17.- HEATING AND COOLING LOAD FOR MINNEAPOLIS

Month	Average temp, °F (a)	Average humidity, percent (a)	Degree days (a)		Load ^(b)			Total load, 10^6 Btu
			Heating	Cooling	Heating 10^6 Btu	Cooling dry air, 10^6 Btu	Drying humid air, 10^6 Btu	
1	12.4	70.0	1631	0	23.9	0	0	23.9
2	15.7	69.0	1380	0	20.3	0	0	20.2
3	27.4	69.5	1166	0	17.1	0	0	17.1
4	44.3	64.0	621	0	9.0	0	0	9.0
5	57.3	63.2	288	94	4.2	1.4	0	5.6
6	66.8	66.0	81	109	1.2	1.6	0	2.8
7	72.3	68.0	22	148	0.3	2.2	3.5	6.0
8	70.0	68.8	31	208	0.5	3.0	2.4	6.0
9	60.4	74.5	189	13	2.8	0.2	0	3.0
10	48.9	71.0	505	0	7.4	0	0	7.4
11	31.2	74.8	1014	0	14.9	0	0	14.9
12	18.1	74.8	1454	0	21.3	0	0	21.3
Total	43.7	69.5	8382	572	122.8	8.5	5.9	137.2

^aMeteorological data from NOAA. Based on 65°F.^bBased on 1500-ft² house of 12,000-ft³ volume, with 1.5 exchanges/hr and an average daily degree day temperature difference.

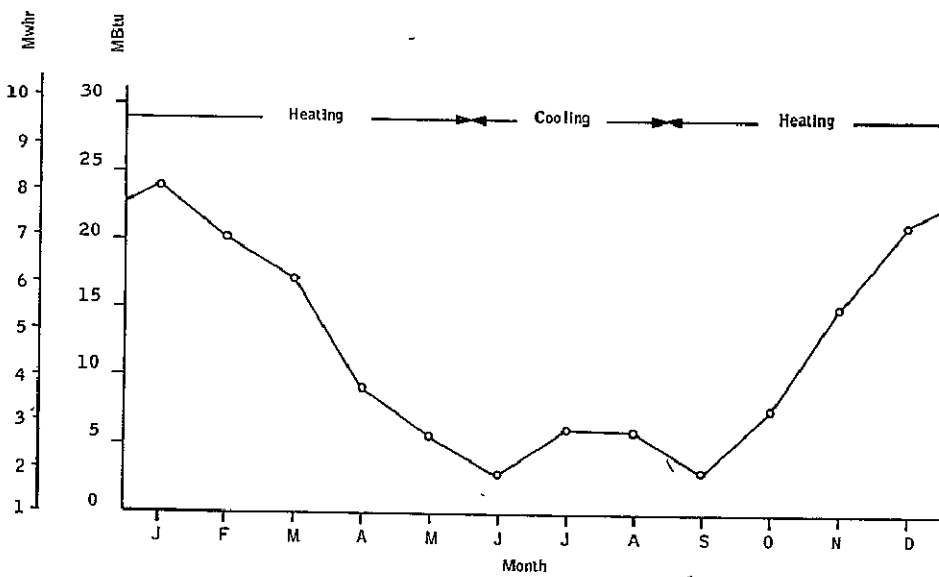


Figure 94. Heating and Cooling Load for a 139 m^2 (1500 ft 2) Minneapolis House

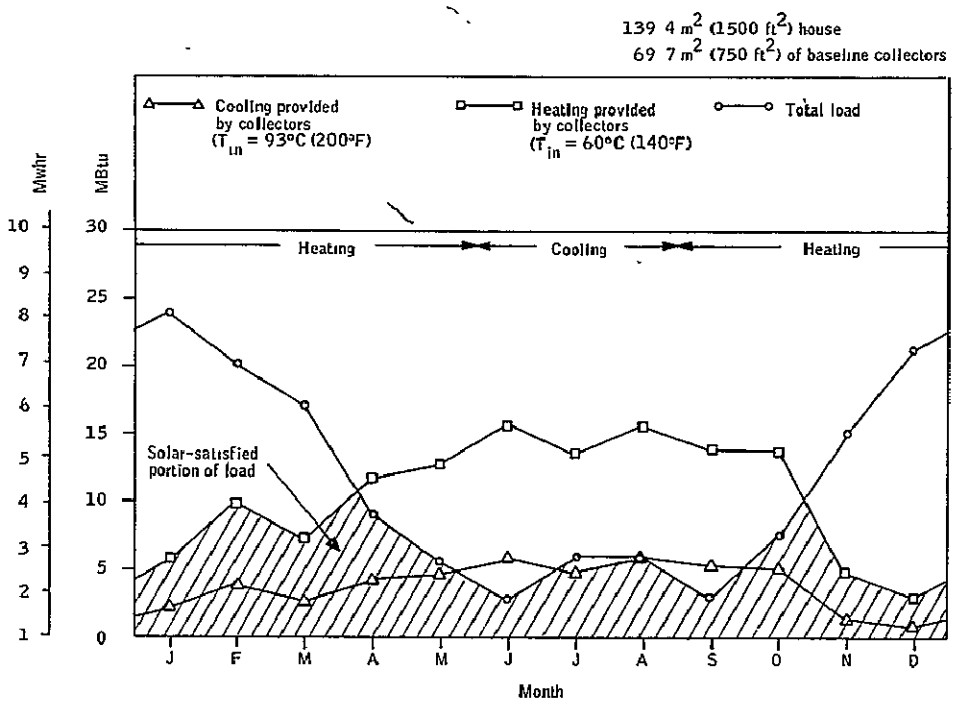


Figure 95. Heating and Cooling Load and Solar-Supplied Portion of a Load for a Minneapolis House

Figure 95 shows the large winter heating load required in Minneapolis and a comparatively small summer cooling load. The portion of the heating load which can be supplied by solar collectors is shown by the 60°C (140°F) (Collector inlet temperature) heating curve and the cooling portion is shown by the 93°C (200°F) cooling curve. The heating mode of operation ends with May, and the cooling mode ends with August. This analysis assumes sufficient storage capacity for total use of collected heat during any particular month. Also, when there is more energy collected than can be used in a given month, the excess energy is disregarded and has no effect on energy supplied in subsequent months. Using these assumptions, 45 percent of the heating load and 92 percent of the cooling load can be provided by 69.7 m² (750 ft²) of solar collectors. Figure 96 shows similar heating and cooling loads for Atlanta. The collectors can provide 85 percent of the heating load and 63 percent of the cooling load. Figure 97 shows the total load for Miami, which is entirely cooling. The collectors would always run at a 93°C (200°F) inlet temperature and would provide 49 percent of the cooling load.

A similar analysis was performed for solar utilization with a light industrial building in Philadelphia. The building load was calculated in the same manner that the house loads were calculated. The results are based on a 464 m² (5000 ft²) building with a 2548 m³ (90,000 ft³) volume. The coefficient of transmission is 0.908 w/m²°C (0.16 Btu/ft²hr°F) for the walls and 0.568 w/m²°C (0.1 Btu/ft²hr°F) for the roof. The same indoor design temperatures were used and internal sensible heat was not included. As noted previously, the total yearly effect of including internal sensible heat may be negligible as it increases the load in the summer but reduces the load in the winter. Table 18 tabulates the results for Philadelphia and Figure 98 shows graphically the portion of the load which can be supplied by 232 m² (2500 ft²) of collectors. A COP of 0.6 was again used for cooling. If the system has sufficient storage capability for 100-percent utilization of collected heat, then the collectors would provide 40 percent of the yearly heating load and 41 percent of the yearly cooling load for the building. Both load and solar collection level data for the remaining locations are presented in Appendix D. The use of these tables will enable calculation of solar utilization for different array sizes.

Typical Solar Utilization System

Several different system configurations are possible to effect utilization of the gathered solar flux. One such system currently under consideration is presented in Figure 99. It is a single-fluid system with a boiler and an absorption air conditioner. The system consists of a conventional oil-fired water heating boiler for heating and an absorption air conditioner for cooling. The solar system consists of the flat plate collectors which can heat the building or supply heat to the absorption air conditioner and a liquid storage tank to store excess energy not needed by the boiler or absorption unit. The boiler can operate independent of the solar system. A separate coil for the solar collectors is included in the air duct so that any solar energy collected

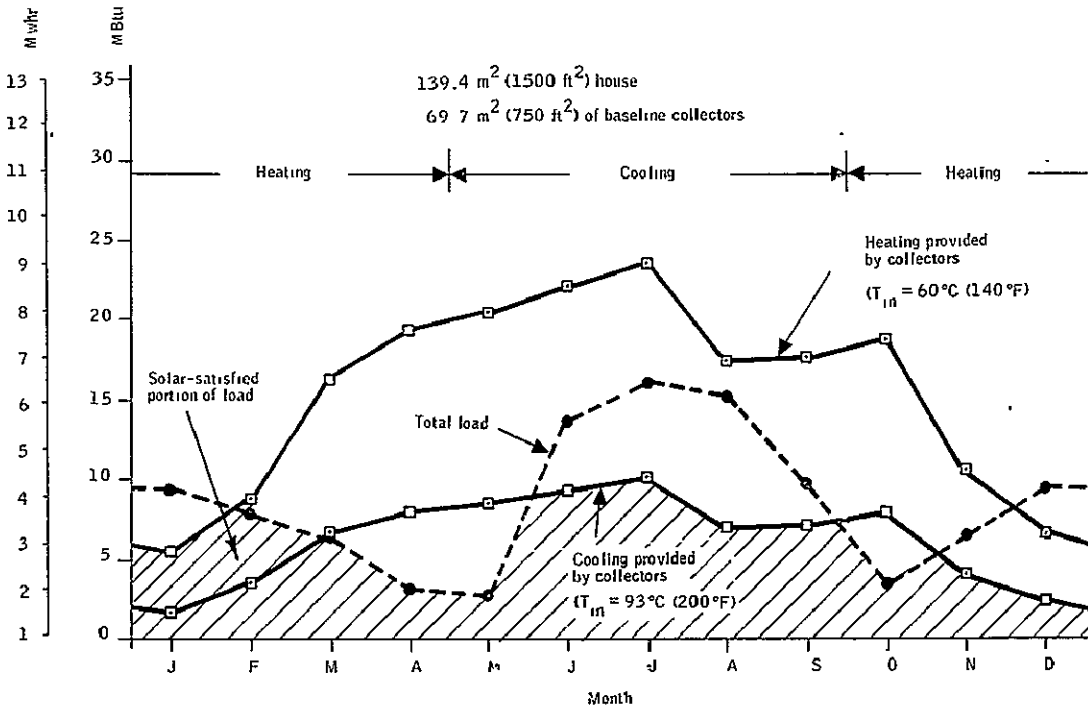


Figure 96. Heating and Cooling Load and Solar-Supplied Portion of a Load for a Atlanta House

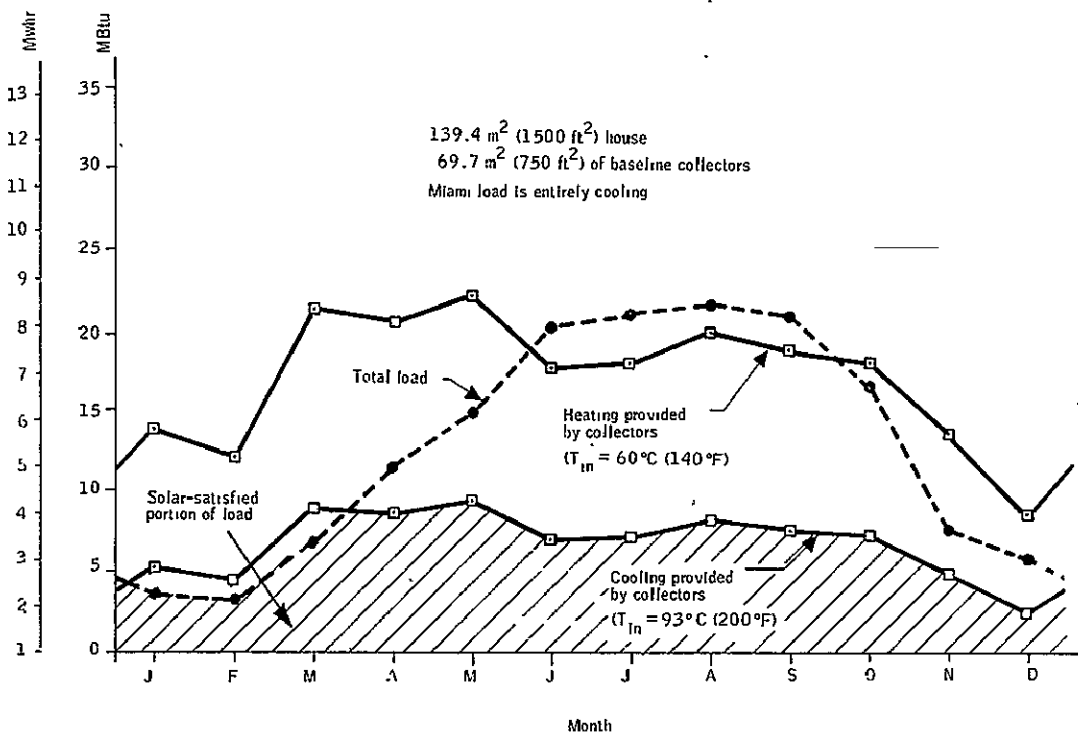


Figure 97. Cooling Load and Solar-Supplied Portion of a Load for a Miami House

ORIGINAL PAGE IS
OF POOR QUALITY

TABLE 18.- HEATING AND COOLING LOAD FOR
PHILADELPHIA INDUSTRIAL BUILDING

Month	Average temp, °F (a)	Average humidity, percent (a)	Degree days (a)		Load ^(b)			Total load 10^6 Btu
			Heating	Cooling	Heating 10^6 Btu	Cooling dry air, 10^6 Btu	Cooling humid air, 10^6 Btu	
1	33.2	70.0	986	0	88.7	0	0	88.7
2	33.6	67.0	879	0	79.1	0	0	79.1
3	42.3	64.8	704	0	63.4	0	0	63.4
4	51.6	63.5	402	0	36.2	0	0	36.2
5	63.1	66.8	104	67	9.4	6.0	0	15.4
6	72.1	68.8	0	223	0	20.1	26.8	46.9
7	76.3	69.0	0	366	0	32.9	48.3	81.2
8	74.0	71.8	0	304	0	27.4	27.5	54.9
9	67.7	72.2	47	131	4.2	99.4	10.4	26.4
10	56.6	71.8	269	13	24.2	1.2	0	25.4
11	45.9	70.0	573	0	51.6	0	0	51.6
12	54.3	68.8	902	0	81.2	0	0	81.2
	54.3	68.8	4866	1104	438.0	99.4	113.0	650.4

^aMeteorological data from NOAA. Based on 65°F.

^bBased on 5250-ft² building of 89,250-ft³ volume, with 1.5 exchanges/hr and an average daily degree day temperature difference.

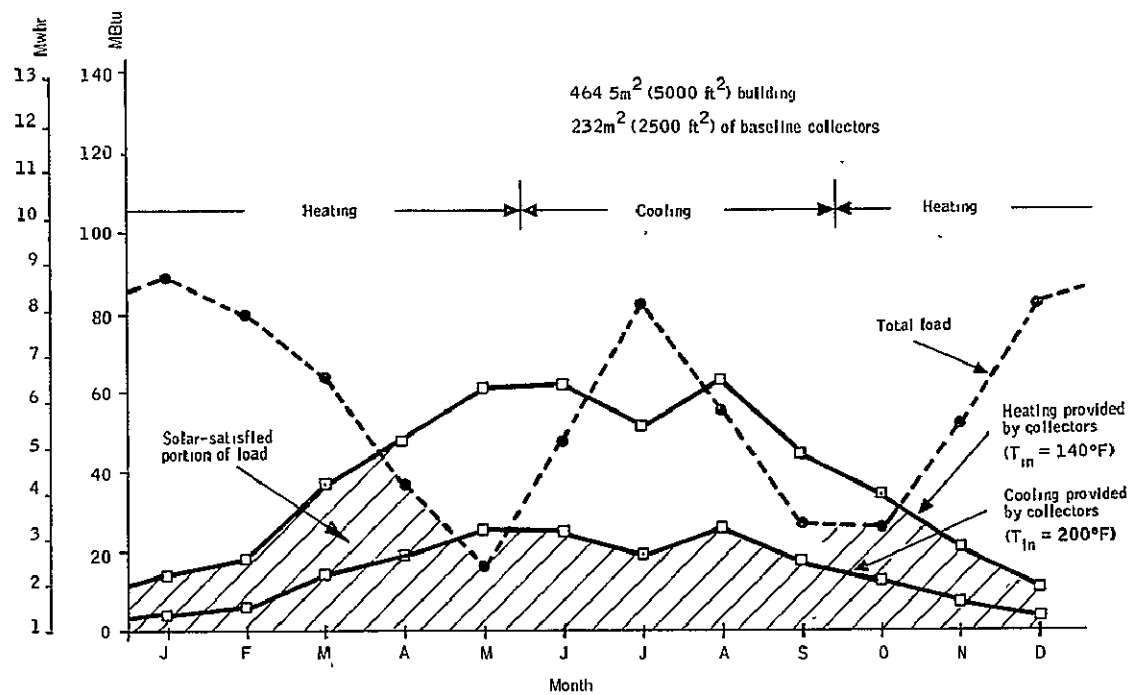


Figure 98. Heating and Cooling Load and Solar-Supplied Portion of a Load for an Industrial Building in Philadelphia

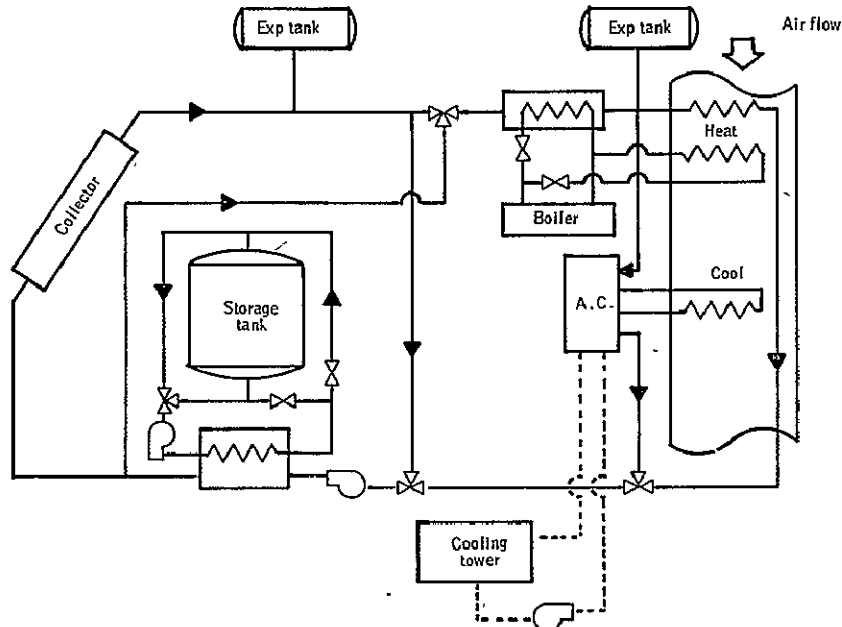


Figure 99. Typical Solar-Assisted-HVAC System

can be utilized for the building demands. Utilizing the solar energy available at low temperatures increases the collector efficiency. Domestic hot water, heated by solar energy, is not included as the demand is small relative to the building loads. The absorption air conditioner was selected because there is a commercially available unit that operates on hot water at approximately 82° - 104°C (180° - 220°F). The other possibility for solar-assisted air conditioning is the Rankine cycle refrigeration system; however, only prototype equipment is being introduced and experience in operation is limited.

The various modes of operation of the solar assisted heating and cooling system can be described as follows:

Heating -- The building demand for heat can be satisfied by taking heat directly from the collectors, from the storage tank, or from the boiler. The collector heat is added in the heating duct prior to the boiler heat so that if the need is satisfied by solar heat alone, the boiler will not have to operate. If the solar heat does not satisfy the load the boiler makes up the difference.

For nighttime operation, or during periods of no sunlight, the storage tank heat, if any, can be used to supply heat to the building.

Cooling -- The building demand for air conditioning is satisfied by taking heat directly from the collectors, from the boiler, or from a combination of the two.

No Heating or Cooling -- If no heating or cooling is needed for the building and sunlight is available, the storage tank temperature can be increased for later or nighttime operation.

CONCLUSIONS AND RECOMMENDATIONS

Conclusions

The program objective was to design, fabricate and test an efficient, low-cost flat plate collector for heating and cooling of buildings. The major emphasis was to develop a $122 \times 122 \text{ cm}$ ($48 \times 48 \text{ in.}$) collector for the cooling application. Therefore, the performance goal set forth was a collection efficiency in excess of 50 percent at a 93°C (200°F) inlet fluid temperature, 27°C (80°F) ambient temperature and 1009 W/m^2 ($320 \text{ Btu/hr - ft}^2$) incident flux. The design of a baseline collector was conducted with the aid of mathematical models of the heat transfer processes in the collector. The baseline collector design has an aluminum absorber plate with an optically selective Black Nickel coating. The absorber plate is backed with 7.6 cm (3 in.) of rigid fiberglass insulation and surrounded with 5 cm (2 in.) of rigid

fiberglass insulation on its four edges. This absorber/insulation sandwich is encased in a sheet metal box and covered with two layers of glass with a 3 cm (1-1/4 in.) air gap between sheets and a 3 cm (1-1/4 in.) air gap between the absorber and the lower layer of glass. The outside dimensions of the collector are 122 x 122 x 15.2 cm (48 x 48 x 6 in.). This collector meets the performance goal.

Variations of the baseline collector design were also examined to evaluate the effect on cost and performance for various collector materials. The variations were concentrated in two major design areas: the absorber and the cover system. Absorber plates were made of both steel and aluminum and coated with selective Black Nickel (steel and aluminum), nonselective black paint (aluminum only), and selective Black Chrome (steel only). The cover systems examined consisted of one glass cover, two glass covers, one outer glass - one inner Tedlar cover, one Lexan cover, and two anti-reflection (AR) etched glass covers. The box design and insulation type and thickness were held constant, as was the cover spacing.

The performance results determined from the solar simulator testing indicated that the selective Black Nickel absorber, on either steel or aluminum panel, covered with two sheets of antireflective etched glass provides the greatest collector efficiency, 61.5 percent, at 93°C (200°F) inlet temperature, 27°C (80°F) ambient temperature, and 1009 W/m² (320 Btu/hr-ft²) incident flux.

Within the bounds of experimental accuracy, the following collector configurations are considered to have met or exceeded the performance goal:

- Black Nickel-coated aluminum absorber panel and two glass covers--50.5 percent collection efficiency.
- Black Nickel-coated steel absorber panel and two glass covers--51.5 percent collection efficiency.
- Black Nickel-coated aluminum absorber panel and two AR etched glass covers--61.5 percent collector efficiency.
- Black Nickel-coated aluminum absorber panel and a glass outer cover and Tedlar inner cover--52.5 percent collection efficiency.
- Black painted aluminum absorber panel and two AR etched glass covers--51.5 percent collection efficiency.
- Black Nickel-coated aluminum absorber panel and a single glass cover--49.5 percent collection efficiency.

- Black Nickel coated aluminum absorber panel and a single Lexan cover--49.0 percent collector efficiency.
- Black Chrome coated steel absorber panel and two glass covers--49.0 percent collection efficiency.

The following collectors did not meet the design goal:

- Black painted aluminum absorber panel and two glass covers--42.5 percent collection efficiency.
- Black painted aluminum absorber panel and an outer glass cover and an inner Tedlar cover--40.5 percent collection efficiency.
- Black painted aluminum absorber panel and a single glass cover--39 percent collection efficiency.
- Black painted aluminum absorber panel and a single Lexan cover--34.5 percent collection efficiency.

In addition to establishing the efficiency of the various collectors relative to the performance goal, the tests conducted with the solar simulator defined their operating characteristics over a wide range of inlet temperatures and incident flux levels. The inlet temperature was adjusted from 27°C (80°F) to 93°C (200°F) and the incident flux level adjusted from 473 to 1010 W/m² (150 to 320 Btu/hr - ft²).

The data from the simulator tests resulted in some general conclusions. These are:

- The tests further substantiate that good collector performance correlation is achieved by using the parameter $T_{in} - T_{amb}/Q_{inc}$, where:
 - T_{in} = inlet temperature
 - T_{amb} = ambient temperature
 - Q_{inc} = incident flux
- For the baseline collector, a reduction in efficiency with increasing incidence angle of the solar flux is caused by the conventional reduction in transmission through the covers with increasing incidence angle.
- The performance of the baseline collector is somewhat reduced when a large fraction (~ 50%) of the incoming energy is diffuse.

- The efficiency of the collector is not strongly dependent on the emittance of the absorber plate in the case of small differences between inlet and ambient temperature ($\sim 28^{\circ}\text{C}$ or 50°F).
- The efficiency of the collector is strongly dependent of the emittance of the absorber plate for larger differences between inlet and ambient temperatures ($\sim 72^{\circ}\text{C}$ or 130°F). This is a typical operating condition for use of the collector with an air conditioner, or a heating application in a cold climate.
- The aluminum and steel absorber plates when coated with Black Nickel had essentially the same performance levels.
- Single cover configurations are more efficient than two cover configurations for low inlet to ambient temperature differences ($\sim 28^{\circ}\text{C}$ or 50°F). (NOTE: The exception to this is the two sheets of AR-coated glass which combined have a higher transmission factor than the single cover sheets tested.)
- Double cover configurations are more efficient than single cover configurations for high inlet to ambient temperature differences ($\sim 72^{\circ}\text{C}$ or 130°F).
- The single versus double cover effects are more pronounced when using the higher heat loss, non-selective absorber surface than when using a selective absorber surface.
- The cover combinations of two glass and one glass/one Tedlar resulted in essentially identical performance.
- The Black Nickel and Black Chrome absorber coatings resulted in similar performance provided the sooty deposit on the Black Chrome was not disturbed. (Removal of the soot reduces the absorptance from 0.94 to 0.80.)

Outdoor collector performance tests were conducted on two collector configurations, the baseline and the black painted aluminum absorber with two glass covers. The two collectors were operated simultaneously to allow direct performance comparisons to be made for identical operating conditions. The performance of the selectively coated baseline collector was measured to be significantly greater than the collector with the non-selective absorber. A comparison was made of the actual measured outdoor performance and empirically predicted performance, based on the simulator test results. The correlation between the predicted and measured results was found to be good, agreeing to within 10 percent in most cases. This result provides added confidence in the positive utility of simulator tests.

In general, outdoor tests are much more difficult to properly conduct and interpret due to the uncontrolled environmental conditions which exist. Therefore, it is difficult, based on outdoor testing, to compare the performance of various collectors without running them simultaneously.

The companion objective to performance was cost. Therefore, a cost analysis was performed on the various collector configurations and combined with the performance results to find a relative cost effectiveness for each collector configuration. Cost effectiveness was defined as the cost per unit heat delivered to the working medium. The costs of the configurations were estimated for small quantities 93 m^2 (1000 ft^2) and limited mass production quantities 9300 m^2 ($100,000 \text{ ft}^2$). For the baseline collector the fabrication cost was reduced by a factor of nearly three when evaluated for the larger quantity.

The cost effectiveness of the Black Nickel, selectively coated collectors was significantly better than for the non-selectively coated collectors (based on prices for the 9300 m^2 ($100,000 \text{ ft}^2$) production and the efficiency for a typical air conditioning application). With the exception of the configuration using a single Lexan cover, all of the collectors with the Black Nickel absorber had similar cost effectiveness values. The total spread in their cost effectiveness was found to be only 13 percent. The most cost-effective design was the collector with an outer glass cover and inner Tedlar cover.

Estimates of thermal heating and cooling leads for both a house and small industrial building were made and compared with estimates of the amount of solar energy which would be collected by an array of baseline collectors with an area equal to approximately one-half the floor area of the house or building. The calculations for the house were made for nine geographic locations utilizing actual weather data and insolation from a typical year. The locations were Atlanta, Chicago, Dallas, Los Angeles, Miami, Minneapolis, Pittsburgh, Philadelphia and Seattle. The industrial building was analyzed for a single location, Philadelphia. With the exception of the Minneapolis and Seattle locations, 50 percent or more of the heating load for the house was satisfied by the baseline collector array. In all locations, 49 percent or more of the estimated energy required for cooling the house was delivered by the baseline solar collectors.

Recommendations

The analysis and testing completed during the course of this research program indicated that significant improvements in collection efficiency could be realized if appropriate design modifications were introduced to reduce collector heat losses. A solar selective coating could be added to the absorber panel to reduce re-radiation losses out through the cover, a second cover layer could be added to the collector to reduce the convection losses through the cover system, insulation could be added around the

absorber panel to reduce conduction losses to the housing, and, finally, performance could be increased by applying an antireflective surface etch to the covers to allow a greater portion of the incident solar flux to actually reach the absorber panel.

Presuming the design analysis to be correct, concurrent incorporation of all of the above mentioned design modifications should enable collection efficiency to approach the theoretical boundary of performance for conventional flat plate collectors. As can be seen from the test data, the collector with a selective Black Nickel absorber coating and two AR-etched glass covers performs significantly better than the other collector design configuration under all combinations of input parameters. Certainly some slight improvements can be made in the performance of this collector. Perhaps the absorptance of the selective coating can be increased to 0.97 or more, and possibly the emittance can be lowered one or two percent; however, these changes are merely fine tuning the existing design, they do not hold promise of a significant breakthrough for improving collector efficiency. It is therefore recommended that further investigation be directed in either or both of two directions:

- Reduce life cycle cost by materials, process, and design development.
- Augment collector performance by non-conventional design modifications, both internal and external to the collector module.

Life cycle cost reduction. - Life cycle costing requires an accounting of all costs associated with the total amount of heat flux delivered over the expected life of the collector. This includes not only the first cost of fabricating and installing the collector, but also the cost of the required maintenance, and the cost of renewal or even replacement of collector components, as may be necessary to achieve the expected collector life. Reduction of present life cycle cost is necessary to improve the economic feasibility of the solar flat plate collector as an alternate energy source. To achieve the necessary reduction in life cycle cost, the following areas of study are recommended:

- (1) Durability of selective coatings: The present selective coatings, such as Black Nickel and Black Chrome, offer a considerable improvement over standard black coatings, in terms of solar performance. However, these selective coatings are susceptible to physical degradation from such sources as humidity and handling. Frequent renewal of a deteriorated absorber coating would seriously impact life cycle cost over the anticipated 15 or 20 year system life. Additional research and development is required to improve coating durability and extend their normal operating life.

- (2) Absorber panel corrosion: As has been expressed in the design section of this report, there is some definite concern about the possibility of internal corrosion of the aluminum roll-bond absorber panel selected for the baseline collector design. To combat this corrosion problem and extend the operating life of the absorber panel it may be necessary to perform considerable periodic maintenance, such as adding and changing filters, flushing the absorber panels, and draining and neutralizing the transfer medium. It may even be necessary to change to a different absorber material, such as copper, which will significantly increase the collector first cost. A rigorous investigation of the rates, types and sources of collector corrosion is necessary before the associated cost questions can be answered. Further material studies are also necessary to reduce potential collector corrosion problems.
- (3) Cover material lifetime: The use of plastic films, such as polyvinyl fluoride or polyesters, for collector covers appears attractive as a means of reducing collector first cost, and also collector weight. However, long term durability and resistance to weathering and U. V. degradation has not been well established for the plastic films. A study program is recommended to examine the expected lifetime of plastic films when exposed to conditions such as temperature and humidity cycling, wind buffeting, and rain and snow loading.
- (4) Collector Redesign: As was mentioned in the Cost Analysis section of this report, the baseline collector design is not considered to be optimized from a production level fabrication standpoint. It is recommended that a formal Value Engineering Study be performed in order to redesign the collector to lower fabrication costs and perhaps increase ease of maintenance.

Collector performance augmentation. - The analysis performed to characterize the thermal processes in flat plate collector operation has been quite successful in revealing those design parameters which must be controlled to achieve improved collector performance. The requirements for successful absorber design and insulation to improve heat transfer and reduce heat losses are quite well understood. It presently appears that the area of collector operation least well understood is that of the use of the cover system. More specifically, a greater amount of the incident solar flux must be made available to the absorber panel for transfer to the working fluid. Two types of studies are recommended to pursue this objective:

- (1) Reduce cover system losses: The collector performance predictions made during the analysis section of this program were consistent in underestimating the amount of collector heat loss. Since the mechanics of the conduction and absorber re-radiation losses are well known, it is expected that the convection losses through the cover are actually the loss component that was underestimated. It is therefore recommended that additional research be performed to more accurately quantify the convection losses, and that design development be pursued to reduce these losses, perhaps through some system of baffling that would disrupt the convection cells without significantly interfering with cover transmission. A second approach might be to evacuate the cover system.
- (2) Increase the insolation level at the absorber panel: The impact of increasing the amount of incident flux that actually reaches the absorber panel can be well appreciated by considering the performance improvement achieved by the use of anti-reflection surface etched glass in the cover system. Collection efficiency increased approximately 10 percent for all combinations of input parameters. This improvement could be further enhanced by the addition of some non-conventional augmentation system to increase the insolation level entering the cover system. One recommended approach that might warrant additional study is the use of external reflectors.

One final recommendation may be made with regard to further flat plate collector development. Both the Cost Analysis and Utilization Study sections of this report indicated that evaluation of collector performance may be deceptive if only pursued for a limited set of collector input parameters. Installed collector performance under the actual operating conditions of a given geographic location may be significantly different than that empirically predicted from test performance for a limited set of design conditions; different even to the extent that some design modifications may actually be vastly more effective than anticipated, and others may not be effective enough to justify the cost of modification. It is therefore recommended that various collector designs be evaluated for extended periods of operation over the naturally varying environmental conditions encountered in the different geographic areas offered as sites for potential applications.

APPENDIX A

FLAT PLATE COLLECTOR PROGRAM

INTRODUCTION

A detailed thermal analysis of the flat plate solar collector was accomplished. The analysis was programmed for computer solution for either the steady-state or transient thermal performance. Using finite difference methods, the heat flows and temperature distribution throughout the collector are obtained. In the following paragraphs the analytical methods and heat transfer correlations are presented, and a flow chart and program listing are given.

Although the flat plate collector has been extensively analyzed by many investigators, the available literature has several deficiencies. First, due to the complex nature of the various radiative and convective thermal processes involved, the literature has tended toward the presentation of simplified formulae for engineering design. Depending on the accuracy and depth of understanding desired by the designer, these relations may be more or less satisfactory. Second, due to the labor involved, a hand calculation cannot take into consideration the transient response of the collector. Since the incident solar flux is inherently time varying, it is desirable to be able to predict the transient performance. This requires the use of a high-speed computer, and no programs are currently available. Third, the effects of a nonuniform temperature distribution in the collector components have not been analyzed. The main source of the nonuniformity is the rise in collector fluid temperature from inlet to outlet, which imposes a similar temperature variation on the absorber and to a lesser extent in the covers. Finally, the large number of geometrical and physical parameters such as absorber material and thickness, number and type of covers, cover spacing, insulation, etc. presents the type of problem that is best handled by automated design analysis.

FLAT PLATE COLLECTOR PROGRAM

To achieve the enumerated design goals, a transient thermal analysis computer program was written. The collector is subdivided into a number of elements, "nodes," which interact thermally. The subdivision is indicated in Figure 100. Although the method of subdivision is arbitrary, the effect of the rise in fluid temperature from inlet to outlet is best examined by the indicated subdivision. The temperature of each node is computed as a function of time using the straightforward explicit method in which the temperature rate of change of node i is related to its present temperature and the temperatures of the neighboring nodes j by

Preceding page blank

Appendix A

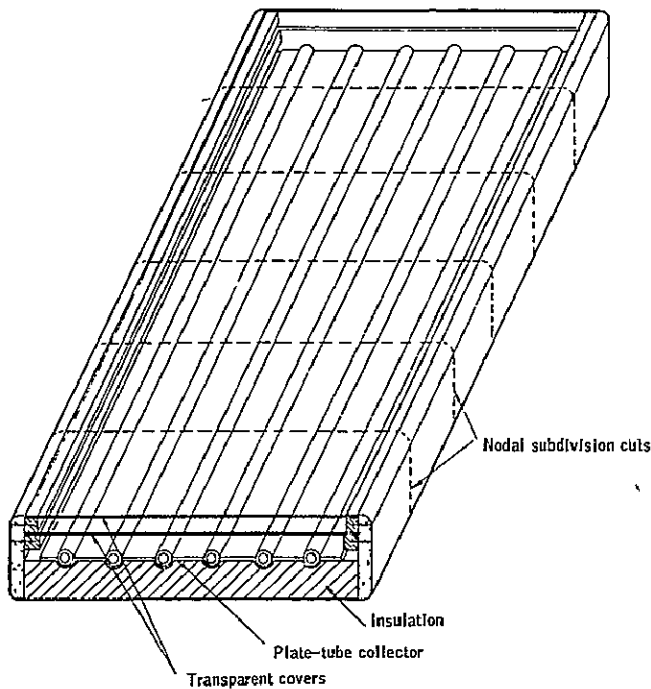


Figure 100. Nodal Subdivision of Flat-Plate Solar Collector

$$C_i \frac{dT_i}{dt} = \sum_j K_{ij} (T_j - T_i) + S_i \quad (A1)$$

where C_i is the heat capacity of node i , T_i is its temperature, dT_i/dt is its rate of change of temperature, T_j is the temperature of node j , and S_i is the solar heat absorption. The coupling coefficients K_{ij} , called conductances, depend on the heat transfer mode and are, in general, temperature dependent.

There are N such equations, one for each mass element, and the solution of these N simultaneous, nonlinear, first order, ordinary differential equations yields the temperature history at N discrete points throughout the collector. Since the temperature of each node is assumed to be given at some initial time, t_0 , the rates $(dT_i/dt)_{t=t_0}$ are given, and the temperatures at $t_0 + \Delta t$ are obtained by

$$T_i(t_0 + \Delta t) = T_i(t_0) + \left(\frac{dT_i}{dt} \right)_{t=t_0} \Delta t \quad (A2)$$

Then the rates at $t_0 + \Delta t$ can be calculated, and the procedure is repeated until the desired time range is covered.

Appendix A

In the following paragraphs the method of obtaining the necessary solar input (S_i) to each node and the internodal conductances (K_{ij}) is discussed.

Solar Energy Absorption

The first step in the analysis is to calculate multiple reflection, absorption, and transmission of incident solar energy in the covers and absorber plate. Equations will be derived for the rate of solar flux absorption in each cover and in the absorber so that these values can subsequently be included as the heat sources S_i in the energy balance of each element of the collector.

The problem will be analyzed using the net radiation method. In this approach energy balance equations are written at each surface in terms of the radiation leaving all the surfaces. The radiation leaving a given surface, its radiosity, is the emitted, reflected, and transmitted (from the interior out) energy. One problem which arises is the number of simultaneous algebraic equations which must be solved, particularly for more than two covers plus an absorber. This problem will be circumvented by the following approach. Reflection, absorption, and transmission coefficients will be derived for a single cover with no absorber. These coefficients are then used in a two-cover analysis to obtain reflection, absorption, and transmission coefficients for the two-cover system. The pattern of the results then emerges such that any number of covers may be analyzed without recourse to the solution of a large number of simultaneous equations. Having obtained the radiation coefficients for the N cover system without absorber, the absorber is then included using the same procedures.

This procedure, which will be clarified in the analysis to follow, allows the solution of four important combinations of specular and/or diffuse conditions:

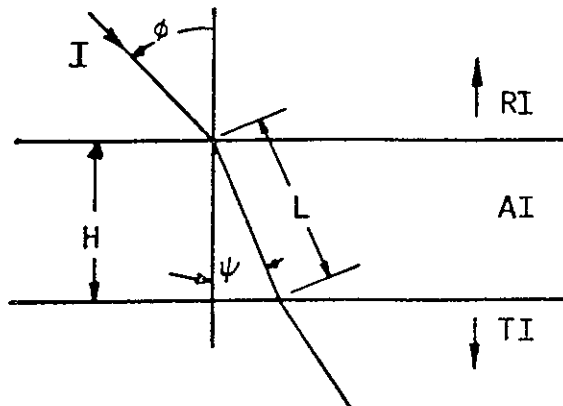
- Direct solar flux with specular absorber
- Direct solar flux with diffuse absorber
- Diffuse solar flux with specular absorber
- Diffuse solar flux with diffuse absorber

The effects of specular versus diffuse absorbing surfaces may be examined, as well as a comparison of the absorption of direct and diffuse solar energy. The program analyzes the reflection, absorption, and transmission of the direct and diffuse components of the incident solar flux separately and then combines the results to obtain the total heat absorption.

Appendix A

Single Layer

The reflection, absorption, and transmission of a single layer will be obtained. The geometry and nomenclature is indicated below.



I = incident flux

R = reflectance (total reflectance due to both first and second surfaces)

A = absorptance

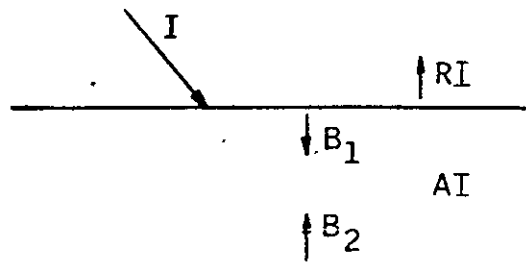
T = transmittance

ϕ = angle of incidence

ψ = angle of refraction, $\sin \phi / \sin \psi = n$ = index of refraction

The reflectance, absorptance, and transmittance are obtained using the radiosity method as follows.

Let B_1 be the flux leaving the first surface in a direction into the layer and B_2 be the flux leaving the second surface in a direction into the material.



Appendix A

Then B_1 consists of energy transmitted across the first surface plus reflection of energy arriving internally,

$$B_1 = (1 - r) I + r e^{-kL} B_2$$

and B_2 consists of only reflection of energy arriving internally,

$$B_2 = r e^{-kL} B_1$$

where k is the extinction coefficient of the absorbing layer and r is the reflectance at a single interface.

The interface reflectance, r , is given by

$$r_{11} = \frac{\sin^2(\phi - \psi)}{\sin^2(\phi + \psi)}, \quad r_i = \frac{\tan^2(\phi - \psi)}{\tan^2(\phi + \psi)}$$

where r_{11} is the reflectance for energy plane polarized in the plane of incidence and r_i is the reflectance for energy polarized in a plane perpendicular to the plane of incidence. The computer program carries out the analysis for each component separately and averages the final reflected, absorbed, and transmitted energies under the assumption that the incident solar flux is unpolarized.

Solving for B_1 and B_2 ,

$$B_1 = \frac{1 - r}{1 - r^2 e^{-2kL}} I$$

$$B_2 = \frac{r(1-r)e^{-kL}}{1 - r^2 e^{-2kL}} I$$

The reflected energy RI consists of first surface reflectance plus that portion of B_2 which remains after absorption in the layer and internal reflection at the first surface; i.e.,

$$RI = rI + (1 - r) e^{-kL} B_2$$

$$= rI + \frac{r(1-r)^2 e^{-2kL}}{1 - r^2 e^{-2kL}} I$$

Appendix A

and the reflectance, R, is

$$R = r \left(1 + \frac{(1-r)^2 e^{-2kL}}{1-r^2 e^{-2kL}} \right) \quad (A3)$$

Similarly, the transmitted energy TI consists of that portion of B_1 which remains after absorption and reflection;

$$TI = (1 - r) e^{-kL} B_1$$

and

$$T = \frac{(1-r)^2 e^{-kL}}{1-r^2 e^{-2kL}} \quad (A4)$$

The absorbed energy is obtained from the energy balance,

$$I = RI + AI + TI$$

or

$$A = 1 - R - T$$

It is noted here that Equation (A4) differs from the commonly stated expression for T,

$$T = \frac{1-r}{1+r} e^{-kL}$$

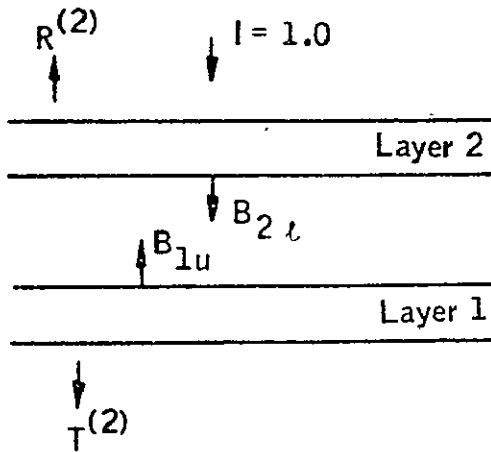
The numerical difference between the two relations is not large for the values of r, k, and H encountered in the flat plate collector. However, since the results are to be obtained by computer analysis, the more precise expression, Equation (A4), will be used.

Multiple Layers

The results for the single layer can now be used to obtain reflectance, absorptance, and transmittance for the two layer system. The analytical procedure will be presented for the two layer case and the results generalized for the N layer case.

Appendix A

The pertinent parameters are indicated on the following sketch. For convenience the incident flux is taken to be unity with no loss in generality.



The superscript in parenthesis is the order (No. of layers) of the system. The subscripts on B refer to the layer number and the upper (u) or lower (l) surface. The following nomenclature is used:

R_1 = reflectance of single layer system having properties (n, r, k, H) of layer 1

R_2 = reflectance of single layer system having properties of layer 2

T_1 = transmittance of single layer system having properties of layer 1

T_2 = transmittance of single layer system having properties of layer 2

$R^{(1)}$ = reflectance of single layer system = R_1

$R^{(2)}$ = reflectance of double layer system

$T^{(1)}$ = transmittance of single layer system = T_1

$T^{(2)}$ = transmittance of double layer system

$A_1^{(2)}$ = absorptance of layer 1 in a double layer system

$A_2^{(2)}$ = absorptance of layer 2 in a double layer system

Appendix A

To assist in following the analysis and to see the generalization to an N layer system the algebra has been organized on Figures 101 through 108 along with sketches of the geometry. Referring to Figure 102 for the two layer system, observe that $B_{2\ell}$ is composed of the transmission T_2 of solar flux by material 2 and the reflection $R_2 B_{lu}$ of the energy leaving the upper surface of layer 1. The interlayer gas is assumed to be nonabsorbing. B_{lu} consists of the reflectance $R^{(1)}$ of a one layer system times $B_{2\ell}$.

The reflection $R^{(2)}$ of the two layer system is the reflection of layer 2 for the incident flux I plus the transmission of flux B_{lu} through layer 2. The transmission $T^{(2)}$ of the two layer system is the transmission $T^{(1)}$ of a one layer system of flux $B_{2\ell}$ through layer 1. The absorption in layer 1, $A_1^{(2)}$, is the absorption of a one layer system for incident flux $B_{2\ell}$, and the absorption of layer 2 is the absorption of incident solar flux I and incident flux B_{lu} . It is noted that, although $R^{(1)} = R_1$, $A^{(1)} = A_1$, and $T^{(1)} = T_1$, the superscript form is used where necessary to show similarity with the three and four layer relations given on Figures 103 and 104.

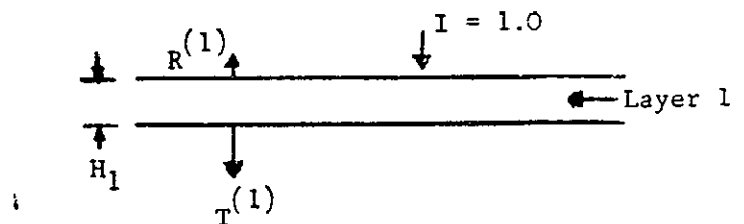
The reflectance $R^{(n, d)}$, absorptances $A_i^{(n, d)}$, and transmittance $T^{(n, d)}$ of an n layer system for diffuse incident solar flux are readily obtained by integration of the above derived direct values over the hemisphere. These results are given in Figure 105.

Multiple Layers Plus Absorber

Expressions for the reflectance and absorptances for an n layer system plus an absorbing material are readily derived using the above results. The relations are presented in Figures 106 through 109 for the four combinations of direct or diffuse solar flux with a specular or diffuse absorber. Some comments on the notation are necessary. The superscript n refers to the number of layers (covers) as before. The superscript $n+a$ refers to a system of n covers plus an absorber. Capital D implies direct incident solar flux. Lower case d implies diffuse incident solar flux and/or diffuse absorber (the second d refers to the absorber). The s superscript implies a specular absorber. Finally, the superscript n^{-1} on a parameter such as $R^{(n-1)}$ means that the reflectance is to be evaluated for the reverse order of the covers; i.e., for incident flux in the opposite direction. This produces the reflectance of the cover system for energy leaving the absorber. Note that although it can be demonstrated that $T^{(n-1)} = T^{(n)}$, the expression $T^{(n-1)}$ is retained where applicable. In general, $R^{(n-1)} \neq R^{(n)}$ and $A_i^{(n-1)}$.

Figure 106 contains the results for the direct incident solar plus specular absorber case. $B_a^{(n+c, D, S)}$ consists of the reflection of energy leaving the lower surface of cover 1. The energy leaving the lower surface of cover 1 consists of transmitted incident solar flux $T^{(n)}$ by an n cover system plus the reflection of $B_a^{(n+c, D, S)}$, and the absorber absorptance $A_a^{(n+a, D, S)}$ are similar and will not be elaborated upon.

Appendix A



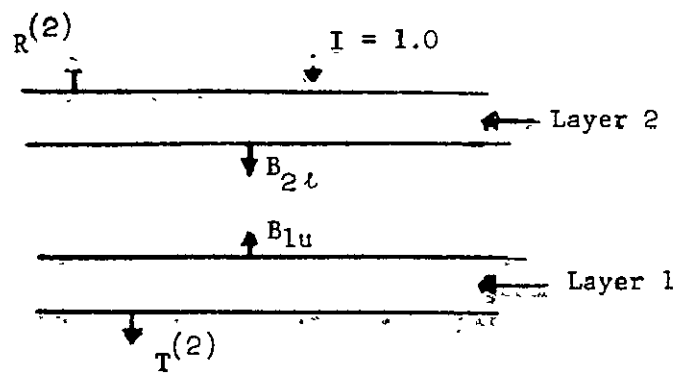
$$R^{(1)} = R_1 = r_1 \left(1 + \frac{(1 - r_1)^2 e^{-2k_1 L_1}}{1 - r_1^2 e^{-2k_1 L_1}} \right), \quad L_1 = \frac{H_1}{\cos \psi}$$

$$A_1^{(1)} = A_1 = 1 - R_1 - T_1$$

$$T^{(1)} = T_1 = \frac{(1 - r_1)^2 e^{-k_1 L_1}}{1 - r_1^2 e^{-2k_1 L_1}}$$

Figure 101. One Layer

Appendix A



$$B_{2L} = T_2 + R_2 B_{1L}$$

$$B_{1L} = R^{(1)} B_{2L}$$

$$R^{(2)} = R_2 + T_2 B_{1L}$$

$$A_1^{(2)} = A_1^{(1)} B_{2L}$$

$$A_2^{(2)} = A_2 + A_2 B_{1L}$$

$$T^{(2)} = T^{(1)} B_{2L}$$

$$B_{2L} = \frac{T_2}{1 - R_1 R_2}$$

$$B_{1L} = \frac{R_1 T_2}{1 - R_1 R_2}$$

$$R^{(2)} = R_2 + \frac{R_1 T_2^2}{1 - R_1 R_2}$$

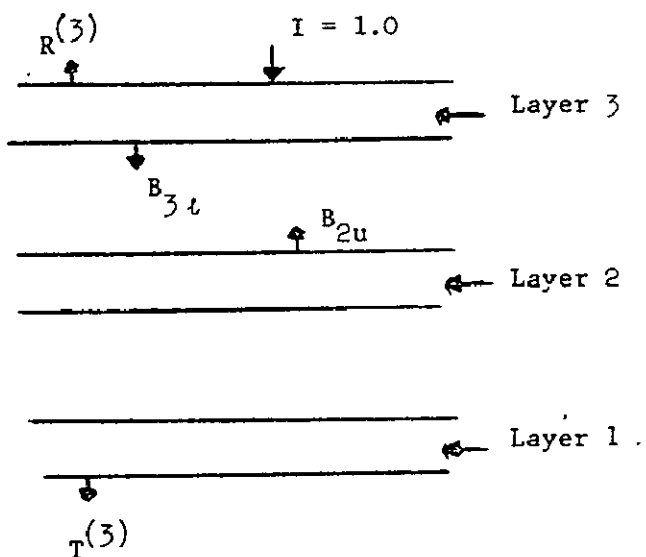
$$A_1^{(2)} = (1 - R_1 - T_1) \frac{T_2}{1 - R^{(1)} R_2}$$

$$A_2^{(2)} = 1 - R_2 - \frac{T_2}{1 - R^{(1)} R_2} (R^{(1)} T_2 - R^{(1)} + 1)$$

$$T^{(2)} = \frac{T_1 T_2}{1 - R^{(1)} R_2}$$

Figure 102. Two Layers

Appendix A



$$B_{3t} = T_3 + R_3 B_{2u}$$

$$B_{2u} = R^{(2)} B_{3t}$$

$$R^{(3)} = R_3 + T_3 B_{2u}$$

$$A_1^{(3)} = A_1^{(2)} B_{3t}$$

$$A_2^{(3)} = A_2^{(2)} B_{3t}$$

$$A_3^{(3)} = A_3 + A_3 B_{3u}$$

$$T^{(3)} = T^{(2)} B_{3t}$$

Figure 103. Three Layers

Appendix A

$$B_{3L} = \frac{T_3}{1-R^{(2)}R_3}$$

$$B_{2U} = \frac{R^{(2)}T_3}{1-R^{(2)}R_3}$$

$$R^{(3)} = R_3 + \frac{R^{(2)}T_3^2}{1-R^{(2)}R_3}$$

$$A_1^{(3)} = (1-R_1-T_1) \left[\frac{T_2}{1-R^{(1)}R_2} \right] \left[\frac{T_3}{1-R^{(2)}R_3} \right]$$

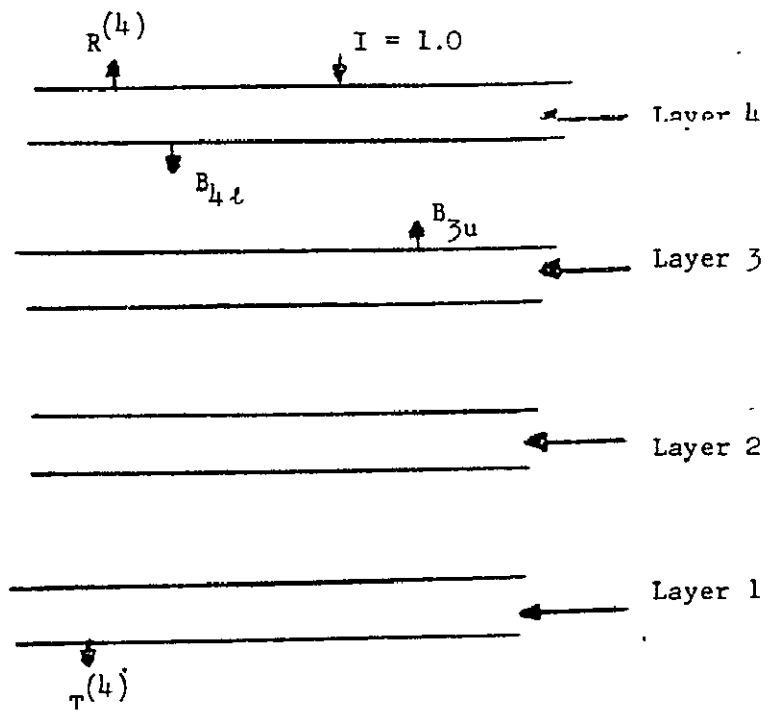
$$A_2^{(3)} = \left[1-R_2 - \frac{T_2}{1-R^{(1)}R_2} (R^{(1)}T_2 - R^{(1)} + 1) \right] \frac{T_3}{1-R^{(2)}R_3}$$

$$A_3^{(3)} = 1-R_3 - \frac{T_3}{1-R^{(2)}R_3} (R^{(2)}T_3 - R^{(2)} + 1)$$

$$T^{(3)} = \frac{T_1 T_2 T_3}{(1-R^{(1)}R_2)(1-R^{(2)}R_3)}$$

Figure 103. Three Layers (Concluded)

Appendix A



$$B_{4\downarrow} = T_4 + R_4 B_{3u}$$

$$B_{3u} = R^{(3)} B_{4\downarrow}$$

$$R^{(L)} = R_4 + T_4 B_{3u}$$

$$A_1^{(4)} = A_1^{(3)} B_{4\downarrow}$$

$$A_2^{(4)} = A_2^{(3)} B_{4\downarrow}$$

$$A_3^{(4)} = A_3^{(3)} B_{4\downarrow}$$

$$A_4^{(4)} = A_4 + A_4 B_{3u}$$

$$T^{(L)} = T^{(3)} B_{4\downarrow}$$

Figure 104. Four Layers

Appendix A

$$B_{4L} = \frac{T_4}{1-R^{(3)}R_4}$$

$$B_{3U} = \frac{R^{(3)}T_4}{1-R^{(3)}R_4}$$

$$R^{(4)} = R_4 + \frac{R^{(3)}T_4^2}{1-R^{(3)}R_4}$$

$$A_1^{(4)} = (1-R_1-T_1) \left(\frac{T_2}{1-R^{(1)}R_2} \right) \left(\frac{T_3}{1-R^{(2)}R_3} \right) \left(\frac{T_4}{1-R^{(3)}R_4} \right)$$

$$A_2^{(4)} = \left[1-R_2 - \frac{T_2}{1-R^{(1)}R_2} (R^{(1)}T_2 - R^{(1)} + 1) \right] \left(\frac{T_3}{1-R^{(2)}R_3} \right) \left(\frac{T_4}{1-R^{(3)}R_4} \right)$$

$$A_3^{(4)} = \left[1-R_3 - \frac{T_3}{1-R^{(2)}R_3} (R^{(2)}T_3 - R^{(2)} + 1) \right] \left(\frac{T_4}{1-R^{(3)}R_4} \right),$$

$$A_4^{(4)} = 1-R_4 - \frac{T_4}{1-R^{(3)}R_4} (R^{(3)}T_4 - R^{(3)} + 1)$$

$$T^{(4)} = \frac{T_1 T_2 T_3 T_4}{(1-R^{(1)}R_2)(1-R^{(2)}R_3)(1-R^{(3)}R_4)}$$

Figure 104. Four Layers (Conclu

Appendix A

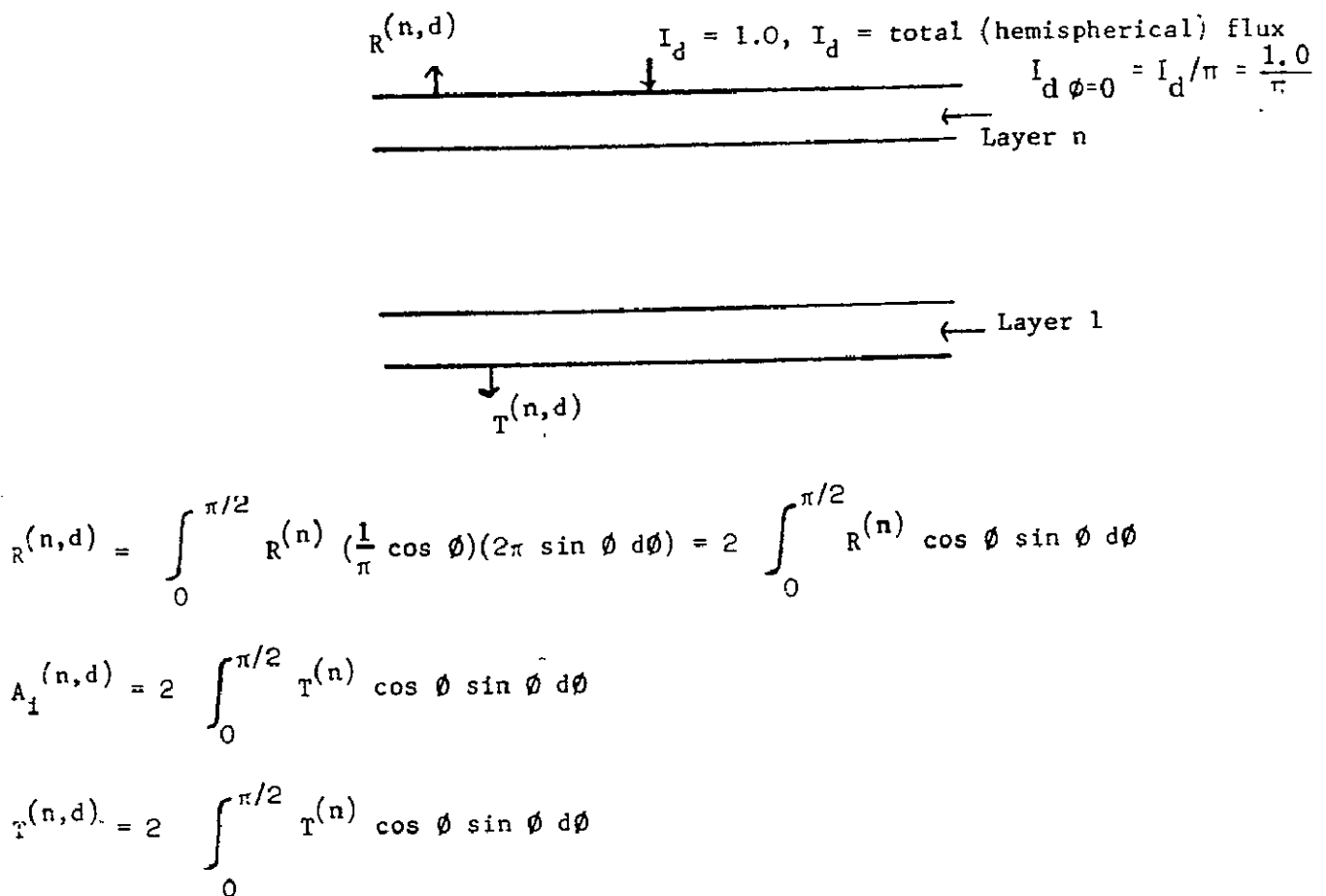


Figure 105. N Layers, Diffuse Incident Flux

Appendix A

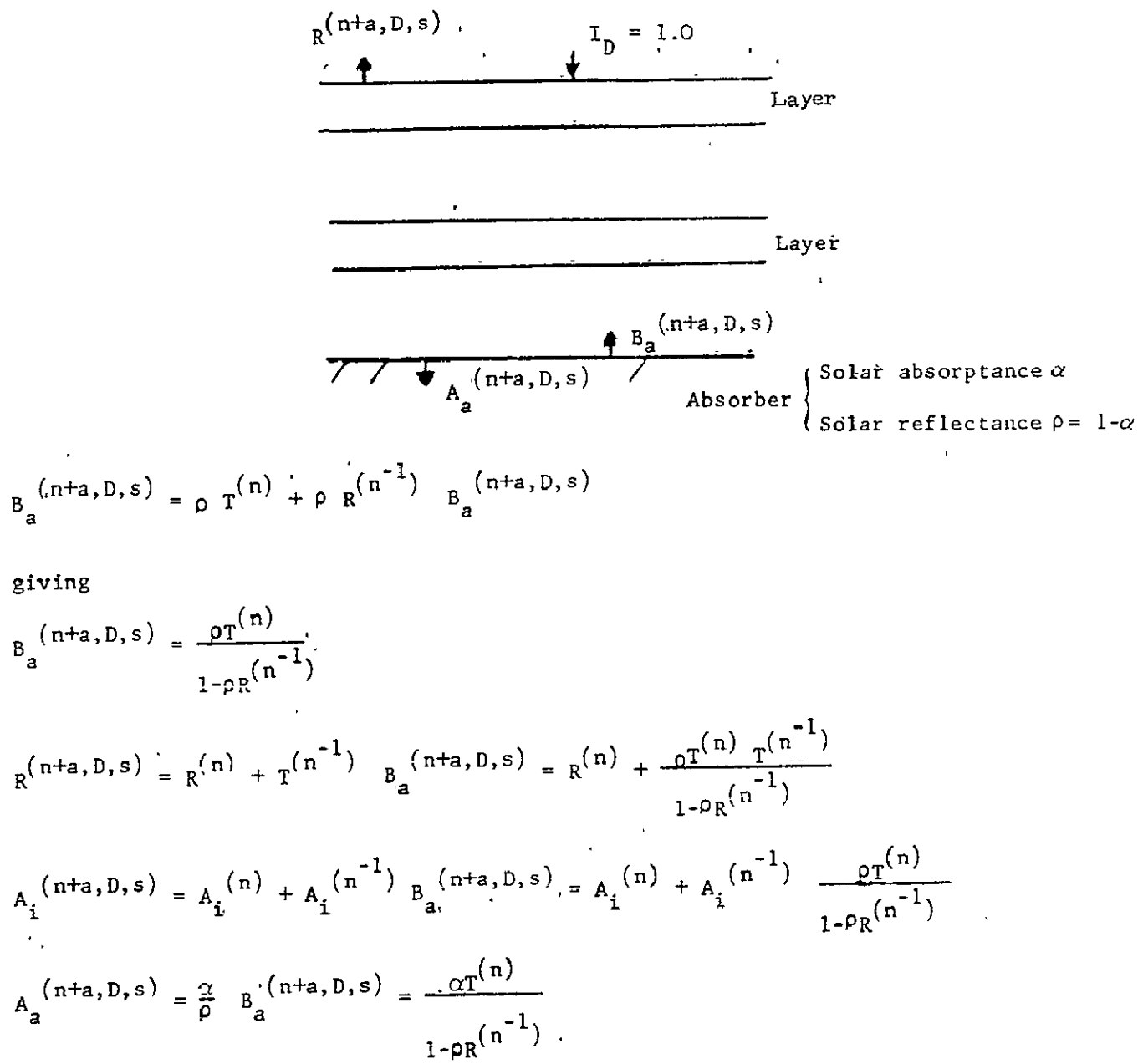


Figure 106. N Layers + Absorber: Direct Incident, Specular Absorber

Appendix A

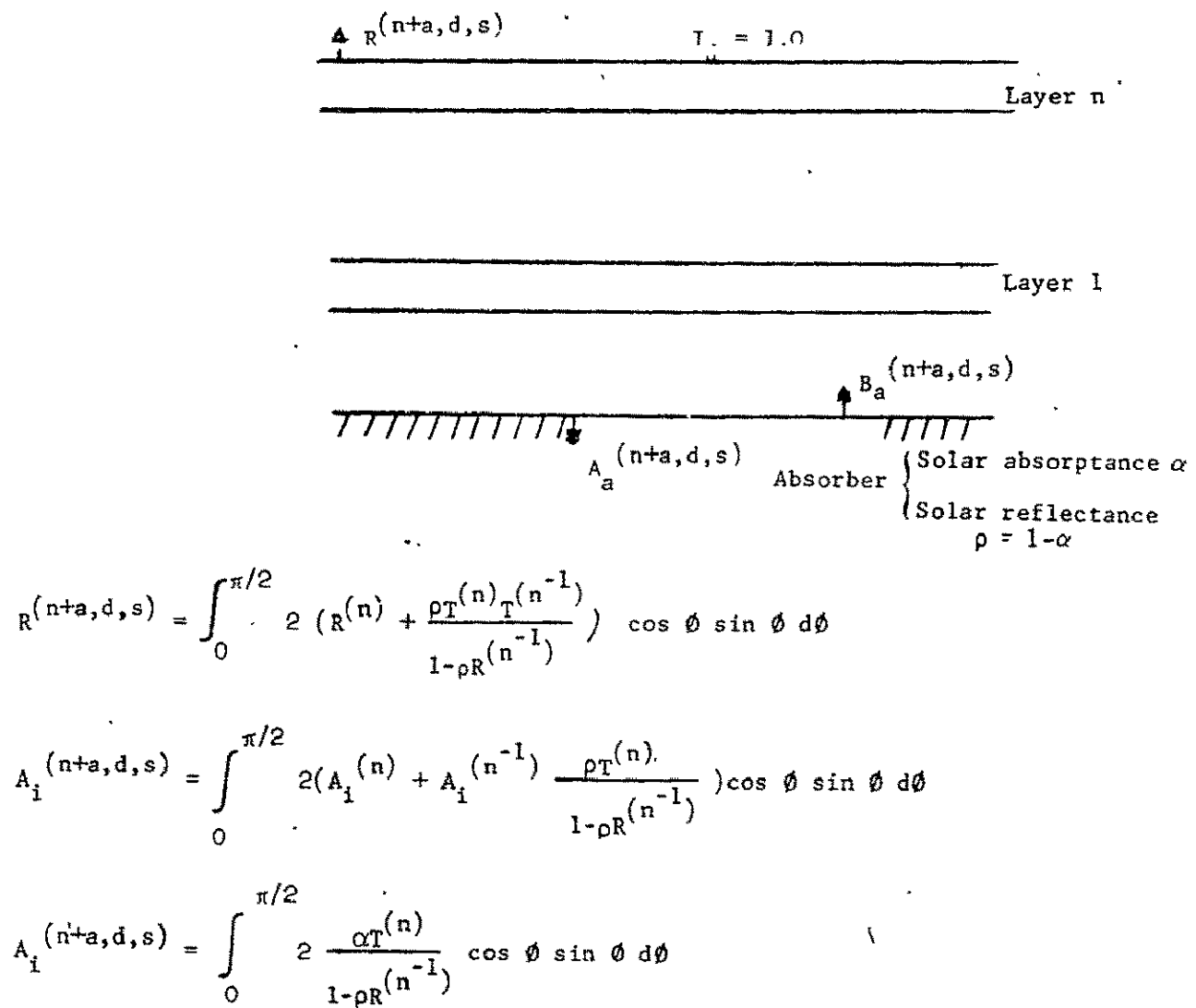


Figure 107. N Layers + Absorber: Diffuse Incident, Specular Absorber

Appendix A

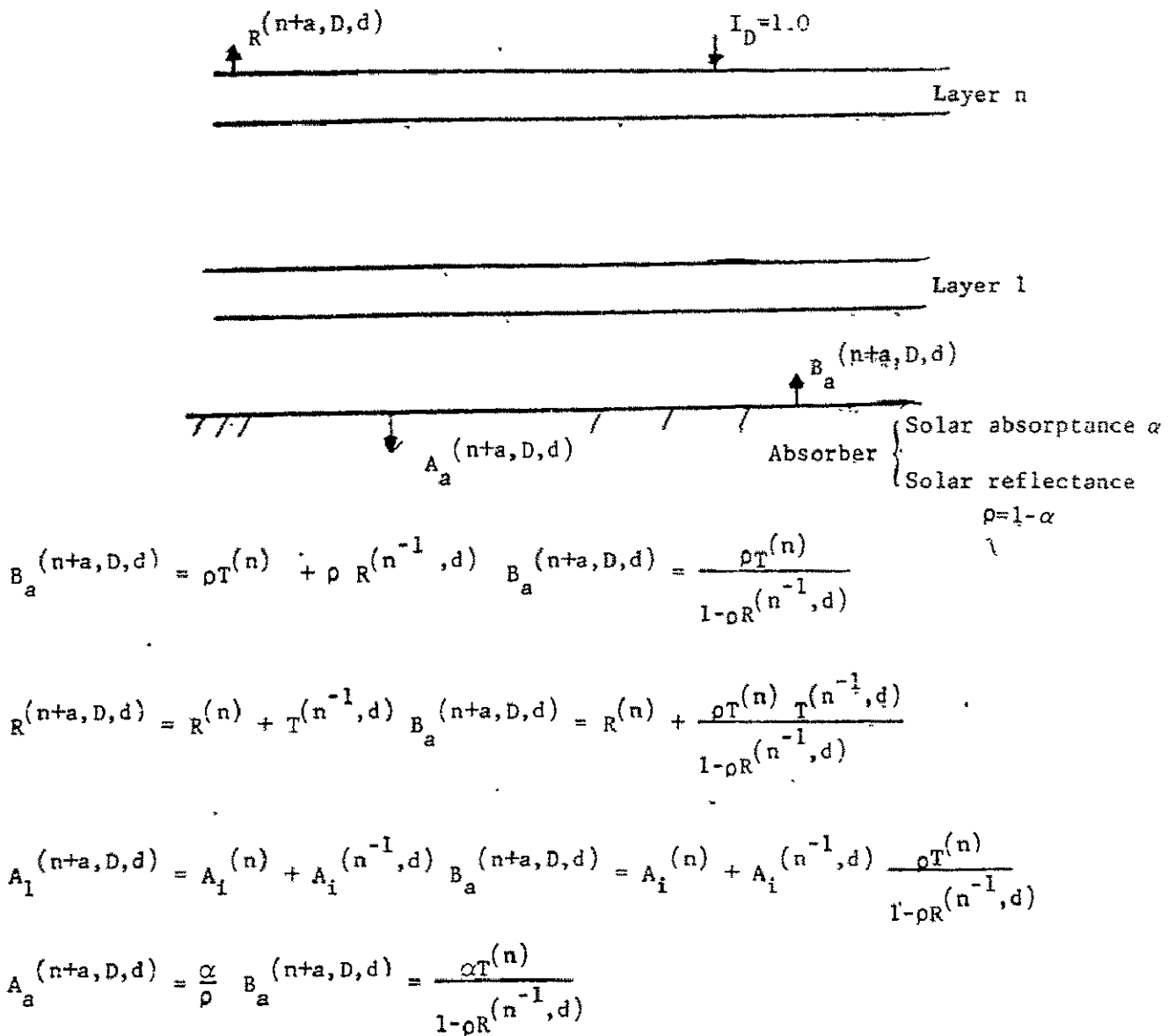


Figure 108. N Layers + Absorber: Direct Incident, Diffuse Absorber

Appendix A

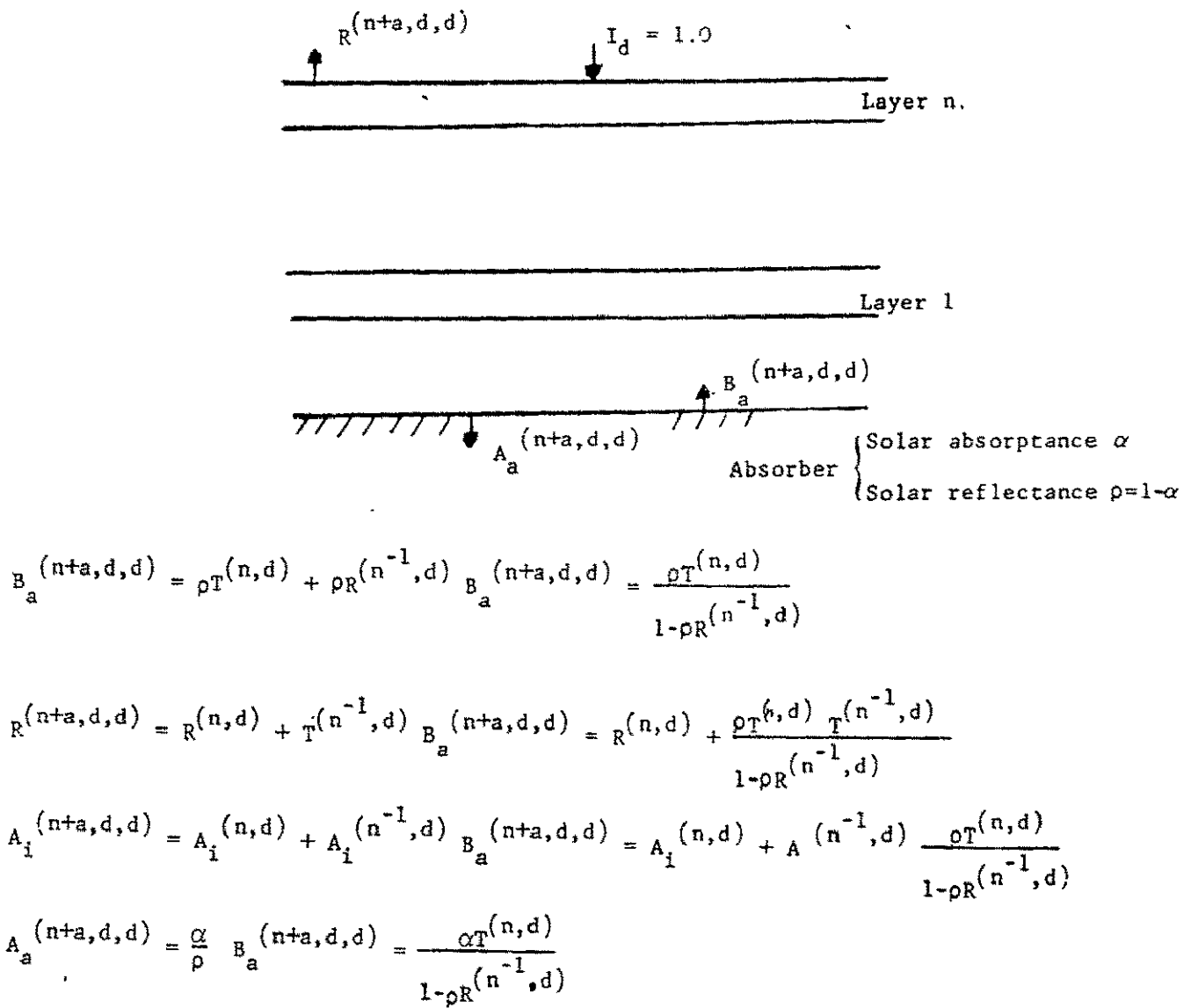


Figure 109. N Layers + Absorber: Diffuse Incident, Diffuse Absorber

Appendix A

Figure 107 indicates the necessary integration of the direct results to obtain reflectance and absorptances for the case of diffuse incident solar flux.

The results in Figure 108 for direct incident solar flux and diffuse absorber and the results of Figure 109 for diffuse incident and diffuse absorber are arrived at by similar arguments. Note that the diffuse incident - diffuse absorber results do not require integration since the energy distribution leaving the absorber is specified (i.e., is diffuse). In the case of the specular absorber with diffuse incident flux, the angular distribution was not known since the covers alter the angular distribution of the originally diffuse incident flux.

Heat Losses

The solar energy absorption by the absorber is partially lost to the environment by convection and radiation between the absorber and the cover system and by conduction through the insulation on the back side of the absorber. In addition, there will be edge losses around the periphery of the collector.

Natural conduction between parallel plates has been treated by several investigators. Tabor⁽⁷⁾ reviewed several proposed correlations and recommends the relations below for the Nusselt number (Nu) which are presented in Ref. (8):

$$Nu = 0.0369 Ra^{0.381}, \text{ vertical planes, } 1.5 \times 10^4 < Gr < 1.5 \times 10^5, \\ Pr = 0.72$$

$$Nu = 0.0685 Ra^{0.327}, \text{ vertical planes, } 1.5 \times 10^5 < Gr < 10^7, Pr = 0.72 \quad (A5)$$

$$Nu = 0.102 Ra^{0.310}, \text{ } 45^\circ \text{ planes } 10^4 < Gr < 10^7, Pr = 0.72$$

$$Nu = 0.168 Ra^{0.281}, \text{ horizontal planes, } 10^4 < Gr < 10^7, Pr = 0.72$$

The heat flow is

$$Q = \frac{NukA}{H} (T_j - T_i)$$

or in terms of a conductance,

$$Q = K_{ij} (T_j - T_i), K_{ij} = NukA/H \quad (A6)$$

Appendix A

where A is the area of the nodal element of the absorber or cover, T is the temperature of the surface indicated by the subscript, H is the gap width, and k is the thermal conductivity of the air in the gap.

The exchange of infrared radiation between the absorber and cover and between adjacent covers is given by the expression

$$\begin{aligned} Q &= \left(\frac{1}{\epsilon_i} + \frac{1}{\epsilon_j} - 1 \right)^{-1} A \sigma (T_j^4 - T_i^4) \\ &= K_{ij} (T_j - T_i), \quad K_{ij} = \left(\frac{1}{\epsilon_i} + \frac{1}{\epsilon_j} - 1 \right)^{-1} A \sigma (T_i^2 + T_j^2) (T_i + T_j) \end{aligned} \quad (A7)$$

where ϵ is the emittance of the surface indicated by the subscript, T is its temperature, and A is the surface area.

The convection loss from the top cover to ambient and from the insulation surface to ambient may be expressed by

$$Q = hA (T_s - T_{amb}), \quad K_{ij} = hA \quad (A8)$$

where A is the convective heat transfer coefficient, T_s is the surface temperature, and T_{amb} is the ambient air temperature. Depending on the wind velocity and turbulence, collector orientation, and the effect of the edge conditions, the flow over the collector may be laminar or turbulent.

A well known heat transfer correlation for laminar flow over a flat plate is

$$NU = \frac{hL}{k} = 0.664 R_e^{1/2} Pr^{1/3} \quad (A9)$$

where the Nusselt and Reynolds numbers are based on the length of the surface in the flow direction. For a boundary layer that is turbulent over the entire collector,

$$NU = 0.037 R_e^{0.8} Pr^{1/3} \quad (A10)$$

In the computer program suitable local values of these heat transfer coefficients are used which are then integrated over the length of the nodal elements. In this way the variation of h with position is accounted for. (The program also has provision for specifying the wind direction.)

Appendix A

The radiation loss from the top cover is ambient and from the insulation to ambient is given by

$$Q = \epsilon A \sigma (T_s^4 - T_{sky}^4) \quad (A11)$$

where ϵ is the infrared emittance of the surface and T_{sky} is the mean radiant temperature of the ambient.

In addition to these heat flows, there is heat transfer by conduction between adjacent absorber nodes, adjacent cover nodes, and adjacent insulation nodes. All of these heat flows take the form

$$Q_{ij} = kA \frac{T_j - T_i}{\Delta x}, \quad K_{ij} = \frac{kA}{\Delta x} \quad (A12)$$

where k is the thermal conductivity of the conducting material and Δx is the path length for heat flow between the two locations of T_i and T_j .

Finally, there will be a flow of enthalpy due to the moving collector fluid. This must be accounted for in the energy balance of the fluid nodes by a term $m c_p$ at the inlet and exit planes of each fluid node.

HEAT ABSORBED BY COLLECTOR FLUID

The primary purpose of the collector is to heat a fluid which flows in physical contact with the absorber. The current version of the computer program assumes an integral tube-plate absorber with parallel flow tubes as indicated in Figure 100. Fluid is assumed to enter the tubes from a common header and empty into a collection header.

The heat transfer from the tube walls to the fluid corresponds to the case of developing thermal and hydrodynamic conditions. Rohsenow (4) presents correlations for four combinations of boundary (uniform wall temperature or uniform heat flux at the wall) and flow conditions. The computer program uses the following relation for the average Nusselt number as a function of the distance x from the inlet,

$$NU_x = \frac{hD}{k} = 4.36 + \frac{0.023 (D/x) RePr}{1 + 0.0012 (D/x) RePr} \quad (A13)$$

where the Reynolds number is based on the tube diameter D . This expression is averaged over the length of the nodal elements to account for the variation in h over the node and to account for the location of the element with respect to the inlet.

Appendix A

SOLUTION STABILITY

The explicit step-by-step solution procedure described earlier is subject to a restriction on the maximum allowable integration time step in order to avoid instability and gross divergence of the solution as time progresses. An automatic stabilization routine has been built into the computer program to minimize the possibility of divergence. At each time step the maximum integration step size is computed from the geometrical and thermal condition and is multiplied by a safety factor, less than or equal to unity. The resulting time interval is used as the integration step size. If the solution diverges outside prespecified bounds on the nodal temperatures, the safety factor is reduced in magnitude and the problem is restarted from the beginning.

APPENDIX B

FLOW DISTRIBUTIONS IN SOLAR COLLECTOR ARRAYS

INTRODUCTION

A typical solar heating installation for a residence might consist of a large number of flat plate collector modules assembled as an array on or in the structure roof. Collection fluid will be supplied to the modules in some form of series-parallel network. The piping network must be designed to provide the proper flow to each module. Also, within a module, the goal is to provide uniform flow per unit area of the collector. In the usual case of uniformly spaced tubes running from a supply header to a collection header as indicated in Figure 110, it is desirable to provide, as nearly as possible, equal flow to each tube. This latter problem, uniform flow within a module, is addressed in the following paragraphs.

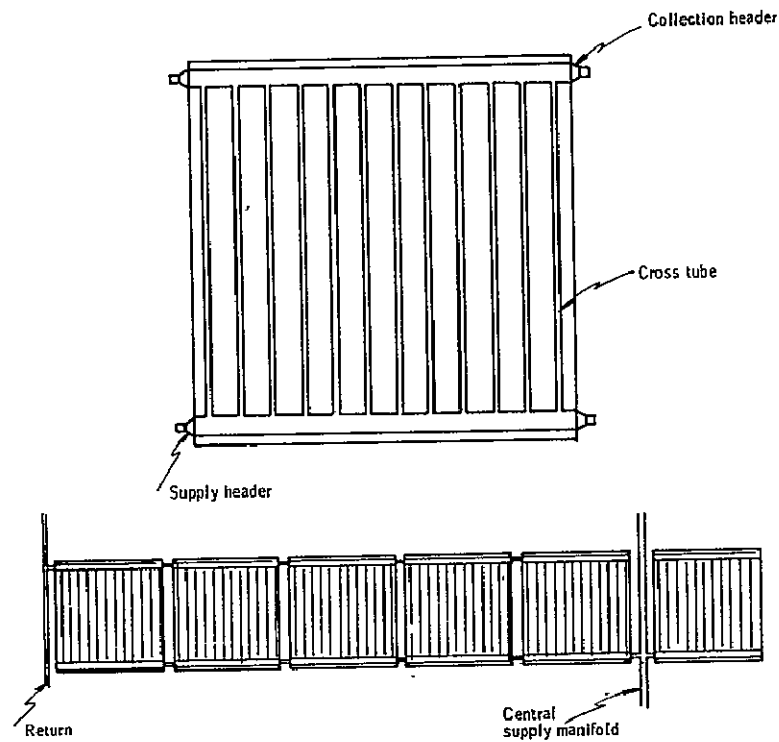


Figure 110. Flat-Plate Solar Collector

Preceding page blank

Appendix B

FLOW ANALYSIS

The flow in a tube is determined by the difference in pressure between the supply header and the collection header at the tube ends. The header pressures will vary along their length due to (1) wall friction losses and (2) momentum flux changes in the headers as fluid is withdrawn or added. The pressure in the supply manifold will fall in the flow direction due to wall shear stress, but the drop will be reduced by pressure recovery at each cross tube due to extraction of fluid and subsequent loss of momentum in the supply header flow. In the collection header, the frictional drop is reinforced by the acceleration drop due to the increased momentum. The resulting pressure difference at the ends of a tube will, therefore, vary from one tube to the next, and the flow rate will vary from tube to tube.

Header Pressure Drop Due to Wall Shear

Pressure drop in the flow in a header between adjacent tubes depends on the flow rate and the flow condition; e.g., laminar or turbulent, developing or fully developed. Since only a small percentage of the header flow is extracted or added at each cross tube, the header flow is assumed to be fully developed at all locations. The flow is assumed to be laminar for Reynolds numbers below 2000 and turbulent above 2000. In either range, the pressure drop, ΔP , over a length, ΔL , may be expressed by:

$$\Delta P = 4f \frac{\Delta L}{D} \frac{1}{2} \rho V^2 \quad (B1)$$

where ΔL is the header passage length between cross tubes, D is the passage equivalent diameter, ρ is the fluid density, and V is the average velocity. The friction factor, f , for laminar flow in a rectangular duct (it is assumed that the headers and cross tubes will be essentially rectangular for reasons which will be discussed later) is given by

$$f = \frac{16}{\phi Re} \quad (B2)$$

where

$$Re = \frac{\rho V D}{\mu}, \mu = \text{dynamic viscosity} \quad (B3)$$

The factor ϕ is a function of the duct aspect ratio, which is the ratio of the short side to the long side. A plot of ϕ versus aspect ratio is presented on page 62, Ref. 8.

Appendix B

In the turbulent range the Blasius equation will be used,

$$f = 0.079 \operatorname{Re}^{-0.25} \quad (\text{B4})$$

It should be noted that this relation is ordinarily applied for Reynolds numbers above 5000. For the transition zone, $2000 < \operatorname{Re} < 5000$, convenient formulae are not available, and the Blasius relation will be used for Re greater than 2000.

Cross-Tube Pressure Drop

The discussion above applies equally well to the cross-tube pressure drop. However, the flow in a cross tube will almost always be in the laminar regime and the pressure drop will be given by

$$\Delta P = \left(4f_t \frac{L_t}{D_t} + K_t \right) \frac{1}{2} \rho V_t^2 \quad (\text{B5})$$

where the friction factor is given by Equation (B2). The factor K_t accounts for entrance pressure losses due to (1) increased wall shear and (2) momentum flux increases in the entrance length. K_t is presented on page 117, Chapter 7 of Ref. (9) as a function of the cross-tube aspect ratio.

Pressure Changes Due to Removal or Addition of Flow at Branches

Fluid is removed from the supply header at each cross tube branch. Considering the control volume as indicated in Figure 111, and equating the net efflux of longitudinal momentum with the net force in the longitudinal direction gives:

$$(P_L - P_R - \Delta P_{\text{shear}}) A_h = M_R V_R - M_L V_L + M V_t \quad (\text{B6})$$

where ΔP_{shear} is the pressure drop over the distance a_t due to wall shear stress.

It is convenient to include the effect of the efflux of longitudinal momentum due to the cross-tube discharge, $M V_t$, as a coefficient C in the form

$$(P_L - P_R - \Delta P_{\text{shear}}) A_h = C(M_R V_R - M_L V_L) \quad (\text{B7})$$

or

$$P_L - P_R = \Delta P_{\text{shear}} - \frac{1}{2} C \rho (V_L^2 - V_R^2) \quad (\text{B8})$$

Appendix B

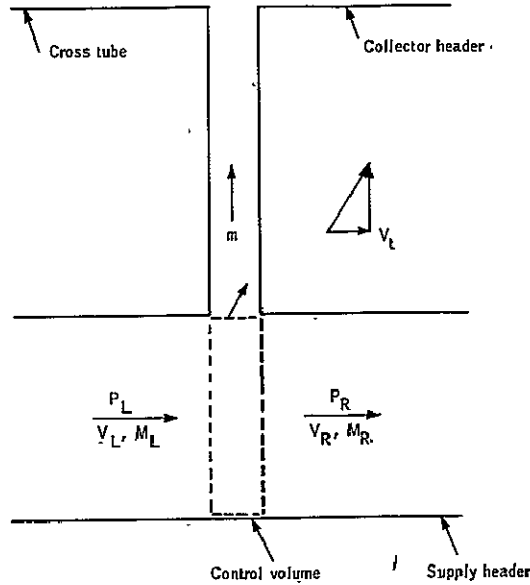


Figure 111. Control Volume Computation

In words, the pressure drop in the supply header from a cross section at the upstream edge of the cross tube to a cross section at the downstream edge is the shear stress ΔP minus the pressure recovery due to loss of longitudinal momentum,

The coefficient C has been studied by Acrivos et al. for air discharging from ports in a header. For fractional changes of header velocity in the range

$$0.2 < \frac{V_L - V_R}{V_L} < 0.5 \quad (B9)$$

they observed values of C on the order of 0.7.

For discharge from a cross tube into the collection header, Equation (B8) takes the form

$$P'_L - P'_R = \Delta P'_{\text{shear}} + \frac{1}{A_h'^2} C' \rho (V_R'^2 - V_L'^2), \quad \text{primes refer to collection header} \quad (B10)$$

where the increased momentum flux in the collection header results in an additional pressure drop.

Appendix B

Cross-Tube Flow Distribution

Using the relations presented above, the following set of equations can be written for the i^{th} cross tube,

$$P_{L,i} = P_{R,i-1} - 4f_{h,i} \frac{\Delta L_h - a_t}{D_h} \frac{1}{2} \rho V_{L,i}^2 \quad (\text{B11})$$

$$P'_{L,i} = P'_{R,i-1} - 4f'_{h,i} \frac{\Delta L_h - a_t}{D_h} \frac{1}{2} \rho V'_{L,i}^2 \quad (\text{B12})$$

$$P_{L,i} - P_{R,i} = 4f_{h,i} \frac{a_t}{D_h} \frac{1}{2} \rho V_{L,i}^2 - \frac{C\rho}{A_h} (V_{L,i}^2 - V_{R,i}^2) \quad (\text{B13})$$

$$P'_{L,i} - P'_{R,i} = 4f'_{h,i} \frac{a_t}{D_h} \frac{1}{2} \rho V'_{L,i}^2 - \frac{C\rho}{A_h} (V'_{L,i}^2 - V'_{R,i}^2) \quad (\text{B14})$$

$$\frac{1}{2} (P_{L,i} + P_{R,i}) - \frac{1}{2} (P'_{L,i} + P'_{R,i}) = \left(4f_{t,i} \frac{L_t}{D_t} + K_t \right) \frac{1}{2} \rho V_{t,i}^2 \quad (\text{B15})$$

$$\rho A_h (V_{L,i} - V_{R,i}) = \rho A_t V_{t,i} \quad (\text{B16})$$

$$\rho A_h (V'_{R,i} - V'_{L,i}) = \rho A_t V_{t,i} \quad (\text{B17})$$

$$V_{L,i} = V_{R,i-1} \quad (\text{B18})$$

$$V'_{L,i} = V'_{R,i-1} \quad (\text{B19})$$

In Equations (B13) and (B14) the friction factors, $f_{h,i}$ and $f'_{h,i}$, will be computed based on the velocities $V_{L,i}$ and $V'_{L,i}$, respectively. The velocities $V_{R,i}$ and $V'_{R,i}$, or the mean values, could equally well have been chosen with very little numerical difference in the final result. The difference in average pressures has been used in Equation (B15) to compute the cross tube flow. Equations (B16) and (B17) express mass conservation at the cross-tube junctions.

Appendix B

Equations (B11) to (B19) are a set of nine equations in nine unknowns: $P_{L,i}$, $P'_{R,i}$, $V_{L,i}$, $V'_{R,i}$, P'_L,i , P_R,i , V'_L,i , V'_R,i , $V_{t,i}$. Considering that a collector may have a dozen cross tubes or that a row of collectors might involve as many as 100 cross tubes, solution of the resulting set of nearly 1000 simultaneous equations would be a formidable task. Fortunately, a much simpler procedure has been employed which will be outlined.

Assuming for the moment that $V'_{R,i-1}$ and $V'_{R,i-1}$ are known, then $V'_{L,i}$ and V'_L,i are known from Equations (B18) and (B19). Then, $P_{L,i}$ and P'_L,i are given by Equations (B11) and (B12). $V_{R,i}$ and V'_R,i can be expressed in terms of the tube flow $V_{t,i}$ from Equations (B16) and (B17). Substituting in Equations (B13), (B14), and (B15) results in three equations in the three unknowns $P'_{R,i}$, P_R,i , $V_{t,i}$. Algebraic elimination of $P'_{R,i}$ and P_R,i results in a quadratic in $V_{t,i}$ which, when solved for $V_{t,i}$, allows direct evaluation of $P'_{R,i}$ and P_R,i and all unknowns have been calculated.

The procedure is started by assuming that the inlet header flow is given and thus $V'_{L,1}$ is known. Similarly it is assumed that the collection header flow is known upstream of tube No. 1 and thus $V'_L,1$ is given. The pressure level of the system is arbitrary, so one pressure, ordinarily the inlet pressure $P_{L,1}$, may be assumed. The solution then proceeds by assuming a value for the velocity, $V_{t,1}$ in tube 1. This permits direct calculation of all other parameters at the supply and collection ends of tube 1. Then the above outlined procedure for solving for the nine unknowns at tube 2 can be followed and repeated for all tubes. If the flow in the supply header is nonzero immediately downstream of the last tube, the solution is repeated for a new value of $V_{t,1}$. By trial and error the proper value of $V_{t,1}$ is found and the problem is solved.

This procedure has been programmed for solution on a digital computer with an on-line plotter. Results have been obtained for a row of 10 collectors as indicated in Figure 110. This number of collectors was chosen as typical for a single family dwelling. A complete array would consist of several rows. The present analysis is concerned with the distribution of flow in one row. The pressure drop in the supply and collection headers in the collectors can be reduced by providing a central supply manifold as indicated in Figure 110, with the flow passing both ways to the outer edge of the array. This produces a significant improvement in the flow uniformity between tubes.

The analysis has thus been carried out for a row of five collectors each having 12 cross tubes for a total of 60 tubes as shown in Figure 110. The supply and collection headers are on 42-inch centers and the cross tubes are 40 inches long on 3.552-inch centers. The headers are rectangular ducts with 1/2-inch by 2-inch inside dimensions. The cross tubes are also rectangular in section and will have 0.050-inch by 0.500-inch inside dimensions. These spacing and dimensions were arrived at from the results of the present analysis.

Appendix B

Figures 112 to 114 present the results of the flow distribution calculations for three possible cross-tube dimensions: 0.050-inch by 0.500-inch, 0.100-inch by 0.500-inch and 0.200-inch by 0.500-inch. The sensitivity of the flow distribution to the cross-tube dimensions is immediately evident. Referring to Figure 112 for the 0.050-inch by 0.500-inch tube, it is seen that the cross-tube pressure drop at a nominal flow of 10 lbm/hr is about 2.5 inches of water. This is a relatively large pressure difference compared with the header pressure variation and, consequently, the cross-tube flow distribution is quite uniform.

As the cross-tube inner height is increased, the associated pressure drop falls rapidly and, as shown in Figure 113 for the 0.100-inch by 0.500-inch tubes, the header pressure variation causes a significant nonuniformity in the flow distribution. The distribution for the 0.200-inch by 0.500-inch tubes, Figure 114, is badly out of balance.

Increasing the cross-sectional dimensions of the headers results in less header pressure variation and more uniform flow. However, the mass of fluid and collector heat capability increase as the header dimensions are increased. For 0.5-inch by 2.0-inch headers and 0.050-inch by 0.500-inch cross tubes, the fluid heat capacity is about 25 percent of the total collector heat capacity, and 90 percent of the fluid is in the two headers.

It should be noted that if a nonuniform flow is present, the resulting variation in the fluid temperature will produce a variation in the hydrostatic pressure distribution which acts in a direction to reduce the nonuniformity. Since the hydrostatic pressure of a 40-inch column of a 50-percent mixture of ethylene glycol and water decreases 0.016-inch of water per °F, the temperature variation will produce a significant improvement in the flow distribution for the 0.200-inch by 0.500-inch tubes, but very little improvement for the thinner tubes.

Appendix B

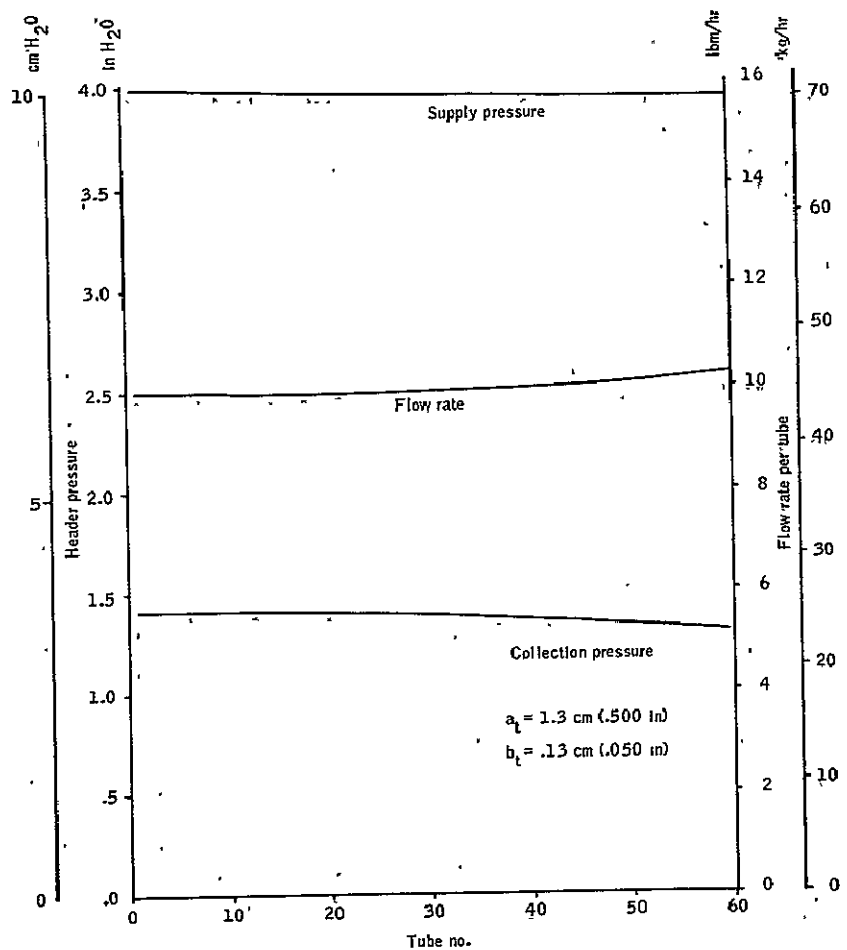


Figure 112. Flow Distribution for $0.13 \text{ cm} \times 1.3 \text{ cm}$
 $(0.05 \text{ in.} \times 0.50 \text{ in.})$ Cross Tube

Appendix B

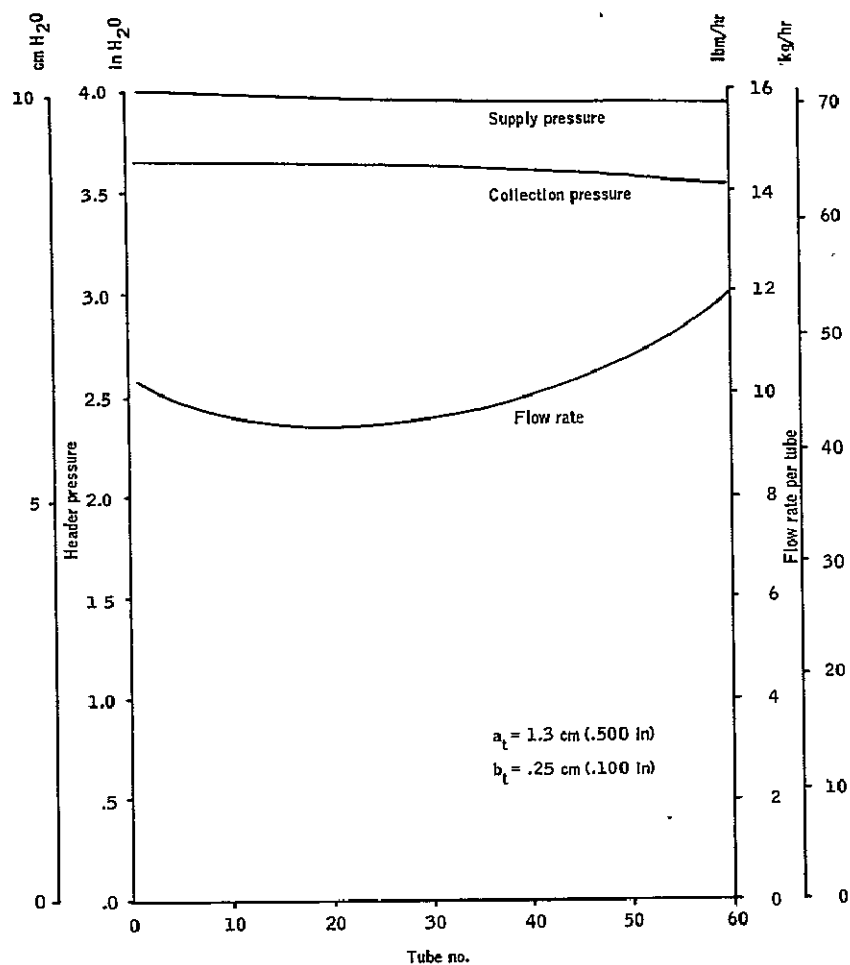


Figure 113. Flow Distribution for
0.25 cm x 1.3 cm
(0.10 in. x 0.50 in.)
Cross Tube

Appendix B

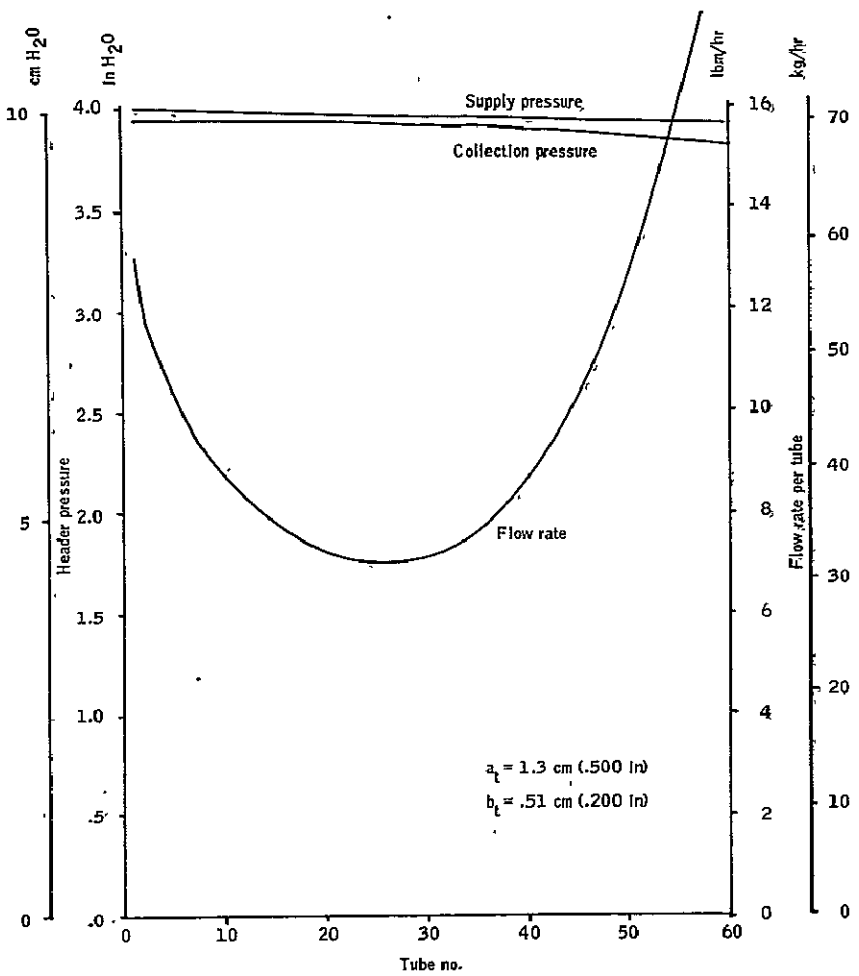


Figure 114. Flow Distribution for
0.5 cm x 1.3 cm
(0.20 in. x 0.50 in.)
Cross Tube

APPENDIX C

SOLAR SIMULATOR AND OUTDOOR TEST DATA

SOLAR SIMULATOR TEST DATA

Solar simulator test data for Black Nickel on aluminum, black paint on aluminum, Black Nickel on steel, and Black Chrome on steel are presented in Tables 19 through 22, respectively, for various combinations of cover, incident angle, and diffuse/direct ratio.

OUTDOOR TEST DATA

Outdoor test data taken at various times of the day over a period of nine different days from 9/26/74 to 10/26/74 are presented in Tables 23 through 31 for selective coated and nonselective coated collectors with two glass covers. In addition to time of day, the data recorded included incident solar flux, ambient temperature, wind velocity, mass flow rate, temperature rise, and fluid inlet temperature.

TABLE 19. - SOLAR SIMULATOR TEST DATA FOR BLACK NICKEL ON ALUMINUM

ABSORBER: Black Nickel on aluminum

(Baseline)

COVER: 2 glass

INCIDENT ANGLE: 0°

50% solution ethylene
glycol with water

DIFFUSE/DIRECT RATIO: 0

Test run	Fluid inlet temp, °F	Mass flow rate, lbm/hr ft ²	Temp rise, °F	Average fluid temp, °F	Collected energy flux, Btu/hr ft ²	Incident energy flux, Btu/hr ft ²	Collector efficiency, percent
6	200.0	10.1	5.0	202.5	44.2	171.1	25.8
7	200.0	10.1	13.3	206.7	117.7	255.5	46.1
8	200.0	10.1	18.8	209.4	166.5	119.0	52.2
9	160.0	9.9	14.8	167.4	126.7	240.0	52.8
58	160.7	10.0	17.1	169.3	147.7	266.8	55.4
10	120.0	10.1	9.7	124.9	82.9	147.8	56.1
14	120.0	9.9	17.5	128.7	145.6	232.0	62.8
50	120.6	10.0	19.5	130.4	164.9	258.2	63.9
15	120.0	10.0	25.1	132.6	212.4	323.3	65.7
53	119.5	10.0	23.5	131.2	198.2	296.3	66.9
13	80.0	9.9	12.7	86.3	103.2	160.2	64.4
12	80.0	9.9	19.5	89.7	158.9	233.0	68.2
11	80.0	9.8	28.0	94.0	226.4	324.0	69.9

TABLE 19. - Continued.

ABSORBER: Black Nickel on aluminum

COVER: 2 glass

INCIDENT ANGLE: 40°

DIFFUSE/DIRECT RATIO: 0

Test run	Fluid inlet temp, °F	Mass flow rate, lbm/hr ft ²	Temp rise, °F	Average fluid temp, °F	Collected energy flux, Btu/hr ft ²	Incident energy flux, Btu/hr ft ²	Collector efficiency, percent
72	201.2	10.0	0.0	202.1	0	146.8	0
74	201.0	10.0	9.4	205.7	82.6	236.3	35.0
76	199.5	10.0	15.9	207.5	140.1	322.3	43.5
59	160.2	10.0	14.4	167.4	124.0	266.8	46.5
48	120.7	10.0	7.2	124.3	60.6	159.4	39.1
51	120.8	10.0	16.6	129.1	140.0	258.2	54.2
54	119.1	10.0	19.1	128.7	161.4	296.3	54.5
33	80.3	10.0	12.3	86.4	101.1	160.5	63.0
35	79.5	10.0	18.4	88.7	151.8	259.1	58.6
37	79.3	10.0	23.9	91.3	197.8	311.2	63.5

TABLE 19. - Continued.

ABSORBER: Black Nickel on aluminum

COVER: 2 glass

INCIDENT ANGLE: 60°

DIFFUSE/DIRECT RATIO: 0

Test run	Fluid inlet temp, °F	Mass flow rate, lbm/hr ft ²	Temp rise, °F	Average fluid temp, °F	Collected energy flux, Btu/hr ft ²	Incident energy flux, Btu/hr ft ²	Collector efficiency, percent
73	201.7	10.0	-3.3	200.0	-29.2	146.8	-19.9
75	201.2	9.9	0.3	201.3	2.3	236.3	1.0
77	200.6	9.4	2.9	202.1	24.1	322.3	7.5
60	160.4	10.0	6.1	163.4	52.1	266.8	19.5
49	120.7	10.0	3.1	122.2	25.8	154.9	16.6
52	120.4	10.0	8.0	124.4	67.3	258.2	26.1
55	117.7	10.0	9.4	122.4	26.7	296.3	26.7
34	79.4	10.0	6.3	82.5	51.5	160.5	32.1
36	79.7	10.0	10.9	85.1	89.5	259.1	34.5
38	79.6	10.0	13.1	86.1	107.7	311.2	34.6

TABLE 19. - Continued.

ABSORBER: Black Nickel on aluminum

COVER: 2 glass

INCIDENT ANGLE: 0°

DIFFUSE/DIRECT RATIO: 0.85

Test run	Fluid inlet temp, °F	Mass flow rate, lbm/hr ft ²	Temp rise, °F	Average fluid temp, °F	Collected energy flux, Btu/hr ft ²	Incident energy flux, Btu/hr ft ²	Collector efficiency, percent
.90	198.0	9.9	3.6	199.8	31.1	160.6	19.4
85	161.0	9.9	6.0	163.5	42.4	141.4	30.0
83	120.0	10.0	6.7	123.4	56.6	130.2	43.5
84	120.0	10.0	10.1	125.0	84.7	166.8	50.8
78	81.1	10.0	21.0	91.6	173.5	253.5	68.5

TABLE 19.- Continued.

ABSORBER: Black Nickel on aluminum

COVER: 1 glass

INCIDENT ANGLE: 0°

DIFFUSE/DIRECT RATIO: 0

Test run	Fluid inlet temp, °F	Mass flow rate, lbm/hr ft ²	Temp rise, °F	Average fluid temp, °F	Collected energy flux, Btu/hr ft ²	Incident energy flux, Btu/hr ft ²	Collector efficiency, percent
23	199.0	9.9	3.0	200.5	26.0	160.6	16.2
24	200.0	10.1	11.8	205.9	105.0	255.4	41.1
25	200.0	10.0	17.9	209.0	157.8	320.9	49.2
19	160.0	10.0	14.5	167.3	125.1	238.6	52.4
16	120.0	9.5	8.1	124.1	65.3	139.0	46.9
17	120.0	9.9	18.6	129.3	156.0	244.0	63.1
18	120.0	9.6	27.5	133.8	244.4	330.2	71.9
20	78.0	10.0	12.0	84.0	98.8	136.5	72.3
21	80.0	10.0	21.7	90.9	179.5	235.9	76.1
22	80.0	10.0	30.6	95.3	253.4	328.1	77.2

TABLE 19.- Continued.

ABSORBER: Black Nickel on aluminum

COVER: 1 Lexan

INCIDENT ANGLE: 0°

DIFFUSE/DIRECT RATIO: 0

Test run	Fluid inlet temp, °F	Mass flow rate, lbm/hr ft ²	Temp rise, °F	Average fluid temp, °F	Collected energy flux, Btu/hr ft ²	Incident energy flux, Btu/hr ft ²	Collector efficiency, percent
69	201.3	10.0	9.7	206.1	85.0	238.3	35.6
57	158.9	10.0	13.6	165.7	117.0	232.8	50.2
56	119.0	10.0	18.7	128.3	157.4	246.3	63.9
39	81.1	10.0	21.5	91.8	177.4	251.1	70.7

TABLE 19. - Continued.

ABSORBER: Black Nickel on aluminum

COVER: Glass/Tedlar

INCIDENT ANGLE: 0°

DIFFUSE/DIRECT RATIO: 0

Test run	Fluid inlet temp, °F	Mass flow rate, lbm/hr ft ²	Temp rise, °F	Average fluid temp, °F	Collected energy flux, Btu/hr ft ²	Incident energy flux, Btu/hr ft ²	Collector efficiency, percent
109	201.0	9.9	10.4	206.2	90.3	226.2	39.9
95	159.0	10.0	15.3	166.6	131.4	239.7	54.8
92	118.0	10.0	18.5	127.3	156.2	249.5	62.6
96	80.0	10.0	20.8	90.4	171.8	237.7	72.3

TABLE 19. - Concluded.

ABSORBER: Black Nickel on aluminum

COVER: 2 antireflection glass

INCIDENT ANGLE: 0°

DIFFUSE/DIRECT RATIO: 0

Test run	Fluid inlet temp, °F	Mass flow rate, lbm/hr ft ²	Temp rise, °F	Average fluid temp, °F	Collected energy flux, Btu/hr ft ²	Incident energy flux, Btu/hr ft ²	Collector efficiency, percent
108	201.0	10.0	12.5	207.3	110.2	226.4	48.7
103	160.0	10.0	15.7	167.9	135.5	229.3	59.1
100	120.0	10.0	19.3	129.9	166.5	231.4	72.0
99	81.0	10.0	21.8	91.9	180.2	226.7	79.5

TABLE 20. - SOLAR SIMULATOR TEST DATA FOR BLACK PAINT ON ALUMINUM

ABSORBER: Black paint on aluminum

COVER: 1 glass

INCIDENT ANGLE: 0°

DIFFUSE/DIRECT RATIO: 0

Test run	Fluid inlet temp., °F	Mass flow rate, lbm/hr ft ²	Temp rise, °F	Average fluid temp., °F	Collected energy flux, Btu/hr ft ²	Incident energy flux, Btu/hr ft ²	Collector efficiency, percent
107	201.0	10.0	3.4	202.7	29.8	229.8	13.0
86	161.0	10.0	10.9	166.4	93.5	228.8	40.9
82	119.0	10.0	7.9	123.0	66.7	146.3	45.6
79	80.0	9.9	15.0	87.5	122.3	162.5	75.2

TABLE 20. - Continued.

ABSORBER: Black paint on aluminum

COVER: 1 Lexan

INCIDENT ANGLE: 0°

DIFFUSE/DIRECT RATIO: 0

Test run	Fluid inlet temp, °F	Mass flow rate, lbm/hr ft ²	Temp rise, °F	Average fluid temp, °F	Collected energy flux, Btu/hr ft ²	Incident energy flux, Btu/hr ft ²	Collector efficiency, percent
67	201.4	10.0	4.3	203.6	38.0	243.4	15.6
62	157.4	10.0	10.1	162.5	87.0	229.7	37.9
46	118.6	10.0	17.7	127.4	148.9	253.9	58.6
41	79.4	10.0	22.6	90.7	186.7	264.0	70.7

TABLE 20.- Continued.

ABSORBER: Black paint on aluminum

COVER: 2 glass

INCIDENT ANGLE: 0°

DIFFUSE/DIRECT RATIO: 0

Test run	Fluid inlet temp, °F	Mass flow rate, lbm/hr ft ²	Temp rise, °F	Average fluid temp, °F	Collected energy flux, Btu/hr ft ²	Incident energy flux, Btu/hr ft ²	Collector efficiency, percent
64	202.5	10.0	-2.5	201.3	-21.6	139.2	-15.5
65	200.7	10.0	8.0	204.7	70.3	237.6	29.6
66	201.2	10.0	12.9	207.6	113.2	291.0	38.9
63	157.1	10.0	12.7	163.5	109.4	233.2	46.9
43	118.2	10.0	8.5	122.4	71.2	152.9	46.5
44	119.6	10.0	19.0	129.1	160.3	257.9	62.1
45	119.8	10.0	23.7	131.6	199.9	302.5	66.1
1	79.0	11.0	11.7	84.9	106.6	157.2	67.8
2	83.0	11.0	20.3	93.2	185.5	256.2	72.4

TABLE 20. - Continued.

ABSORBER: Black paint on aluminum

COVER: Glass/Tedlar

INCIDENT ANGLE: 0°

DIFFUSE/DIRECT RATIO: 0

Test run	Fluid inlet temp, °F	Mass flow rate, lbm/hr ft ²	Temp rise, °F	Average fluid temp, °F	Collected energy flux, Btu/hr ft ²	Incident energy flux, Btu/hr ft ²	Collector efficiency, percent
91	198.0	10.0	7.0	201.5	61.4	241.6	25.4
94	159.0	10.0	11.3	164.7	97.4	237.6	41.0
93	120.0	10.0	15.7	127.8	132.1	236.3	55.9
97	80.0	10.0	20.5	90.2	169.0	230.6	73.3

TABLE 20. - Concluded.

ABSORBER: Black paint on aluminum

COVER: 2 antireflection glass

INCIDENT ANGLE: 0°

DIFFUSE/DIRECT RATIO: 0

Test run	Fluid inlet temp, °F	Mass flow rate, lbm/hr ft ²	Temp rise, °F	Average fluid temp, °F	Collected energy flux, Btu/hr ft ²	Incident energy flux, Btu/hr ft ²	Collector efficiency, percent
106	201.0	10.0	8.7	205.4	76.7	230.3	33.3
102	161.0	10.0	14.9	168.5	128.7	232.7	55.3
101	119.0	10.0	17.2	127.6	145.0	233.4	62.0
98	81.0	10.0	21.6	91.8	178.5	227.7	78.4

TABLE 21.- SOLAR SIMULATOR TEST DATA FOR BLACK NICKEL ON STEEL

ABSORBER: Black Nickel on steel

COVER: 2 glass

INCIDENT ANGLE: 0°

DIFFUSE/DIRECT RATIO: 0

Test run	Fluid inlet temp, °F	Mass flow rate, lbm/hr ft ²	Temp rise, °F	Average fluid temp, °F	Collected energy flux, Btu/hr ft ²	Incident energy flux, Btu/hr ft ²	Collector efficiency, percent
89	198.0	10.0	10.6	203.3	93.0	230.0	40.4
104	160.0	10.0	13.7	166.8	177.6	233.9	50.3
81B	119.0	10.0	10.7	124.3	89.7	149.8	59.9
80	81.0	10.0	20.8	91.4	171.9	250.7	68.6

TABLE 22. - SOLAR SIMULATOR TEST DATA FOR BLACK CHROME ON STEEL

ABSORBER: Black Chrome on steel

COVER: 2 glass

INCIDENT ANGLE: 0°

DIFFUSE/DIRECT RATIO: 0

60% solution ethylene
glycol with water

Test run	Fluid inlet temp, °F	Mass flow rate, lbm/hr ft ²	Temp rise, °F	Average fluid temp, °F	Collected energy flux, Btu/hr ft ²	Incident energy flux, Btu/hr ft ²	Collector efficiency, percent
116	201.0	10.0	7.9	204.9	65.9	208.3	31.6
115	162.0	10.0	11.3	167.6	92.0	209.2	44.0
114	121.0	10.0	14.9	128.5	118.6	209.3	56.6
113	82.0	10.0	18.1	91.1	140.1	210.4	66.6

TABLE 23. - OUTDOOR TEST DATA FOR 9/26/74

Time	Incident solar flux, Btu/hr ft ²	Ambient temp, °F	Wind velocity, mph	Selective coated collector			Nonselective coated collector		
				Mass flow rate, lbm/hr ft ²	Temp rise, °F	Fluid inlet temp, °F	Mass flow rate, lbm/hr ft ²	Temp rise, °F	Fluid inlet temp, °F
9:30	186.7	62.6	5-7	9.3	4.7	157.1	9.1	2.7	156.1
9:45	209.9	66.1	3-5	9.3	7.5	163.8	8.9	5.5	163.1
10:17	231.1	67.5	3-5	10.0	9.9	170.4	9.8	7.3	169.4
10:32	243.9	70.3	6-7	9.6	10.7	174.4	9.8	9.1	173.7
10:50	259.4	72.4	4-6	9.2	12.3	178.4	9.7	9.9	177.4
11:05	267.5	76.2	5	11.5	12.1	181.7	9.9	12.2	180.7
11:14	276.4	74.8	8-10	9.7	15.3	180.4	9.7	14.2	179.4
11:32	283.9	75.5	8-10	8.7	15.9	178.1	9.7	13.9	176.7
11:48	286.6	75.8	7-11	10.2	15.5	182.1	9.3	13.9	180.4
12:01	292.5	76.9	10-12	10.2	15.2	184.0	9.1	14.5	182.4
12:17	295.2	78.6	9-11	10.3	16.3	186.3	10.5	13.7	184.4
12:32	297.6	77.9	10-12	10.2	17.6	185.7	10.4	15.2	184.4
12:49	299.1	80.7	9-11	10.0	19.5	176.1	10.1	18.3	174.7
1:25	290.1	82.1	9-12	9.9	16.5	188.0	9.9	13.9	186.7
1:41	285.1	82.4	5-10	9.9	16.5	189.0	8.4	14.9	188.4
1:55	280.3	81.4	5-10	9.0	18.3	189.0	10.2	13.9	188.0
2:10	269.9	84.9	10-15	11.8	13.5	189.7	9.7	13.5	188.4
2:25	263.9	83.5	5-10	10.4	14.7	188.4	9.9	13.1	187.4
2:47	251.7	83.5	8-10	10.5	14.2	177.7	9.9	11.1	177.1

TABLE 23. - Concluded.

Time	Incident solar flux, Btu/hr ft ²	Ambient temp, °F	Wind velocity, mph	Selective coated collector			Nonselective coated collector		
				Mass flow rate, lbm/hr ft ²	Temp rise, °F	Fluid inlet temp, °F	Mass flow rate, lbm/hr ft ²	Temp rise, °F	Fluid inlet temp, °F
3:00	241.8	83.5	8-10	10.4	14.0	179.4	9.9	11.1	178.4
3:15	227.2	84.5	10-15	10.4	11.9	179.1	9.9	11.8	178.4
3:30	213.8	83.5	10-15	10.4	13.1	179.1	10.0	10.5	178.4

TABLE 24.- OUTDOOR TEST DATA FOR 10/2/74

Time	Incident solar flux, Btu/hr ft ²	Ambient temp, °F	Wind velocity, mph	Selective coated collector			Nonselective coated collector		
				Mass flow rate, lbm/hr ft ²	Temp rise, °F	Fluid inlet temp, °F	Mass flow rate, lbm/hr ft ²	Temp rise, °F	Fluid inlet temp, °F
9:17	173.6	38.0	3-5	8.9	5.9	114.6	6.6	5.1	113.6
9:32	195.3	39.4	5-8	11.2	7.4	117.5	12.8	5.1	116.9
9:47	215.3	40.4	6-8	8.9	9.5	123.9	10.0	6.7	123.5
10:02	234.1	42.5	6-10	8.7	12.3	129.9	10.2	8.3	129.2
10:16	246.0	43.9	5-10	10.3	12.0	133.8	10.3	9.7	133.2
10:33	256.8	44.6	5-10	10.1	13.7	139.5	10.1	10.8	138.8
10:48	269.3	45.6	5-10	9.8	15.1	143.5	10.3	12.1	142.8
11:03	283.6	44.2	5-10	9.7	16.9	147.8	10.4	13.1	147.5
11:17	294.0	44.6	5-10	9.7	17.6	150.8	10.2	13.9	150.1
11:32	302.1	45.6	5-10	9.5	19.1	153.8	10.0	14.9	153.5
11:46	305.1	46.0	5-10	9.6	19.7	156.8	9.9	15.7	156.5
12:00	310.1	49.8	5-10	9.1	20.3	159.4	9.6	15.9	158.8
12:16	315.2	47.7	5-10	8.7	21.7	163.8	8.5	17.1	163.4
12:30	316.4	48.7	5-10	13.3	14.7	167.1	13.8	12.4	166.8
12:45	318.8	44.9	5-10	10.4	18.0	170.4	11.1	13.6	169.8
1:00	316.4	46.7	5-10	10.3	18.2	173.7	10.5	14.5	173.1
1:15	315.5	47.7	5-10	10.0	18.5	176.4	9.8	14.8	175.7
1:30	309.8	47.7	5-10	8.5	20.5	178.7	9.5	14.5	178.1
1:45	303.9	49.4	5-10	8.0	21.7	180.4	8.5	15.3	180.1

ORIGINAL PAGE IS
OR POOR QUALITY

TABLE 24. - Concluded.

Time	Incident solar flux, Btu/hr ft ²	Ambient temp, °F	Wind velocity, mph	Selective coated collector			Nonselective coated collector		
				Mass flow rate, lbm/hr ft ²	Temp rise, °F	Fluid inlet temp, °F	Mass flow rate, lbm/hr ft ²	Temp rise, °F	Fluid inlet temp, °F
2:01	297.3	51.5	5-10	15.6	13.0	181.1	12.6	13.1	180.4
2:15	290.7	52.2	5-10	9.5	16.0	179.7	11.0	11.4	179.1
2:30	284.5	50.9	5-10	10.5	15.5	182.4	11.7	10.0	181.7
2:47	273.2	51.2	10-15	9.8	14.3	182.7	8.5	12.1	182.1
3:00	260.6	53.3	10-15	10.4	13.6	182.1	10.7	8.9	181.7
3:15	245.1	51.5	10-15	10.5	12.1	181.7	10.2	3.2	181.4
3:30	234.1	51.9	5-10	10.2	9.2	181.7	9.8	3.5	181.1
3:43	217.7	52.2	10-15	10.3	2.9	181.1	9.6	5.0	180.4
3:56	205.5	53.9	5-10	10.3	7.8	180.4	9.3	2.9	179.4

TABLE 25.- OUTDOOR TEST DATA FOR 10/8/74

Time	Incident solar flux, Btu/hr ft ²	Ambient temp, °F	Wind velocity, mph	Selective coated collector			Nonselective coated collector		
				Mass flow rate, lbm/hr ft ²	Temp rise, °F	Fluid inlet temp, °F	Mass flow rate, lbm/hr ft ²	Temp rise, °F	Fluid inlet temp, °F
8:50	115.4	41.8	0	19.7	0.7	80.3	16.2	0.9	80.0
9:11	144.3	41.8	0-2	13.1	2.9	94.0	11.7	1.9	93.6
9:35	178.9	53.9	0-2	10.5	6.8	118.2	10.9	4.7	117.5
9:49	194.1	56.0	1-3	10.6	8.3	125.9	10.8	5.7	125.2
10:03	210.8	58.5	2	10.6	9.4	133.2	10.8	6.8	132.5
10:17	226.3	59.5	2	10.6	10.7	140.2	10.9	7.7	139.5
10:36	242.1	59.5	2	10.8	12.0	149.1	10.6	9.3	148.8
10:50	252.6	59.5	0-5	10.7	13.0	155.8	10.2	10.0	155.5
11:05	260.6	60.6	0-4	9.8	13.9	162.8	8.4	11.7	162.4
11:20	270.8	60.2	3-5	8.5	17.5	167.8	13.6	9.0	167.8
11:35	278.2	60.9	3-7	10.9	13.6	173.4	9.9	11.1	173.1
11:50	285.4	62.3	3-6	11.1	14.9	178.1	8.0	13.5	177.4
12:09	292.5	63.3	3-6	10.4	15.4	181.4	8.5	14.9	180.7
12:21	298.2	64.4	3-5	10.1	17.8	178.1	9.3	19.1	177.7
12:36	296.7	65.8	4-8	10.2	13.8	182.7	8.6	13.8	182.4
12:50	305.1	63.0	5-8	10.0	18.5	183.1	9.9	16.3	182.4
1:03	312.5	64.0	7-11	11.6	18.3	182.1	10.6	16.7	181.4
1:32	221.0	63.7	4-8	8.2	4.5	184.4	9.5	0.1	184.0
1:49	343.2	65.8	5-8	10.4	21.2	175.7	9.0	17.9	175.1

TABLE 25. - Concluded.

Time	Incident solar flux, Btu/hr ft ²	Ambient temp., °F	Wind velocity, mph	Selective coated collector			Nonselective coated collector		
				Mass flow rate, lbm/hr ft ²	Temp rise, °F	Fluid inlet temp., °F	Mass flow rate, lbm/hr ft ²	Temp rise, °F	Fluid inlet temp., °F
2:02	314.6	65.1	5-8	10.1	16.3	180.1	11.4	10.8	179.7
2:18	243.6	65.4	4-8	11.2	11.5	182.4	11.2	7.0	182.1
2:39	252.0	64.7	4-8	13.7	10.3	182.1	9.2	7.7	181.4
3:06	75.4	62.3	3-6	8.1	-1.9	180.7	Shadow		
3:25	73.7	61.2	8-14	7.7	4.3	180.7	Shadow		

TABLE 26. - OUTDOOR TEST DATA FOR 10/15/74

Time	Incident solar flux, Btu/hr ft ²	Ambient temp, °F	Wind velocity, mph	Selective coated collector			Nonselective coated collector		
				Mass flow rate, lbm/hr ft ²	Temp rise, °F	Fluid inlet temp, °F	Mass flow rate, lbm/hr ft ²	Temp rise, °F	Fluid inlet temp, °F
9:30	158.9	38.3	5-10	7.3	2.1	136.5	5.8	-1.4	134.8
9:45	195.6	39.7	5-6	8.8	4.7	142.8	10.8	0.9	142.2
10:01	234.7	42.1	5-10	8.9	7.0	153.5	11.0	2.1	152.8
10:30	113.3	43.5	5-10	8.4	-7.2	169.8	11.5	-9.8	169.4
10:45	236.2	43.9	5-10	10.4	4.9	175.1	10.0	-3.1	174.1
11:01	180.1	45.6	8-12	9.6	7.3	178.7	8.9	4.5	177.4
11:18	148.2	47.7	6-10	9.0	4.7	181.4	8.8	1.7	180.4
11:30	120.8	47.3	8-13	8.9	2.3	179.1	10.1	-1.5	178.4
11:45	112.1	48.4	9-14	9.1	2.5	177.1	11.0	-1.5	176.1
12:00	175.3	49.4	8-12	11.6	4.3	175.1	11.1	0.5	174.1
12:15	240.3	51.5	10-15	10.2	4.7	177.4	11.2	-0.8	176.1
12:30	171.2	51.9	11-17	9.7	1.5	181.7	9.7	-2.7	181.1
12:47	136.9	51.9	10-15	8.6	-2.3	183.7	8.9	-7.7	183.1

TABLE 27. - OUTDOOR TEST DATA FOR 10/18/74

Time	Incident solar flux, Btu/hr ft ²	Ambient temp, °F	Wind velocity, mph	Selective coated collector			Nonselective coated collector		
				Mass flow rate, lbm/hr ft ²	Temp rise, °F	Fluid inlet temp, °F	Mass flow rate, lbm/hr ft ²	Temp rise, °F	Fluid inlet temp, °F
9:30	173.6	48.7	0-5	11.4	1.6	126.9	20.3	2.3	126.2
9:45	191.4	49.8	0-2	10.0	1.9	146.1	11.5	-2.0	145.1
10:00	209.6	49.8	0-3	10.0	4.0	161.4	10.1	0.1	160.1
10:15	227.8	48.0	2-4	9.8	5.5	174.4	9.5	1.3	173.1
10:30	241.2	49.8	0-5	9.7	7.3	184.7	11.1	1.9	183.4
10:45	255.3	49.8	0-7	8.8	13.9	181.1	8.6	9.4	180.1
11:00	266.0	48.0	5-10	9.3	15.0	181.1	7.7	13.3	181.4
11:15	275.2	48.7	5-10	11.7	14.5	181.7	11.5	12.1	180.4
11:30	283.6	48.4	5-7	11.5	14.8	179.7	11.5	12.3	178.1
11:45	288.4	50.1	5-7	11.3	15.4	181.1	11.6	12.5	179.7
12:00	295.2	50.5	5-10	11.2	16.7	182.1	11.2	13.1	180.7
12:15	300.0	52.2	5-7	11.2	17.0	182.7	11.1	14.0	181.1
12:30	271.4	52.6	5-7	11.1	17.9	183.4	11.0	14.5	181.7
12:45	289.3	54.0	5-7	11.0	17.7	183.1	10.8	14.5	181.4
1:00	320.6	53.9	3-5	10.8	15.7	182.7	10.8	12.9	180.7
1:15	303.9	53.3	5-7	10.9	17.9	182.1	10.9	13.5	180.4
1:30	301.8	52.2	5-10	11.0	16.4	181.7	10.7	12.4	179.7
1:45	289.9	52.9	5-10	11.1	17.4	181.4	10.8	14.1	179.4
2:00	281.8	54.6	5-10	11.1	16.3	181.4	10.8	13.1	179.14

C
W
TABLE 27. - Concluded.

Time	Incident solar flux, Btu/hr ft ²	Ambient temp, °F	Wind velocity, mph	Selective coated collector			Nonselective coated collector		
				Mass flow rate, lbm/hr ft ²	Temp rise, °F	Fluid inlet temp, °F	Mass flow rate, lbm/hr ft ²	Temp rise, °F	Fluid inlet temp, °F
2:15	274.9	54.3	5-10	11.1	15.8	181.7	10.8	12.5	180.1
2:30	262.1	53.9	0-5	11.1	14.9	182.4	10.9	11.6	180.4
2:45	248.1	53.9	5-10	11.0	13.7	182.7	10.6	9.9	181.1
3:00	234.7	55.3	5-10	10.9	12.7	183.4	Shadow		
3:15	221.9	56.0	5-10	11.1	10.2	183.1	Shadow		

TABLE 28.- OUTDOOR TEST DATA FOR 10/20/74

Time	Incident solar flux, Btu/hr ft ²	Ambient temp, °F	Wind velocity, mph	Selective coated collector			Nonselective coated collector		
				Mass flow rate, lbm/hr ft ²	Temp rise, °F	Fluid inlet temp, °F	Mass flow rate, lbm/hr ft ²	Temp rise, °F	Fluid inlet temp, °F
9:18	160.4	36.9	5-10	10.2	-0.3	131.5	12.0	-3.3	130.5
9:32	181.0	36.9	0-5	10.7	-0.4	146.1	9.5	-3.5	144.8
9:45	197.4	38.0	5-10	10.9	1.6	155.8	10.9	-2.0	154.5
10:00	216.5	39.0	5-10	11.0	2.5	167.4	11.0	-1.1	165.8
10:15	233.2	39.4	10-15	10.4	4.2	178.4	10.3	-0.5	176.7
10:30	248.4	39.7	10-15	9.8	5.8	187.0	9.6	1.3	185.7
10:45	261.2	41.1	5-10	9.5	13.5	177.7	9.6	4.0	176.1
11:00	271.1	41.4	10-15	9.2	13.6	177.7	9.0	9.9	176.1
11:15	281.5	41.8	10-15	10.0	14.3	178.7	8.7	11.9	177.4
11:30	290.4	42.1	7-12	9.6	16.6	178.7	9.9	12.7	177.4
11:45	295.5	43.2	10-15	10.3	17.2	179.4	9.7	13.5	178.1
12:00	300.0	44.9	10-15	9.6	18.3	179.7	10.8	14.1	178.4
12:15	304.5	45.3	5-10	9.3	18.8	181.4	8.9	15.0	180.1
12:30	306.5	45.3	5-10	8.7	21.1	180.1	8.7	16.9	178.4
12:45	308.0	44.9	5-10	10.8	17.9	179.4	9.8	15.5	178.1
1:00	306.3	47.3	5-10	10.5	17.8	180.1	10.2	15.1	178.7
1:15	304.5	46.0	5-10	10.3	17.6	180.7	10.0	14.7	179.1
1:30	300.0	48.0	10-15	11.2	18.1	182.4	9.9	14.9	180.7
1:45	296.4	47.3	5-10	10.3	18.5	182.7	9.9	14.4	181.4

TABLE 28. - Concluded.

Time	Incident solar flux, Btu/hr ft ²	Ambient temp., °F	Wind velocity, mph	Selective coated collector			Nonselective coated collector		
				Mass flow rate, lbm/hr ft ²	Temp rise, °F	Fluid inlet temp., °F	Mass flow rate, lbm/hr ft ²	Temp rise, °F	Fluid inlet temp., °F
1:45	296.4	47.3	5-10	10.3	18.5	182.7	9.9	14.4	181.4
2:00	287.8	46.7	5-10	9.4	18.8	182.4	9.5	14.4	181.1
2:15	281.2	47.3	5-10	9.3	18.3	183.1	9.3	13.7	181.7
2:30	272.3	48.7	10-15	10.1	18.1	182.4	9.8	13.0	181.1
2:48	256.2	48.0	10-15	8.9	16.9	182.1	9.2	11.3	180.7
3:00	246.3	49.1	5-10	8.9	15.7	182.4	9.1	9.9	181.1
3:15	230.8	47.7	5-10	8.7	18.5	181.7	Shadow		
3:31	202.8	48.0	5-10	8.8	11.8	181.1	Shadow		

ORIGINAL PAGE IS
OF POOR QUALITY

TABLE 29. - OUTDOOR TEST DATA FOR 10/24/74

Time	Incident solar flux, Btu/hr ft ²	Ambient temp, °F	Wind velocity, mph	Selective coated collector			Nonselective coated collector		
				Mass flow rate, lbm/hr ft ²	Temp rise, °F	Fluid inlet temp, °F	Mass flow rate, lbm/hr ft ²	Temp rise, °F	Fluid inlet temp, °F
11:00	208.4	57.8	0-2	9.8	10.0	108.9	10.2	7.7	112.2
11:15	219.5	55.7	0-2	9.2	10.1	125.5	9.7	6.6	130.2
11:30	225.1	56.0	0-2	10.1	6.5	141.2	8.5	5.5	145.5
11:45	228.7	57.1	1-3	10.0	8.5	155.5	10.1	4.7	160.8
12:00	238.3	55.3	0-2	9.8	8.7	169.1	9.5	4.8	174.1
12:15	240.9	55.0	3-5	7.8	13.9	179.1	5.6	9.7	184.7
12:30	253.8	58.5	0-2	11.3	13.9	174.4	10.6	13.2	180.1
12:45	251.7	59.9	0-2	10.9	11.9	180.4	10.3	9.9	186.4
1:00	250.5	60.6	1-3	10.2	15.6	178.1	10.3	12.7	183.7
1:15	250.5	60.2	0-2	10.0	15.2	178.4	10.2	11.9	183.7
1:30	248.4	61.9	0-5	10.0	15.3	178.7	10.3	11.8	184.0
1:45	240.9	60.9	2-5	9.9	15.3	178.7	10.2	11.2	183.4
2:00	239.2	60.9	3-6	9.9	14.4	178.1	10.2	10.1	182.7
2:15	222.8	61.2	3-6	10.3	12.9	177.7	10.2	9.1	182.4
2:30	213.5	60.9	3-7	10.2	12.8	176.4	10.0	8.8	181.1
2:45	204.3	61.9	3-5	10.2	10.8	177.7	10.1	6.5	182.4
3:00	187.6	61.6	3-6	10.2	10.4	177.1	10.1	5.8	181.4
3:15	178.9	61.6	3-6	10.2	8.5	176.7	Shadow
3:30	172.3	61.6	4-7	10.2	7.3	176.1	Shadow

TABLE 30.- OUTDOOR TEST DATA FOR 10/25/74

Time	Incident solar flux, Btu/hr ft ²	Ambient temp., °F	Wind velocity, mph	Selective coated collector			Nonselective coated collector		
				Mass flow rate, lbm/hr ft ²	Temp rise, °F	Fluid inlet temp, °F	Mass flow rate, lbm/hr ft ²	Temp rise, °F	Fluid inlet temp, °F
9:15	167.6	42.1	0-5	4.8	-23.7	146.5	5.8	-35.3	146.5
9:45	207.5	44.6	3-9	10.8	2.4	154.5	10.5	-1.3	154.5
10:00	196.5	44.2	3-6	10.7	3.3	154.4	10.4	-0.4	154.4
10:15	178.6	44.6	2-5	10.8	4.2	173.4	10.3	0.3	173.4
10:30	232.9	44.6	2-5	9.8	4.4	183.4	10.3	-0.5	183.4
10:46	257.9	44.6	2-5	9.9	14.1	179.1	10.1	10.4	179.1
11:00	230.5	45.3	5-10	9.8	10.9	179.7	10.2	7.7	179.7
11:15	276.7	44.9	5-7	9.8	16.0	179.4	10.0	12.0	179.4
11:30	274.9	44.6	3-5	9.7	14.9	179.1	10.1	11.0	179.1
11:45	245.7	46.3	2-5	9.7	13.9	178.4	9.9	10.3	178.4
12:00	222.2	45.3	2-5	9.8	11.1	179.4	9.9	7.8	179.4
12:15	259.4	48.7	2-5	9.7	14.0	181.4	9.9	10.3	181.4
12:30	273.4	47.3	0-5	9.7	16.4	182.1	10.0	12.5	182.1
12:45	283.3	47.7	0-5	9.7	17.9	182.1	10.2	13.9	182.1
1:00	286.0	51.9	0-3	9.7	17.6	183.4	9.9	13.8	183.4
1:15	283.0	50.1	0-3	9.5	18.3	183.4	9.6	14.2	183.4
1:30	274.9	51.5	3-7	9.5	17.3	184.0	9.6	12.7	184.0
1:46	272.9	51.9	3-7	9.4	17.5	184.4	9.2	12.5	184.4
2:00	249.9	52.9	3-7	9.2	15.3	184.4	9.1	11.1	184.4

ORIGINAL PAGE IS OF POOR QUALITY.

TABLE 30. - Concluded.

Time	Incident solar flux, Btu/hr ft ²	Ambient temp, °F	Wind velocity, mph	Selective coated collector			Nonselective coated collector		
				Mass flow rate, lbm/hr ft ²	Temp rise, °F	Fluid inlet temp, °F	Mass flow rate, lbm/hr ft ²	Temp rise, °F	Fluid inlet temp, °F
2:15	248.7	52.3	3-7	9.4	14.7	184.0	9.4	10.6	184.0
2:30	235.3	51.2	2-5	10.7	12.3	183.1	9.6	9.0	183.1
2:51	220.7	52.6	0-5	11.0	10.6	183.1	9.9	7.4	183.1
3:00	214.7	53.3	0-5	11.2	9.9	183.1	10.1	6.8	183.1
3:15	199.2	53.6	0-5	11.0	9.7	183.1	Shadow		

TABLE 31. - OUTDOOR TEST DATA FOR 10/26/74

Time	Incident solar flux, Btu/hr ft ²	Ambient temp, °F	Wind velocity, mph	Selective coated collector			Nonselective coated collector		
				Mass flow rate, lbm/hr ft ²	Temp rise, °F	Fluid inlet temp, °F	Mass flow rate, lbm/hr ft ²	Temp rise, °F	Fluid inlet temp, °F
9:00	131.8	42.1	5-8	11.2	-4.3	145.8	11.0	-8.1	144.8
9:15	153.6	43.9	5-8	11.2	-2.1	157.4	11.2	-4.9	154.1
9:30	174.4	44.6	5-8	11.5	-1.3	167.8	10.7	-4.1	164.1
9:45	192.0	46.0	5-8	10.6	-0.4	178.7	9.5	-3.1	174.7
10:00	210.2	48.0	5-8	10.6	2.0	187.0	10.3	-1.1	183.4
10:17	229.3	49.8	5-7	10.6	8.9	179.4	10.2	7.7	175.7
10:30	242.1	51.5	3-6	10.7	8.9	182.1	10.1	7.1	178.7
10:45	253.8	48.0	3-6	10.7	10.7	181.7	10.1	9.1	178.7
11:00	263.3	52.2	3-6	10.7	11.7	179.7	10.1	10.1	179.1
11:15	272.6	54.6	2-5	10.8	13.7	179.4	10.1	11.8	179.4
11:30	282.1	55.3	5-10	10.0	14.7	179.4	10.1	12.5	180.4
11:45	287.2	56.7	3-5	10.3	15.5	182.7	10.2	13.1	181.1
12:00	289.0	56.4	3-5	10.2	16.1	184.0	10.4	13.1	182.7
12:15	294.6	56.4	3-7	10.1	17.3	183.1	10.5	14.5	181.4
12:30	295.5	57.4	5-9	10.2	17.3	183.7	10.4	14.3	182.1
12:45	295.2	60.2	5-8	10.2	16.8	185.0	8.9	15.1	183.7
1:00	295.8	59.5	5-8	10.0	18.1	184.0	10.0	15.6	182.4
1:15	291.6	60.9	3-5	9.6	18.1	184.4	9.9	15.2	182.4
1:30	289.3	61.6	3-6	9.6	18.1	184.7	9.7	15.3	183.1

ORIGINAL PAGE IS
OF POOR QUALITY.

TABLE 31. - Concluded.

Time	Incident solar flux, Btu/hr ft ²	Ambient temp., °F	Wind velocity, mph	Selective coated collector			Nonselective coated collector		
				Mass flow rate, lbm/hr ft ²	Temp rise, °F	Fluid inlet temp., °F	Mass flow rate, lbm/hr ft ²	Temp rise, °F	Fluid inlet temp., °F
1:45	283.0	61.6	5-10	10.2	17.1	185.0	9.3	15.5	183.4
2:00	277.6	61.2	6-12	10.2	16.3	184.4	9.4	14.8	182.4
2:15	266.3	62.3	5-10	10.2	14.9	184.0	9.4	13.7	182.1
2:30	255.6	64.0	6-10	10.3	13.6	184.0	9.5	11.5	183.1
2:45	243.0	62.6	9-13	10.2	12.9	182.7	9.5	10.7	180.4
3:00	221.3	63.0	5-10	10.4	11.4	182.7	Shadow		

APPENDIX D
HEATING AND COOLING LOAD AND
SOLAR-LEVEL COLLECTION DATA

HEATING AND COOLING LOAD

The heating and cooling load, tabulated by month for a 12-month period, for the cities of Atlanta, Chicago, Dallas, Los Angeles, Miami, Pittsburg, Philadelphia, and Seattle are presented in Tables 32 through 39, respectively. Data recorded include average temperature, average humidity, number of degree days of heating and cooling, load (heating, cooling dry air, and drying humid air) in 10^6 Btu's, and total load in 10^6 Btu's.

SOLAR-LEVEL COLLECTION DATA

Incident and collected solar energy data, tabulated by month for a 12-month period, are presented in Tables 40 through 47 for the cities of Atlanta, Chicago, Dallas, Los Angeles, Miami, Pittsburg, Philadelphia, and Seattle, respectively. The data for collected energy are based on a selective-coated, two-glass cover collector and inlet temperatures of 60°C (140°F) and 93°C (200°F).

TABLE 32.- HEATING AND COOLING LOAD FOR ATLANTA

Month	Average temp., °F (a)	Average humidity, percent (a)	Degree days (a)		Load (b)			Total load, 10 ⁶ Btu
			Heating	Cooling	Heating, 10 ⁶ Btu	Cooling dry air, 10 ⁶ Btu	Drying humid air, 10 ⁶ Btu	
1	44.7	69.2	639	0	9.4	0	0	9.4
2	46.1	64.8	529	0	7.8	0	0	7.8
3	51.4	62.5	437	0	6.4	0	0	6.4
4	60.2	64.5	168	38	2.5	0.6	0	3.1
5	69.1	68.2	25	115	0.4	1.7	0.6	2.7
6	76.6	74.0	0	374	0	5.5	8.1	13.6
7	78.9	78.2	0	378	0	5.3	10.7	16.0
8	78.2	77.0	0	371	0	5.4	9.7	15.1
9	73.1	75.2	18	265	0.3	3.9	5.5	9.7
10	62.4	70.0	127	95	1.9	1.4	0	3.3
11	51.2	68.8	414	13	6.1	0.2	0	6.3
12	44.8	70.8	626	5	9.2	0.1	0	9.3
Total	61.4	70.2	2983	1634	44.0	24.1	34.6	102.7

^aMeteorological data from U. S. Weather Bureau.

^bBased on 1500-ft² house of 12,000-ft³ volume, with 1.5 exchanges/hr and an average daily degree day temperature difference.

TABLE 33. - HEATING AND COOLING LOAD FOR CHICAGO

Month	Average temp, °F (a)	Average humidity, percent (a)	Degree days (a)		Load (b)			Total load, 10 ⁶ Btu
			Heating	Cooling	Heating, 10 ⁶ Btu	Cooling dry air, 10 ⁶ Btu	Drying humid air, 10 ⁶ Btu	
1	26.0	68.0	1209	0	17.7	0	0	17.7
2	27.7	63.5	1044	0	15.3	0	0	15.3
3	36.3	64.5	890	0	13.1	0	0	13.1
4	49.0	64.5	480	0	7.0	0	0	7.0
5	60.0	60.0	211	53	3.1	0.8	0	3.9
6	70.5	61.8	48	191	0.7	2.8	1.6	5.1
7	75.6	65.0	0	301	0	4.4	5.3	9.7
8	74.2	67.2	0	277	0	4.1	3.7	7.8
9	66.1	66.0	81	84	1.2	1.2	0	2.4
10	55.1	62.5	326	19	4.8	0.3	0	5.1
11	39.9	69.2	753	0	11.0	0	0	11.0
12	29.1	74.8	1113	0	16.3	0	0	16.3
Total	50.8	65.75	6155	925	90.2	13.6	10.6	111.4

^aMeteorological data from U. S. Weather Bureau.^bBased on 1500-ft² house of 12,000-ft³ volume, with 1.5 exchanges/hr and an average daily degree day temperature difference.

TABLE 34.- HEATING AND COOLING LOAD FOR DALLAS
 $[U_{wall} = 0.166; U_{roof} = 0.041]$

Month	Average temp, °F (a)	Average humidity, percent (a)	Degree days (a)		Load (b)			Total load, 10 ⁶ Btu
			Heating	Cooling	Heating, 10 ⁶ Btu	Cooling dry air, 10 ⁶ Btu	Drying humid air, 10 ⁶ Btu	
1	45.5	68.0	614	0	9.0	0	0	9.0
2	49.2	65.2	448	6	6.6	0.1	0	6.7
3	55.9	65.5	319	21	4.8	0.3	0	5.1
4	64.8	69.2	99	71	1.5	1.0	0	2.5
5	72.7	73.2	0	195	0	2.9	4.9	7.8
6	81.5	66.8	0	546	0	8.0	9.8	17.8
7	85.4	59.5	0	606	0	8.9	11.3	20.2
8	85.4	63.2	0	456	0	6.7	11.5	18.2
9	78.4	71.2	0	382	0	5.6	8.9	14.5
10	67.9	68.0	65	171	1.0	2.5	1.0	4.5
11	57.8	67.5	324	36	4.8	0.5	0	5.3
12	47.7	70.5	536	1	7.9	0	0	7.9
Total	65.8	67.2	2405	2491	35.6	36.5	47.4	119.5

^aMeteorological data from U. S. Weather Bureau.

^bBased on 1500-ft² house of 12,000-ft³ volume, with 1.5 exchanges/hr and an average daily degree day temperature difference.

TABLE 35.- HEATING AND COOLING LOAD FOR LOS ANGELES

Month	Average temp, °F (a)	Average humidity, percent (a)	Degree days (a)		Load (b)			Total load, 10 ⁶ Btu
			Heating	Cooling	Heating, 10 ⁶ Btu	Cooling dry air, 10 ⁶ Btu	Drying humid air, 10 ⁶ Btu	
1	55.8	57.8	310	71	4.5	1.0	0	5.5
2	57.1	61.8	230	28	3.4	0.4	0	3.8
3	59.4	62.5	202	16	3.0	0.2	0	3.2
4	61.8	64.8	123	46	1.8	0.7	0	2.5
5	64.8	66.8	68	50	1.0	0.7	0	1.7
6	68.0	62.8	18	131	0.3	1.9	0.2	2.4
7	73.0	67.5	0	291	0	4.3	4.0	8.3
8	73.1	68.5	0	435	0	6.4	4.2	10.6
9	71.9	65.0	6	296	0.1	4.3	3.0	7.4
10	67.4	65.2	31	176	0.5	2.6	0.2	3.3
11	62.7	54.2	132	17	1.9	0.2	0	2.1
12	58.2	54.8	229	0	3.4	0	0	3.4
Total	64.4	63.2	1349	1557	19.9	22.7	11.6	54.2

^aMeteorological data from U. S. Weather Bureau.

^b Based on 1500-ft² house of 12,000-ft³ volume, with 1.5 exchanges/hr and an average daily degree day temperature difference.

TABLE 36.- HEATING AND COOLING LOAD FOR MIAMI

Month	Average temp, °F (a)	Average humidity, percent (a)	Degree days (a)		Load (b)			Total load, 10 ⁶ Btu
			Heating	Cooling	Heating, 10 ⁶ Btu	Cooling dry air, 10 ⁶ Btu	Drying humid air, 10 ⁶ Btu	
1	66.9	73.5	74	85	1.1	1.2	1.2	3.5
2	67.9	71.0	56	59	0.8	0.9	1.5	3.2
3	70.5	70.5	19	239	0.3	3.5	3.0	6.8
4	74.2	69.8	0	425	0	6.2	5.3	11.5
5	77.6	72.2	0	446	0	6.5	8.5	15.0
6	80.8	78.8	0	518	0	7.6	12.6	20.2
7	81.8	76.0	0	558	0	8.2	12.8	21.0
8	82.3	75.5	0	596	0	8.7	12.9	21.6
9	81.3	79.5	0	522	0	7.7	13.2	20.9
10	78.8	78.2	0	457	0	6.7	9.8	16.5
11	72.4	74.0	0	185	0	2.7	4.9	7.6
12	68.1	72.2	65	213	1.0	3.1	1.7	5.8
Total	75.1	74.2	214	4303	3.2	63.0	87.4	153.6

^aMeteorological data from U. S. Weather Bureau.

^bBased on 1500-ft² house of 12,000-ft³ volume, with 1.5 exchanges/hr and an average daily degree day temperature difference.

TABLE 37.- HEATING AND COOLING LOAD FOR PITTSBURG

Month	Average temp, °F (a)	Average humidity, percent (a)	Degree days (a)		Load (b)			Total load, 10 ⁶ Btu
			Heating	Cooling	Heating, 10 ⁶ Btu	Cooling dry air, 10 ⁶ Btu	Drying humid air, 10 ⁶ Btu	
1	32.2	65.3	1017	0	14.9	0	0	14.9
2	32.8	64.0	902	0	13.2	0	0	13.2
3	41.6	60.3	725	0	10.6	0	0	10.6
4	51.3	56.3	411	7	6.0	0.1	0	6.1
5	62.5	57.7	123	74	1.8	1.1	0	2.9
6	71.3	61.7	11	199	0.2	2.9	1.9	5.0
7	75.7	62.3	0	298	0	4.4	4.7	9.1
8	73.4	64.7	5	254	0.1	3.7	3.8	7.6
9	67.1	65.3	57	103	0.8	1.5	0	2.3
10	56.1	64.3	285	13	4.2	0.2	0	4.4
11	45.4	64.3	588	0	8.6	0	0	8.6
12	34.8	64.7	936	0	13.7	0	0	13.7
Total	53.7	62.7	5060	948	74.1	13.9	10.4	98.4

^aMeteorological data from U. S. Weather Bureau.^bBased on 1500-ft² house of 12,000-ft³ volume, with 1.5 exchanges/hr and an average daily degree day temperature difference.

TABLE 38.- HEATING AND COOLING LOAD FOR PHILADELPHIA

Month	Average temp, °F (a)	Average humidity, percent (a)	Degree days (a)		Load (b)			Total load, 10 ⁶ Btu
			Heating	Cooling	Heating, 10 ⁶ Btu	Cooling dry air, 10 ⁶ Btu	Drying humid air, 10 ⁶ Btu	
1	33.2	70.0	986	0	14.5	0	0	14.5
2	33.6	67.0	879	0	12.9	0	0	12.9
3	42.3	64.8	704	0	10.3	0	0	10.3
4	51.6	63.5	402	0	5.9	0	0	5.9
5	63.1	66.8	104	67	1.5	1.0	0	2.5
6	72.1	68.8	0	223	0	3.3	3.6	6.9
7	76.3	69.0	0	366	0	5.4	6.5	11.9
8	74.0	71.8	0	304	0	4.5	3.7	8.2
9	67.7	72.2	47	131	0.7	1.9	1.4	4.0
10	56.6	71.8	269	13	3.9	0.2	0	4.1
11	45.9	70.0	573	0	8.4	0	0	8.4
12	35.9	69.8	902	0	13.2	0	0	13.2
Total	54.3	68.8	4866	1104	71.3	16.3	15.2	102.8

^aMeteorological data from U. S. Weather Bureau.

^bBased on 1500-ft² house of 12,000-ft³ volume, with 1.5 exchanges/hr and an average daily degree day temperature difference,

TABLE 39.- HEATING AND COOLING LOAD FOR SEATTLE

Month	Average temp, °F (a)	Average humidity, percent (a)	Degree days (a)		Load (b)			Total load, 10 ⁶ Btu
			Heating	Cooling	Heating, 10 ⁶ Btu	Cooling dry air, 10 ⁶ Btu	Drying humid air, 10 ⁶ Btu	
1	38.3	79.8	828	0	12.2	0	0	12.2
2	40.8	74.5	678	0	10.0	0	0	10.0
3	43.8	73.8	657	0	9.6	0	0	9.6
4	49.2	73.5	474	0	7.0	0	0	7.0
5	55.5	70.2	295	4	4.3	0.1	0	4.4
6	59.8	68.2	159	2	2.3	0	0	2.3
7	64.9	66.5	56	106	0.8	1.6	0	2.4
8	64.1	68.8	62	107	0.9	1.6	0	2.5
9	59.9	74.8	162	0	2.4	0	0	2.4
10	52.4	79.5	391	0	5.7	0	0	5.7
11	43.9	80.2	633	0	9.3	0	0	9.3
12	40.8	81.5	750	0	11.0	0	0	11.0
Total	51.1	74.5	5145	219	75.5	3.3	0	78.8

^aMeteorological data from U. S. Weather Bureau.

^bBased on 1500-ft² house of 12,000-ft³ volume, with 1.5 exchanges/hr and an average daily degree day temperature difference.

Appendix D

TABLE 40.- INCIDENT AND COLLECTED SOLAR ENERGY
INCLUDING CLOUD COVER FOR ATLANTA

Month	Incident flux, Whr/m ² - mo. (Btu/ft ² - mo.)	Collected energy from selective coated collector, Whr/m ² - mo. (Btu/ft ² - mo.)	
		T _{in} = 60°C (140°F)	T _{in} = 93°C (200°F)
1	82,920 (26,282)	23,151 (7,337)	12,036 (3,815)
2	104,307 (33,061)	37,251 (11,807)	23,609 (7,403)
3	156,245 (49,523)	68,038 (21,565)	46,211 (14,647)
4	169,578 (53,749)	81,235 (25,748)	56,159 (17,800)
5	172,787 (54,766)	85,848 (27,210)	58,860 (18,656)
6	174,989 (55,464)	93,315 (29,577)	65,422 (20,736)
7	184,028 (58,329)	98,916 (31,352)	69,902 (22,156)
8	148,380 (47,030)	72,988 (23,134)	48,398 (15,340)
9	150,727 (47,774)	73,284 (23,228)	49,410 (15,661)
10	164,003 (51,982)	78,373 (24,841)	54,585 (17,301)
11	110,592 (35,053)	43,246 (13,707)	28,124 (8,914)
12	90,946 (28,826)	27,572 (8,739)	15,762 (4,996)
Total	1,709,499 (541,838)	783,210 (248,244)	528,472 (167,503)

Appendix D

**TABLE 41. INCIDENT AND COLLECTED SOLAR ENERGY
INCLUDING CLOUD COVER FOR CHICAGO**

Month	Incident flux, Whr/m ² - mo. (Btu/ft ² - mo.)	Collected energy from selective coated collector, Whr/m ² - mo. (Btu/ft ² - mo.)	
		T _{in} = 60°C (140°F)	T _{in} = 93°C (200°F)
1	92,227 (29,232)	24,376 (7,726)	13,295 (4,214)
2	101,007 (32,015)	29,483 (9,345)	18,627 (5,904)
3	116,401 (36,894)	36,137 (11,454)	20,974 (6,648)
4	127,222 (40,324)	48,284 (15,304)	28,423 (9,009)
5	131,276 (41,609)	54,036 (17,127)	31,351 (9,937)
6	137,949 (43,724)	65,444 (20,743)	40,920 (12,970)
7	129,588 (41,074)	58,528 (18,551)	34,762 (11,018)
8	126,197 (39,999)	56,516 (17,913)	33,850 (10,729)
9	148,197 (46,972)	69,883 (22,150)	47,297 (14,991)
10	146,525 (46,422)	67,123 (21,275)	44,697 (14,167)
11	75,935 (24,068)	17,797 (5,641)	8,276 (2,623)
12	64,059 (20,304)	10,487 (3,324)	5,509 (1,746)
Total	1,396,517 (442,636)	538,092 (170,552)	327,981 (103,956)

Appendix D

TABLE 42.- INCIDENT AND COLLECTED SOLAR ENERGY
INCLUDING CLOUD COVER FOR DALLAS

Month	Incident flux, Whr/m ² - mo. (Btu/ft ² - mo.)	Collected energy from selective coated collector, Whr/m ² - mo. (Btu/ft ² - mo.)	
		T _{in} = 60°C (140°F)	T _{in} = 93°C (200°F)
1	81,431 (25,810)	20,325 (6,442)	11,528 (3,654)
2	88,618 (28,088)	29,682 (9,408)	17,015 (5,393)
3	138,410 (43,870)	57,405 (18,195)	36,939 (11,708)
4	127,263 (40,337)	52,991 (16,796)	31,676 (10,080)
5	143,022 (45,332)	66,009 (20,922)	41,479 (13,147)
6	161,741 (51,265)	82,961 (26,295)	56,478 (17,901)
7	190,534 (60,391)	105,847 (33,549)	75,180 (23,829)
8	187,271 (59,357)	103,743 (32,882)	75,244 (23,849)
9	156,860 (49,718)	79,963 (25,345)	54,831 (17,379)
10	135,999 (43,106)	60,731 (19,249)	40,018 (12,684)
11	94,833 (30,058)	31,941 (10,124)	19,173 (6,077)
12	119,139 (37,762)	47,956 (15,200)	29,745 (9,428)
Total	1,625,122 (515,094)	739,557 (234,408)	489,299 (155,087)

Appendix D

**TABLE 43.- INCIDENT AND COLLECTED SOLAR ENERGY
INCLUDING CLOUD COVER FOR LOS ANGELES**

Month	Incident flux, Whr/m ² - mo. (Btu/ft ² - mo.)	Collected energy from selective coated collector, Whr/m ² - mo. (Btu/ft ² - mo.)	
		T _{in} = 60°C (140°F)	T _{in} = 93°C (200°F)
1	102,392 (32,454)	36,727 (11,641)	22,546 (7,146)
2	128,301 (40,666)	56,374 (17,868)	37,567 (11,907)
3	161,943 (51,329)	72,950 (23,122)	51,341 (16,273)
4	146,177 (46,332)	63,993 (20,283)	42,469 (13,461)
5	187,129 (59,312)	91,804 (29,098)	65,757 (20,842)
6	176,484 (55,938)	84,355 (26,737)	58,020 (18,390)
7	190,985 (60,534)	95,764 (30,353)	68,949 (21,854)
8	189,650 (60,111)	96,824 (30,689)	69,968 (22,177)
9	176,311 (55,883)	89,107 (28,243)	64,668 (20,497)
10	124,316 (39,403)	53,178 (16,855)	34,314 (10,876)
11	114,312 (36,232)	47,035 (14,908)	29,742 (9,427)
12	110,242 (34,942)	43,750 (13,867)	27,808 (8,914)
Total	1,810,768 (573,136)	831,863 (263,665)	573,150 (181,664)

Appendix D

**TABLE 44.- INCIDENT AND COLLECTED SOLAR ENERGY
INCLUDING CLOUD COVER FOR MIAMI**

Month	Incident flux, Whr/m ² - mo. (Btu/ft ² - mo.)	Collected energy from selective coated collector, Whr/m ² - mo. (Btu/ft ² - mo.)	
		T _{in} = 60°C (140°F)	T _{in} = 93°C (200°F)
1	130,721 (41,443)	58,831 (18,647)	35,118 (11,131)
2	114,050 (36,149)	50,101 (15,880)	30,512 (9,671)
3	174,484 (55,384)	89,397 (28,335)	62,207 (19,717)
4	166,710 (52,840)	85,822 (27,202)	60,261 (19,100)
5	178,213 (56,486)	93,205 (29,561)	65,829 (20,065)
6	148,099 (46,941)	73,795 (23,390)	48,442 (15,354)
7	150,913 (47,833)	75,259 (23,854)	49,527 (15,698)
8	159,722 (50,625)	83,207 (26,373)	57,140 (18,111)
9	151,440 (48,000)	78,351 (24,834)	52,998 (16,798)
10	150,809 (47,800)	75,928 (24,066)	50,770 (16,092)
11	122,597 (38,858)	56,664 (17,960)	33,408 (10,589)
12	93,394 (29,602)	35,491 (11,249)	16,343 (5,180)
Total	1,741,440 (551,962)	856,112 (271,351)	562,552 (178,305)

Appendix D

**TABLE 45.- INCIDENT AND COLLECTED SOLAR ENERGY
INCLUDING CLOUD COVER FOR PITTSBURG**

Month	Incident flux, Whr/m ² - mo. (Btu/ft ² - mo.)	Collected energy from selective coated collector, Whr/m ² - mo. (Etu/ft ² - mo.)	
		T _{in} = 60°C (140°F)	T _{in} = 93°C (200°F)
1	61,917 (19,625)	6,215 (1,970)	2,231 (707)
2	72,025 (22,829)	13,667 (4,332)	6,367 (2,018)
3	122,524 (38,835)	41,570 (13,176)	25,066 (7,945)
4	125,402 (39,747)	49,496 (15,688)	30,250 (9,588)
5	151,935 (48,157)	67,924 (21,529)	43,725 (13,859)
6	142,186 (45,067)	65,965 (20,908)	42,425 (13,447)
7	153,500 (48,653)	72,868 (23,096)	47,571 (15,078)
8	154,216 (48,880)	73,319 (23,239)	48,196 (15,276)
9	127,314 (40,353)	55,158 (17,451)	34,639 (10,979)
10	106,200 (33,661)	35,904 (11,380)	20,233 (6,413)
11	77,462 (24,552)	18,968 (6,012)	9,963 (3,158)
12	75,095 (23,802)	17,914 (5,678)	10,415 (3,301)
Total	1,369,775 (434,160)	518,865 (164,458)	321,081 (101,769)

Appendix D

TABLE 46.- INCIDENT AND COLLECTED SOLAR ENERGY
INCLUDING CLOUD COVER FOR PHILADELPHIA

Month	Incident flux, Whr/m ² - mo. (Btu/ft ² - mo.)	Collected energy from selective coated collector, Whr/m ² - mo. (Btu/ft ² - mo.)	
		T _{in} = 60°C (140°F)	T _{in} = 93°C (200°F)
1	79,049 (25,055)	17,078 (5,413)	7,985 (2,531)
2	85,952 (27,243)	20,933 (6,635)	11,008 (3,489)
3	129,200 (40,951)	44,552 (14,121)	27,392 (8,682)
4	141,177 (44,747)	57,560 (18,244)	37,106 (11,761)
5	161,362 (51,445)	73,903 (23,424)	49,414 (15,662)
6	154,851 (49,081)	74,953 (23,757)	49,108 (15,565)
7	136,977 (43,416)	62,444 (19,792)	36,996 (11,726)
8	155,153 (49,177)	76,159 (24,139)	50,915 (16,138)
9	124,370 (39,420)	53,922 (17,091)	34,437 (10,915)
10	109,116 (34,585)	40,794 (12,930)	24,499 (7,765)
11	84,740 (26,859)	24,719 (7,835)	13,043 (4,134)
12	63,763 (20,210)	11,882 (3,766)	5,559 (1,762)
Total	1,425,703 (451,887)	558,896 (177,146)	347,454 (110,128)

Appendix D

**TABLE 47.- INCIDENT AND COLLECTED SOLAR ENERGY
INCLUDING CLOUD COVER FOR SEATTLE**

Month	Incident flux, Whr/m ² - mo. (Btu/ft ² - mo.)	Collected energy from selective coated collector, Whr/m ² - mo. (Btu/ft ² - mo.)	
		T _{in} = 60°C (140°F)	T _{in} = 93°C (200°F)
1	50,158 (15,098)	5,089 (1,613)	2,215 (702)
2	63,059 (19,987)	10,329 (3,274)	4,414 (1,399)
3	86,494 (27,415)	17,917 (5,679)	7,342 (2,327)
4	113,899 (36,101)	39,141 (12,406)	22,908 (7,261)
5	115,744 (36,686)	40,838 (12,944)	21,624 (6,854)
6	118,824 (37,662)	45,678 (14,478)	24,319 (7,708)
7	123,411 (39,116)	49,294 (15,624)	27,679 (8,773)
8	152,371 (48,295)	68,482 (21,706)	45,350 (14,374)
9	122,181 (38,726)	49,467 (15,679)	32,247 (10,221)
10	73,591 (24,910)	19,555 (6,198)	10,850 (3,439)
11	57,197 (18,129)	7,894 (2,502)	3,452 (1,094)
12	54,345 (17,225)	9,083 (2,879)	4,228 (1,340)
Total	1,136,073 (360,150)	362,768 (114,982)	206,624 (65,491)

APPENDIX E

BLACK NICKEL SELECTIVE COATING AND ANTIREFLECTIVE GLASS-ETCH PROCESS DESCRIPTIONS

The results of the test program indicate the gains in both performance and cost effectiveness that can be achieved by using solar-selective coatings in collector design. Two such coatings, examined during the course of the program, but not yet commercially available, are discussed here. The first is a selective coating process which electroplates Bright Nickel over a copper or steel surface and then Black Nickel over the Bright Nickel substrate. The second is a glass-etch process which effectively reduces the reflectance of both surfaces of a collector cover glass.

BLACK NICKEL COATING PROCESS DESCRIPTION

The Black Nickel selective coating process requires the following equipment:

- Alkaline electro-cleanser tank with heater and power supply
- Muriatic acid tank
- Two rinse tanks
- Bright Nickel plating tank with heaters and plating power supply
- Black Nickel (nickel-zinc-sulfide) plating tank with heaters and plating power supply.

The absorber panel is mounted in a plating rack and cleaned by muriatic acid and electro-cleanser to remove all rust and grease from the surface. The panel is rinsed after each cleaning to prevent contamination or degradation of any of the process solutions. When all rust and grease are removed, the panel is given a final preplating surface-activation dip in the acid bath, then rinsed and placed in the Bright Nickel plating tank.

A minimum of 1 mil of Bright Nickel is electroplated on the front surface for coating durability (i. e., rust prevention). The panel is again rinsed and put in the Black Nickel (nickel-zinc-sulfide) plating tank. The current density is changed during this plating process to achieve a two-layer selective coating. The panel is removed and rinsed with deionized water and allowed to dry. Care must be taken to move the panel from the final acid bath to the subsequent tanks as rapidly as possible to avoid panel surface oxidation which will weaken the durability of the coating.

Preceding page blank

Appendix E

ANTIREFLECTIVE GLASS-ETCH PROCESS DESCRIPTION

rich
ous

The glass is etched by immersion in a silica supersaturated hydrofluosilicic acid bath of controlled composition and temperature. The acid attacks the glass surface and leaves a skeletonized porous silica layer which has an effective refractive index between that of glass and air. This porous silica layer constitutes the antireflection (AR) coating. Etched AR coatings have been prepared which reduce the two-surface reflection loss from the original 8 percent to less than 2 percent in the solar spectrum.

The parameters of the etching process are:

- Degree of solution supersaturation (potency)
- Solution temperature
- Immersion time
- Glass pretreatment
- Type of glass

The glass-etch process requires the following facilities:

- Hydrofluoric acid pretreatment tank
- Rinse tank
- Silica supersaturated hydrofluosilicic acid tank with heater and stirring method.

The glass sheet is mounted in a dipping rack and cleaned in the hydrofluoric acid tank to remove the weathered surface layer. The HF concentration used is between 0.5 and 1 percent. The glass is then rinsed and placed in the hydrofluosilicic acid etching tank. The tank contains hydrofluosilicic acid which is saturated with silica and then supersaturated by adding boric acid. The degree of supersaturation is termed "potency" and the required etching potency varies for different types of glass. The bath must also be heated and stirred so that the solution is homogeneous and without a temperature gradient from bottom to top. The effect of high solution temperature is to shorten the emmersion time for the etching process.

Both of these coating processes, while not yet fully commercialized, offer good potential for solar collector applications in that they provide significant improvements in collector performance without requiring extensive and costly processing.

REFERENCES

- (1) H. C. Hottel and B. B. Woertz, The Performance of Flat Plate Solar Heat Collectors, Trans. ASME 64, 91 (1942).
- (2) H. C. Hottel and A. Whillier, Trans. Conf. on the Use of Solar Energy, Vol. 2, Part I, p. 74, Univ. Arizona Press (1958).
- (3) R. W. Bliss, The Derivation of Several "Plate Efficiency Factors" Useful in the Design of Flat Plate Solar Heat Collectors, Solar Energy 3, 55 (1959).
- (4) W. M. Rohsenow, H. Choi, Heat, Mass and Momentum Transfer, Prentice-Hall (1961), p. 142.
- (5) H. C. Hottel and A. Whillier, "Evaluation of Flat Plate Solar Collector Performance," Solar Energy Conversion Research Project, Publication No. 53, Massachusetts Institute of Technology, Cambridge, Massachusetts.
- (6) F. F. Simon and Paul Harlamert, "Flat Plate Collector Performance Evaluation - the Case for a Solar Simulation Approach," NASA TMX 71427.
- (7) H. Tabor, "Radiation, Convection and Conduction Coefficients in Solar Collectors," Bull. Res. Council of Israel, Vol. 6C, pp. 155-176 (1958).
- (8) Housing Research Paper No. 32, "The Thermal Insulating Value of Airspaces," Housing and Home Finance Agency, U. S. Govt. Printing Office (1957).
- (9) A. Acrivos, B. D. Babcock, R. L. Pigford, Flow Distribution in Manifolds, Chemical Engineering Science, Vol. 10, pp. 112-124 (1959).
- (10) J. P. Hartnett and W. M. Rohsenow, Handbook of Heat Transfer, McGraw-Hill (1973).
- (11) K. Yass and H. Curtis, "Low-Cost, Air Mass 2 Solar Simulator," NASA TMX-3059.
- (12) G. E. McDonald, "Spectral Reflectance Properties of Black Chrome for Use as a Solar Selective Coating," NASA TMX-71696 (1974).